UNIVERSITY TRANSPORTATION CENTER
FOR UNDERGROUND TRANSPORTATION INFRASTRUCTURE

UNCERTAINTY ANALYSIS IN ROCK MASS CLASSIFICATION AND ITS APPLICATION TO RELIABILITY EVALUATION IN TUNNEL CONSTRUCTION

FINAL PROJECT REPORT

by
Dr. Hui Lu[1]
Dr. Marte Gutierrez[1]
[1] Colorado School of Mines

Sponsorship
UUTC-UTI and cost matching external sponsors)

For
University Transportation Center for
Underground Transportation Infrastructure
(UTC-UTI)

October 30, 2020

COLORADO SCHOOL OF MINES
EARTH • ENERGY • ENVIRONMENT

Disclaimer

The contents of this report reflect the views of the authors, who are responsible for the facts and the accuracy of the information presented herein. This document is disseminated in the interest of information exchange. The report is funded, partially or entirely, by a grant from the U.S. Department of Transportation's University Transportation Centers Program. However, the U.S. Government assumes no liability for the contents or use thereof.

1. Report No. UTC-UTI 004	2. Government Accession No.	3. Recipient's Catalog No.
4. Title and Subtitle UNCERTAINTY ANALYSIS IN ROCK MASS CLASSIFICATION AND ITS APPLICATION TO RELIABILITY EVALUATION IN TUNNEL CONSTRUCTION		5.October 30, 2020 6. Performing Organization Code
7. Authors: Hui Lu (Orcid.org/ 0000-0001-5180-5114) Marte Gutierrez (Orcid.org/0000-0001-5070-8726)		8. Performing Organization Report No. UTC-UTI 004
9. Performing Organization Name and Address University Transportation Center for Underground Transportation Infrastructure (UTC-UTI) Tier 1 University Transportation Center Colorado School of Mines Coolbaugh 308, 1012 14th St., Golden, CO 80401		10. Work Unit No. (TRAIS) 11. Contract or Grant No. 69A355174711
12. Sponsoring Agency Name and Address United States of America Department of Transportation Research and Innovative Technology Administration		13. Type of Report and Period Covered Final Project Report 14. Sponsoring Agency Code
15. Supplementary Notes Report also available at: https://zenodo.org/communities/utc-uti		

16. Abstract

With the increasing demand for tunnels in sensitive urban environments, pressure balance mechanized tunneling is employed in most soft ground tunnel construction projects. Segmental tunnel lining is used in pressure balance mechanized tunneling as temporary and final support. With common service life requirements of 100 and even 150 years, efficient design of pre-cast concrete segments can have considerable serviceability and economic importance. The aim of this thesis is to improve the understanding of ground-structure interaction of segmental lining in soft ground mechanized tunneling both in the main running tunnels and at cross-passage openings. Incorporating rare field data collected from the Northgate Link project in Seattle together with advanced three-dimensional (3D) finite-difference modeling (FDM), this research seeks to provide insight into segmental lining ground-structure interaction.

As part of the effort to reduce surface settlement, pressure outside the TBM shield plays an important role in pressure balance mechanized tunneling. An advanced 3D FDM model is presented for pressure balanced tunneling, where the annulus between the shield and ground is full of pressurized material, simplifying the modeling of the shield. The FDM results show that the final lining loads are controlled by the shield and chamber pressure, and the modeling of the TBM shield is not required, as the ground convergence is smaller than the annulus gap size. Extending the 3D FDM model for cross-passages, an advanced 3D ground-structure interaction model is proposed for cross-passages connecting segmentally lined tunnels. Validated using field data, the results show the difference between the loading processes of the break-in and break-out. At the break-out opening, the loading process is controlled by the cross-passage opening formation, while at the break-in opening, the loading is controlled by the advance of the cross-passage excavation, as the ground confining the break-in area is gradually removed. The most critical points with regards to the load capacity of the cross-passage opening support elements were found to be the segmental lining above and below the openings, and the bicone dowel shear capacity. In addition, this thesis investigates the ground response of a tunnel excavated by pressure balance mechanized TBMs in soft ground characterized by the hardening-soil small-strain (HSS) model. A comprehensive parametric analysis using a series of 3D and axisymmetric FDM modeling is employed. The results show that longitudinal displacement profiles (LDP) assuming linear-elastic or elastic perfectly plastic (EPP) soil behavior compared to the more realistic HSS model can result in overestimation of pre-convergence prior to liner installation. This over-estimation of the pre-convergence by EPP MC is

shown to be as much as 20%. A new LDP solution for HSS is proposed for application in pressure balance TBM tunneling in soft ground, and the practical application of the new HSS LDP solution is described.			
17. Underground transportation tunnels, safety and reliability, Rock mass quality prediction; Rock mass classification Q-system; Markov chain; Monte Carlo simulations; probabilistic analysis.		18. Distribution Statement No restrictions.	
19. Security Classification (of this report) Unclassified	20. Security Classification (of this page) Unclassified	21. No of Pages 224	22. Price NA

ABSTRACT

Creation of underground infrastructures and facilities provides a viable solution to rapid urbanization and population growth with the limited and increasingly congested space on the surface, which has posed a critical challenge to urban population's demands on the living environment. This includes road and rail transport systems, utility tunnels, water and sewage, parking, storage, and even living quarters. These underground structures are constructed in rock and soil materials, which are not precisely known before excavation. This means that there is intrinsic uncertainty due to the inherently heterogeneous nature of the ground, which can have adverse effects on the design and construction of underground works. Traditional deterministic design methods are based on a limited understanding of this inherent uncertainty, which may result in over- or under- design of underground structures. To address this issue, a systematic assessment of uncertainties in rock mass classification systems has been conducted in this study, in conjunction with a reliability-based approach, to evaluate the stability of underground openings. The rock mass quality Q-system has been used as an example of rock mass classification systems in this study, but the approach can also be applied to other rock mass classifications such as rock mass rating (RMR) and geological strength index (GSI).

First, a Markovian prediction model based on the rock mass classification Q-system has been proposed to provide the probabilistic distribution of the rock mass quality Q for unexcavated tunnel sections using the Monte Carlo Simulation (MCS) technique. In addition, an analytical approximation approach has been proposed to derive the statistics (mean, standard deviation, and coefficient of variation) of the Q value based on statistics of Q-parameters (input parameters in the Q-system). The proposed prediction model and analytical approach were applied to a case study of a water tunnel and have been validated by the recorded Q data during tunnel construction.

Next, an MCS-based uncertainty analysis framework has also been developed to probabilistically characterize the uncertainty in the rock mass quality Q-system and

its propagation to rock mass characterization and ground response evaluation. The Shimizu highway tunnel was used as the case study for validation. The probabilistic distribution of the Q value was obtained using the MCS technique based on relative frequency histograms of the Q-parameters. Similarly, probabilistic estimates of rock mass parameters were also derived with Q-based empirical correlations, which were subsequently used as inputs in numerical models for the evaluation of excavation response. In addition, the probabilistic sensitivity analysis was also conducted in the MCS process to identify the most influential Q-parameters. The effects of the correlation and distribution types of uncertain Q-parameters on the Q value and associated rock mass parameters were also examined.

Finally, a reliability assessment with a strain-based failure criterion has been performed using the First Order Reliability Method (FORM) algorithm. The probabilistic critical strain and Q-based empirically estimated tunnel strain were incorporated in the performance function. The Shimizu tunnel case study was also utilized to perform reliability analysis as a basis for the evaluation of tunnel excavation stability. Reliability analysis was also performed using the MCS technique for comparison. In addition, the effects of correlation, distribution types and coefficient of variation in input parameters on the reliability (reliability index and probability of failure) have also been studied. The reliability assessment results show that the Shimizu tunnel was not expected to experience instability after excavation. The excavation stability has also been evaluated using analytical and numerical approaches, and results were consistent with those derived from the reliability approach.

Uncertainty and reliability assessment using rock mass classification systems, as presented in this report, can probabilistically characterize uncertainties and risks and provide an improved rock mass characterization and excavation response evaluation as compared to traditional use of safety factor. It can also offer insightful information and valuable input for the probabilistic analysis and design of excavation and support strategies as we as construction time and cost estimation for underground structures.

TABLE OF CONTENTS

LIST OF FIGURES

LIST OF TABLES

CHAPTER 1

INTRODUCTION

1.1 Background and motivation

Increasing global population and urbanization has increased the demands for additional living spaces of all kinds (Goel et al., 2012). Creation of underground space offers a feasible strategy for development of additional functional spaces since the underground space can include infrastructures that are difficult, if not impossible, to build above ground. Underground space also offers natural protection and great safety against different kinds of disasters (Goel et al., 2012). The use of underground space with tunnels is expected to be a viable solution in view of the increasingly limited and congested space on the surface, especially in urban areas (Brox, 2017). Tunnels have been used for a range of infrastructure needs, including road, water and wastewater, utility, oil and gas pipeline, access and ventilation in mining, waste disposal, storage, defense, etc. However, since tunnels are constructed in geo-materials (rock and soil), which are known to involve some degree of uncertainty before tunnels are excavated, there is an intrinsic risk for encountering unknown geological conditions (Spackova, 2012). Thus, the uncertainty in geological conditions poses a critical challenge in underground construction.

Rock mass classification systems, including the rock mass rating (RMR) (Bieniawski, 1976), Q-system (Barton et al., 1974) and geological strength index (GSI) (Hoek and Brown, 1997), allows the overall rock mass quality to be described and rock mass properties to be characterized, and can also offer initial estimates of support requirements of underground excavations (Hoek, 2007). Rock mass classification systems have been used as empirical rock design tools and have enjoyed widespread application due to the easy use of simple observations and measurements to offer a quantitative index of overall rock mass quality (Palmstrom and Stille, 2010). Traditionally, however, most empirical methods, including the rock mass classifications, rely on single mean (or expected) values, and there may be significant variations

between the upper and lower bound values (Palmstrom and Stille, 2010). In other words, uncertainties in rock mass classifications are often treated deterministically, which fails to cover the possible wide range of rock mass quality and may result in over- or under-design of the engineering structure. The overdesign indicates the conservative approach, where the safety is assured while cost and schedule overruns are the end result. In contrast, the under-design implies an aggressive approach, involving higher risks of failure and damage to the surrounding structure or safety implications. In traditional deterministic design methods, uncertainties in rock mass classifications are not logically characterized and estimates of reliability are not provided. There is a lack of complete understanding of how uncertainties in rock mass parameters propagate and affect the characterization of rock mass behavior. Modeling and evaluating uncertainties in rock mass classifications before construction is critical and can provide insightful information for the optimum design of underground excavation and support on the basis of safety and economic risk. Thus, it is necessary to adequately assess uncertainties in rock mass classifications, and to analyze the effects on the rock mass characterization and evaluate ground behavior in a more rigorous way.

Uncertainty and reliability based methods represent more rational approaches to quantitatively describe uncertainties in input parameters as well as providing a consistent and complete measure of level of reliability and risks in the analysis and design process. In this report, uncertainty analysis in the rock mass classification was conducted using the Q-system as an example. The uncertainty in the Q-system was probabilistically characterized and its effects on the characterization of rock mass properties and the evaluation on the tunnel excavation response were examined. Moreover, a reliability approach with the strain-based failure criterion has also been used to assess the stability of underground tunnel after excavation.

1.2 Research objectives

To improve the understanding on the probability-based uncertainty analysis in the rock mass classification, using the Q-system in this study, and its application to the reliability assessment for the underground excavation stability, the research objectives

in this report are as follows:

(1) Probabilistically characterize and predict uncertainties in rock mass classification Q-system before tunnel excavation and validate the predicted results with rock mass quality data collected during tunnel construction.

(2) Investigate the effects of uncertainties in input parameters in the Q-system on the overall Q value and associated rock mass characterization and ground response evaluation for underground structures.

(3) Perform reliability analysis with probabilistic Q-system on the basis of a strain-based failure criterion to evaluate the tunnel excavation stability.

1.3 Report outline

This report is composed of six chapters, which are outlined below. All references are placed at the end of the report.

Chapter 1 presents the general background, the motivation for this research, research objectives and report outline.

Chapter 2 presents the literature review in the report. The commonly used modern rock mass classification systems, sources of uncertainties in rock mass classifications and treatment approaches are introduced. In addition, reliability-based methods and the application in underground construction are also described.

Chapter 3 presents a rock mass classification Q-system-based prediction model using the Markov Chain technique to probabilistically assess rock mass quality before tunnel excavation. Based on the proposed prediction model, the probability distribution of the overall Q value can be derived at arbitrary locations along the tunnel alignment using Monte Carlo simulations. In addition, an analytical approximation approach to deriving statistics (mean, standard deviation, and coefficient of variation) of the Q value has also been developed given statistics of input parameters in the Q-system. The proposed prediction model and analytical approach have been applied to a case study of a water tunnel and validated by the actual Q value recorded during tunnel construction.

Chapter 4 presents a paper titled “Monte Carlo simulation (MCS)-based

uncertainty analysis of rock mass quality Q in underground construction" This paper has been published in The Journal of Tunneling and Underground Space Technology. An MCS-based uncertainty analysis framework has been proposed to probabilistically quantify the uncertainty in the rock mass classification Q-system. The proposed framework has been implemented in the Shimizu highway tunnel case study. Based on relative frequency histograms of Q-parameters (input parameters in the Q-system), the probability distribution of the Q value is obtained using the MCS technique, which is then used to probabilistically estimate rock mass properties and responses with appropriate empirical correlations. The probabilistic estimates of rock mass properties are also adopted as inputs in a finite element model for the probabilistic evaluation of the excavation-induced tunnel displacement. In addition, the probabilistic sensitivity analysis is conducted in the MCS process to identify the most important Q-parameters in the Q-system based on several ranking criteria. The effects of correlation and distribution types of input parameters in the probabilistic Q-system on the Q value and associated rock mass parameters have also been investigated.

Chapter 5 presents a reliability assessment using the Q-based empirical approach for the preliminary evaluation of the excavation stability using the FORM algorithm. The probabilistic critical strain and the Q-based empirically estimated tunnel strain are incorporated in the limit state function for reliability analysis. Reliability analysis is also conducted using the MCS technique for comparison. The Shimizu tunnel case study is also utilized as an example to perform reliability assessment on the excavation stability. The effects of the correlation, distribution types and coefficient of variation in input parameters on the reliability have also been investigated. The reliability results on the stability evaluation of the excavated tunnel have been compared to those derived using analytical and numerical approaches.

Chapter 6 is the final chapter of this report. Major findings and conclusions are summarized, and directions for future work are also presented.

CHAPTER 2

LITERATURE SURVEY

This chapter presents the literature review for this research, which mainly includes uncertainty analysis in rock mass classification systems and reliability-based assessment in underground construction. The commonly used rock mass classification systems, involved uncertainties and treatment approaches have been introduced. Reliability-based methods, the comparison with factor of safety and reliability assessment in underground construction are also presented.

2.1 Uncertainty analysis in rock mass classification systems

2.1.1 Rock mass classification system

Rock mass classification involves the process of placing rock masses into groups or classes based on defined relationships and has played an indispensable part in engineering design and practice (Bieniawski, 1989). Rock mass classification systems provide a basis for understanding the characteristics and behavior or rock mass, serving as the basis of the empirical design and relating to experiences obtained in rock mass conditions at one site to another. The objectives of the rock mass classification are proposed (Bieniawski, 1989):

(1) Identify the most important parameters impacting the rock mass behavior.
(2) Subdivide a particular rock mass formation into groups or classes of similar behavior.
(3) Provide a basis for understanding the characteristics of each rock mass class.
(4) Relate the experience of rock mass conditions at one site to the conditions and experience gained at another.
(5) Derive quantitative data and guidelines for rock engineering design, e.g. support guidance for underground excavations.
(6) Provide a common basis for communication between engineers and geologists

The advantages of rock mass classifications have also been summarized(Bieniawski, 1989):

(1) Rock mass classification systems can provide a checklist for the ground parameters to be collected, thus improving the quality of site investigation

(2) Classification systems can provide quantitative information for engineering design purposes

(3) These quantitative classifications enable better engineering judgement and more effective communication on a project.

Problems in the application of rock mass classifications arise when (Bieniawski, 1993):

(1) Using rock mass classification as the ultimate design solution, i.e. neglecting the analytical, numerical and observational methods;

(2) Using on rock mass classification only without cross-checking with other classification systems

(3) Using rock mass classification without sufficient input data

(4) Using rock mass classifications without realizing the conservatism and limits arising from the databases on which they are based.

Commonly used rock mass classification systems are briefly introduced below, namely the RMR system, Q-system and the GSI system.

RMR system

The Geomechanics Classification or the RMR system was developed by Bieniawski (1976) to evaluate the excavation stability and support requirements of tunnels. Since then it has been improved based on more collected case histories, and the 1989 version of the classification is introduced herein. The RMR system has six input parameters, i.e. uniaxial compressive strength (UCS) of rock material, rock quality designation (RQD), the spacing of discontinuities, condition of discontinuities, groundwater conditions and the orientation of discontinuities (Bieniawski, 1989). Ratings are given to each input parameter, and the summation of these ratings is the overall RMR value.

In applying the RMR system, the rock mass is subdivided into a number of structural zones (Bieniawski, 1989). Each zone is relatively geologically homogeneous

and classified separately. A major structural feature such as a fault or the change of rock types may be considered as the boundary of structural zones (Hoek, 2007). In terms of the application of the RMR system, it provides a set of guidelines for excavation and support of 10 m span rock tunnels constructed using drill and blast methods (Hoek, 2007). The RMR is also applied to estimate the unsupported span and stand-up time for excavated tunnels. In addition, the RMR system can also be used to estimate rock mass properties based on some empirical correlations (Bieniawski, 1989).

Q-system

The rock mass classification Q-system was developed for the determination of rock mass characteristics and support requirements (Barton et al., 1974). This empirical rock mass classification was proposed based on 212 case records of hard rock tunnel from Scandinavia. The numerical value of the Q index ranges from 0.001 to a maximum of 1000 on a logarithmic scale, and the overall Q value is defined by the Q-equation as follows (Barton et al., 1974):

$$Q = \frac{RQD}{J_n} \times \frac{J_r}{J_a} \times \frac{J_w}{SRF} \tag{2.1}$$

where RQD is the Rock Quality Designation; J_n is the joint set number; J_r is the joint roughness number; J_a is the joint alteration number; J_w is the joint water reduction factor and SRF is the stress reduction factor.

As seen in the Q-equation, the Q value is the product of three quotients of its input parameters. The first quotient (RQD/J_n) represents the rock mass structure and is a measure of the block size; the second quotient (J_r/J_a) indicates inter-block shear strength and relates to the roughness and frictional characteristics of joint walls, and the third quotient (J_w/SRF) is an empirical factor describing the active stress . Based on the incorporation of new case records, the Q-system has been updated and improved. A normalization factor considering the UCS of the intact rock has been incorporated into the Q-equation and a new value Q_c is generated (Barton, 2002). A support chart based on the overall Q value has been developed and updated for the rock support estimation by relating the Q value and the equivalent dimension of excavated openings (Barton,

2002; Barton et al., 1974; Grimstad, 1993). Relationships between the Q value and the seismic velocity, depth, deformation modulus of rock mass, required support pressure, have been developed, and these parameters can be roughly estimated using the empirical correlations based on obtained Q value (Barton, 2002).

GSI system

The GSI system was introduced to estimate the reduction in rock mass strength under different geological conditions (Hoek and Brown, 1997). The GSI can be estimated based on field observation and geological descriptions by combing the rock mass structure (block size) and the rock discontinuity surface conditions (roughness and alteration). It is also recommended to use a range of GSI values rather than single number or value (Hoek, 1998a). The GSI has been modified to cover more complex geological conditions, such as shear zones or heterogeneous rock masses, and the GSI chart are updated to incorporate these categories (Hoek and Marinos, 2000a; Hoek et al., 1998). In addition, the GSI system has been interpreted in a more quantitative manner by many authors (Cai et al., 2004; Hoek et al., 2013; Hoek et al., 1998; Marinos et al., 2005).

In terms of the application, the GSI system has been used to estimate the rock mass properties in rock engineering (Hoek et al., 2002; Marinos and Hoek, 2000). It also serves as a tool to estimate the parameters in the Hoek-Brown criterion of rock masses (Hoek and Brown, 1997; Hoek et al., 2002).

2.1.2 Sources of uncertainty in rock mass classification system

Uncertainty can be categorized as aleatory or epistemic uncertainty (Baecher and Christian, 2003). Aleatory uncertainty relates with the natural, intrinsic randomness which may be dealt with probabilistic or statistical analysis. In contrast, the epistemic uncertainty results from incomplete knowledge and can be reduced when additional information is available. Einstein and Baecher (1983) also divided the sources of uncertainty in geotechnical engineering as: (1) inherent spatial and temporal variability; (2) measurement errors; (3) model uncertainty; (4) load uncertainty; and (5) omissions.

Rock mass classification systems are based on experience and thus have similar inherent uncertainties (Stille and Palmström, 2003). Input parameters in the rock mass classification have inherent uncertainties due to the spatial variability and heterogeneity of rock mass itself. The determination of the ratings for input parameters in the rock mass classification systems also involves uncertainty. For example, RQD can often lead to a sampling bias due to a preferential distribution of joints (Grenon and Hadjigeorgiou, 2003). In addition, uncertainties also take place in observing and recording joint characteristics. The mapping results for the joint location for different observers along the same scanline are very different (Ewan et al., 1983). Some input parameters relating to joint features in the rock mass classifications are prone to mischaracterization (Palmstrom and Broch, 2006).

Hadjigeorgiou and Harrison (2011) also noted that rock mass classification systems have uncertainties and not considering them may lead to statistical errors. Two groups of errors can be generated in the use of rock mass classifications. The first group relates with the intrinsic errors in the rock mass classifications, such as the errors of omission, errors of superfluousness, and errors of taxonomy. The omission means the failure to consider pertinent characteristics in rock mass classifications, such as the absence of UCS in the Q-system and the in-situ stress condition in the RMR system. The consideration of rock mass anisotropy is also omitted in both RMR and the Q-system. With regard to the superfluousness, the RQD and discontinuity spacing are a good example since these two parameters are not mutually independent, indicating that either can be estimated from the other. The errors of taxonomy are due to the requirement to pick a number or rating value for a geomechanical property. For example, for the joint water reduction factor J_w in the Q-system, it is not clear how to classify “medium inflow with significant outwash of joint fillings”. In contrast to the first group of error types, the second group is associated with implementation, such as the errors of human error and errors of ignoring variability or uncertainty. The assignment of only one value, instead of a range of distribution, ignores the heterogeneous and random nature of rock mass properties. The risk analysis for a

certain rock engineering project also depends on the level of confidence in known relevant parameters, which is dependent on the amount of available information, the variation of input parameters in rock mass classifications and its impact on the probable rock mass quality index and the required minimum rock mass quality for compatibility with proposed excavation requirements (Carter, 1992).

2.1.3 Dealing with uncertainty in rock mass classification system

Empirical assessment methods, including those based on rock mass classification systems, are essentially deterministic approaches (Carter, 1992). However, the use of only one subjectively assigned value cannot consider the wide range of actual rock mass characteristics that are often encountered in engineering practice. It is appropriate to provide a range of values, instead of a single value, to each input parameter in rock mass classification systems and to assess the significance of the final result (Hoek, 2007). The obtained mean value can be used in choosing the basic rock support while the range can provide an indication of the possible adjustments that may be required to meet different conditions encountered during tunnel excavation. It is also recommended by Hoek (1998a) that a range of values of GSI should be used in preference to a deterministic value. Barton et al. (1994) have used the Q-histogram logging approach to collect the histogram of input parameters in the Q-system, and statistics (min, max, mean, and mode) of the Q value can be obtained using the interval analysis. However, Panthi (2006) pointed out that the mean and range values have poor statistical properties and are sensitive to extreme values. Similarly, Bedi (2013) also stated that the possible wide range of Q value intervals lacks sufficient information and may cause difficulty in decision-making. Carter (1992) suggested that it is advantageous to replace the subjectivity associated with a selecting single value with the use of probabilistic sampling approaches accounting for the uncertain and variable nature of rock masses. These probabilistic approaches can provide some insights into the degree of uncertainty in the input parameters in the rock mass classifications. Carter (1992) also stated that geological-geomechanical factors, such as rock strength and rock structure, are particularly amenable to the probabilistic treatment and that it is

advocated to evaluate the collected geotechnical site investigation data for rock engineering projects from a probabilistic point of view. The probabilistic approach in evaluating rock mass classifications, rather than straightforward use of deterministic assessment, can provide the designer not only with a better understanding on the sensitivity of the output to variations in the input parameters, it also reflect the basic uncertainties inherent in the rock mass parameter data on which the design is predicated (Carter, 1992). If the uncertainty and variability in the rock mass classifications are not sufficiently characterized, they might propagate through the analysis and design process and adversely impact the ground response and support performance (Langford, 2013).

Fortunately, probabilistic evaluation on the rock mass classification, which enables the description of the complete probability distribution function (PDF) of rock mass parameters, is capable of quantifying the uncertainty and its effect on the design performance. Cai (2011) presented that both the intrinsic and subjective uncertainties in rock mass classifications can be captured in the probabilistic evaluation and the probabilistic design can be accordingly conducted. Bedi (2013) derived the probability density function of the Q value in the Gjovik cavern using the Monte Carlo simulation (MCS) method based on the assumed triangular distributions of Q-parameters. Carter (1992) also performed similar simulations to derive the distribution of the Q value and suggested that simple triangular distributions often provide sufficient accuracy. Panthi (2006) assumed the normal or lognormal distributions for RQD, J_r and J_a parameters while the triangular distributions for J_n, J_w and SRF parameters in the Q-system, and the PDF of the Q value was obtained using the MCS technique for the Himalayan mountainous tunnels. Analogously, the distribution of GSI was also estimated from the statistical distributions of joint characteristics in field mapping, which was then used as the input in the numerical model for probabilistically evaluating the excavation response and stability of underground construction (Cai, 2011; Idris et al., 2015; Tiwari et al., 2017). The probability distributions of RMR and GSI were derived based on the probabilistic descriptions of discontinuities and intact rock properties using the MCS

technique, and the strength and deformability properties of rock mass were also probabilistically estimated based on some empirical relationships (Sari, 2009; Sari et al., 2010).

However, few researchers have investigated the contributions of input parameters in the rock mass classification systems within a probabilistic framework. In addition, the majority of studies fail to consider the interdependency between uncertain input parameters and its impact in rock mass classifications. Further, although rock mass parameters are amenable to probabilistic treatment, few studies have examined the effects of distribution types of input parameters in rock mass classifications on the overall rock mass quality and associated rock mass characterization and response.

2.2 Reliability-based assessment in underground construction

2.2.1 Factor of safety and reliability concept

Traditionally, the deterministic factor of safety (*FS*) is applied to deal with the uncertainties in the geotechnical engineering. The factor of safety is calculated as the ratio of characteristic resistance over the characteristic load. The characteristic resistance and load are conservative estimates of resistance and load in the system (Fenton and Griffiths, 2008). When the characteristic values are equal to the means, then the factor of safety can be defined in terms of the mean resistance and mean load:

$$FS = \frac{\mu_R}{\mu_Q} \tag{2.2}$$

where *FS* is the factor of safety, μ_R is the mean resistance, μ_Q is the mean load.

Griffiths and Fenton (2007) stated that all uncertainty is lumped into the single factor of safety, and the factor of safety does not provide information on the level of safety in the design. The same factor of safety can generate two designs that have different levels of safety. This may be due to factors of safety agreed on in design codes or standards not being calibrated to each other. It is also common to apply the same factor of safety for a given type of geo-structures, such as long-term slope stability, without considering the uncertainties involved in the calculation (Duncan, 2000).

Fenton and Griffiths (2008) stated an example of three geotechnical designs, having the same mean factor of safety, can have considerably different probabilities of failure. The actual design safety is not adequately reflected in the mean factor of safety. Tapia et al. (2007) also showed an example of slope design A and B, in which the FS_A (1.35) is smaller than the FS_B (1.50). However, the greater uncertainty in design B, indicated by larger spread, results in higher probability of failure despite the larger *FS* value in design B in comparison to design A. This is an example for the slope design, however, it can be equally applicable to underground construction.

The factor of safety in the conventional geotechnical engineering is generally determined heuristically, based on experiences of similar projects. However, as questioned by Griffiths and Fenton (2007), what if we do not have experience, such as using new construction materials or in a new environment? What if the experience that we have is not positive? The traditional factor of safety approach cannot answer the above questions. Griffiths and Fenton (2007) also suggested that it is difficult to pick an optimum factor of safety since the FS has no real meaning in terms of reliability.

The ambiguous nature of the factor of safety has also been reported by Low and Einstein (2013), and two different definitions on the factor of safety against the wedge falling were discussed. Each definition has its rationale while the values of *FS* can differ by an order of magnitude. Lilly and Li (2000) also stated that the factor of safety, by definition, is a binary criterion. Either the excavation is stable ($FS>1$) or fails ($FS<1$) due to the fact that excavations at limit equilibrium ($FS=1$) are very rare in practice. Zhang and Goh (2012) also pointed out that failure in underground excavation may occur even when the *FS* is larger than 1.0.

To overcome these issues, reliability-based approaches have been developed to provide a more consistent and complete measure of the safety level considering the uncertainties involved. The subsection below will briefly introduce the reliability theory.

2.2.2 Overview of reliability theory

(1) The general case

The performance function *G(X)* is used to describe the performance of geotechnical structures, which also defines the acceptance criterion for the system in terms of the limit state function (where *X* is the collection of all relevant input random variables).The resistance *R(X)* and the load acting on the system *Q(X)* can be used to construct the performance function, and the relationship can be expressed as follows:

$$G(X) = R(X) - Q(X) \tag{2.3}$$

The critical limit state, indicated by $G(X) = 0$, defines the boundary between safe and unsafe regions. $G(X) > 0$ means stable conditions are expected while $G(X) < 0$ indicates the system has failed to meet the acceptance criterion.

Note that in underground construction, the resistance and load can rarely be separated since the ground response depends on the support type and installation sequence. The performance function can therefore be expressed with respect to a limiting value for the ground response parameter (e.g. displacement, strain, plastic radius) (Langford, 2013).

The probability of failure, or the probability of unsatisfactory performance, can be defined as:

$$p_f = P[G(X) \le 0] = \int ... \int_{G(X) \le 0} f_X(x) dx \tag{2.4}$$

where $f_X(x)$ is the joint probability density function of the collection of random variables X. This integral is generally non-tractable or impossible to solve analytically when many random variables are involved. Thus, approximate methods, including First Order Second Method (FOSM), First Order Reliability Method (FORM), Point Estimate Method (PEM) and Monte Carlo Simulation (MCS), are used to evaluate the integral.

(2) Reliability index

In geotechnical engineering, the safety margin *M* is defined as the difference between the resistance *R* and the load *Q* (Baecher and Christian, 2003).

$$M = R - Q \tag{2.5}$$

The mean value of the safety margin *M* is

$$\mu_M = \mu_R - \mu_Q \tag{2.6}$$

where μ_M , μ_R, μ_Q are the mean value of safety margin *M*, the resistance *R*, and the load *Q*, respectively.

The variance of the safety margin *M* is

$$\sigma_M^2 = \sigma_R^2 + \sigma_Q^2 - 2\rho_{RQ}\sigma_R\sigma_Q \tag{2.7}$$

where σ_M , σ_R , σ_Q are the standard deviation (SD) of the safety margin *M*, the resistance *R* and the load *Q*, respectively; ρ_{RQ} is the correlation coefficient between *R* and *Q*.

The reliability index β is defined as:

$$\beta = \frac{\mu_M}{\sigma_M} = \frac{\mu_R - \mu_Q}{\sqrt{\sigma_R^2 + \sigma_Q^2 - 2\rho_{RQ}\sigma_R\sigma_Q}} \tag{2.8}$$

The probability of failure p_f can be given according to the following equation based on the assumption that the safety margin *M* is normally distributed.

$$p_f = P(M \le 0) \approx \Phi(-\beta) = 1 - \Phi(\beta) \tag{2.9}$$

where p_f is the probability of failure, $\Phi(\cdot)$ is the cumulative distribution function of the standard normal variable, β is the reliability index.

Unlike the factor of safety, the reliability approach enables the consideration of uncertainties in the input parameters and the level of safety and reliability can be quantified. Based on this, consistent levels of reliability can be achieved among different designs. In addition, different to the experience-based factor of safety, the reliability-based approach can provide the ability to develop new designs which achieve a specified reliability target. Moreover, by quantifying the reliability, the cost-benefit analysis can also be carried out to balance the construction costs against the risk of failure (Griffiths and Fenton, 2007).

However, despite the advantages of the reliability approach over the traditional factor of safety, reliability approaches have not yet gained widespread application in geotechnical practice. There are two main reasons (Duncan, 2000): first, reliability theory contains some statistical terms that may not be very familiar to geotechnical engineers; second, there is misconception that the application of the reliability approach requires more data, time and effort than the traditional geotechnical analysis. Duncan (2000) stated that simple reliability analyses, which require neither complex theory nor unfamiliar statistical terms, require minimal additional effort compared to the conventional analyses and should be used in geotechnical practice. Several example applications were used to illustrate the simplicity and practicality of the reliability approach. It has also been advocated that the reliability approach should complement, instead of replacing, the factor of safety analyses in providing measures of acceptable geotechnical design (Duncan, 2000).

2.2.3 Reliability-based methods

The following subsections describe the reliability methods that are commonly used in reliability analysis and reliability-based design in underground structures. These reliability methods can account for the effects of the variability of input parameters on the resulting output variable, including the First Order Second Moment (FOSM), the First Order Reliability Method (FORM), the Point Estimate Method (PEM) and the Monte Carlo simulation (MCS).

FOSM

The FOSM method uses the first terms of a Taylor series expansion of the performance function to evaluate the mean value and variance of the performance function (Baecher and Christian, 2003). The Taylor expansion is truncated after the linear term, and this is called the first order. The first two moments of the output variable are to be estimated, in which the variance is a form of the second moment and the highest order statistics in the analysis, and this is termed as second moment (Fenton and Griffiths, 2008). If the number of the random variable is N, this method needs either

estimating N partial derivatives of the performance function or performing a numerical approximation with evaluations at 2N+1 points (Baecher and Christian, 2003).

The FOSM method is relatively simple and widely used since it requires the evaluation of a minimal number of terms and only the first statistic moments are needed. The evaluation points in the FOSM method are similar to those that are used in parametric sensitivity analysis, thus the contributions of each input parameter can also be revealed (Langford, 2013). However, it should be noted that the accuracy of the FOSM method deteriorates caused by the truncation of the Taylor expansion series after the linear terms if the second and higher derivatives of the performance function are significant, e.g. in situations where the performance functions are highly non-linear (Fenton and Griffiths, 2008). In addition, the probability distribution functions are not taken into account for input parameters, and only the mean and standard deviation are used, which may also result in the approximation errors. Moreover, different values for the probability of failure are obtained using different performance functions for the same problem, indicating the non-uniqueness and inconsistency of reliability evaluation using FOSM (Baecher and Christian, 2003).

FORM

To overcome the problems in the FOSM method, the FORM method was developed by Hasofer and Lind (1974) based on a geometric interpretation of the reliability index as a measure of the distance in dimensionless space between the mean point of the multivariate distribution of input parameters to the boundary of limit state surface. The point where the reliability index ellipsoid touches the limit state surface is termed the design point. A spreadsheet method using the SOLVER add-in with the optimization routine for the Excel can be efficiently used to determine the reliability index in the reliability analysis (Low and Tang, 1997). The distribution types for the input random variables can be defined, and the correlation structure between variables can be captured by the correlation coefficient matrix. The probability of failure can also be approximated based on the assumption that the performance function is normally distributed.

The design point in the FORM spreadsheet, i.e. the x^* value, indicates the most likely failure point on the limit state surface. The distance between the design point and the mean value point of each input parameter reflects the sensitivity of the performance function to that input variable. The ratio of the mean value to the design point value (x^*) is also similar to the partial factor in limit state design in Eurocode 7. However, the partial factors are specified in Eurocode 7 while the design point values are determined automatically in the FORM spreadsheet. The design point values can reflect sensitivities, correlation structures, standard deviations, and probability distributions in a fashion that the prescribed partial factors cannot reflect (Low, 2008b).

PEM

The PEM method was proposed by Rosenblueth (1975) to approximate the mean and standard deviation of the performance function. It is used to obtain the statistical moments of the performance function by evaluating at a set of selected points. The PEM method is a weighted average method, and solutions at different evaluation points are combined with proper weights to get an approximation of the statistic moments of the output variable. The two-point estimate method for the first two moments of uncorrelated random variables is commonly used, and sampling points are selected at one standard deviation above and below the mean value of each random variable. If the performance function has N random variables, then there will be 2^N sampling points considering all combinations of evaluation points (Fenton and Griffiths, 2008). If all random variables are uncorrelated, then the weight value is simply $1/2^N$ for each random variable (Langford, 2013).

The PEM method is preferable to other methods for cases with five or fewer random variables in terms of computation efficiency. However, the number of 2^N evaluations can be a very large number if many random variables are involved. In addition, as with FOSM method, it does not account for the probability distribution off the performance function. Generally the normal distribution is assumed both for the input and output variable. Further, little information is known about the low probability conditions since the performance function is only evaluated at one standard deviation

above and below the mean value. In other words, values beyond the bounds are not considered and these low probability events outside of the bounds may lead to high consequences, thus posing a great risk to the design (Langford, 2013). It is also noted that the PEM method does not perform well in capturing mixed behavior or mode switches since the abrupt change in behavior will not be detected in the PEM (Valley et al., 2010).

MCS

In situations where the performance function is complicated and difficult to assess, the probability of failure can be evaluated directly using the MCS simulation technique. The distributions of the input parameters should be assigned first, and then single values of the input variables are randomly sampled in one iteration according to their respective distributions. This set of sampled input values are then used to calculate a value of the output parameter. With a number of iterations, more input values are sampled and accordingly a number of output values are generated. The statistical moments of the output can be estimated and an appropriate distribution function can be determined for the output variable. Based on the obtained distribution of the performance function, the probability of failure can be calculated as the probability that the performance function is less than or equal to zero.

The MCS technique is straightforward and has the advantage of conceptual simplicity. The distributions for the input parameters can be specified based on the collected information, and the correlation structure between input variables can also be captured. The major disadvantage is that it is computationally expensive and time consuming. The computation efforts are extremely high if adequate accuracy of calculation is to be satisfied especially when the estimated probability of failure is very low (Baecher and Christian, 2003). The considerable computational effort can be reduced using variance reduction techniques in which the accuracy level is sustained while the required number of computations is reduced. The MCS simulation can be used as a complement to discrete sampling methods to ensure an accurate evaluation of the system performance especially for complex problems (Langford, 2013).

2.2.4 Reliability evaluation in underground construction

Uncertainties are unavoidable in geotechnical engineering, including underground construction, and they stem from loads, geotechnical properties, measurement errors, calculation models etc. (Ang and Tang, 2007; Baecher and Christian, 2003). The limitations of the FS-based design approach, which has been traditionally used in the geotechnical practice, have been pointed out, and alternatives including the partial factor design in Eurocode 7 and the load and resistance factor design (LRFD) approach in United States, which is equivalent to limit state design (LSD) in Canada, have been developed (Ang and Tang, 2007; Baecher and Christian, 2003; Fenton and Griffiths, 2008). The LRFD, LSD and partial factor approaches, are philosophically similar and the focus is the re-distribution of the factor of safety into separate load and resistance factors or partial factors for ground parameters (Phoon et al., 2003).

The LRFD approach subjectively incorporates uncertainties of load and resistance into the design process by assigning separate factors to each. The LRFD approach has been used extensively in North America for geotechnical structures, in which the prescribed limit state in LRFD should yield a constructed system having a target reliability or an acceptable probability of failure (Fenton and Griffiths, 2008). The LRFD is used relatively straightforward in gravity-driven structures, such as the foundation and retaining wall design, as the loads and resistances can be considered separately in the design (Langford, 2013). However, the LRFD approach is more complicated in underground structures. The system performance is defined by the relationship between deformations, loads that have been induced by rock mass stresses, and the capacity of support elements, thus limiting its applicability in the underground works (Langford, 2013). Fortunately, reliability methods are capable of assessing how uncertainty in rock mass parameters propagates through the analysis and design to obtain a measure of uncertainty in the system performance. The reliability-based approach provides a more consistent and complete measure of risk since it not only defines the expected case (as with a deterministic analysis) but it also provides a

measure of design performance based on the probability of failure (Langford, 2013). The reliability-based approach using the FORM spreadsheet with an expanding ellipsoid has the ability to seek the most-probable design point without presuming any partial factors and to automatically reflect sensitivities from case to case (Low, 2008b). The superiority of reliability-based methods to approaches including the traditional factor of safety, LRFD and the partial factor approach is summarized in (Phoon et al., 2003).

Despite its benefits, the reliability analysis in the geotechnical engineering has been focused on surface geotechnical projects and has not yet achieved widespread in the design of underground construction (Langford 2013). While some productive research has been done on the reliability analysis in underground construction (Bjureland et al., 2017; Langford and Diederichs, 2013; Liu and Low, 2017; Low and Einstein, 2013; Mollon et al., 2009a, b, 2010), more attention should be paid to some issues in this area. To start with, the reliability analyses in the current research are mostly based on analytical solutions or numerical procedures. However, in the analytical solutions, the ground-support interaction is often used to establish the performance function, and this is always based on some simplistic assumptions that are rarely met in practice (Li and Low, 2010; Su et al., 2011). For example, the convergence-confinement method (Carranza-Torres and Fairhurst, 2000; Panet and Guenot, 1983) was adopted by Li and Low (2010) to construct the performance function of tunnel response for reliability analysis, in which a circular tunnel was assumed to be subjected to hydrostatic stresses with uniform internal pressure around the tunnel perimeter. Due to the implicit characteristics of the performance function in underground construction, numerical procedures with finite element or finite difference models using different algorithms have been used to construct the limit state function, including the response surface method (Hamrouni et al., 2017; Lü et al., 2011; Mollon et al., 2010), regression methods (Basarir, 2008; Zhang and Goh, 2015; Zhu et al., 2008), artificial neural networks (Adoko et al., 2013; Lü et al., 2012; Mahdevari and Torabi, 2012), support vector machines (Tan et al., 2011; Zhao, 2008; Zhao et al., 2014) and

radial basis functions (Bai et al., 2012; Fang et al., 2005; Wang et al., 2016). However, the numerical procedures are generally computationally expensive, which requires a great deal of computational effort. In addition to the analytical and numerical procedures, some empirical relationships or evidences with regard to tunnel response (e.g. displacement, strain, and plastic radius) have also been developed to evaluate the excavation stability (Barton, 2002; Barton et al., 1994; Marinos and Hoek, 2000; Sakurai, 1983). However, no current research has adopted such empirical correlations in reliability evaluation to preliminarily assess the stability of underground excavations. In addition, the focus of the majority of the research is the illustration of the newly proposed reliability analysis approaches or algorithms, and hypothetical examples are generally used with assumed statistical data of rock mass parameters, indicating few case studies with real rock mass parameter data have been adopted to validate proposed approaches or algorithms. Moreover, previous work has focused only on the deterministic critical strain using the strain-based limit state function in the reliability assessment on underground construction. In other words, the previous work failed to consider the uncertainty in the critical strain itself.

CHAPTER 3

A STUDY OF A PROBABILISTIC Q-SYSTEM USING A MARKOV CHAIN MODEL TO PREDICT ROCK MASS QUALITY IN TUNNELING

3.1 Abstract

Uncertainties in rock mass conditions are mainly caused by the inherently inhomogeneous nature of rock masses. Assessment of rock mass quality without accounting for inherent uncertainty often leads to excessive conservatism in design and construction, resulting in a negative effect on overall design and construction processes; thus, accurate prediction of rock mass quality is critical to save project cost and time. In this study, to advance rock mass quality assessment, a Q-based prediction model to assess probabilistic rock mass quality has been proposed using the Markov chain technique with quantitatively characterized uncertainties. Based on the Markovian prediction model, the statistical distribution of the Q value has been derived from arbitrary locations along a tunnel alignment using Monte Carlo simulations. The predicted results derived using the proposed probabilistic prediction model have also been compared to those obtained using the deterministic prediction approach. In addition, an analytical approximation approach to deriving the statistics (mean, standard deviation, and coefficient of variation) of the Q value given statistics of Q-parameters has also been developed. In this study, the proposed prediction model and analytical calculation approach were applied to a case study of a water tunnel and have been validated by the actual Q values recorded during construction. The proposed Q-based prediction model is capable of assessing the rock mass quality of unexcavated tunnel sections using a probabilistic approach, thus serving as a supplement to geologic exploration and prospecting in planning and preliminary design stage. The proposed Q-based model is also useful in evaluating excavation support strategies as well as construction time and cost, providing decision support for the optimization of tunnel design and construction.

3.2 Introduction

Accurate prediction of rock mass conditions is a main focus in the underground construction and tunneling industry (Haas and Einstein, 2002). However, most subsurface rock mass conditions are not sufficiently known before construction. In general, rock mass conditions have been mostly evaluated for the worst-case scenario in traditional deterministic analyses, leading to biased conclusions since the inherent uncertainty of the rock mass conditions is not considered, resulting in serious construction delays and cost overruns of projects (Langford, 2013; Sousa and Einstein, 2012). In contrast, if this uncertainty is well modeled and analyzed before construction start, it can help significantly reduce risks as well as project costs, providing proper decision support for excavation-support strategies (Spackova, 2012).

Many geologic prediction techniques, such as geostatistical approaches and Markov models, have been developed to assess geological uncertainty in tunneling and underground construction (Chan, 1981; Chen et al., 2017; Ferrari et al., 2014; Ioannou, 1987; You and Lee, 2006). The Markov process approach is of particular interest because geological processes can be well addressed by the Markov process (Chan, 1981; Guan et al., 2012; Ioannou, 1987). Chan (1981) has shown that geological parameters can be probabilistically predicted using the Markov Chain technique. In addition, the Markov process approach has some advantages over semivariogram and autocovariance-based geostatistical methods because a Markov chain model can be implemented with limited data (less than ten boreholes) to simulate geological uncertainty, whereas variograms or autovariance functions require a great amount of data, e.g. more than tens of boreholes (Qi et al., 2016). Additionally, the transitional probability used in the Markov process approach can be geologically interpreted more easily than the variogram or autocovariance function, contributing to the popularity of the Markov model (Carle, 2000; Elfeki and Dekking, 2001; Elfeki and Dekking, 2005; Guan et al., 2012; Park et al., 2005; Ye and Khaleel, 2008). For these reasons, the Markov process has been widely used for geologic predictions in diverse fields in

geotechnical engineering (Bi et al., 2015; Elfeki and Dekking, 2001; Felletti and Beretta, 2009; Haas and Einstein, 2002; Min et al., 2008; Ruwanpura et al., 2004).

In the field of underground construction, the ground is often described behaviorally and allocated a ground class based on the field observations (Stille and Palmström, 2003). However, as a descriptive and behavioral system, the documentation of ground conditions in some ground classifications based on field observations does not seem to be very clear since the ground classifications rely largely on subjective observations (Palmstrom and Stille, 2007). The rock mass is subjectively classified without a numerical quality rating; in other words, the ground conditions are described qualitatively (Bieniawski, 1989). In addition, a limited number of geologic parameters and parameter states are generally used to characterize the ground conditions, which may lead to inadequate evaluation of the overall rock mass conditions. For instance, only two parameters (the N value in the standard penetration test and the percentage of clay content) were used to describe geologic classes (Leu and Adi, 2011), and only two fuzzy states (severe and not severe) were adopted to characterize weathering grades (Ioannou, 1987). Thus, the importance of some geological input parameters in ground classification seems to be ignored in current research and practice. Additionally, interdependency or correlation among geological input parameters in ground classifications is disregarded (Leu and Adi, 2011). Often, a ground classification is determined by several case-dependent geologic parameters based on a specific individual project. However, most of the aforementioned limitations of ground classification can be overcome using a probabilistic Q-system.

The Q-system — proposed by (Barton et al., 1974) in the Norwegian Geotechnical Institute (NGI) for the design of support in underground excavations — is a quantitative rock mass classification system. As an empirical method, the Q-system has been developed based and updated on a large number of case histories and updates of global tunneling projects and contains six parameters that are critical during underground construction (Hoek, 2007). Each input parameter of the Q-system has several states with different numerical values, which provides relatively complete descriptions of

ground conditions (Hoek, 2007); thus, the Q-system as a quantitative rock mass classification system has an advantage relative to the qualitative ground classifications. In the Q-system, the numerical Q value can be calculated with individual ratings assigned to each input parameter within its range according to the Q-equation (Barton et al., 1974). Consequently, sensitivity analyses can be performed by investigating the effect of each Q-parameter on the overall Q value by changing one parameter while keeping the other parameters constant. The correlation among the Q-parameters can be quantitatively characterized in the Q-equation. Furthermore, in the Q-based support chart, several rock classes and possible support patterns have been defined with extensive case histories and updates (Barton, 2002; Barton et al., 1974; Grimstad, 1993), and a support pattern can be determined from the obtained Q value. Empirical rock mass classification systems, including the rock mass rating (RMR), the Q-system and the geological strength index (GSI), have inherent uncertainties (Palmstrom and Stille, 2007; Palmstrom and Stille, 2010). However, it is possible to probabilistically characterize the uncertainties in the Q-system and to specify the excavation support strategies using the Q-based rock classes in a probabilistic way.

The Q-system is advantageous over the ground classification in quantitatively characterizing the rock mass conditions, which accounts for the inherent uncertainty involved. Thus, in this chapter, a Q-based prediction model for rock mass quality is proposed with the Markov process prediction approach by considering the uncertainties in the Q-system. We have demonstrated that the proposed Q-based prediction model is capable of the quantitative prediction of rock mass quality before tunnel excavations with a probabilistic method, providing useful information not only for assessing excavation support strategies but also for saving project time and cost in underground construction and tunneling.

3.3 Methodology

3.3.1 The Markovian prediction approach

Markov process and Markov chain

The Markov process refers to a stochastic process that has a Markov property, and the Markov chain is a special case of the Markov process with discrete states (Benjamin and Cornell, 2014). The Markov property, also named memoryless or single-step memory, denotes that the probability of the future states of the process depends only on the present state but not the past sequence of states (Benjamin and Cornell, 2014). Tunnel geology can be viewed as a random process, and each geological parameter follows a continuous-space and discrete-state Markov process (Chan, 1981; Ioannou, 1987). To be more specific, the spatial variability of geological parameters can be characterized by transitions in and out of their parameter states, each of which has an extent of persistence. Each particular geologic parameter is considered a scalar random process *X(t)* whose state probability is a function of the distance *t* from an arbitrary point, such as the tunnel portal (Chan, 1981; Ioannou, 1987). Thus, the Markov property, or the single-step memory, can be expressed in mathematical terms as follows:

$$P[X(t_{i+1}) = x_{i+1} \mid X(t_i) = x_i, X(t_{i-1}) = x_{i-1}, ...] = P[X(t_{i+1}) = x_{i+1} \mid X(t_i) = x_i] \quad (3.1)$$

where $x_{i+1}, x_i, x_{i-1}, ...$ are the outcomes of the random variables $X(t_{i+1}), X(t_i), X(t_{i-1}), ...$ at locations $t_{i+1}, t_i, t_{i-1}, ...$ $(t_{i+1} > t_i > t_{i-1} > ...)$ along the tunnel axis from the arbitrary origin, respectively.

Elements of the Markov process

The Markov process is defined by three elements: the transition probability, the transition intensity coefficient, and the interval transition probability of geological parameters, all of which can be estimated with general geologic information of the tunnel area (Chan, 1981; Ioannou, 1987). The transition intensity matrix *A* contains the transition intensity coefficient c_i and the transition probability P_{ij} and is useful in predicting the state probability of geological parameters.

$$A = [a_{ij}] \ \ i, j = 1, 2, ...n, \text{ where } a_{ij} = \begin{cases} -c_i & i = j \\ c_i P_{ij} & i \neq j \end{cases} \quad (3.2)$$

The parameter P_{ij} denotes the probability that the next state of a geological parameter is *j* given that the present state is *i*. It can be estimated as the ratio of the

number of transitions from the state *i* to the state *j* to the total number of transitions out of the state *i*. The transition intensity coefficient c_i has a physical meaning of the reciprocal of the extent of a geological parameter state, which indicates at what length the parameter state will persist before a transition to other states takes place.

Both P_{ij} and c_i can be estimated by statistical procedures if sufficient information is available in the tunnel area, including the geologic profile or the geologic map. If the amount of available data is limited in practice, subjective judgments are required from experienced experts who are familiar with the geology of the tunnel area. The Markov process is assumed to be homogeneous within some areas that have the same geologic history, in which the parameters P_{ij} and c_i are considered constant independent of location (Chan, 1981; Ioannou, 1987).

The interval transition probability matrix *V*, the matrix of the interval transition probability v_{ij}, is used to characterize the probabilistic behavior of the Markov process *X(t)* over several transition intervals. It can be expressed as follows:

$$V(t_0,t)=[v_{ij}(t_0,t)],\ v_{ij}(t_0,t)=v_{ij}(t-t_0)=P[X(t)=j\mid X(t_0)=i] \tag{3.3}$$

where $V(t_0,t)$ is the interval transition probability matrix, and $v_{ij}(t_0,t)$ is the interval transition probability, denoting that the probability of the Markov process *X(t)* will be in state *j* at location *t* given that the current state is *i* at location t_0.

The interval transition probability *V(u)* of a Markov process satisfies the forward Kolmogorov differential equation, and the solution can be written as follows:

$$V(u)=e^{uA}=I+uA+(1/2!)u^2A^2+\ldots+(1/m!)u^mA^m+\ldots \tag{3.4}$$

where *I* is the unit matrix and the distance $u=t-t_0$.

State probability interpolation of a geologic parameter between boreholes

When imperfect observations are made at location-specific boreholes, the states of the geological parameters can be described probabilistically. The state probability of a geologic parameter *X* at a location between two boreholes can be calculated as shown in Figure 3.1. The equation can be expressed as follows (Chan, 1981):

$$P[X(t)=j]=\sum_{m=1}^{n}P[X(t_{i-1})=m]\sum_{k=1}^{n}P[X(t_i)=k]\frac{v_{Xjk}(t_i-t)v_{Xmj}(t-t_{i-1})}{v_{Xmk}(t_i-t_{i-1})} \qquad (3.5)$$

where m and k are known states of the geologic parameter X at two observation locations (e.g. boreholes) t_{i-1} and t_i ($t_i > t_{i-1}$), respectively. The location t is an arbitrary unknown point between these two observation locations t_{i-1} and t_i, whose state of the parameter X is j.

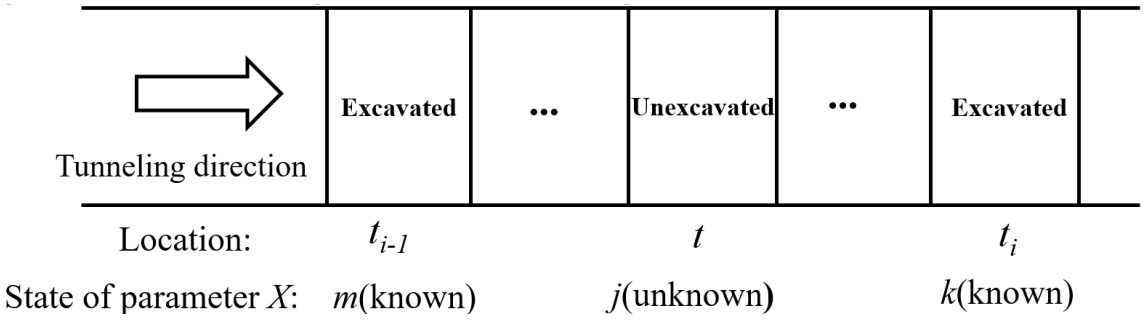

Figure 3.1 Interpolation of the parameter state probability at an unknown location.

As seen in Figure 3.1, the state probability of geologic parameter X at location t can be interpolated given the state probabilities at two observation locations t_{i-1} and t_i according to Eq. (3.5). The calculation procedure can also be similarly applied to the interpolation of cells between other adjacent boreholes. Thus, the probabilistic state profile of this geologic parameter could be calculated at any cells along the tunnel alignment. Analogously, the probabilistic profile of other parameters can also be obtained. By integrating these probabilistic profiles of all the parameters, the probabilistic profile of rock mass classification can be derived accordingly. More detailed explanations about the Markovian geological prediction approach are available in reference papers (Chan, 1981; Ioannou, 1987).

3.3.2 Probabilistic rock mass classification based on Q-system

In the Markovian geological prediction approach in Section 3.3.1, location-specific information (e.g., exploratory borehole data) can be incorporated to predict the state probability of geological parameters. The observation results of the geological parameter states can be nondeterministic, e.g. because of imperfect exploration. In the

Q-system, the likelihood matrix of Q-parameters using a particular exploration method (e.g., subsurface borehole and face logging) at a certain location can be defined as:

$$L_{jk}(t_b) = [l_{jk}(t_b)];\ \ l_{jk}(t_b) = P[Y(t_b) = k \mid X(t_b) = j] \qquad (3.6)$$

where $Y(t_b)$ is the observation result of a Q-parameter state at location t_b; $X(t_b)$ is the true state of a Q-parameter at location t_b; $l_{jk}(t_b)$ is the likelihood (or reliability) of the observation result k given that the true state of a Q-parameter is j at location t_b, and $L_{jk}(t_b)$ is the likelihood matrix of a Q-parameter at location t_b.

The likelihood matrix of each Q-parameter is estimated by on-site engineering geologists, which relies on the reliability of the exploration data or the experts' judgment. In practice, the likelihood matrix can vary due to the particular combination of exploration methods and geologic parameters. The likelihood matrix is also a function of location; however, for the purpose of simplicity, it is often assumed to be constant.

3.3.3 Implementation procedures of the proposed model

The implementation procedures of the proposed model can be described as follows:
(1) Adapt state definitions, descriptions and ratings of Q-parameters to an individual project.

The state definitions, descriptions and ratings of the Q-parameters have been modified from Barton (2002) to individual project characteristics to establish transition matrices of input parameters, as shown in Appendix A. For example, in cases where squeezing and swelling are not expected to occur, SRF states characterizing these two categorical features might not be included in the transition matrix for the parameter SRF.

(2) Estimate the transition probability P_{ij} and transition intensity coefficient c_i.

The transition probability P_{ij} and transition intensity coefficient c_i of each Q-parameter state are used to construct the transition matrix, which was the input for the Markovian prediction model. These parameters could be determined by the statistical frequency calculation if sufficient geologic data is available in the project area, by

subjective judgment from on-site engineering geologists based on limited available data or by a combination of both.

(3) Evaluate observation results and the likelihood of Q-parameters at particular locations.

The observed state of Q-parameters can be evaluated by experienced experts at particular locations. The likelihood of Q-parameter states, which reflects the experts' confidence level, can also be assessed by on-site engineering geologists.

(4) Interpolate the state probability of Q-parameters between particular observation locations.

Based on Eq. (3.5), the state probability of Q-parameters can be interpolated between two adjacent observation locations given the probabilistic descriptions obtained from Step (3) at these known observation locations. If we repeat this procedure to interpolate the state probability of the Q-parameters at all adjacent observation locations, then the probabilistic profile for Q-parameter states can be derived along the entire tunnel alignment.

(5) Integrate probabilities of Q-parameters to obtain the probability distribution of the Q value.

Based on the Q-equation in Eq. (2.1), if we integrate the state probabilities of all Q-parameters using the MCS technique at arbitrary locations, the probability distribution of the Q value can be obtained. If we repeat this procedure at other locations along the alignment, the probability distribution of the Q value can be generated along the tunnel axis.

3.3.4 Application to a case study

A water tunnel in western Canada, was selected for application of the proposed Q-based prediction model. The tunnel is 7.2 km in length and located predominantly within quartz diorite and granodiorite, with overburden varying from 185 m to 650 m. It was excavated by an open-type hard rock tunneling boring machine with the diameter of 3.8 m. The geological profile map is shown in Figure 3.2. In this case study, a tunnel section with relatively homogeneous ground condition in quartz diorite formation with

1000 m length (from Chainage +1610 to +2610 m) was selected. The layout of the tunnel section is illustrated in Figure 3.3. Actually, the entire tunnel section in Figure 3.3 has been excavated and the tunnel mapping data has been recorded. Due to the limited availability of site investigation borehole data in this section, mapping data collected during tunnel construction have been used for implementation and validation of the proposed model. In this study, as can be seen in Figure 3.3, this section was divided into two subsections: Subsection 1 with 400 m in length from Chainage +1610 to +2010 m and Subsection 2 with about 600 m length from Chainage +2010 to + 2610 m. Subsection 1 has been excavated and known exactly while Subsection 2 was assumed to be unknown except for 13 observation cells (OCs).

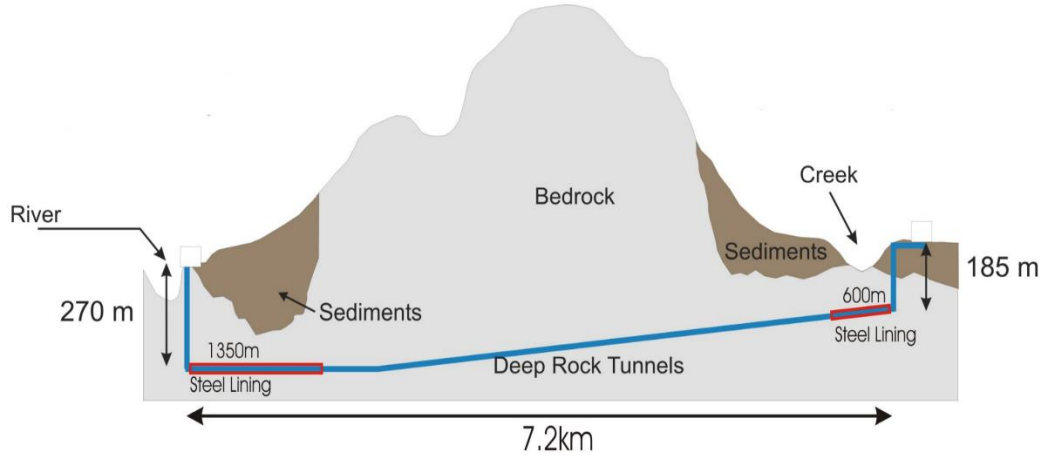

Figure 3.2 Geological profile of the tunnel project.

Due to the stationarity of rock mass conditions in the entire tunnel section, the transition intensity matrices of Q-parameters can be treated as constant. Thus, the actually recorded data set of the Q-system in Subsection 1 with 400 m in length was used as input for establishing the transition matrix of the prediction model, while Subsection 2 was used for testing the prediction performance by comparing the predicted Q-results with the actually recorded ones in Subsection 2. In practice, the Q-log mapping was performed every 5 m during construction in this tunnel section, and a single numerical value was assigned to each Q-parameter and the overall Q value. For the convenience of comparison between predicted and actually recorded Q results, Subsection 2 was subdivided into cells with 5 m length for each cell. The total length

of Subsection 2 is 605 m and thus 121 cells are obtained with 13 OCs. The OC 1 is at Chainage +2010~2015 m, which is the starting cell in Subsection 2. This cell was considered as the reference starting point for the subsequent prediction. In other words, OC 1 is the starting Cell 1 while OC 13 is Cell 61 in Subsection 2.

To investigate the effects of the input data, i.e. Q data in Subsection 1, on the prediction performance, two additional scenarios, including the Subsection 1 with 200 m (Chainage +1610~1810 m) and 300 m (Chainage +1610~1910 m), have also been conducted. The Subsection 2 with 600 m (Chainage +2010~2610) is used as the test subsection to verify the prediction performance with input data obtained from Subsection 1 with different length (200 m, 300 m and 400 m). The following section in this chapter focuses on the results derived from the scenario with Subsection 1 of 400 m. The main results for the other two scenarios with Subsection 1 of 200 m and 300 m are listed in Appendix D.

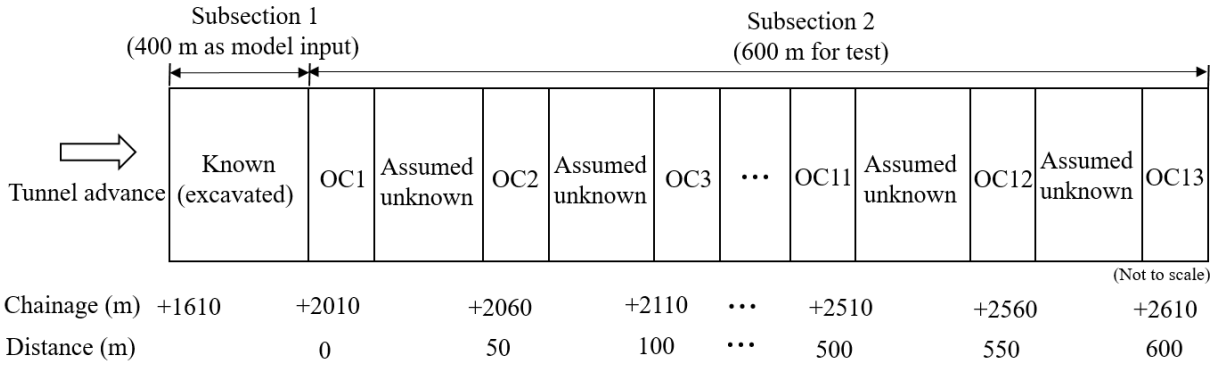

Note: The tunnel section is in homogeneous quartz diorite, and has been excavated and known; Subsection 1 for constructing prediction model, Subsection 2 for testing prediction performance; OC1-13 are observation cells with actually mapped data, and each cell is 5 m in length.

Figure 3.3 Layout of observation cells in this tunnel section.

3.4 Results and discussion

3.4.1 Probabilistic profiles of Q-system

Probabilistic Profile of States of Q-parameters

The state definitions, descriptions and ratings for Q-parameters in this case study are shown in Appendix A. Note that SRF states for squeezing and swelling rocks are not included in Appendix A since these scenarios are not expected to be encountered

in the case study. The transition intensity matrices of Q-parameters were calculated based on state transition frequency calculations of Q-parameters in Subsection 1, as shown in Appendix B. The observed states for Q-parameters at observation cells are shown in Table 3.1. The likelihood matrices for Q-parameters are demonstrated in Appendix C. Combining the observed states at observation cells and the likelihood of Q-parameter states, the imperfect observation results are described probabilistically at these observation cells. Since the states for Q-parameters are discrete, the occurrence probabilities of states for Q-parameters are, in fact, in form of probability mass functions (PMFs). Based on the transition intensity matrices of Q-parameters and the probabilistic descriptions of Q-parameter states at these observation cells, the probabilistic state profile for each Q-parameter was predicted along the tunnel axis. This calculation process in the prediction model was coded and performed using MATLAB sotfware based on Eq. (3.5). The obtained probabilistic state profiles of Q-parameters (RQD, J_n, J_r, J_a, J_w and SRF) are shown in Figure 3.4, respectively. As seen in Figure 3.4, greater variations in parameters J_n and RQD were observed while the predicted probability profiles for other Q-parameters (J_r, J_a, J_w and SRF) in Subsection 2 are more stable.

Table 3.1 Observation cell locations and observed states.

No. of cell	Chainage (m)	Distance (m)	Observed states					
			RQD	J_n	J_r	J_a	J_w	SRF
1	2010	0	4	5	4	3	1	5
2	2060	50	3	5	4	3	1	5
3	2110	100	3	5	4	3	1	5
4	2160	150	3	5	4	3	1	5
5	2210	200	3	5	4	3	1	5
6	2260	250	4	3	4	3	1	5
7	2310	300	4	5	4	3	1	5
8	2360	350	4	3	4	3	1	5
9	2410	400	4	5	5	3	1	5
10	2460	450	4	4	4	2	1	5
11	2510	500	4	3	4	3	1	5
12	2560	550	4	3	4	3	1	5
13	2610	600	4	3	4	3	1	5

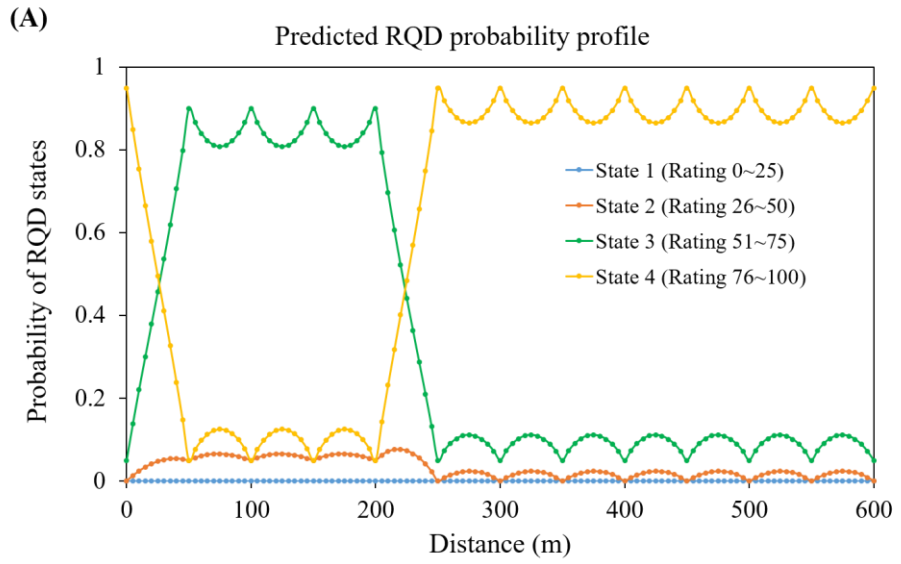
(A)
Predicted RQD probability profile
Probability of RQD states
Distance (m)
State 1 (Rating 0~25)
State 2 (Rating 26~50)
State 3 (Rating 51~75)
State 4 (Rating 76~100)

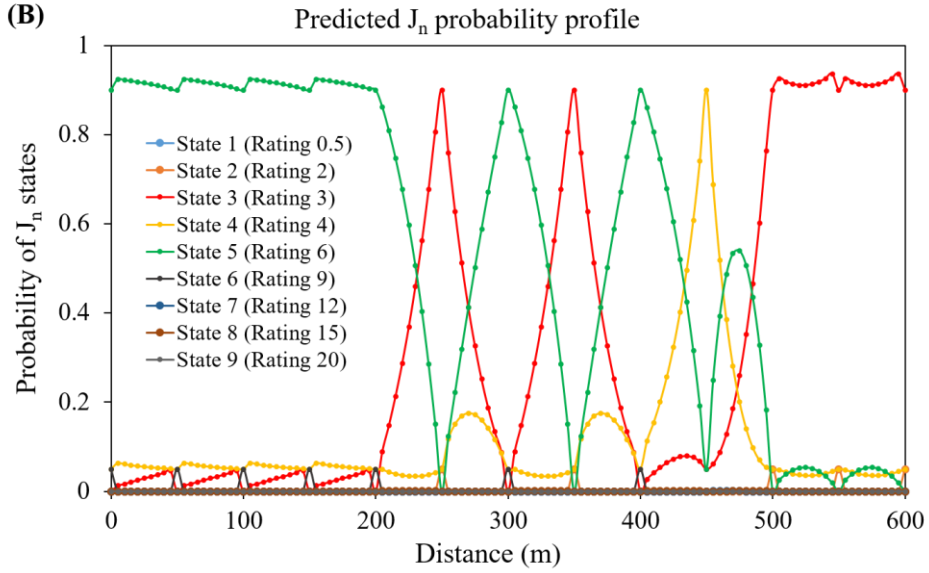
(B)
Predicted J_n probability profile
Probability of J_n states
Distance (m)
State 1 (Rating 0.5)
State 2 (Rating 2)
State 3 (Rating 3)
State 4 (Rating 4)
State 5 (Rating 6)
State 6 (Rating 9)
State 7 (Rating 12)
State 8 (Rating 15)
State 9 (Rating 20)

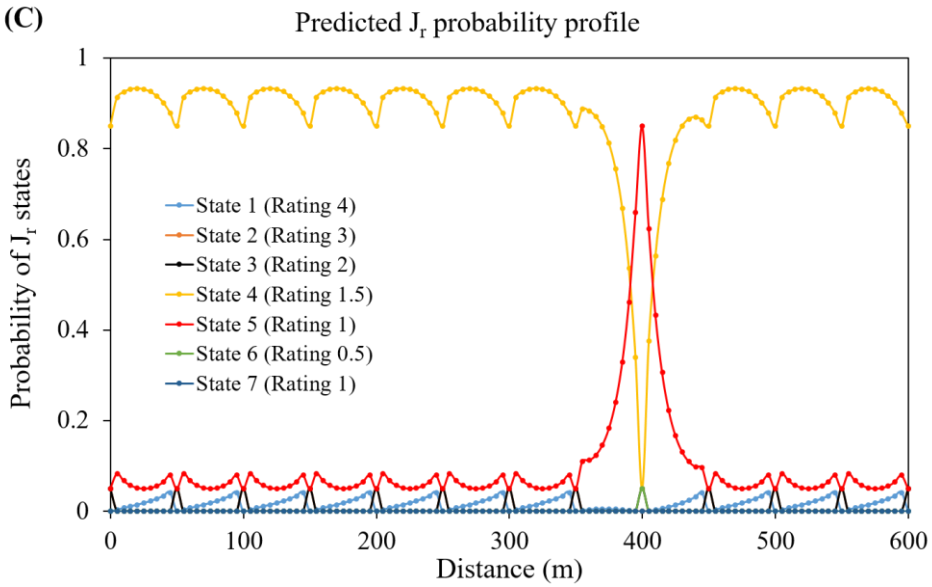
(C)
Predicted J_r probability profile
Probability of J_r states
Distance (m)
State 1 (Rating 4)
State 2 (Rating 3)
State 3 (Rating 2)
State 4 (Rating 1.5)
State 5 (Rating 1)
State 6 (Rating 0.5)
State 7 (Rating 1)

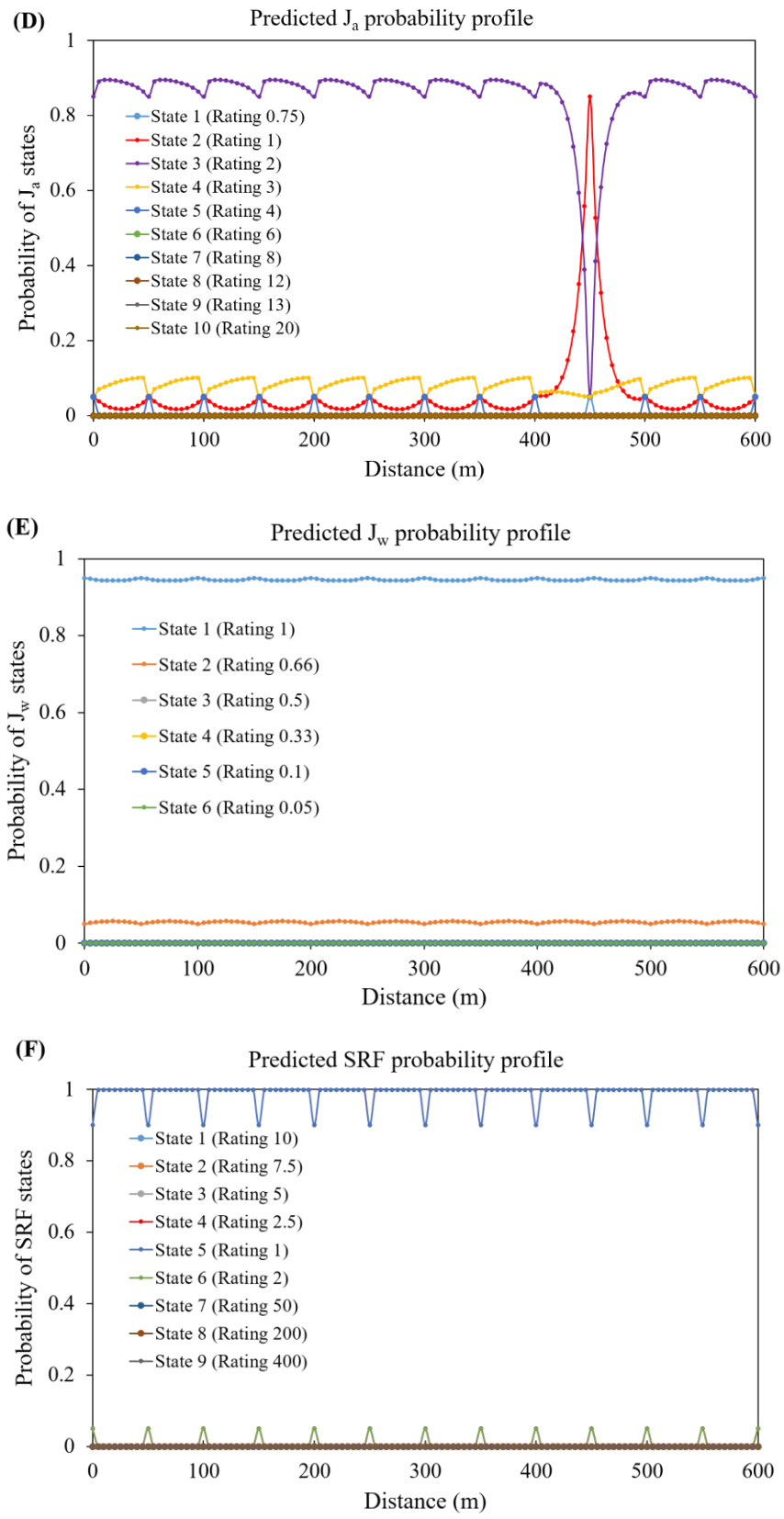

Figure 3.4 Predicted probabilistic state profiles of Q-parameters in Subsection 2: (A) RQD; (B) J_n; (C) J_r; (D) J_a; (E) J_w; (F) SRF

Probabilistic distribution of Q value

As the PMF of Q-parameter states has been obtained, the resultant PDF of the overall Q value can be calculated using the MCS technique according to Eq. (2.1). In this case study, the MCS simulation was carried out with 10,000 iterations using the @RISK software. Figure 3.5 illustrates an example of the obtained PDF and cumulative distribution function (CDF) of the Q value at OC 3 (distance 100-105 m). Results also shows that lognormal distribution is the best fit for the simulated distribution based on the Bayesian Information Criterion (BIC). The BIC is calculated from the log-likelihood function and takes into account the number of parameters of the fitted distribution, and it is recommended for the distribution fit (Palisade Corporation, 2016). The comparison of statistics for the Q value between the simulated distribution and fitted lognormal distribution is also shown in Figure 3.5. Analogously, the statistical distribution of the Q value can also be derived at other cells, and thereby the probabilistic distribution of Q value can be obtained at any locations along the tunnel alignment.

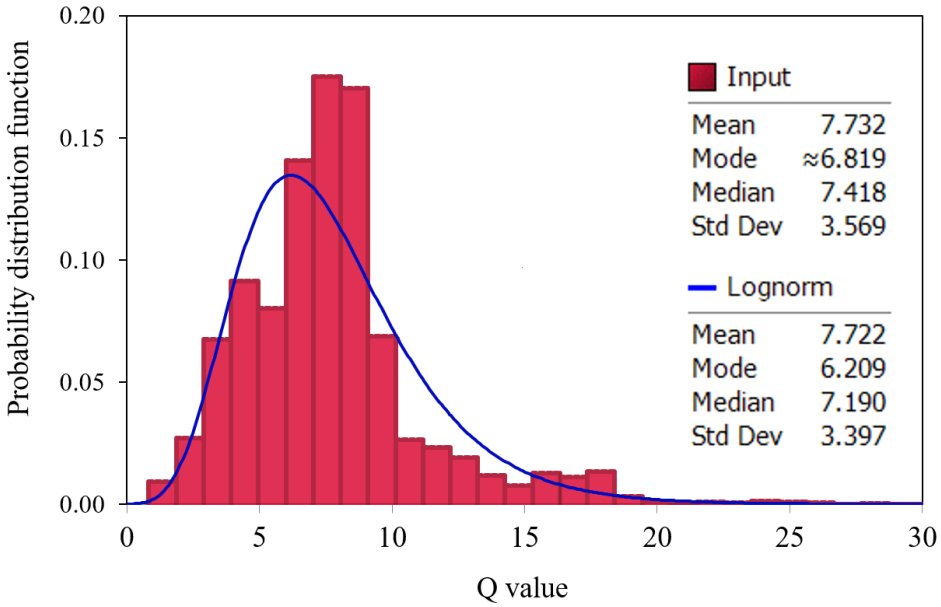

Figure 3.5 An example of the statistical distribution of MCS-simulated Q value at OC 3 (distance 100-105 m).

Probabilistic Profile of Q-based rock class

Given the statistical distribution of Q value, as shown in Figure 3.5, the relative percentage of Q-based rock class (RC) can be obtained at that cell. According to the Q-based rock mass classification (Barton et al. 1974), RC 1–3 herein represent "good" rock, "fair" rock and "poor" rock with Q values in the ranges of 10–40, 4–10, 1–4, respectively. The probability profile of Q-based rock classes has been obtained along the tunnel section, as illustrated in Figure 3.6. At the beginning of Subsection 2, the leading rock class is RC1 with "good" rock for about 20 m before its transition to RC2 with "fair" rock. The RC2 dominates for about 200 m before its transition to RC1 at the distance about 220 m, consistent with the changes of RQD and J_n to better quality rock mass. After that, RC1 is mostly likely again for the remaining 380 m except locally where RC2 is most likely at the distance of 400 m.

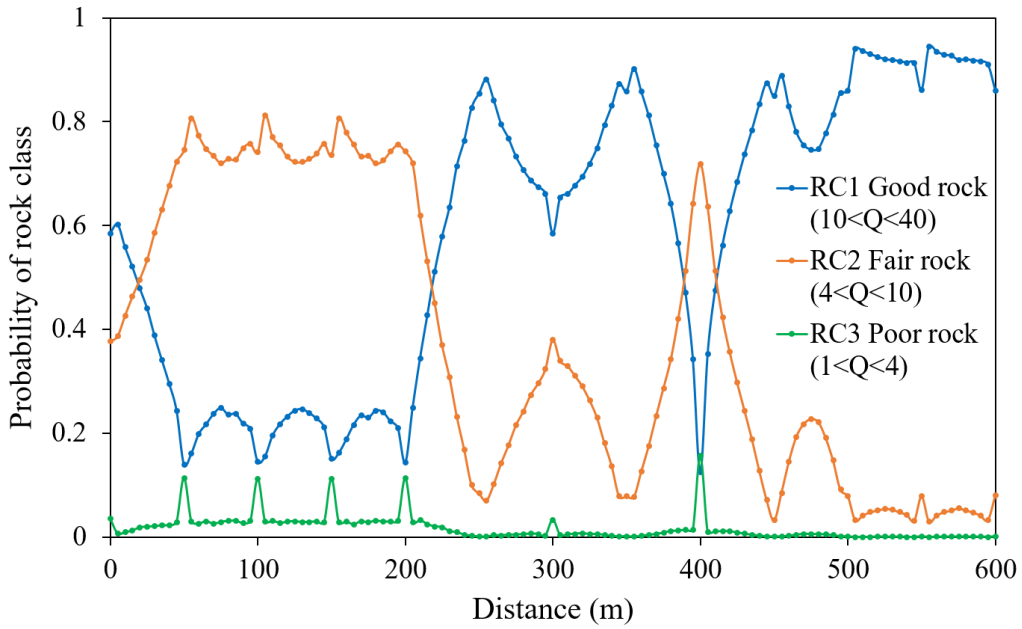

Figure 3.6 Predicted probability profile of Q-based rock classes in Subsection 2.

3.4.2 Comparison between predicted results and field observations

The Q-log mapping data has been actually collected during construction, and this type of data set was used to compare with predicted results of the Q value for the validation of the proposed prediction model. Since the ratings for each Q-parameter and the overall Q value were recorded in each cell during tunnel mapping, the validation

can be performed by comparing predicted Q-parameter states, Q values and Q-based rock classes with those actually collected during tunnel construction.

Comparison criterion of Q-parameter states

To test predicted results of Q-parameter states, the accuracy plot has been used. In the accuracy plot for predicted Q-parameter states, the horizontal axis indicates the probability interval of predicted mostly likely outcome for each Q-parameter, which can be obtained in Figure 3.4. The vertical axis means the proportion of the actually recorded results in this interval in all cells of the Subsection 2. A perfect prediction corresponds to the 1:1 line in the accuracy plot. Figure 3.7 and Figure 3.8 illustrate the accuracy plots for the predicted RQD and J_n in Subsection 2, respectively. The probability interval is in unit of 10% in this case. Take the accuracy plot of RQD as an example, in the interval of 0.8~0.9, the middle value of 0.85 is used. The number of cells in which the predicted modal probabilities are in this interval of 0.8~0.9 is 79 in Subsection, as obtained in the predicted probability profile of RQD in Figure 3.4. Based on the actually recorded RQD states in Subsection 2, there are 66 out of 79 cells where the predicted modal outcomes correspond to the actually mapped states, giving the proportion of true states about 84% in this interval of 0.8~0.9. The calculated proportion value in certain probability interval reflects the actual prediction correctness in this probability interval. Similarly, the proportion values in other probability intervals for the predicted RQD and for other Q-parameters were also derived and the accuracy plots have been obtained for Q-parameters.

The measures of prediction accuracy, including the RMSE (Root Mean Square Error) and R^2 (coefficient of determination), have also been derived in the accuracy plots. It can be seen in Figure 3.7 and Figure 3.8 that R^2 values for both predicted RQD and J_n are above 0.8 and RMSE values are around 0.1, indicating the relatively good prediction performance. As can be seen in Figure 3.4, there are greater variations in the predicted probability profiles for RQD and J_n while a certain state is dominant in the majority of Subsection 2 for other Q-parameters (J_r, J_a, J_w and SRF). Actually recorded results also reveal that the mapped state results for RQD and J_n are more variable than

other Q-parameters in Subsection 2. The dominance of a certain state for other Q-parameters (J_r, J_a, J_w and SRF) is also observed in the actually recorded data during tunnel mapping, indicating the relatively high prediction accuracy for these parameters. Thus, the prediction accuracy of the proposed prediction model is relatively high based on the comparison criterion of Q-parameter states.

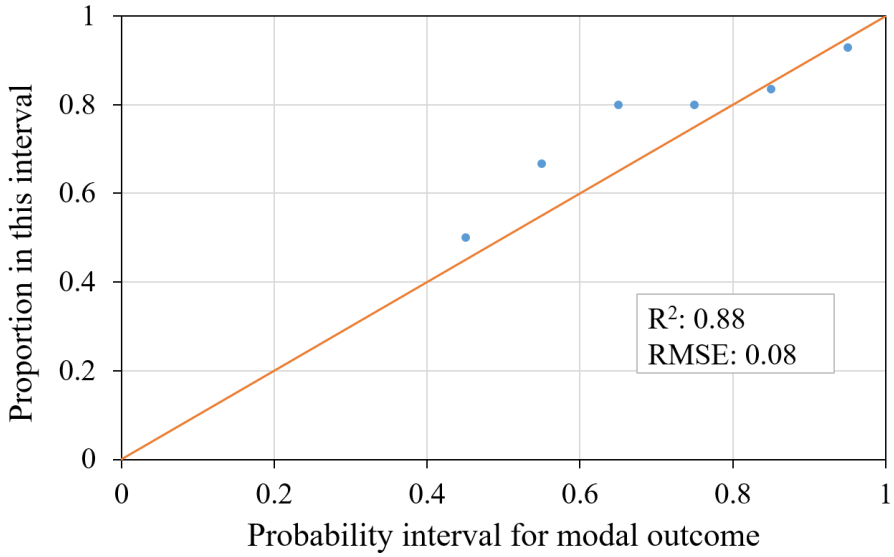

Figure 3.7 Accuracy plot for predicted RQD

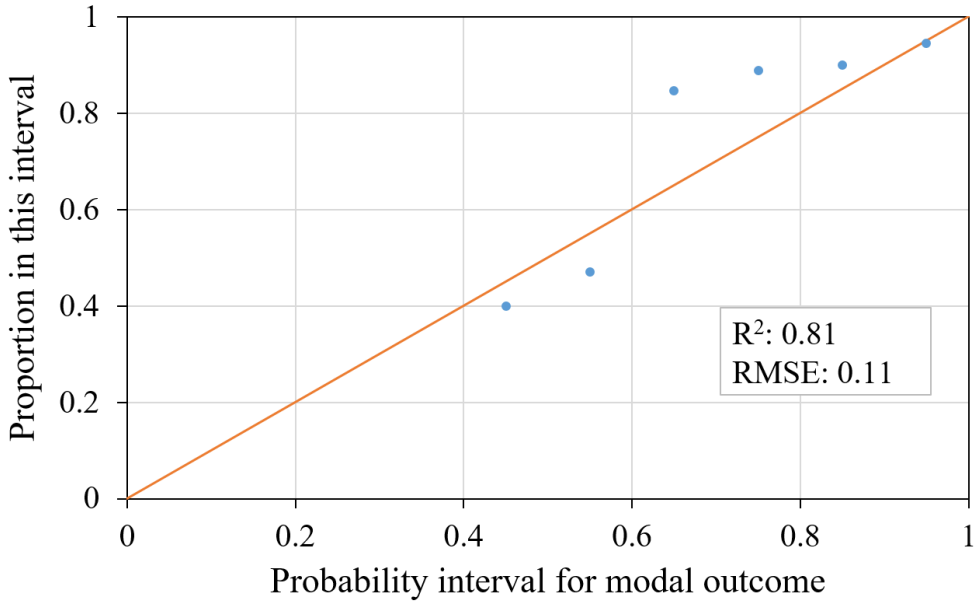

Figure 3.8 Accuracy plot for predicted J_n

Comparison criterion of the Q value

Different to the Q-parameters that are categorical variables, the Q-value is a continuous variable, and the accuracy plot has been made using the symmetric intervals

centered on the cumulative distribution function median (Goovaerts, 2001). A series of symmetric *p*-probability intervals (percentiles 0.1 to 1.0 in increments of 0.1) bounded by the (1-*p*)/2 and (1+*p*)/2 are used to construct the accuracy plot (Goovaerts, 2001). An indicator function is used to assign a value of 1 if the true value falls within the probability interval in a test location and 0 if the true values falls outside of the probability interval. For example, if the *p*-probability is 0.5, the corresponding probability interval is 0.25~0.75. The number of true Q values falling within the 0.5-probability interval of the Q value, i.e. 0.25~0.75, can be calculated at each cell in Subsection 2, and the proportion of true Q values in this probability interval can accordingly derived. For a prediction model with high prediction accuracy, the proportion in the probability interval should be close to the *p* in the accuracy plot.

The accuracy plot for the predicted Q value is shown in Figure 3.9. The derived accuracy plot is very close the 1:1 line. The obtained R^2 is at a very high value of 0.99 and the calculated RMSE is as low as 0.04. This indicates that the prediction accuracy is very high for the proposed prediction model based on the comparison criterion of the Q value.

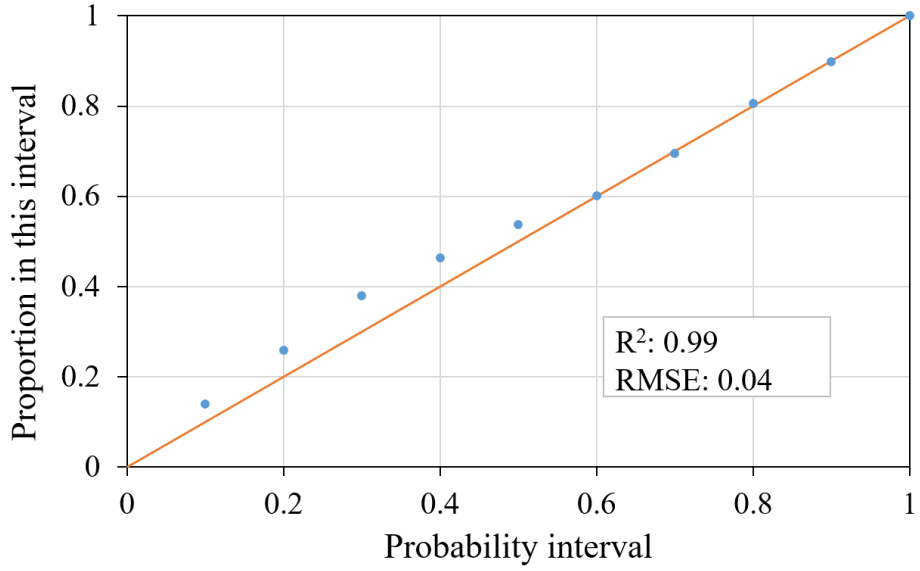

Figure 3.9 Accuracy plot for predicted Q value

Comparison criterion of Q-based rock class

As with Q-parameters, the accuracy plot for the Q-based rock class has also been obtained by comparing the predicted probability interval for modal outcome with the proportion of true states in that interval, as shown in Figure 3.10. The obtained R^2 value is 0.92 and RMSE value is 0.07, indicating the relatively high prediction accuracy of the proposed prediction model based on the comparison criterion of Q-based rock class.

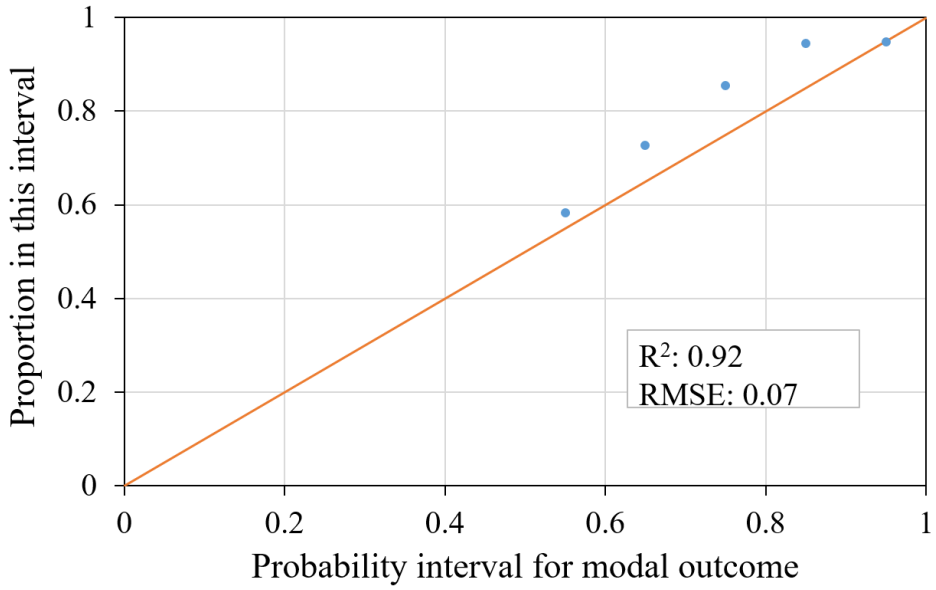

Figure 3.10 Accuracy plot for predicted Q-based rock class

In addition, the accuracy plots for individual rock class have also been made. As can be seen in Figure 3.6, GC1 with "good" rock and GC2 with "fair" rock are dominant in Subsection 2, and the accuracy plots have been generated for these two dominant rock classes. Figure 3.11 illustrates the accuracy plots for GC1 and GC2, respectively. Both plots reveal the relatively high prediction accuracy for individual rock class, which agrees well with that derived from the accuracy plot for the predicted overall Q-based rock class shown in Figure 3.10.

Discussion on the validation of the proposed prediction model

The proposed Q-based prediction model has been validated by comparing predicted Q-parameter states, Q values and Q-based rock classes with observed values. By contrast, with regard to the ground classification-based prediction model, the model validation was carried out by comparing the predicted ground class that had the maximum

probability with the real on-site ground class (Guan et al., 2014; Guan et al., 2012; Leu and Adi, 2011). For commonly used rock mass classification systems, comparisons between the predicted and actual rock class, based on RMR and Q-system, have been used to test the accuracy of the rock mass classification prediction model (Panthi and Nilsen, 2007; Ravnjak et al., 2014). However, these validation processes were based on comparisons of overall rock mass quality described by the ground class, RMR or Q-

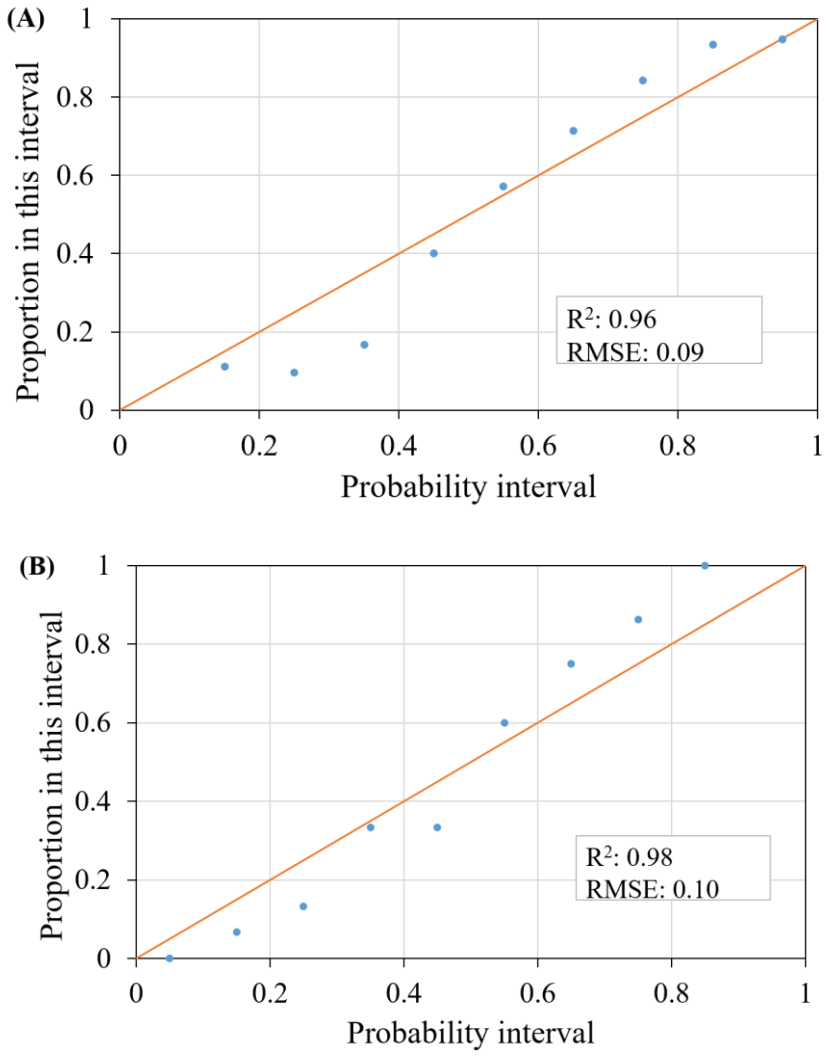

Figure 3.11 Accuracy plot for predicted ground classes: (A) GC1; (B) GC2

based rock class. As the Q-system is a quantitative rock mass classification with numerical ratings for each input parameter, the prediction model can also be validated by comparing its input parameter states and the overall Q values between the predicted and actual recorded results in addition to the comparison of rock classes. Thus, the

proposed Q-based prediction model, in this study, provides a means in a more comprehensive way to compare the predicted and actual results for validation purpose.

In addition, the probabilistic prediction results have been evaluated in a probabilistic framework using the accuracy plot. In the ground class-based prediction model proposed by (Guan et al., 2014; Guan et al., 2012; Leu and Adi, 2011), the probabilistic predictions of ground class or geology class were directly compared to deterministic ground-truth data. If the predicted dominant ground class matches the actual one at one location, then the prediction is considered accurate at that location. In other words, the probabilistic predictions were evaluated in a deterministic way and the uncertainties in the predicted probabilistic model are not explicitly quantified. The accuracy plot used in this study can address this issue, and characterize the uncertainties and prediction accuracy of the proposed probabilistic prediction in a probabilistic way.

3.4.3 Sensitivity analysis

Different sensitivity analysis techniques can be used to determine the sensitivity of the output parameter to its input parameters, including one at a time sensitivity analysis, differential sensitivity analysis, factorial design, importance factors and the sensitivity index (Hamby 1994). Probabilistic sensitivity analysis can be performed in the MCS process to determine the relative importance of input parameters in the Q-system using the @RISK software. The tornado graphs generated from the MCS process show the ranking of relative importance of the input distributions. Input parameters that have the longest bars in the graph indicate that input distribution has greatest impact on the output distribution.

Sensitivity analysis at one cell

Figure 3.12 illustrates the relative importance for Q-parameters in OC 3 in tornado graphs ranked by 4 different criteria: i.e. the effect on output mean, the regression coefficient, the Spearman correlation coefficient and the contribution to output variance, respectively. As seen in Figure 3.12, the rank of relative importance for Q-parameters is different based on different ranking techniques. However, all the tornado graphs indicate, in general, J_r, J_a and RQD are the most influential input

parameters while J_n, SRF and J_w are less significant. This is related to the state probability assigned for each Q-parameter in OC 3.

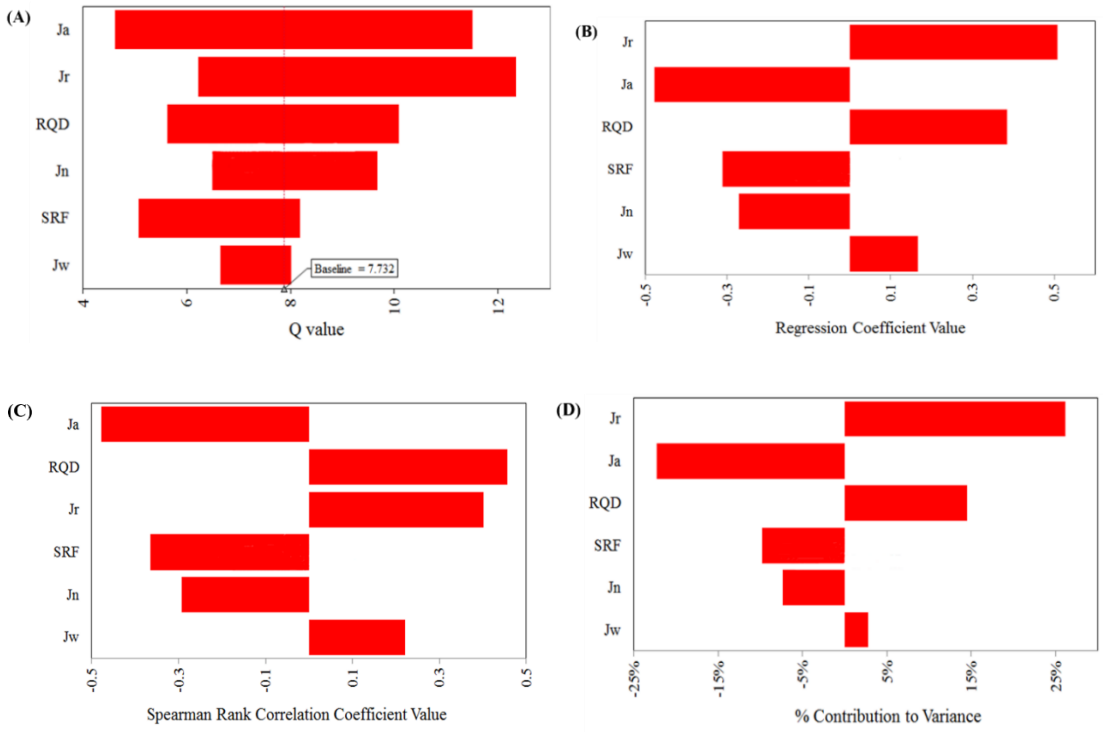

Figure 3.12 Rank of relative importance of Q-parameters at OC 3. (A) ranked by effect on output mean; (B) ranked by regression coefficient; (C) ranked by Spearman correlation coefficient; (D) ranked by contribution to variance

Sensitivity analysis in Subsection 2

The Q-parameter logging data has been collected during tunnel construction, and the relative frequency histograms for these Q-parameters can be obtained in Subsection 2, as shown in Figure 3.16. The distribution of the Q value can also be derived using the MCS technique based on statistical distributions of actually recorded Q-parameter data based on the Q-equation Eq. (2.1). Figure 3.14 shows the obtained distribution of Monte Carlo-simulated Q value and its best fit in Subsection 2. The distribution of simulated Q value is also well described by a lognormal distribution. On the other hand, the statistical distribution of the actually recorded Q value data during construction is also obtained in Subsection 2, as shown in Figure 3.15. By comparing Figure 3.14 and Figure 3.15, it is seen that statistics of MCS-derived Q value (mean of 12.96, standard deviation of 6.78) are close to those of the actually recorded Q values (mean of 13.34,

standard deviation of 7.10), indicating the effectiveness of the MCS technique in characterizing uncertainty propagation from input parameters to the output. In addition, the relative percentage of Q-based rock class was also compared for simulated and actually recorded results, as illustrated in Figure 3.16. In general, the simulated and actually recorded Q-based rock class results agree well with each other. It is also found that "good" and "fair" rocks are dominant, covering more than 95% in total, for both simulated and actually recorded Q-based rock classes. Thus, the MCS-derived rock class percentage can also provide preliminary estimation of the overall rock mass quality in the tunnel section before excavation.

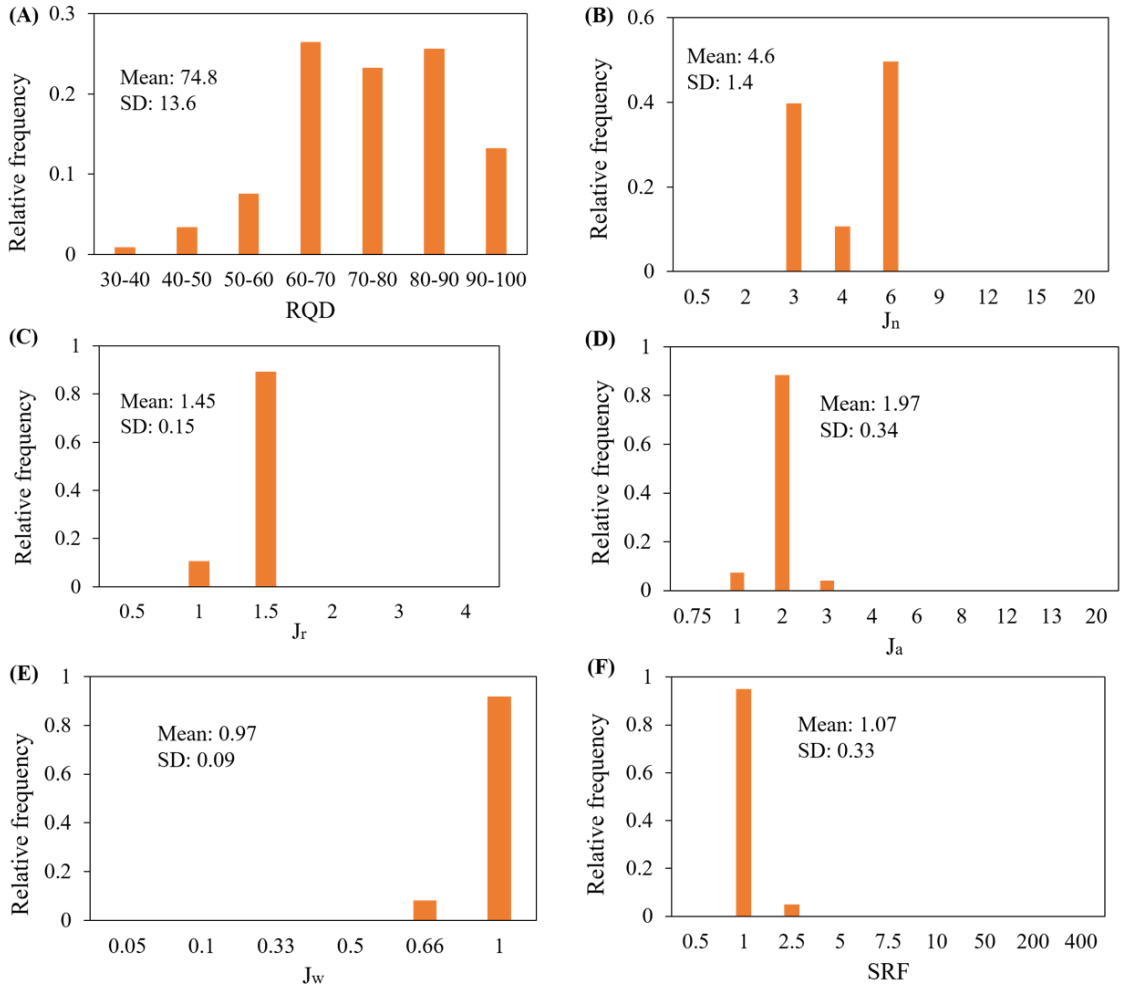

Figure 3.13 Relative frequency histogram collected in Subsection 2: (A) RQD; (B) J_n; (C) J_r; (D) J_a; (E) J_w; (F) SRF

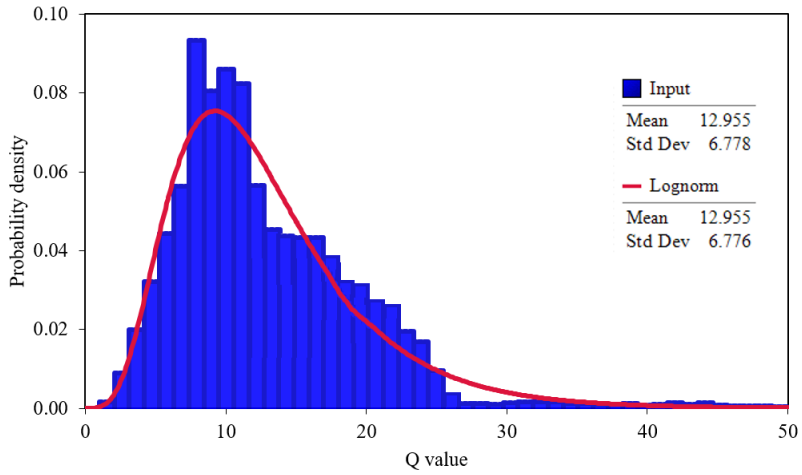

Figure 3.14 Statistical distribution of MCS-derived Q value in Subsection 2.

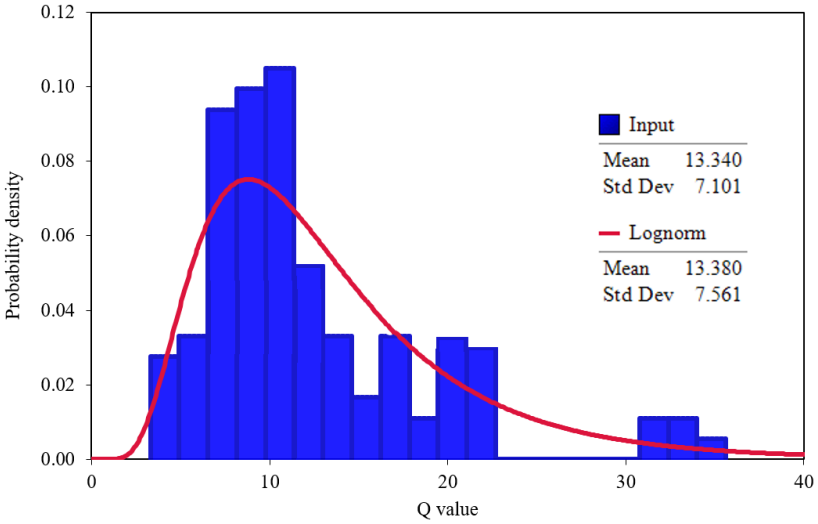

Figure 3.15 Statistical distribution of actually recorded Q value in Subsection 2.

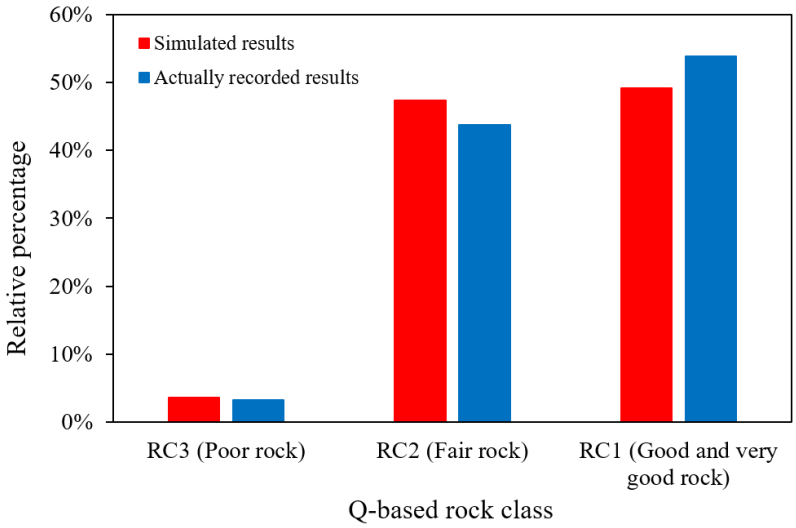

Figure 3.16 Comparison of rock class distribution between simulated and actual results in Subsection 2.

Sensitivity analysis has also been carried out on the statistical distribution of Monte Carlo simulated Q value in Subsection 2. Figure 3.17 depicts the tornado graphs displaying the rank of relative importance for Q-parameters in Subsection 2. The sensitivity analysis results show that J_n, RQD and J_a are more significant than other input parameters in this case study. Parameters J_n and RQD are most influential, indicating greater uncertainties in distributions of these two input parameters, and this also corresponds to the observed greater variations in the predicted probabilistic profile of these two parameters in Figure 3.4. As can be seen in Figure 3.13, the histograms for RQD and J_n are more dispersed than other Q-parameters, indicating greater variabilities. Note that the more importance of the RQD and J_n in the sensitivity results is valid in this case study of the water tunnel project. The rank of relative importance for Q-parameters can be different based on individual characteristics for different projects. However, the sensitivity analysis in the MCS process provides a feasible method to examine the impact of uncertainties in input distributions on the output Q value based on different ranking criteria in a probabilistic way.

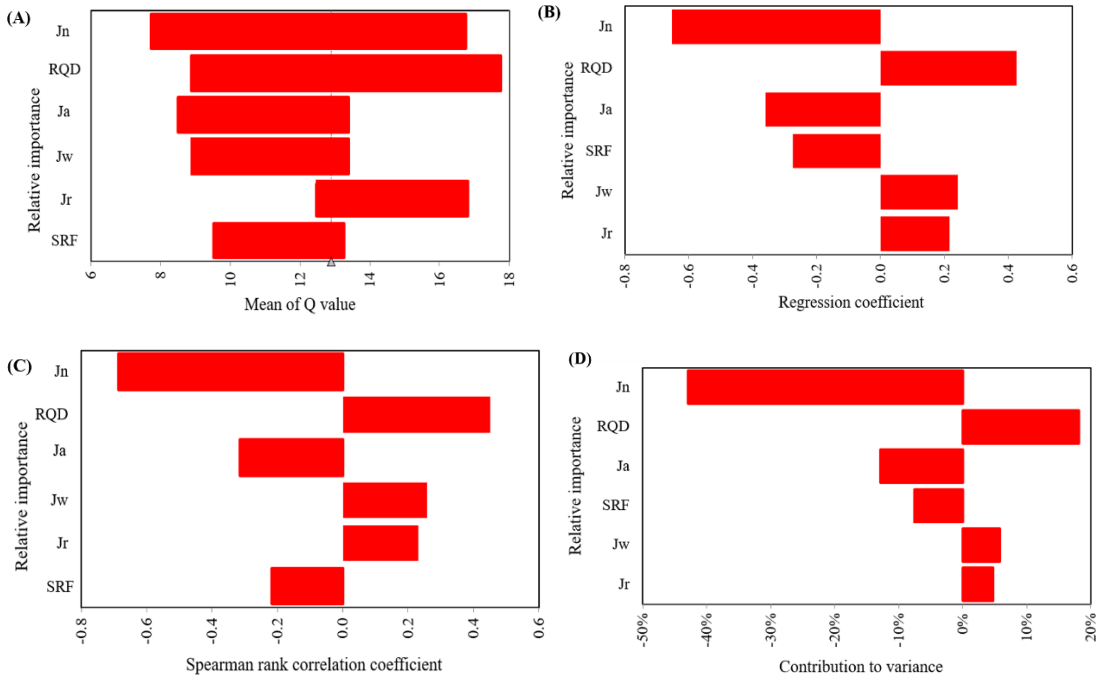

Figure 3.17 Rank of relative importance of Q-parameters in Subsection 2: (A) ranked by effect on output mean; (B) ranked by regression coefficient; (C) ranked by Spearman correlation efficient; (D) ranked by contribution to variance

3.4.4 Analytical calculation approach to deriving statistics of Q value

Analytical approximation on statistics of Q value

The statistics of a product of several input parameters, including the mean, standard deviation and coefficient of variation (COV), can be approximated using Taylor expansions given those statistics of input parameters (Elandt-Johnson and Johnson, 1980). Since the Q value is the product of three quotients as shown in the Q-equation in Eq. (2.1), statistics of the Q value can be accordingly calculated given statistics of Q-parameters. In this section, an analytical approximate calculation approach to deriving statistics of the Q value is proposed accounting for the uncertainties in Q-parameters, and the derivation procedures are shown in Appendix E in detail. It should be noted that for the derivation COV of Q value, it can either be calculated as the ratio of standard deviation to the mean of obtained Q value by definition, or derived through the COV of Q-parameters. For the simplicity of calculation, all the Q-parameters are assumed to be independent in this derivation process.

Comparison between analytical and simulated Q value

The relative frequency histogram for each Q-parameter has been obtained at each cell in the tunnel section, and statistics for each Q-parameter has also been obtained using the @RISK software. Given the statistics of Q-parameters, the statistics of the Q value can be approximated using the developed analytical calculation approach. Table 3.2 compares statistics of the Q value among analytical, Monte Carlo-simulated and actually recorded results in OC 3 and Subsection 2, respectively. The Q-equation approach in the analytical solution is also included, in which the mean of Q value was calculated directly based on the Q-equation in Eq. (2.1) with the mean of each Q-parameter as the only input. In this Q-equation approach, only the mean value rather than the standard deviation and COV of the Q value is calculated since the dispersion (e.g. SD and COV) of Q-parameters is not considered. In contrast, in the proposed calculation approach, the standard deviation and COV of Q-parameters are taken into

account, and statistics (mean, SD and COV) of the Q value have also been derived accordingly.

Table 3.2 Comparison of Q statistics among analytical, simulated and actual results.

Area	Solutions		Statistics of the Q value			
			Mean	SD	COV	
					Calculated by definition	Calculated through COV of Q-parameters
Subsection 2	Analytical solution	Q-equation approach	10.71	N/A	N/A	
		Proposed calculation approach	13.21	6.64	0.50	0.51
	MCS solution	2,000 iterations	12.93	6.71	0.52	
		5,000 iterations	12.94	6.74	0.52	
		10,000 iterations	12.95	6.77	0.52	
		20,000 iterations	12.95	6.78	0.52	
		30,000 iterations	12.99	6.84	0.53	
	Actually recorded Q value		13.34	7.10	0.53	
OC 3 (distance 100~105 m)	Analytical solution	Q-equation approach	7.04	N/A	N/A	
		Proposed calculation approach	8.20	3.96	0.48	0.55
	MCS solution	3,000 iterations	7.73	3.57	0.46	
		5,000 iterations	7.74	3.59	0.46	
		10,000 iterations	7.74	3.60	0.46	
		20,000 iterations	7.74	3.61	0.47	
		30,000 iterations	7.75	3.65	0.47	
	Actually recorded Q value		8.75	N/A	N/A	

Note that only a single value was given for the rating of the Q value during tunnel mapping at OC 3, thus the standard deviation and COV are not applicable for actually recorded results at OC 3. As can be seen in Table 3.2, the analytical, MCS-

simulated and actually recorded results in terms of the mean, standard deviation and COV of the Q value are, in general, close in both OC 3 and Subsection 2. The generated statistics in analytical and simulated solutions are smaller than that in actually recorded results, but the differences are insignificant. With regard to the analytical solution, the obtained mean value in the proposed calculation approach (13.21) is closer to the recorded value (13.34) than that derived from the Q-equation approach (10.71) in Subsection 2. In addition, the measure of variations (SD and COV) for the estimated Q value can also be obtained in the proposed calculation approach, as shown in Table 3.2. In terms of the MCS solution, it is seen that greater mean and dispersion of the Q value are obtained with increased iterations. However, the differences are also limited, meaning the effect of iteration runs on simulated results is insignificant in this case study.

As mentioned above, the results derived from the proposed calculation approach were close to MCS-simulated and actually recorded results in OC 3. This analytical approximation procedures can also be performed at other cells in Subsection 2. The analytical approximation process has been carried out at all cells in Subsection 2.

Figure 3.18 shows the comparison of derived mean and standard deviation of Q values between analytical and simulated results (3,000 iterations) in Subsection 2. The comparison of COV for Q values is illustrated in Figure 3.19. It is shown that the analytical means of Q values are very close to those of simulated ones along the section. Compared to the mean values, the standard deviation and COV have greater variations between analytical and simulated results. The analytical calculation results reveal less dispersion in the Q value than the MCS-derived results. The relative difference of statistics of the Q value between analytical and simulated results along Subsection 2 is demonstrated in Figure 3.20. The relative difference is calculated as the absolute difference between the analytical and simulated Q statistics divided by the analytical values. It is seen that the relative difference of the mean is low between the analytical and simulated results along Subsection 2 with the maximum value around 5%. In contrast, the relative difference values for SD and COV are higher with the majority of

values below 10% and the maximum values around 20% locally. Overall, the differences of standard deviation and COV results derived from the analytical approximation and the MCS solutions are insignificant.

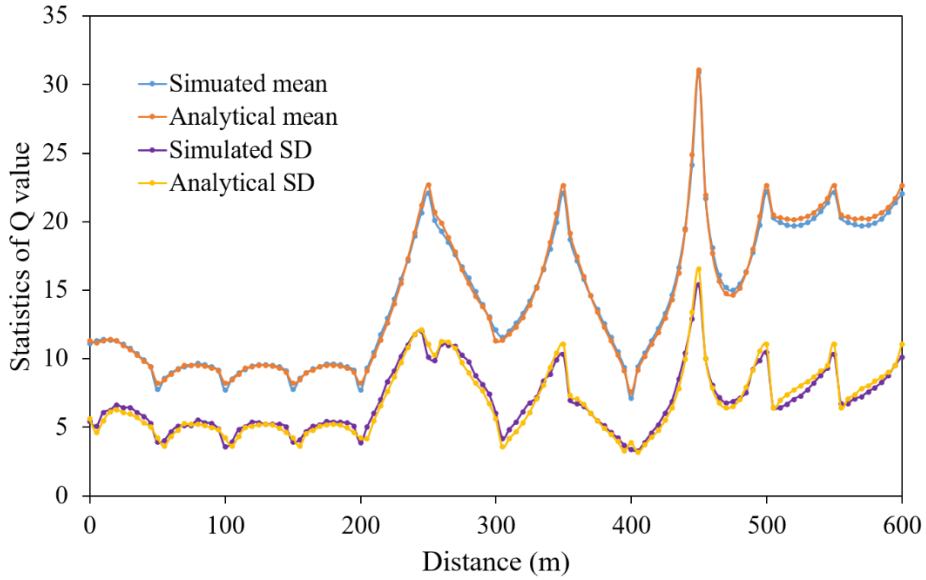

Figure 3.18 Comparison of the mean and standard deviation of Q values between analytical and simulated results along Subsection 2.

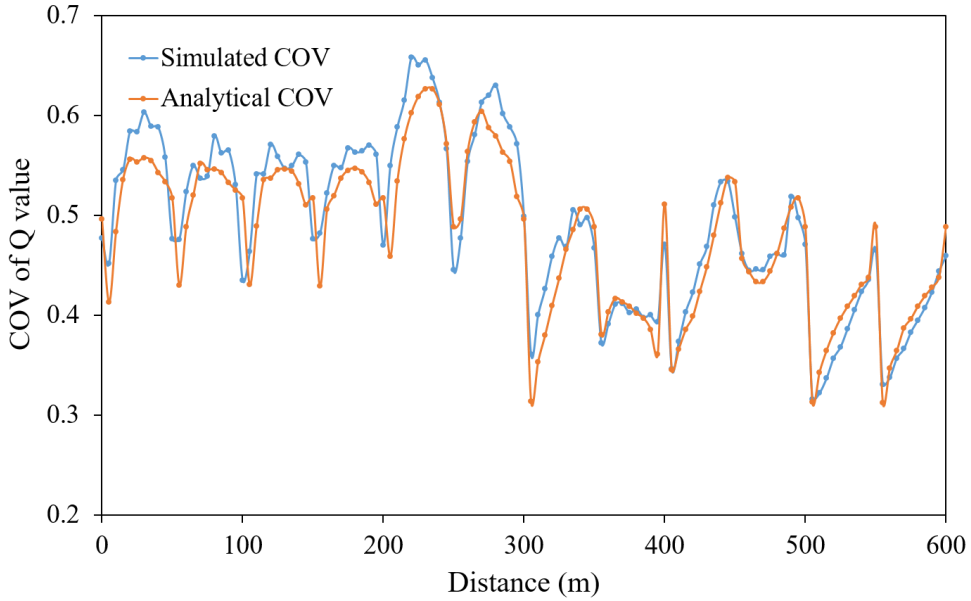

Figure 3.19 Comparison of COV of Q values between analytical and simulated results along Subsection 2.

Discussion on the comparison between analytical and simulated Q value

Results show that the proposed analytical approximate calculation approach provides a higher accuracy than that of the Q-equation approach in the analytical solution. This is because the dispersion (SD and COV) of Q-parameters is taken into consideration in addition to the mean value in the proposed calculation approach. As shown in the derivation of the statistics of the Q value in Appendix E, the degree of uncertainty expressed by the standard deviation and COV of the Q value, in addition to the mean value, also has effects on the statistics of the Q value. The dispersion parameters of the Q value derived from the proposed calculation approach are very useful in probabilistic analysis and reliability evaluation for a geostructure design (Fenton and Griffiths, 2008; Hoek, 2007). Thus, the proposed analytical calculation reflects the actual uncertainty or variability of the rock mass quality with the dispersion or uncertainty of the Q value.

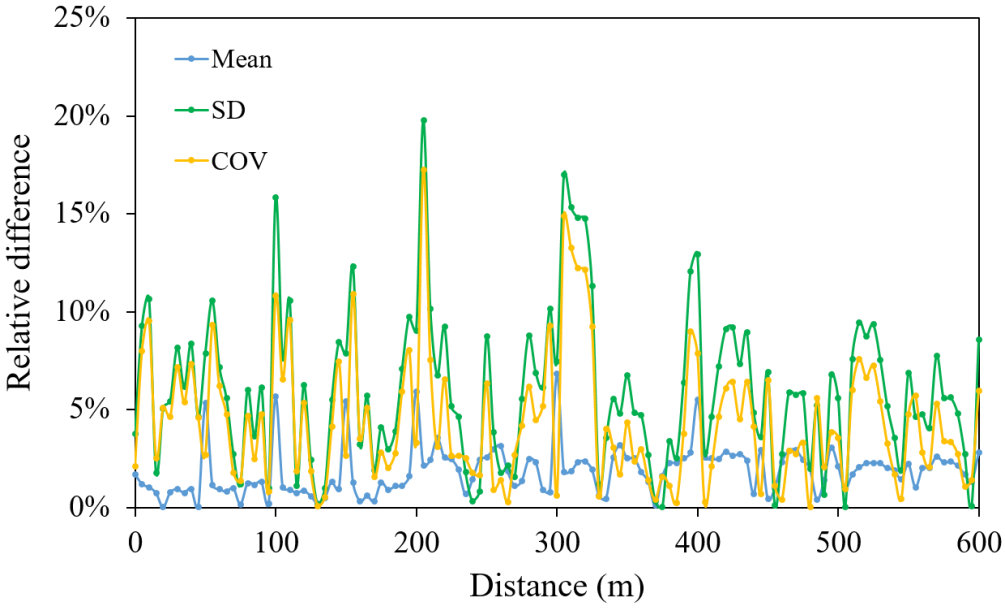

Figure 3.20 Relative difference of Q statistics between analytical and simulated results along Subsection 2

The statistics of the Q value derived from the analytical calculation and the MCS simulation are smaller than the actual recorded ones. This underestimation may be due to the approximation process caused by Taylor expansion for the analytical calculation and the Monte Carlo sampling from input distributions for the simulated results. However, in general, the differences among the analytical, simulated, and recorded results are insignificant. Thus, the accuracy of the estimated results using the proposed

analytical calculation approach and the MCS technique has been validated by the actually recorded Q value. The MCS technique is capable of providing a complete probability distribution of the estimated Q value and associated statistics, and its advantage in describing the uncertainty propagation in rock mass classifications has also been reported in literature (Bedi, 2014; Cai, 2011; Panthi, 2006; Sari, 2009; Sari et al., 2010). Thus, the MCS technique can be helpful in providing good estimates of the actual rock mass quality and associated uncertainties in the tunnel section before construction.

3.4.5 Effects of the correlation between Q-parameters on Q value

Correlation between RQD and Jn

A correlation between RQD and volumetric joint frequency λv was reported by Palmstrom (2005), and can be described as:

$$RQD = 110 - 2.5\lambda v \quad (4 \le \lambda v \le 44) \tag{3.7}$$

The volumetric joint frequency λv can be expressed as (Palmstrom and Stille, 2010):

$$\lambda v = \sum_{i=1}^{N} (\frac{1}{s_i}) + \frac{N_r}{5} \tag{3.8}$$

where s_i is the mean joint set spacing in meters of the i_{th} joint set; N is the total number of joint sets; and N_r is the number of random joints.

It is seen that RQD is negatively correlated to the volumetric joint frequency λv from Eq. (3.7) and that λv is positively correlated to the total number of joint sets N from Eq. (3.8). Combining these two equations, it is obtained that RQD is negatively correlated to the number of joint sets N, which is consistent with the rating of J_n in Q-system. Therefore, it is concluded that RQD is negatively correlated to J_n.

Effects of correlation between RQD and J_n on Q value

The effects of correlation coefficients between RQD and J_n on the Q value in OC 3 and Subsection 2 are shown in Table 3.3. It is shown that the stronger the negative correlation between RQD and J_n, the larger the statistics (mean, standard deviation and COV) of the Q value. This reveals that the variation in the Q value may be under-estimated if the correlation is not modeled. The statistics of actually recorded Q value

in Subsection 2 are also listed in Table 3.3 for comparison. It is found that the statistics of actually recorded Q value (mean of 13.34, SD of 7.10, COV of 0.53) are within the range of Q statistics derived from simulated results with different correlation coefficients (from 0 to -1). In contrast, the scenario in OC 3 is different. The recorded Q value is larger than any simulated mean of Q values considering different correlation coefficients. This may be due to the smaller variations in parameters RQD and J_n in OC 3, as can be shown in Figure 3.4.

Table 3.3 Effect of correlation between RQD and J_n on statistics of Q value.

Area	Correlation coefficient between RQD and Jn	Statistics of Q value		
		Mean	Standard Deviation	Coefficient of Variation (COV)
Subsection 2	-1	13.62	8.29	0.61
	-0.75	13.43	7.85	0.58
	-0.5	13.26	7.45	0.56
	-0.25	13.10	7.15	0.55
	0	12.95	6.77	0.52
	Actually recorded Q value	13.34	7.10	0.53
OC 3 (distance 100~105 m)	-1	7.87	4.08	0.52
	-0.75	7.83	3.94	0.50
	-0.5	7.81	3.81	0.49
	-0.25	7.76	3.71	0.48
	0	7.75	3.62	0.47
	Actually recorded Q value	8.75	N/A	N/A

3.4.6 Effects of distribution types of Q-parameters on Q value

Distribution pattern of Q-parameters

Based on a number of on-site collected data of Q-parameters, statistical distributions of these Q-parameters can be obtained and fitted with certain probability distribution models. Table 3.4 summarizes probability distribution models of Q-parameters in literature based on various research and case studies. In this case study, the RQD parameter is relatively important based on the sensitivity analysis results and can be well fitted by a continuous probability distribution. Thus, the parameter RQD is

taken as an example, and the effect of RQD distribution on the Q value has been investigated. As seen in Table 3.4, RQD can be characterized in form of a normal, lognormal, exponential, or triangular distribution in the MCS process.

Table 3.4 Summary of distribution of Q-parameters.

Q-parameter	Distribution patterns	Literature
RQD	Exponential distribution	Şen and Kazi 1984; Tavakoli and Ranjbar 2004; Onsel et al. 2011;Esfahani and Asghari 2013
	Normal distribution	Panthi 2006; Şen 2016
	Lognormal distribution	Wines and Lilly 2001; Panthi 2006; Onsel et al. 2011
	Triangular distribution	Bedi 2013
J_n	Triangular distribution	Panthi 2006; Panthi and Nilsen 2010
J_r	Normal distribution	Beer et al. 2002; Panthi 2006; Andrade and Saraiva 2008; Panthi and Nilsen 2010; Cai 2011
	Lognormal distribution	Panthi 2006
	Triangular distribution	Bedi 2013
J_a	Normal distribution	Panthi 2006; Panthi and Nilsen 2010; Cai 2011
	Lognormal distribution	Panthi 2006
	Triangular distribution	Bedi 2013
J_w	Triangular distribution	Panthi 2006
SRF	Triangular distribution	Panthi 2006

The recorded RQD data from tunnel mapping, and the statistical distribution can be described in form of a histogram with statistics estimated using the @RISK software. These statistics, including min, mode, mean, max and standard deviation, derived from the histogram can be used to define probability distribution models under different assumptions. To investigate the effect of distribution pattern of RQD on statistics of Q value, the normal, lognormal, exponential and triangular distributions, were adopted based on summarized RQD distribution types in Table 3.4 in comparison to the actual

relative frequency histogram. Meanwhile, relative frequency histograms for other Q-parameters are also used in the MCS process. To be more specific, in the scenario of Subsection 2, the relative frequency histograms based on actually collected data are adopted for other Q-parameters in the MCS simulation. In the scenario for OC 3, the predicted PMFs for other Q-parameters using the proposed prediction model were used in the MCS simulation. The MCS simulations were performed with 10, 000 iterations using the @RISK software.

Effects of distribution types of RQD on Q value

Table 3.5 Comparison of Q value between simulated and actual results with different RQD distributions.

Area	Distribution pattern of RQD	Statistics of Q value		
		Mean	Standard Deviation	Coefficient of Variation (COV)
Subsection 2	Histogram	12.96	6.78	0.52
	Normal distribution	12.76	6.54	0.51
	Lognormal distribution	12.68	6.49	0.51
	Triangular distribution	10.33	6.29	0.61
	Exponential distribution	10.59	5.94	0.56
	Actually recorded Q value	13.34	7.1	0.53
OC 3 (distance 100~105 m)	Histogram	7.74	3.64	0.47
	Normal distribution	7.76	3.63	0.47
	Lognormal distribution	7.72	3.55	0.46
	Triangular distribution	7.12	3.86	0.54
	Exponential distribution	6.81	3.94	0.58
	Actually recorded Q value	8.75	N/A	N/A

Table 3.5 compares statistics of simulated Q value with different assumptions of RQD distribution patterns in both OC 3 and Subsection 2. The actually recorded Q value during tunnel mapping is also included for comparison. It is found that the simulated results with RQD histogram are closest to actual results in Subsection 2,

followed by those with normal distribution and lognormal distribution. This is because the RQD histogram was derived from the actually recorded RQD data in the tunnel section. The distribution fitting results also show that normal and lognormal distributions are good fits for the RQD histogram, and this is why simulated scenarios with these two distribution assumptions also generated close results to the actual results. The RQD histogram based on the actually recorded RQD data is shown in Figure 3.21 with the normal distribution fit. By contrast, greater deviations were observed between actually recorded results and simulated ones with triangular and exponential distributions of RQD, indicating these two distribution types are not good fits in this case.

In the scenario of OC 3, as shown in Table 3.5, similar results can be observed in the normal, lognormal and triangular distributions compared to the RQD histogram. This may be related with the characteristics of RQD histogram at OC 3. As can be seen in Figure 3.4, the probability for state 3 (RQD: 50~75) of RQD parameter is 90%, and the probability for state 2 (RQD: 25~50) and state 4 (75~100) are both 5% at the OC 3. Due to the single peak of state 2 in the RQD histogram at OC 3, the goodness-of-fit differences for normal, lognormal and triangular distributions are limited and thus similar results are generated using these distributions.

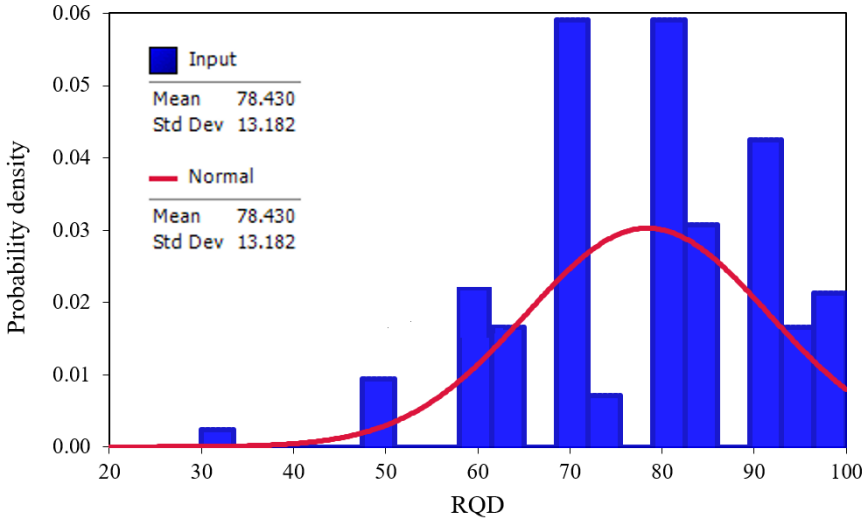

Figure 3.21 Statistical distribution of actually recorded RQD data in Subsection 2 and normal distribution fit

3.4.7 Perspective of the study

The proposed Q-based prediction model provides a framework for predicting rock mass quality using the Markov Chain technique in the planning and preliminary design stage of underground construction. The probability distributions of rock mass quality can be predicted along the tunnel alignment before tunnel excavation based on site investigation data, including the rock mass quality data in the regional area and location-specific exploration boreholes. Note that the availability of Q data in the tunnel area and boreholes are limited in this case study. In view of this, the Q data collected in Subsection 1 of the excavated tunnel section was used as the input for the prediction model, and Subsection 2 of the excavated tunnel section has been used as the test section, considering the ground stationarity of the selected tunnel section. The proposed probabilistic prediction model should also be applied to tunnel cases with Q data available from the tunnel area and boreholes in the site investigation stage to test prediction robustness. In addition, as reported by some researchers (Bieniawski, 1989; Palmstrom and Stille, 2010), it is recommended to use more than one rock mass classification (e.g. RMR, Q-system, GSI) in tunnel design for comparison. Thus, the extension of the probabilistic Q-based prediction model to other rock mass classification systems such as RMR and GSI should be incorporated into future work. Further, the proposed prediction model should be updated based on new rock mass quality data available during tunnel construction, and Bayesian updating technique or equivalent can be used. It should also be noted that the selected tunnel section from the water tunnel case study is in relatively stationary ground conditions. In a tunnel with heterogeneous and complex geologic conditions, the tunnel section can be divided into several relatively stationary subsections, and the Markov Chain-based prediction model can be implemented in relatively stationary subsections. The proposed prediction model should be applied to tunnel cases with more variable geologic conditions to test its prediction performance for further study. Nevertheless, the proposed prediction model enables the prediction of probabilistic distributions of rock mass quality along the tunnel alignment before construction with a relative high prediction accuracy in this

case study, thus providing a supplement to the geology exploration and prospecting in the planning and preliminary design stage of underground excavations.

3.5 Conclusions

The probabilistic distribution of rock mass quality Q index in the unexcavated tunnel sections has been predicted before excavation by a Q-based prediction model using the Markov chain technique. The proposed prediction model has been applied to selected sections of a water tunnel for the purpose of validation. The predicted probabilistic results of Q-parameter states, Q values and Q-based rock classes were compared with those recorded during tunnel construction. The average prediction accuracy for the predicted results was relatively high based on the accuracy plots in comparison to the actually recorded Q data, indicating the effectiveness of the proposed prediction model.

In addition to Monte Carlo-simulated results, an analytical calculation approach for approximating the statistics of the Q value has also been developed given the statistics of Q-parameters. The statistics of Q values estimated from the analytical calculation approach were also compared to the MCS-derived and actually recorded Q results, and the comparability among these results was confirmed.

Probabilistic sensitivity analysis was also carried out in the MCS process and the relative importance of Q-parameters was ranked in tornado graphs based on four different ranking criteria. All the ranking criteria show similar sensitivity results with J_n and RQD being most influential, in consistent with the greater variations in the predicted probabilistic profile of J_n and RQD compared to other Q-parameters.

Moreover, the negative correlation between RQD and J_n has been presented, and the estimated mean and dispersion of the Q value would be underestimated if the correlation was neglected. The effects of distribution for RQD on the Q value have also been examined. The normal distribution was a good fit for the actually recorded RQD data in this case study, and the generated Q value under this normal assumption of RQD agreed well with the actually recorded Q results during tunnel construction.

The proposed Q-based prediction model is capable of quantitatively predicting rock mass quality in the unexcavated tunnel section using a probabilistic approach and can be used to complement geology exploration in the planning and preliminary design stages of tunnel projects. It can also be helpful in probabilistically evaluating excavation support strategies as well as the construction time and cost, thus contributing greatly to decision support for the tunnel design and construction.

CHAPTER 4

MONTE CARLO SIMULATION (MCS)-BASED UNCERTAINTY ANALYSIS OF ROCK MASS QUALITY Q IN UNDERGROUND CONSTRUCTION

Modified from a paper published in *Journal of Tunneling and Underground Space Technology*

Hui Lu, Eunhye Kim, Marte Gutierrez

4.1 Abstract

Uncertainty in rock mass quality as it pertains to tunnel design is due largely to the inherently heterogeneous nature of rock masses. Traditional deterministic methods for the assessment of rock mass quality are based on a limited understanding of this inherent uncertainty, which results in adverse effects on the overall design and possibly on the performance of the structure. To address this problem, a Monte Carlo simulation (MCS)-based uncertainty analysis framework is proposed to probabilistically quantify uncertainties in the rock mass quality assessment by the rock mass classification Q-system. The proposed framework has been successfully implemented in a highway tunnel case study. The probabilistic distribution of the Q value was obtained using the MCS technique with the relative frequency histograms of Q-parameters, which was then used to assess rock mass properties and responses with appropriate empirical correlations. The probabilistic estimates of rock mass properties were also adopted as the inputs for a finite element model for the probabilistic evaluation of excavation-induced tunnel displacement. In addition, the probabilistic sensitivity analysis was conducted in the MCS process to rank the relative importance of Q-parameters based on criteria of regression coefficients, Spearman's rank-order correlation coefficients, contributions to variance and effects on output mean. The negative correlation between Rock Quality Designation (RQD) and J_n was also presented, and its effects on the Q value and associated rock mass parameters have been investigated. Moreover, the effects of the distribution types of uncertain input parameters in the Q-system have also been examined. The proposed framework is capable of systematically assessing the uncertainty in the rock mass quality measure before tunnel construction as well as providing insightful information for the probabilistic evaluation of the ground response and support performance of underground structures.

4.2 Introduction

Rock mass classification systems have been widely used to provide a quantitative assessment of rock mass quality and guidelines for engineering design (Palmstrom and Stille, 2010). Empirical rock mass classification systems, including the rock mass rating (RMR), rock mass quality Q-system, and geological strength index (GSI), have inherent uncertainties (Palmstrom and Stille, 2007; Stille and Palmström, 2003). For example, in the Q-system, the joint characteristics, J_r, J_a and especially J_n, in addition to the RQD, are prone to mischaracterization (Palmstrom and Broch, 2006). The traditional deterministic analysis methods, which are based on ground characterization and rock mass classification, disregard the inherent uncertainties in the rock mass itself and thus may cause conservative estimates to be used in the design and construction phases that inflate the costs of underground construction (Guan et al., 2014; Ioannou, 1987).

The Q-log chart is commonly used to record the statistics of all the input parameters in the Q-system for the field mapping of surface exposures, core logging or underground excavation logging (Barton, 2002). The mean, mode and the range interval of each input parameter are estimated based on the collected Q-log data, and these statistics for the overall Q value could be calculated using an interval analysis. However, Panthi (2006) reported that the mean and range values have poor statistical properties and are sensitive to extreme values. A Q-log example from a case study showed that the typical Q value range was 0.008–100 with a mean value of 4.44 (Morelli, 2015). This cautious estimate of the range covers several rock classes, from exceptionally "poor" to "extremely good", and the mean value indicates that the rock mass is "fair" on average. Bedi (2013) also reported that the lack of information on intervals could cause difficulty in decision-making, as exemplified by the wide range of the calculated Q interval. In addition, if the uncertainties and variabilities in the rock mass classifications are insufficiently characterized, they may propagate through the design process and have an adverse impact on the ground response and tunnel support performance (Baecher and Christian, 2003; Langford, 2013).

However, probabilistic analysis, which encompasses the complete probability distribution of the rock mass parameters, is capable of adequately characterizing the uncertainties in rock mass conditions. The probabilistic rock mass quality can capture the intrinsic and subjective variability of the rock mass conditions and has a significant influence on the probabilistic design in underground construction (Cai, 2011). Once uncertainties in the Q-system are quantified probabilistically, probabilistic estimates of the rock mass properties can be made through a forward

uncertainty analysis based on the empirical relationships. The derived probabilistic rock mass properties can be used as the inputs for a probabilistic analyses using numerical modeling, in which the rock mass response and design performance can also be evaluated probabilistically. Sari (2009) developed the probability distributions of the RMR and GSI based on probabilistic descriptions of the discontinuities and intact rock properties using Monte Carlo simulation (MCS) and derived a probabilistic estimate of the rock mass strength and deformability properties. Cai (2011) analyzed GSI from probabilistic evaluations of the joint characteristics in field mapping and performed a probabilistic analysis of tunnel and cavern stability which considered the variability of the rock mass parameters and in situ stress.

Similarly, Tiwari et al. (2017) estimated the rock mass parameters from the GSI in tunnel case studies and used them to assess the uncertainty in the yield zone and tunnel displacement. Idris et al. (2015) quantified the deformation modulus of a rock mass at the Laisvall mine based on the probabilistic distribution of GSI and adopted it to evaluate the pillar stability using numerical simulations. Bedi (2013) developed the probability density distribution (PDF) of the Q value in the Gjovik cavern using the MCS technique based on triangular PDFs of Q-parameters.

However, no attempts in the past research have been made to consider the relative importance of the input parameters in the probabilistic Q-system. Additionally, the majority of studies fail to take into account the interdependencies between uncertain Q-parameters and the effects of the distribution types of the Q-parameters. In this chapter, an MCS-based uncertainty analysis framework for the Q-system has been proposed. By conducting the MCS, the probabilistic sensitivity analysis has been used to investigate the impact of the input parameters on the Q-system and associated rock mass parameters. The effects of the correlations between input parameters and the effects of the input parameter distribution types on the Q value and associated rock mass properties and responses have also been examined. The proposed MCS-based uncertainty analysis framework for the Q-system is described in detail in Section 4.3, in which the MCS-based stochastic model of the rock mass quality Q and the uncertainty analysis of the probabilistic Q-system are introduced. The framework has been implemented in a case study of the Shimizu highway tunnel in Japan for illustrative purposes. The results and discussion on the case study are in Section 4.4, followed by the major conclusions in Section 4.5.

4.3 Methodology

4.3.1 Stochastic modeling of the rock mass quality

Probabilistic Q value from Monte Carlo simulation

The MCS is a stochastic simulation method where the distribution of possible outcomes is produced from different randomly sampled sets of values from the probability distributions of the input parameters. The probability distribution is specified for each input parameter, and the randomly selected input values are used to simulate a wide range of possible output values (Palisade Corporation, 2016). The disadvantages of MCS are that it requires substantial computational resources, along with explicit probability distribution functions for the input variables (Cai, 2011). For a more comprehensive description of MCS, the reader can refer to the literature (Gentle, 2013; Law et al., 1991; Vose, 2008).

The Excel add-in program @RISK is an advanced statistical risk analysis system that implements MCS in a standard spreadsheet package, in which the uncertainty in the input parameters can be explicitly characterized to produce outputs that describe all the possible outcomes (Palisade Corporation, 2016). It allows the definition of different types of continuous and discrete probability distributions for the input parameters in the spreadsheet, and it is capable of making a best-fit for the available data as well as generating statistics for the data and the fit curve. The @RISK program enables stochastic simulation using both Monte Carlo and Latin hypercube sampling techniques for any number of iterations per simulation and any number of simulations in a single analysis (Palisade Corporation, 2016). For the Monte Carlo sampling, samples are more likely to be drawn from the areas of the distribution that have a higher probability of occurrence due to its entirely random feature. Clustering becomes an issue when a distribution includes low probability outcomes, which could have a major impact on the results, especially when a small number of iterations are carried out.

In contrast, the Latin Hypercube sampling requires fewer iterations due to the use of stratified sampling from the input probability distributions. Stratification divides the cumulative density function (CDF) of the input parameter into equal intervals, and a sample is then randomly selected from each interval or stratification of the input probability distribution. Sampling thus draws representative samples from each interval, which then recreates and more accurately reflects the input probability distribution. Compared with traditional Monte Carlo sampling, Latin hypercube sampling provides increased sampling efficiency and faster runtimes due to fewer iterations. The

Latin hypercube sampling also aids the analysis in situations where low probability outcomes are represented in the input probability distributions (Palisade Corporation, 2016).

In the Q-system, all the input parameters can be regarded as random variables. The variability of the input parameters can be described by their relative frequency histograms, which can be accessed from the Q-histogram logging data by drilled core logging, exposed outcrop mapping, and tunnel mapping. When the statistical distributions are developed for the six input parameters, the distribution of the Q value can be calculated according to Eq. (2.1) using MCS with Latin hypercube sampling in the @RISK program. The Q-input parameter values are randomly sampled from their distributions, and the probability distribution of the Q value is generated from the simulation runs. A statistical analysis can be performed on the probability distribution of the Q value that is produced, and the statistics for rock mass quality can be derived.

Probabilistic evaluation of the rock mass properties and responses

Once the probability distributions of the Q value and other input parameters have been determined, the rock mass properties and responses can be similarly characterized probabilistically according to empirical equations using the MCS with the @RISK program.

parameters (e.g., the tunnel wall displacement or the radius of the plastic zone), either an MCS or the point estimate method (PEM) (Rosenblueth, 1981) can be used for the numerical analysis. The RS2 FEM program is capable of performing probabilistic analysis using MCS with both Monte Carlo and Latin Hypercube sampling as well as PEM techniques. The MCS and PEM techniques can be used to probabilistically characterize the uncertainties in the input parameters of the numerical model.

Table 4.1 and Table 4.2 list the empirical correlations between the Q value and the rock mass properties and responses, respectively. The parameters that must be calculated for the rock mass responses include the displacement and plastic zone radius of the underground opening; based on Hoek and Marinos (2000b), the Duncan Fama (1993), and the Barton (2002) approach, are introduced. Note that the Q-based empirical correlations for evaluating the rock mass responses only serve as a preliminary estimation. These empirical correlations were either derived using several simplified theoretical assumptions or obtained from the databases of different case histories. For a more reliable and accurate assessment of the rock mass responses of underground excavations, a numerical analysis should be conducted.

Probabilistic analysis of the rock mass response with numerical modeling

Once the probability distributions of the rock mass properties have been determined, they can be used as the inputs for a numerical model to evaluate the rock mass responses. To achieve this, a finite element method (FEM) or a finite difference method stress analysis may be performed, taking the variability of the input parameters into account and including the rock mass properties and the in situ stress (Cai, 2011). To calculate the probability distributions of the tunnel response parameters (e.g., the tunnel wall displacement or the radius of the plastic zone), either an MCS or the point estimate method (PEM) (Rosenblueth, 1981) can be used for the numerical analysis. The RS2 FEM program is capable of performing probabilistic analysis using MCS with both Monte Carlo and Latin Hypercube sampling as well as PEM techniques. The MCS and PEM techniques can be used to probabilistically characterize the uncertainties in the input parameters of the numerical model.

Table 4.1 Empirical correlations based on the Q value for estimating rock mass properties.

Parameters		Equation No.	Empirical equations	Source
Rock mass properties	Deformation modulus	4.1	$E_m = 25\log Q (Q \geq 1)$	Grimstad and Barton 1993
		4.2	$E_m = 10(Q\frac{\sigma_c}{100})^{\frac{1}{3}}$	Barton 1996
		4.3	$E_m = 10^{(15\log Q+40)/40}$	Barton 2002
		4.4	$E_{in} = E_i \exp(0.8625\log Q - 2.875)$	Ramamurthy 2004
	Compressive strength	4.5	$\sigma_{cm} = 7\gamma\frac{\sigma_c}{100}Q^{\frac{1}{3}} (Q \geq 10)$	Singh et al. 1997
		4.6	$\sigma_{cm} = 7\gamma Q^{\frac{1}{3}} (Q < 10)$	
		4.7	$\sigma_{cm} = 5\gamma(Q_0\frac{\sigma_c}{100})^{\frac{1}{3}}$	Barton 2000
		4.8	$\sigma_{cm} = \sigma_{ci}\exp(0.6\log Q - 2)$	Ramamurthy 2004
	Cohesion	4.9	$c_m = (\frac{RQD}{Jn} * \frac{1}{SRF} * \frac{\sigma_{ci}}{100})$	Barton 2002
	Friction angle	4.10	$\phi_m = \tan^{-1}(\frac{Jr}{Ja} * \frac{Jw}{1})$	

Table 4.2 Empirical correlations based on the Q value for estimating rock mass responses.

Parameters			Equation No.	Empirical equations	Source
Rock mass responses	Displacement	Hoek and Marinos approach	4.11	$\delta = r_0(0.002 - 0.0025\frac{p_i}{p_0})(\frac{\sigma_{cm}}{p_0})^{(2.4\frac{p_i}{p_0}-2)}$	Hoek and Marinos 2000
		GRC approach	4.12	$u_{ie} = \frac{r_0(1+v)}{E_m}(p_0 - p_i)$	Duncan Fama 1993
			4.13	$u_{ip} = \frac{r_0(1+v)}{E_m}[2(1-v)(p_0 - p_{cr})(\frac{r_p}{r_0})^2 - (1-2v)(p_0 - p_i)]$	
		Barton approach	4.14	$\Delta_v = \frac{SPAN}{100Q}\sqrt{\frac{\sigma_v}{\sigma_{ci}}}$	Barton 2002
			4.15	$\Delta_h = \frac{HEIGHT}{100Q}\sqrt{\frac{\sigma_h}{\sigma_{ci}}}$	
	Plastic zone radius	Hoek and Marinos approach	4.16	$\frac{r_p}{r_0} = (1.25 - 0.625\frac{p_i}{p_0})(\frac{\sigma_{cm}}{p_0})^{(\frac{p_i}{p_0}-0.57)}$	Hoek and Marinos 2000
		GRC approach	4.17	$r_p = r_0[\frac{2(p_0(k-1)+\sigma_{cm}}{(1+k)((k-1)p_i+\sigma_{cm})}]^{\frac{1}{(k-1)}}$	Duncan Fama 1993

The PEM is capable of combining probabilistic input parameters and evaluating the probability distribution of the output variables. In the PEM, several estimation points are sampled to calculate the possible values of the outcome, and proper weights should be assigned to obtain an approximation of the probability distribution for the output variable (Baecher and Christian, 2003). The two-point estimate is commonly used, and the evaluation points of an input variable are located at one standard deviation above and below its mean. The probabilistic input parameters are often assumed to be uncorrelated and to follow a normal distribution for the sake of simplicity. Compared to an MCS, which requires a large number of simulations and thus is computationally expensive, the PEM needs much less computational effort, i.e., 2^n solutions, to find the mean and standard deviation of the output variable, where n is the number of input variables. The main limitation of the PEM is that it is only suitable when the variables follow a normal distribution (mean and standard deviation). If either the input or output variables differ from a normal distribution, the approximation obtained by using the PEM will lead to inaccuracies.

For PEM-based probabilistic modeling in RS2, the normal distribution is assumed for all the uncertain input and output parameters, and the mean and standard deviation from the estimated distributions of the rock mass properties are used as the inputs for numerical modeling. For the MCS model, the distribution types of the rock mass parameters are derived from the best fit distribution for each parameter, while the statistical values, such as the mean, standard deviation, min, and max, are estimated from the actual relative frequency histograms which are used for the Q-parameters. After performing the numerical calculations and interpretations, the statistics (mean,

standard deviation) of the rock mass response parameters can be obtained at arbitrary points in the model based on a certain number of iterations.

4.3.2 Uncertainty analysis in the Q-system

Probabilistic sensitivity analysis in the Q-system

The sensitivity analysis of the Q value to its input parameters can be conducted in the @RISK program. The sensitivity analysis results are shown using tornado graphs that display the rank of the input distributions relative to the impact on the output distribution. Inputs with the largest impact on the output distribution have the longest (and topmost) bars in the graph (Palisade Corporation, 2016). Four tornado graphs in @RISK are commonly used for ranking the relative importance of input parameters: the regression coefficients, the Spearman correlation coefficients, the contribution to output variance, and the effect on output mean. For the tornado graphs showing regression coefficients or Spearman correlation coefficients, the length of the bar shown for each input distribution is based on the coefficient value calculated between the output and the input parameter. It should be noted that the regression coefficient describes the size of the effect each input has on the output. In contrast, the correlation coefficient indicates whether increasing the input generally increases or decreases the output and how consistent that trend is, but it tells nothing about the strength of the influence. In the @RISK program, the regression coefficient for an input variable shown on a tornado graph is the scaled value normalized by its standard deviation and the standard deviation of the output, which also reflects the impact of the input parameters on the output. For tornado graphs showing the contribution to variance, the length of the bar is the amount of change in the output attributable to each input. These values are calculated during the regression analysis. Unlike a regression coefficient, this measurement is unaffected by the magnitude of the input. In the tornado graph, to visualize the effect on the output mean, the double-sided tornado has one bar for each selected input. The output means are calculated for the output values in each iteration as the input varies over its range.

In the tornado graphs, the numbers shown at the two ends of a bar graph describe the calculated values for the different ranking techniques used during the simulation process. Note that the numbers at the two ends of the double-sided tornado, showing the effect on the output mean, are the means of the output variable from the iterations with the lowest and highest 10% of input values, respectively. The rank of the input parameters is based on the range between the highest and the lowest mean value caused by that input parameter, i.e., the length of the bar. The regression

coefficient and the percentage contribution to variance are obtained based on a stepwise multiple regression, an iterative process where input variables are entered into the regression sequentially. Spearman's correlation coefficient is calculated based on the Spearman rank-order correlation, which works well for linear or nonlinear correlations. In addition to the tornado graphs, @RISK also provides a spider graph of input parameters which show how the output mean value varies with an increase in the input parameter across its range. The steeper the gradient of the trend line is, the greater the effect this input parameter has on the output. A spider graph shows more information than a tornado graph, when used to describe the effect on an output mean, since the spider graph shows the rate of change for the input parameters while only the overall range of the output is shown in the tornado graph.

Correlation between input parameters in the Q-system

As mentioned in Section 3.4.6 in Chapter 3, the correlation between RQD and J_n has been previously documented, and the effect of the correlation on the Q value can be studied. The Spearman rank-order correlation coefficients between RQD and J_n can be specified at values between -1 and 1 in different scenarios using the correlation matrix function in the @RISK program. The probability distributions of the Q values and the statistics generated under the different simulation scenarios can then be compared. Since the rock mass properties and responses are associated with the Q value, the effect of the negative correlation between RQD and J_n on these output variables can also be investigated.

Distribution types for input parameters in the Q-system

In rock engineering, the uncertainty components include the aleatory variability, caused by randomness, and the epistemic uncertainty, caused by the lack of knowledge (Baecher and Christian, 2003). The best way to quantitatively measure these uncertainties is to use probability distribution models that are expressed in the form of a mathematical distribution (Panthi, 2006). Because of the variable nature of rock masses, it is difficult, or sometimes even impossible, to give a single representative value of Q (Barton and Grimstad, 2014). To better represent and record the locally variable properties, the Q-histogram logging chart is introduced and has been widely used to register the Q-parameter data. Based on the Q-histogram logging chart, the relative frequency of these Q-parameters can be intuitively observed, and statistics (e.g., mean, mode, min, max) can also be obtained. Using the @RISK program, the best-fit PDF for each Q-parameter can be determined by the distribution fitting function that can meet the fit test. However, the geotechnical

data collected from the project site are often limited and incomplete in terms of rock engineering data. In such cases, an alternative method is to assume appropriate PDF models for the geotechnical parameters with perceived uncertainty on the basis of limited experimental or field measured results and logical engineering judgment (Hoek, 1998a; Sari, 2009). Sen and Kazi (1984) stated that the distribution function of the RQD is unique since it is a random variable that is a function of discontinuous spacings and numbers. The most commonly used probability distribution models for rock mass quality evaluation have been summarized in **Error! Reference source not found.** in Section 3.4.7 in Chapter 3 based on various research and case studies. The various distribution types can be assumed for the input parameters in the Q-system and then compared to the collected Q-histogram logging data to investigate their effects on the Q value and the associated rock mass parameters.

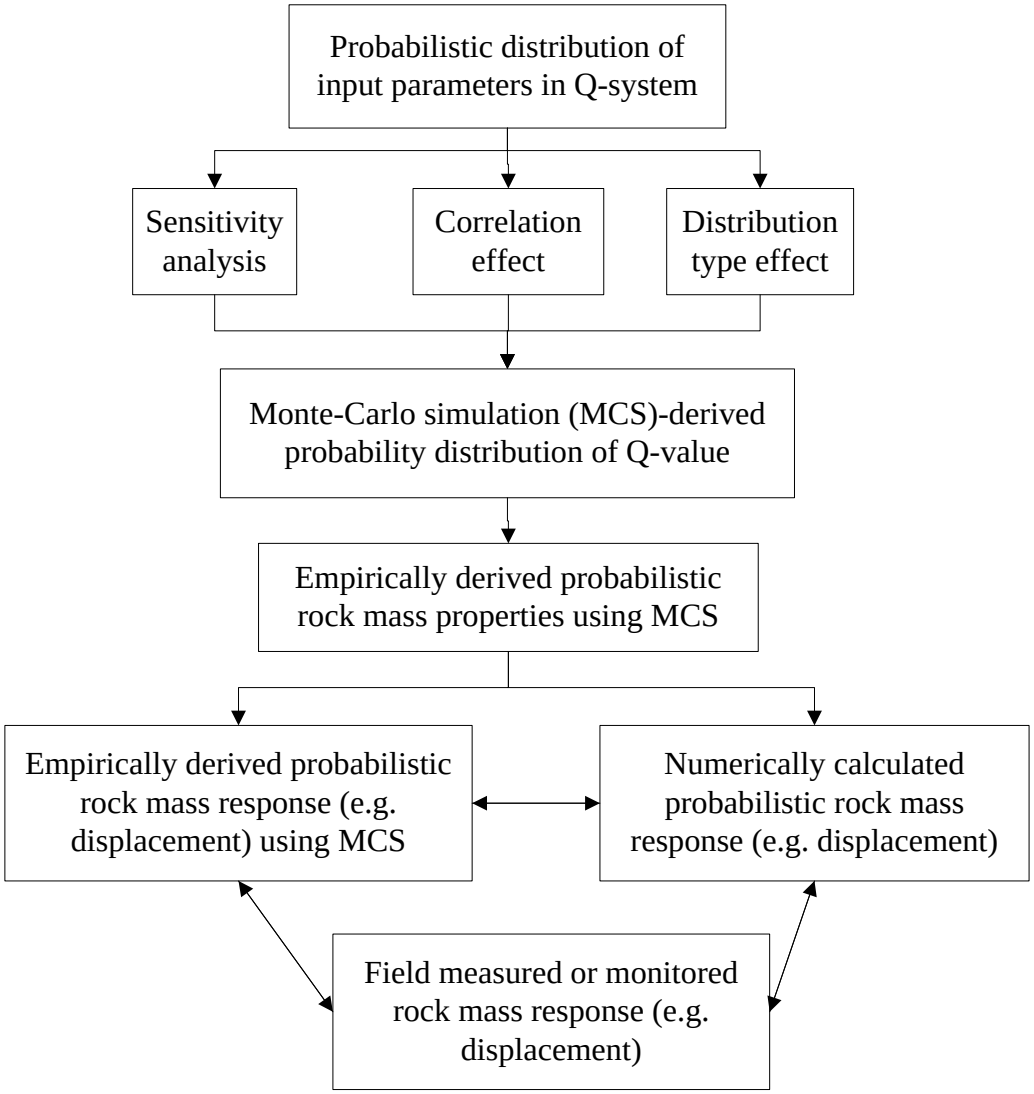

Figure 4.1 Block diagram of the proposed framework.

The proposed framework is illustrated in Figure 4.1. The uncertainty in the rock mass is characterized by the probability distribution of input parameters in the Q-system. Using the MCS technique, the probability distribution of the Q value, rock mass properties and responses (e.g. displacement, plastic radius) can be obtained based on the Q-derived empirical relationships. In this process, the uncertainty is propagated from the Q-parameters to the Q value and to the Q-based rock mass parameters. To quantitatively characterize the process, the sensitivity analysis, the effects of the correlation, and the effects of distribution types among the input parameters in the Q-system can be performed. On one hand, the empirically derived probabilistic rock mass properties can be used to evaluate the rock mass responses empirically using the MCS technique; on the other hand, these probabilistic rock mass properties can also serve as the input in numerical modeling to estimate the probabilistic distribution of rock mass responses. The empirically and numerically derived probabilistic distribution of rock mass responses can be compared with each other and should be validated in comparison to the field measured or monitored rock mass response data.

4.3.3 Application to a case study of the Shimizu tunnel

The Shimizu tunnel No. 3, located in the city of Shimizu in Japan, is an important section of Japan's Tomei-Meishin Expressway project. It is a research tunnel with a length of 1.12 km (height 12 m, width 18 m). The depth varies from 30 m to 190 m with an average of approximately 83 m. The average in-situ stresses are 2 MPa and 1.73 MPa in the vertical and horizontal directions, respectively, giving a stress ratio of 0.83 (Vardakos, 2003). Figure 4.2 shows the longitudinal geologic section along the western and central sector tunnel. Field investigations showed that the ground was composed of soft sedimentary rock formations, including weathered soft sandstone (W_{ss}) and interbedded mudstone-sandstone (Walt 1 and Walt 2). The tunnel was excavated mainly through the W_{ss} sandstone formation with a density of 2.5 g/cm^3. Three major joint sets were recognized in the weathered soft sandstone. The geotechnical data are collected by the Norwegian Geotechnical Institute by inspecting drilled cores, field mapping, geophysical investigations and laboratory tests on intact rock samples, and a detailed Q logging was made (Barton et al., 1995). Core logging was carried out for a total of four selected drill cores in the western and central sector from the Shimizu tunnel site. Two horizontal borings were drilled in the western portals with about

100 m in length for each, and one vertical and one inclined borings were drilled in the central sector. Extensive core photo analysis was also conducted to determine the parameter values in the Q-system. As a result, a complete Q-classification based on about 400 Q-logging data, was obtained for the western and central sector of the Shimizu tunnel. Extensive rock mechanics tests were also performed on the collected drilled cores. The lab test results on the core samples collected in the western and central sector showed that the uniaxial compressive strength (UCS) for the intact rock samples is in the range of 20-78 MPa, and the intact rock elastic moduli are in the range of 5.4-15 GPa. The friction angles of the rock samples are in the range of 37-53 degrees, and the cohesion of the intact rock is in the range of 1.9-6.8 MPa (Vardakos, 2003).

At the Shimizu tunnel No. 3, the tunneling boring machine (TBM) pilot tunneling and enlargement method was utilized. The TBM tunnel was first bored within the top heading cross-section using a 5 m diameter triple shield TBM. After the advance of the TBM pilot tunnel, the gradual enlargement of the tunnel was performed by drilling and blasting top heading, a bench and finally an invert. Since the Shimizu tunnel No. 3 is a research tunnel, extensive instrumentation was installed to monitor the tunnel response during tunnel construction. Total stations with reflex targets and 12 m long multipoint extensometers were used to monitor the tunnel deformation (Vardakos, 2003). However, the measured data that is available is mainly for the top heading excavation, which can be used to compare the estimated and measured displacement for validation. Thus, the analysis below is focused on the top heading stage of the tunnel excavation. For more details about the Shimizu tunnel No. 3, the reader may refer to the literature (Vardakos, 2003)

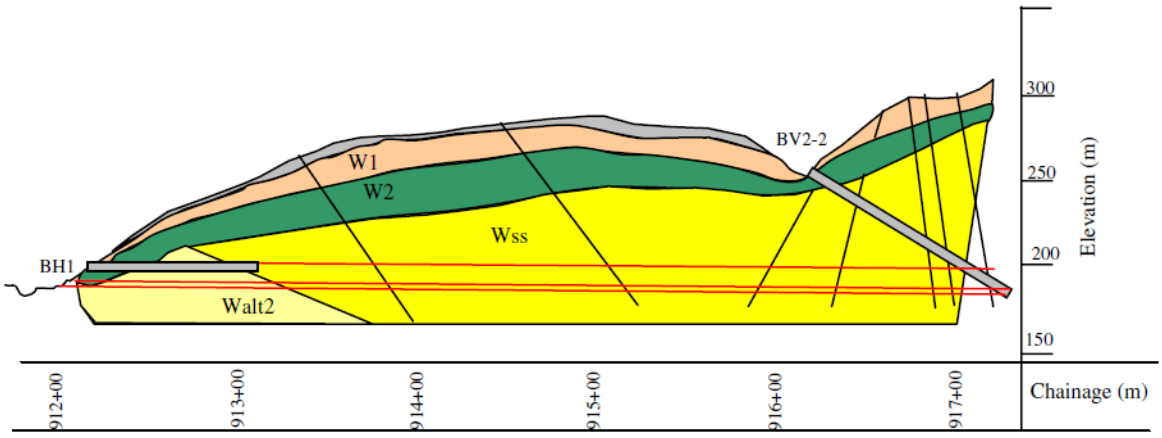

Figure 4.2 The longitudinal geologic section in the western and central sector tunnel. BH1 and BV2-2 are locations of two boreholes (Vardakos et al., 2007)

4.4 Results and Discussion

4.4.1 Probabilistic analysis in the Q-system

Distribution of the Q value

According to Barton et al. (1995), the Q-histogram logging data (about 400 data in total) was collected in the western-central sector of the Shimizu tunnel, and Figure 4.3 shows the relative frequency histograms of the Q-parameters. It is obvious that the RQD is taken as a continuous random variable expressed in the form of a histogram, while the other input parameters are expressed as discrete random variables in the form of probability mass functions. The RQD is bimodal and approximately negatively skewed towards low values on the left. For the other input parameters, the relative frequency on the vertical axis represents the percentage of each discrete value for each parameter. The qualitative statistics of all the input parameters in the Q-system have been conducted using the @RISK program and are depicted in Table 4.3. The statistical distribution of the Q value was obtained using MCS in the @RISK program according to Eq. (2.1) and based on the relative frequency histograms of the Q-parameters. The Latin hypercube sampling technique was used, and a simulation was performed with 10,000 iterations.

The distribution of the Monte Carlo simulation Q values and the best fit PDF are shown in Figure 4.4. The mean and standard deviation of the MCS-simulated Q value are 6.63 and 7.52, respectively, and the lognormal distribution is the best fit distribution. In the same western-central sector of the Shimizu tunnel, Tiwari et al. (2017) derived the probability distribution of GSI based on statistical intact rock and joint properties, and the obtained mean of GSI is 47 and the standard deviation is 2.25. The obtained GSI distribution is consistent with the derived distribution of the Q value, with both indicating the best estimate of “fair” rock mass quality in this tunnel area. The distribution of the logarithm (base of 10) of the Q value is also shown in Figure 4.4 with the normal distribution fit. The mode, median and mean values of the simulated Q value are increasing, corresponding to approximately 1.08, 3.82 and 6.63, respectively, which is consistent with the characteristics of a lognormal distribution. Similarly, the lognormal distribution was found to be a good fit of the statistical distribution of the predicted or mapped Q values for the rock tunnels (Daraei and Zare, 2018; Lu et al., 2018b). The logarithms of the actual mapped Q values in the Northern Link project in Stockholm, Sweden, were also found to conform to a normal distribution, which also supports the lognormality of the Q value distribution (Benhalima, 2016).

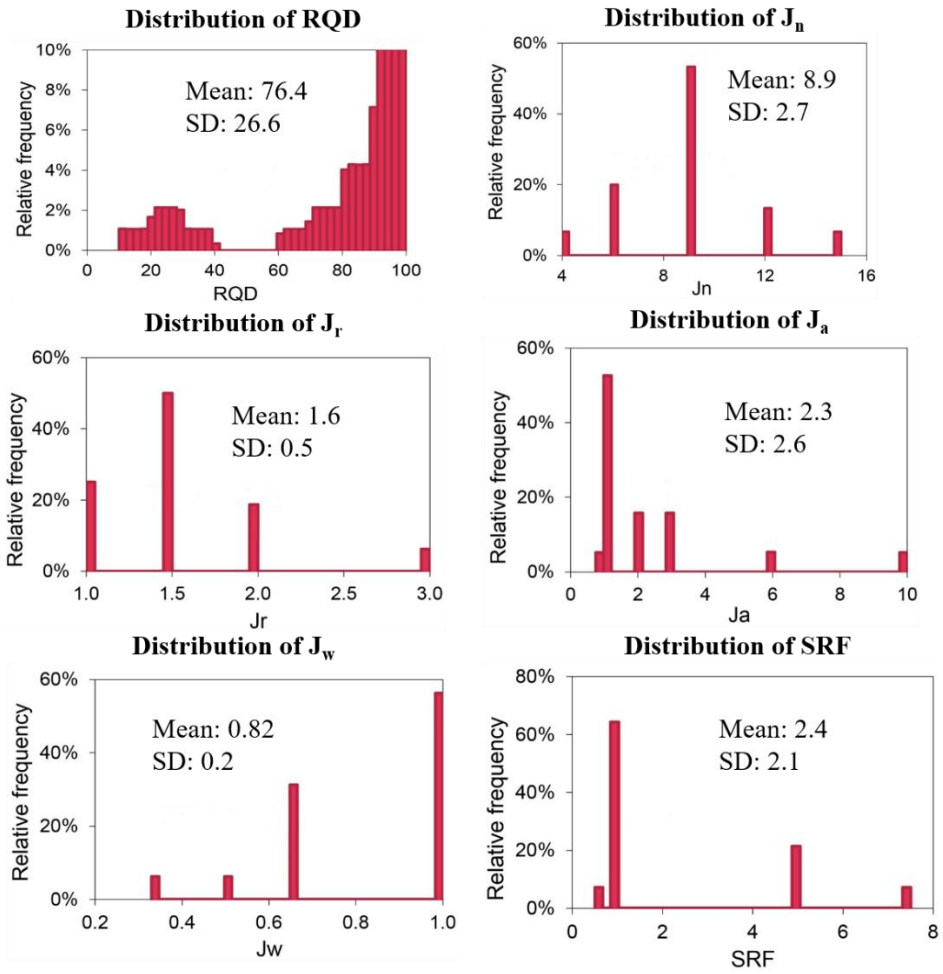

Figure 4.3 Histograms of Q-parameters: (A) RQD; (B); J_n; (C) J_r; (D) J_a; (E) J_w; (F) SRF

Table 4.3 Comparison of the Q value statistics calculated by different methods.

		(RQD	/	Jn)	*	(Jr	/	Ja)	*	(Jw	/	SRF)	=	Q	Monte-Carlo simulated Q
Interval analysis	Typical min	15	/	15	*	1	/	10	*	0.33	/	7.5	=	0.004	0.013
	Typical max	100	/	4	*	3	/	0.75	*	1	/	0.5	=	200	74.03
	Mode	95.0	/	9	*	1.5	/	1	*	1	/	1	=	15.83	1.08
	Arithmetic mean	76.4	/	8.9	*	1.6	/	2.3	*	0.82	/	2.4	=	2.01	6.63
Weighted average (Barton, 1993)		88.5	/	8.1	*	1.9	/	1.8	*	0.9	/	1.5	=	7.08	
Geometric mean (Sing and Goel, 1999)		$= (Q_{min} * Q_{max})^{0.5} = (0.004 * 200)^{0.5}$											=	0.94	
Monte Carlo Simulation	Standard Deviation	26.6		2.7		0.5		2.6		0.2		2.1			7.52
	Coefficient Of Variation (COV)	35%		30%		32%		113%		24%		88%			113%
Note: A weighted average for Q-input parameter=10% * poorest value + 60% * most frequent value + 30% * best value; The arithmetic mean, standard deviation are estimated in the @RISK program.															

Traditionally, an interval analysis based on the statistics obtained from the Q-histogram logging in the site investigation stage is used to estimate the Q value. Table 4.3 compares the statistics of the Q value calculated from different methods. The interval analysis results show that the Q value is in the range of 0.004-200, from "exceptionally poor" to "exceptionally good", based on the rock mass classification. The arithmetic mean and mode (most frequent value) of the Q value is also calculated directly by substituting the mean and mode of all the Q-parameters into Eq. (2.1), giving mean and mode values of 2.01 and 15.83, respectively. For the derivation of the typical min and max of the output Q value, the extreme values are selected for input parameters, and it is based on the assumption that the numerators for all the input parameters are achieved at the maximum (or minimum) values while at the same time the denominators are achieved at the minimum (or maximum) values. In other words, all the numerators (or denominators) are assumed perfectly positively correlated while perfectly negative correlations are assumed between numerators and denominators. Similarly, for the derivation of mode and mean of the Q value, the respective mode and mean values for each input Q-parameter are used. This is assumed that the mode and mean values for all the Q-parameters take place simultaneously. These idealized assumptions are not logical and rarely met in practice. Clearly, these derivation processes using the interval analysis do not realistically reflect the relationship among the input parameters in the Q-system and the derived range is relatively large.

By contrast, the Monte Carlo simulated Q value has a much narrower range (0.013-74.03) with a mean and mode of 6.63 and 1.08, respectively, as shown in Figure 4.4. The standard deviation and the arithmetic mean were obtained for each Q-parameter and the overall Q value in the @RISK program. The coefficient of variation (COV), a dimensionless measure of uncertainty and defined as the quotient between the standard deviation and the mean, was also obtained for the Q-parameters and the Q value in Table 4.3. To ensure the selection of representative values for the Q-parameters, Barton (1993) proposed a method to calculate the weighted average value for each Q-parameter. First, the weighted average value, calculated by adding the 10% poorest, 60% most typical and 30% best values, is obtained for each Q-parameter. Then, the weighted average Q value is obtained by substituting the weighted average values of all the Q-parameters into Eq. (2.1). The calculated weighted average Q value is 7.08, which is close to the mean (6.63) of the Monte Carlo simulation Q value. Singh and Goel (1999) also suggested that a geometric mean obtained from the minimum and maximum values can be considered as a representative Q value,

which would reduce the bias and generate confidence among users. The geometric mean of the Q value, briefly calculated as the square root of the product between the minimum and maximum Q values, Q_{min} and Q_{max}, can be assumed in the design calculations (Singh and Goel, 1999). In this case study, the minimum (0.004) and maximum (200) values, calculated from the interval analysis results, are taken as Q_{min} and Q_{max}, respectively. The calculated geometric mean of the Q value is 0.94, which is smaller than the mean values calculated by other methods.

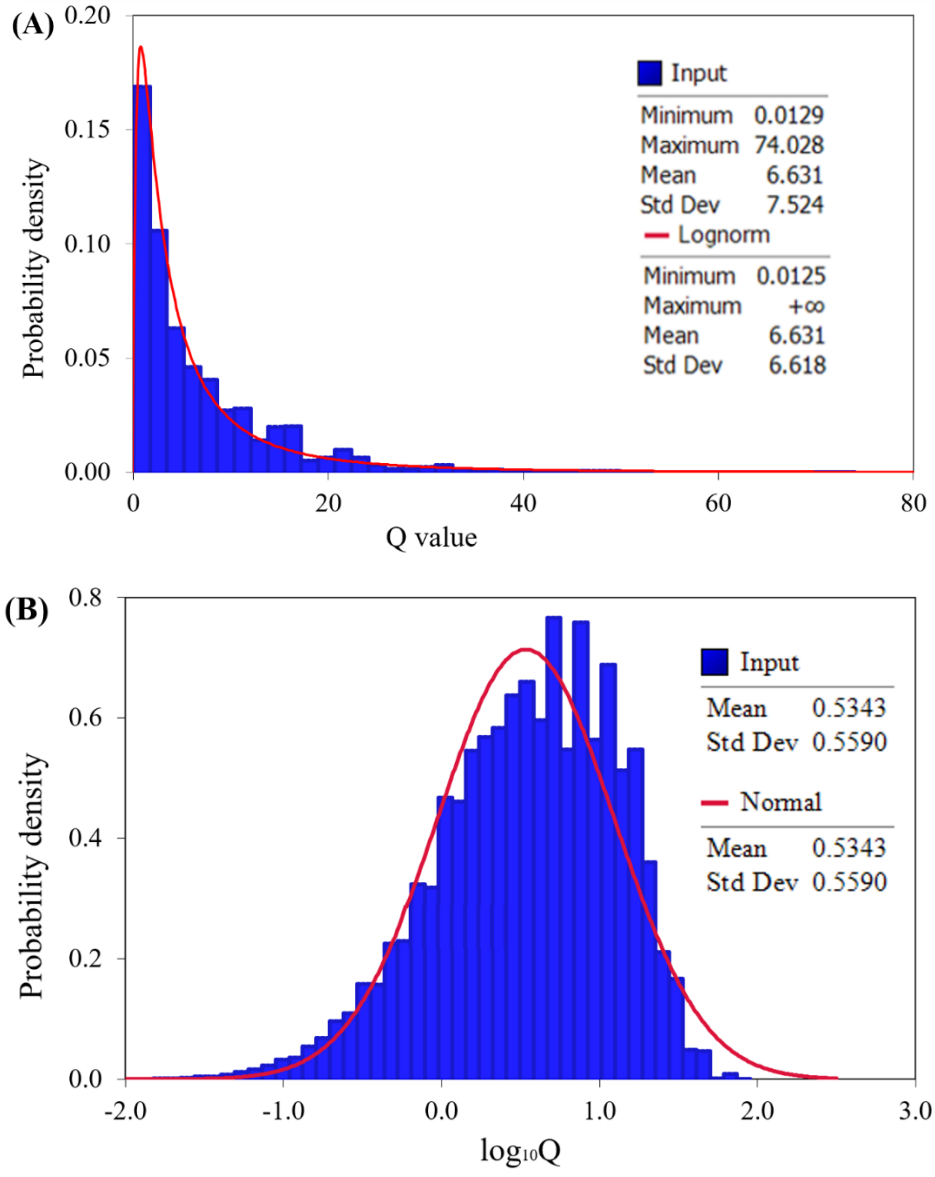

Figure 4.4 Statistical distribution of Monte Carlo simulated Q value and distribution fit. (A) Q value; (B) logarithm of Q value on the base of 10

From the results, the Monte Carlo simulation is superior to the interval analysis in estimating the statistics of the Q value. The MCS technique can more realistically account for the correlations, e.g. RQD and J_n, among input parameters and provides the full probability distribution and a much narrower range for the Q value compared with the interval analysis method. The probability that the Q value would be less than a certain value or in a certain interval could be determined from the PDF or CDF of the Monte Carlo-simulated Q value. By contrast, the interval analysis only produces an interval that provides little information with which to make an engineering design decision, and the uncertainty is too large to make a subjective judgment (Bedi, 2013). In addition, the statistics of the Q value calculated using the MCS are more reliable than those from the interval analysis. The statistics (min, max, arithmetic mean, standard deviation, mode, and median) of the Monte Carlo simulation Q value were obtained based on a larger number (10,000 in this case) of generated samples during the MCS process. In contrast, in the interval analysis the mean and mode of the Q value are directly calculated from the mean and mode of all the input parameters. In the calculation of the mean Q value during the MCS process, the effect of the standard deviations of the Q-parameters has been taken into account. By contrast, this effect is neglected in the interval analysis and may lead to some inaccuracies. Table 4.3 also shows that the calculated mode (15.83) is much larger than the arithmetic mean (2.01) in the interval analysis, while the mode (1.08) is smaller than the mean (6.63) in the Monte Carlo simulation results. According to the lognormality of the Q value distribution, the mode should be smaller than the arithmetic mean. In this sense, the Monte Carlo simulation results reflect the characteristics of a lognormal distribution for the Q value. Furthermore, the standard deviation, a measure of spread, can be obtained for each input parameter and the generated Q value in the MCS process. Consequently, the COV can be calculated for each input parameter and enables the quantitative characterization of uncertainty in the input parameters and the effects on the overall Q value.

In addition to the interval analysis, both the geometric mean and the weighted average calculations are deterministic approaches to obtaining a representative value of the Q index. By definition, the geometric mean is calculated as the n_{th} root of the product of n (nonnegative) random variables (Fenton and Griffiths, 2008). However, in the geometric mean calculation method used by Barton (1993), only the extreme values, i.e., the minimum and maximum, are included in the calculation for the geometric mean of the Q value. The result is highly sensitive to the extreme values, and the role that other Q values in the Q value range play in the geometric mean value has

been overlooked. A geometric mean Q value of 0.94 was generated, which greatly underestimated the actual rock mass quality. In comparison to the geometric mean, the weighted average method (Barton, 1993) accounts for the effect of the mode in addition to the extreme values in the input parameters. As a result, the weighted average (7.08) is closer to the mean (6.63) of the Monte Carlo simulation Q value. However, both the geometric mean and weighted average methods do not provide the full probability distribution of the Q value and do not reflect the uncertainties involved. Thus, it is also inferior to the MCS method in probabilistically estimating the Q value.

Probability distributions of the rock mass properties and responses

Table 4.4 lists the Q-based empirical relationships for estimating the rock mass properties and responses for the Shimizu tunnel case study. There are two approaches for estimating the rock mass properties from the Q value, i.e., the independent and normalized estimation approaches (Vásárhelyi and Kovács, 2017; Zhang, 2017). In the independent approach the rock mass properties can be calculated independently of the intact rock properties, and thus Eqs. (2-4) and (7) belong to this approach. By contrast, the normalized estimation approach indicates the dependence of the rock mass properties on the intact rock properties, and Eqs. (5) and (9) are examples of this approach. The intact rock properties are also included in Table 4.4 for comparison. The UCS and the elastic modulus of the intact rock samples are assumed to follow a normal and a lognormal distribution, respectively, which is based on published data from the literature (Hoek, 1998a; Li and Low, 2010; Sari, 2009; Tiwari et al., 2017). The means and standard deviations of the distributions for the intact rock parameters are estimated using the three sigma rule. The independent estimating approach does not work well in this case study since the estimated elastic modulus values of the rock mass are even larger than those of the intact rock as seen by comparing the mean (10.2) of the intact rock with the mean values calculated by Eqs. (2-4). This is not reasonable and should be discarded. Additionally, the rock mass elastic modulus calculated from Eq. (4.1) shows the minimum value as negative, which is not physically possible. This is because there is approximately an 18% probability that the Q value is smaller than 1, as can be estimated from Figure 4.4, and the logarithms of values less than 1 yield negative results. Recall that Eq. (4.1) in

parameters (e.g., the tunnel wall displacement or the radius of the plastic zone), either an MCS or the point estimate method (PEM) (Rosenblueth, 1981) can be used for the numerical analysis. The RS2 FEM program is capable of performing probabilistic analysis using MCS with both Monte

Carlo and Latin Hypercube sampling as well as PEM techniques. The MCS and PEM techniques can be used to probabilistically characterize the uncertainties in the input parameters of the numerical model.

Table 4.1 applies to cases where the Q value is greater than 1 and is generally for hard rock masses. Thus, great care should be taken to select the appropriate empirical correlations for estimating the rock mass properties.

Additionally, the UCS of the rock mass estimated from Eq. (4.8) using the normalized estimating approach is more reliable than that calculated from Eq. (4.6) using the independent approach, which accounts for the actual "fair" to "poor" quality in the jointed rock mass in this case study. Similarly, Hoek (2007) proposed that estimated rock mass property results are usually more reliable taking into account the intact rock strength. Vásárhelyi and Kovács (2017) also showed that the normalized rock mass properties calculated using the intact rock data usually provide a better regression coefficient. The probabilistic distributions of the rock mass properties estimated by the normalized estimation approach (Vásárhelyi and Kovács, 2017), including the UCS, deformation modulus, cohesion, and friction angle of the rock mass, are shown in Figure 4.5. These probabilistic rock mass properties are then used as the inputs to an empirical estimation of the tunnel displacement without support, (P_i=0), according to the empirical correlations shown in Table 4.4Table 4.4. For the Hoek and Marinos (2000a) approach in Eq. (4.11) and the Duncan Fama (1993) approach in Eq. (4.12), it is assumed that the tunnel is circular and that the in situ stress is hydrostatic. The equivalent radius is approximately 4.83 m for a circular opening based on the same area criterion as the actual area of the top heading. The hydrostatic stress is calculated as the product of the unit weight and the overburden in this case study. For the Barton (2002) approach, the actual span of 18 m for the top heading was used. The tunnel displacements (without support) estimated using these three approaches are compared in Table 4.4. The actual measured displacement obtained from the total stations and extensometers in the top heading excavation was on the order of 10 mm. This displacement value indicates the tunnel displacement after the support was installed and effective, and the pre-convergence before the support installation was not considered. Thus, the measured displacement cannot be directly used to validate the empirically estimated displacement.

Table 4.4 Comparison of the estimated rock mass properties and displacement values using different empirical correlations.

Parameters		Equation No.	Empirical equations	Mean	SD	Min	Max	Distribution
Elastic modulus (GPa)	Intact rock Ei			10.2	1.6	5.4	15	Normal
	Rock mass Em	4.1	$E_m = 25\log Q$	13.3	14.1	-52	50	Lognormal
		4.2	$E_m = 10(Q\frac{\sigma_c}{100})^{\frac{1}{3}}$	12.9	5.22	1.7	38	
		4.3	$E_m = 10^{(15\log Q+40)/40}$	17.6	7.86	1.6	50	
		4.4	$E_m = E_i \exp(0.8625\log Q - 2.875)$	1.01	0.48	0.1	3.5	
UCS (MPa)	Intact rock σci			49	9.66	20	78	Normal
	Rock mass σcm	4.6	$\sigma_{cm} = 7\gamma Q^{\frac{1}{3}} (Q \le 10)$	31	12.33	4.2	83	Lognormal
		4.8	$\sigma_{cm} = \sigma_{ci} \exp(0.6\log Q - 2)$	9.62	3.62	1.4	25	
Displacement (mm)	Hoek and Marinos approach	4.11	$\delta = r_0(0.002 - 0.0025\frac{p_i}{p_0})(\frac{\sigma_{cm}}{p_0})^{(2.4\frac{p_i}{p_0}-2)}$	0.72	0.87	0	15	Lognormal
	Duncan Fama approach	4.12	$u_{ie} = \frac{r_0(1+v)}{E_m}(p_0 - p_i)$	16.4	10.4	2.8	118	
	Barton approach	4.14	$\Delta_v = \frac{SPAN}{100Q}\sqrt{\frac{\sigma_v}{\sigma_{ci}}}$	28.9	79.1	0.4	389	

Fortunately, the simulation results using the UDEC software and the convergence-confinement method by Vardakos et al. (2007) were validated by the measured displacement, and the established UDEC model was considered valid and reliable. The ground characteristic curves generated from the UDEC model showed that the displacement without support is in the range of 30~40 mm.

Figure 4.6 shows the probability distribution of tunnel displacement estimated using the tunnel squeezing problems. In the Duncan Fama model, it is assumed that the surrounding weak rock mass behaves as an elastic-perfectly plastic material with no plastic volume change during failure.

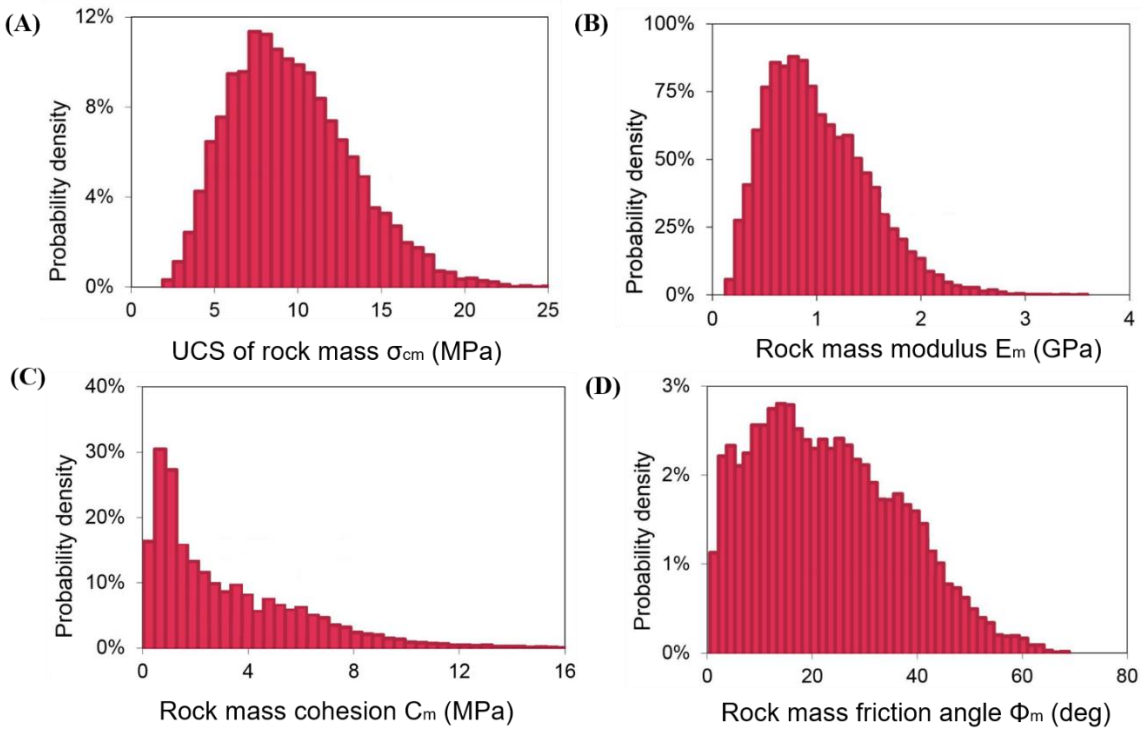

Figure 4.5 Statistical distributions of estimated rock mass properties. (A) UCS; (B) deformation modulus; (C) cohesion; (D) friction angle

According to the derived Q value and rock mass properties, this approach does not fit the case of the Shimizu tunnel. Thus, the Hoek and Marinos approach and the Duncan Fama approach, which work best for weak and very weak rock masses with assumptions of a circular tunnel and hydrostatic stress, are not suitable for estimating tunnel displacement in the current case study. In contrast, the Barton approach, empirically derived from hundreds of case records, uses the actual tunnel span and does not restrict the stress conditions, thus providing a more reliable estimate of tunnel displacement. Therefore, for this case study, the Barton approach performs better for empirically deriving the preliminary estimate of the tunnel displacement, which can be compared with the displacement generated from the detailed analysis using the FEM numerical modeling program.

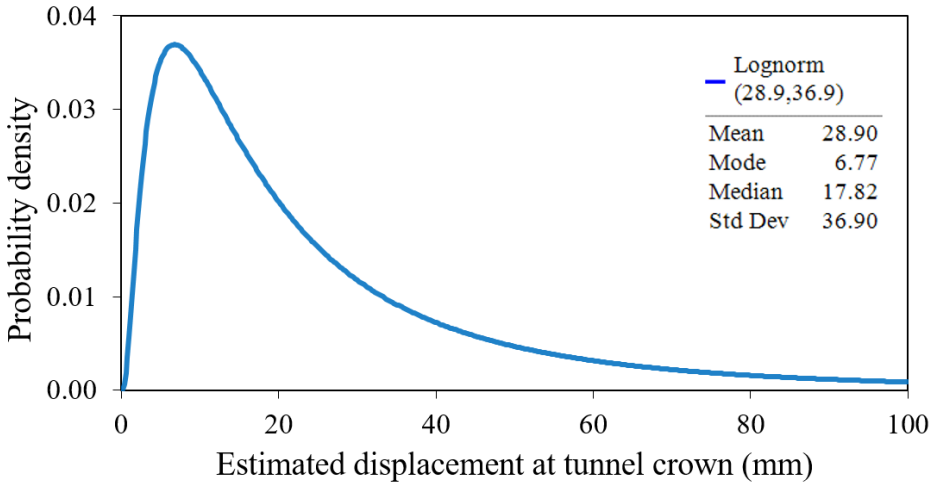

Figure 4.6 Probability distribution of tunnel displacement estimated using the Barton approach

Distribution comparison of rock properties between intact rock and rock mass

The distributions of rock properties, including the UCS, elastic modulus and cohesion, are compared between intact rock and rock mass, as shown in Figure 4.7. Due to the weakening effect of joints, the rock mass properties are smaller than those of intact rock, and the distributions of rock mass are accordingly to the left of the distributions of intact rock.

Due to the limited availability of in-situ rock mass property data in the Shimizu tunnel case, alternatively, the predicted rock mass properties can be compared to back-calculated values from measured or instrumented data in the numerical models for verification. The rock mass modulus value of 1 GPa, which was used in the numerical models in the discrete element modeling by Barton and Chrysanthakis (1996) agrees very well with the mean value (1.01 GPa) of the predicted distribution of rock mass modulus, as marked in Figure 4.7(b). Similarly, as seen in Figure 4.7(c), the cohesion value of 2 MPa for the rock mass, used in UDEC models by Vardakos (2003), is between the mode (1.64 MPa) and median value (2.67 MPa) of the predicted distribution. The cohesion value of 2 MPa is also within the range of one standard deviation of the mean value (0.68~6.16 MPa) and has a high probability of occurrence in the predicted distribution of rock mass cohesion. Thus, the probabilistic estimates of rock mass properties have, to some extent, been verified by the back-calculated values used in the numerical models.

4.4.2 Probabilistic analysis in numerical modeling

The Shimizu tunnel No. 3 is a research tunnel, and instrumentation and measurement were performed accordingly. The displacement data during the heading construction at the section STA

913+65 in the western sector of the tunnel, as can be seen in Figure 4.2, is available, thus the top heading construction at this section will be modeled in the following numerical studies using the FEM RS2 software.

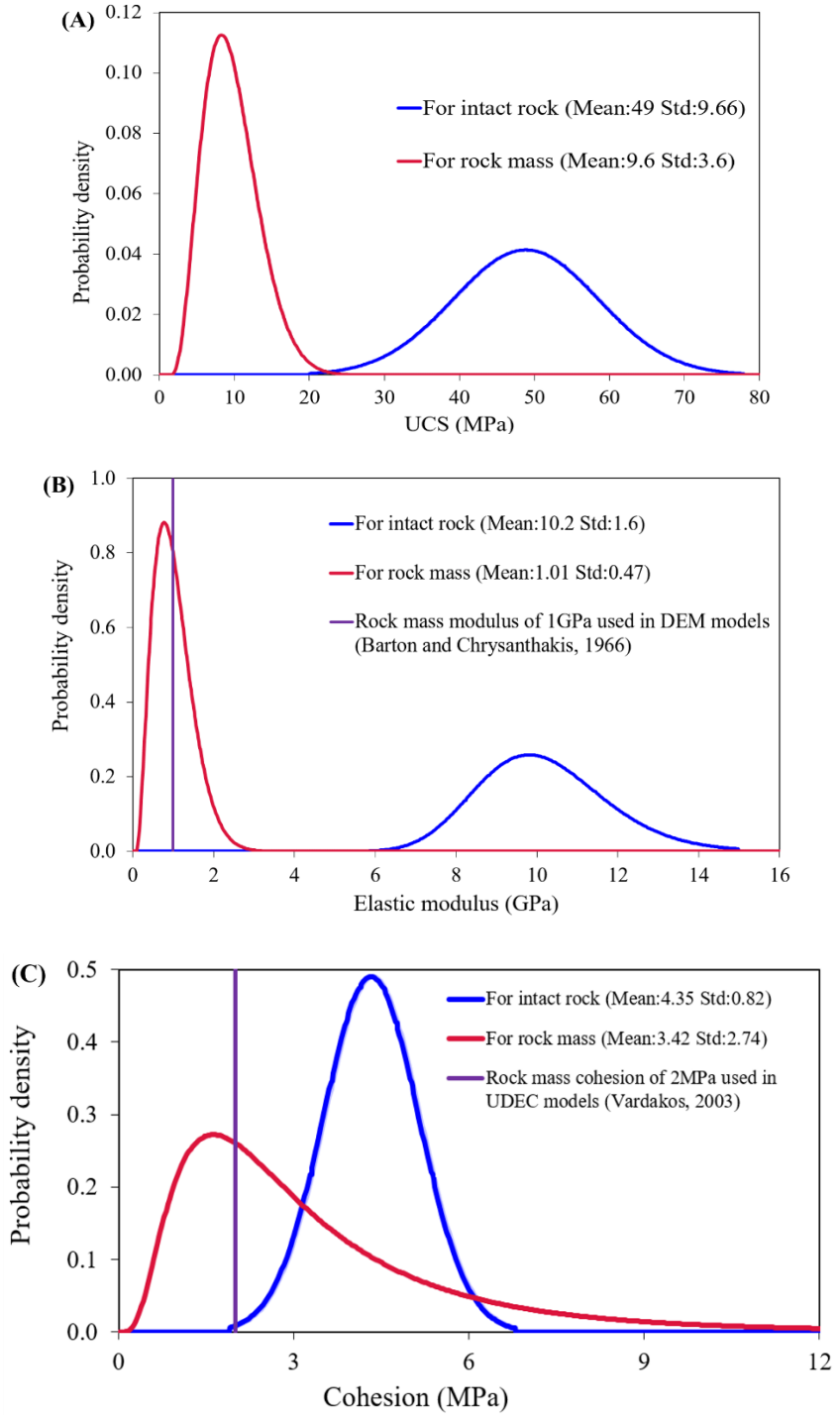

Figure 4.7 Comparison of rock properties between intact rock and rock mass: (A) UCS; (B) elastic modulus; (C) cohesion

It should be noted that the data for actual Q value is not available at the section STA 913+65. However, the rock mass quality data obtained from core logging at the end of the BH1, which is close to the STA 913+65, is available. The Q index is in the range of 1-10 and the independent RMR logging reveals the range of 55-63. This indicates the "fair" rock mass quality at the section based on RMR and Q classifications.

Unsupported tunnel case

The FEM program RS2 was used to conduct the numerical analysis for this case study. Recall that the mode, median and mean for the estimated distribution of the Q value are 1.08, 3.82 and 6.63, respectively. According to the Q-based rock class, the rock mass quality at the western-central sector is mainly "fair" and "fair" to "poor". It is also revealed from the site investigation results that three major joint sets existed in this tunnel area. As seen in Figure 4.5, the estimated rock mass properties using the normalized estimation approach also indicate the fair to poor quality of the jointed rock mass in this tunnel area. Based on these rock mass properties and characteristics, according to the descriptions and guidelines on post-failure behavior or rock mass given by Hoek and Brown (1997), it is reasonable to assume that the surrounding rock mass followed the Mohr-Coulomb failure criterion and that the material behaved in an elastic perfectly-plastic way. The tensile strength of the intact rock was not available in this case study; thus, the following equation was used to estimate the tensile strength (Hoek and Brown, 2018):

$$\frac{\sigma_c}{|\sigma_t|} = 0.81m_i + 7 \tag{4.18}$$

where σ_c is the UCS of the rock mass; σ_t is the tensile strength of the intact rock; m_i is the material constant for the intact rock, related to the rock type and texture.

The UCS of the rock mass has been estimated using Eq. (4.8), and its distribution is shown in Figure 4.5. The Shimizu tunnel was mainly excavated through weathered soft sandstone, and the m_i value was assumed to follow a normal distribution with a mean of 17 and a standard deviation of 4 (Tiwari et al., 2017). Therefore, the probability distribution of the intact rock tensile strength can be characterized according to Eq. (4.18). The tensile strength of rock mass can be calculated as follows (Hoek et al., 2002):

$$\sigma_{tm} = -\frac{s\sigma_c}{m_b} \tag{4.19}$$

where σ_{tm} is the tensile strength of rock mass; s is the material constant of rock mass; m_b is the reduced (rock mass) value of the material constant m_i.

According to Tiwari et al. (2017), the mean values for s and m_b are 0.0029 and 2.57, respectively in the Shimizu tunnel case. Thus, the calculated tensile strength of rock mass is about 0.055 MPa, which is used as the input in the FEM RS2 model. In the RS2 model, the rock mass properties, including the deformation modulus, cohesion and friction angle, can be treated as random variables. The statistical values of the probabilistic rock mass parameters were estimated from the Monte Carlo simulation results based on the Q-based empirical correlations. For the deterministic rock mass properties, the means were taken as the representative input values. In this Shimizu tunnel case, the deformation modulus, cohesion and friction angle of the rock mass were taken as the probabilistic inputs while the deterministic tensile strength and Poisson's ratio were used in the RS2 model. In addition, the stress variability was also considered in this model. Stresses have been assumed to be normally distributed, and the COV of 25% was used by researchers based on the published literature (Cai, 2011; Hadjigeorgiou and Harrison, 2011; Lü et al., 2013; Şen and Sadagah, 2002). In this Shimizu tunnel case, taking the near surface excavation into account, the gravity field stress was used in the RS2 model, which changes linearly with depth as measured from the actual ground surface. Due to the limited information of the in-situ stress in the Shimizu tunnel case, the horizontal-to-vertical stress ratio was assumed to follow a normal distribution with a mean of 0.83 and a COV of 25% in the model. The inputs for the RS2 model are summarized in Table 4.5. The FEM mesh used in the model is displayed in Figure 4.8. No joint pattern was explicitly modeled in the mesh, despite the existence of three joint sets. This is because the deteriorating effect of the joints had already been taken into account in the estimation of the Q-based rock mass properties. Singh and Goel (1999) also suggested that double-counting the effect of the joints should be avoided. The joints should not be considered in the analysis if these have been accounted for in the classification and estimation of the rock mass properties.

The interpreted crown displacement of the unsupported tunnel in the PEM-based probabilistic analysis from the RS2 program is depicted in Figure 4.8, in which uncertainties in both rock mass properties and in-situ stress are considered The maximum displacement at the crown occurs at the point labeled "Crown C" and has a mean of 38.8 mm which agrees well with the displacement predicted by the previously published UDEC model (Vardakos et al., 2007) and the empirically derived displacement of 28.9 mm estimated using the Barton approach. The yield zone,

represented by sheared or tensioned elements in Figure 4.8, were developed mainly in the corner of the unsupported heading, and no yielded element was observed in the crown.

To investigate the effects of uncertainty in the rock mass properties and in situ stress in the crown displacement, deterministic and probabilistic analyses were performed in RS2 using PEM and MCS modeling. For the deterministic scenarios, only single mean values of the rock mass properties and in situ stress were used. For the probabilistic scenarios, uncertain input parameters, such as the rock mass properties and in situ stress, were defined based on prescribed distributions. In the PEM model, the mean and standard deviation of the probabilistic parameters were used as model inputs. In the MCS model in RS2, the best-fit distribution type, mean, standard deviation, and min and max of the probabilistic parameters were required as model inputs. Note that for a normally distributed parameter, the max and min can be estimated at 3 standard deviations above and below the mean value according to the three-sigma rule (Duncan, 2000). The Poisson's ratio and the horizontal-to-vertical stress ratio, in this Shimizu tunnel case, were assumed normally distributed, and the max and min values were estimated using the three-sigma rule. For the MCS model in RS2, the Latin hypercube sampling was applied, and 1,000 iterations were performed.

Table 4.5 Input in the FEM RS2 model for probabilistic analysis

Deterministic/Probabilistic	Input parameters		Mean	SD	COV
Probabilistic	Rock mass properties	Deformation modulus/GPa	1.01	0.47	47%
		Cohesion/MPa	3.42	2.74	80%
		Friction angle/degree	38.4	18	47%
Deterministic		Tensile strength/MPa	0.055	0	0%
		Poisson's ratio	0.3	0	0%
Probabilistic	In-situ stress	Stress ratio	0.83	0.21	25%

Table 4.6 compares the displacements at different crown points using both the deterministic and probabilistic modeling methods in RS2. The advantage of the probabilistic analysis over the deterministic analysis is clearly shown in Table 4.6. The standard deviation and COV can be obtained in the probabilistic analysis scenarios, while in the deterministic analysis of Scenario 1, only a single displacement value was obtained at certain crown points. The results also show that the uncertainty in the rock mass properties has a greater influence on the statistical displacements

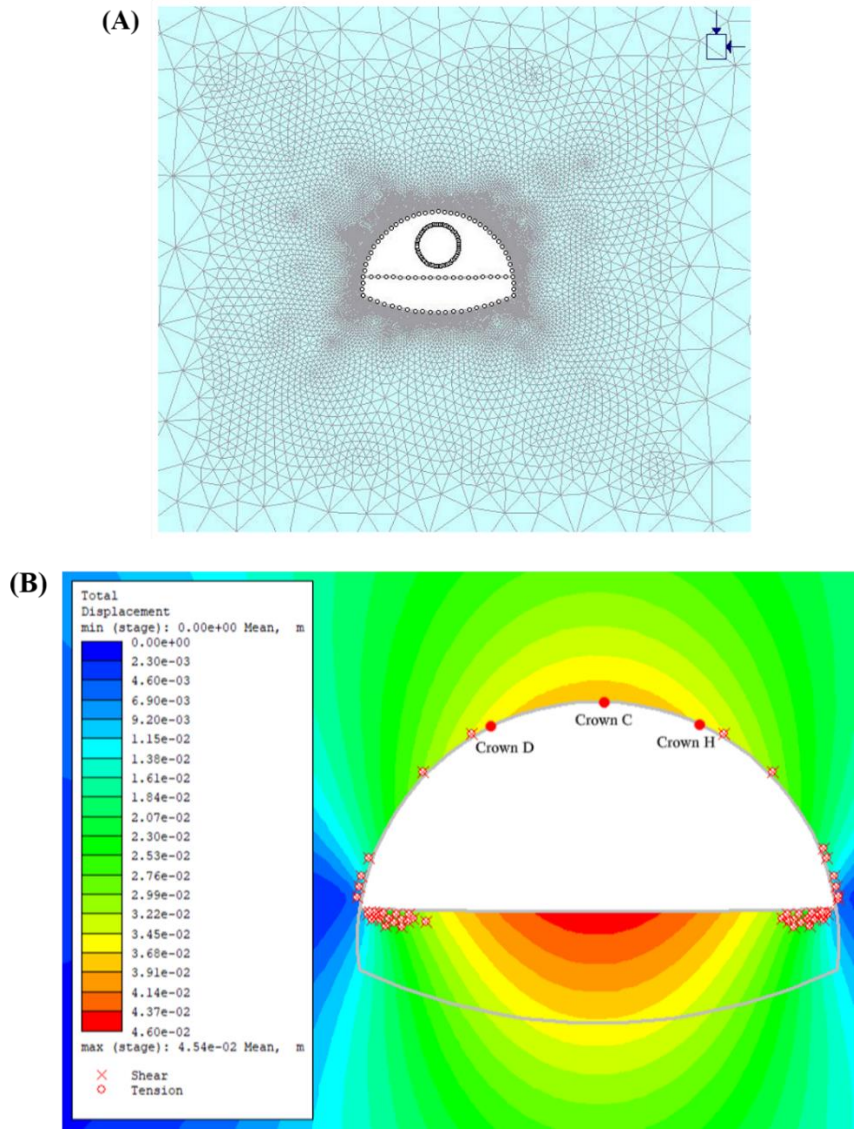

Figure 4.8 FEM mesh and total displacement contour (without support) in RS2: (A) FEM mesh; (B) displacement contour after top heading excavation

than the in-situ stress does. This indicates that the tunnel displacement is more sensitive to the uncertainties in the rock mass properties than those in the in-situ stress in this case study. If the in situ stress is deterministic, the probabilistic rock mass properties generate larger mean displacements (38.7 mm for the PEM method in Scenario 4 and 40.5 mm for the MCS in Scenario 5) than the displacement (29.0 mm) obtained in the deterministic case in Scenario 1. Similar results can be obtained by comparing the generated mean displacements in Scenarios 2 and 6, Scenarios 3 and 7 when the in situ stress is probabilistic. In contrast, the statistical displacement is not sensitive to the uncertainty in the in situ stress. This can be shown when Scenarios 1 and 2 are

compared in the case of deterministic rock mass properties and when Scenarios 4 and 6 are contrasted in the case of probabilistic rock mass properties.

It is also revealed in Table 4.6 that the crown displacement derived from the MCS model has greater variation, described by the generated COV, than that calculated by the PEM model. This may be attributed to the differences in the distribution types and sampling mechanisms used in these two probabilistic modeling methods. In the PEM model in Scenario 6, three input parameters, the rock mass deformation modulus, Poisson's ratio, and in situ stress, are assumed to be normally distributed, and only 8 (i.e., 2^3) values were sampled at one standard deviation above and below the mean for each input parameter. In contrast, in the MCS model, the actual lognormal distribution for the rock mass deformation modulus was used. A total of 1000 values have been sampled across the parameter range, and the distribution tails are well represented during the MCS process. The importance of distribution types and distribution tails has been reported by Jimenez and Sitar (2009). The use of the actual distribution form and the sampled values from the tail distribution may contribute to the greater variation of tunnel displacement generated by the MCS model. However, the computation effort required by the MCS model is much greater than that required by the PEM model in this case study. The results from Table 4.6 also show that the displacements at Crown points D and H are the same, which may be due to the similar stress conditions at these two symmetrical points on the tunnel crown. Recall that the joint sets were not explicitly modeled in the study, and this may also contribute to the same displacements which are shown at Crown points D and H.

Supported tunnel case

In practice, during the construction of the section STA 913+65, the standard support, including steel beams, shotcrete and rock bolts, was used as the primary support. The standard support was selected for CI class (corresponding to Q=4~10) based on the Japanese highway rock mass classification systems. The support system used in the tunnel section is summarized in Table 4.7. According to Vardakos (2003), the rock bolts were assumed to be installed at the 50% relaxation in order to consider the elastic displacement occurred before the support, while beam and shotcrete supports were installed at the 65% relaxation. The PEM sampling was used in the RS2 model to perform the probabilistic deformation analysis with the prescribed support, designated as Scenario 10 in Table 4.6. Figure 4.9 illustrates the prescribed tunnel support pattern and tunnel displacement contour with support. As summarized in Table 4.6, the displacement at

Table 4.6 Summary of tunnel crown displacement in different scenarios

Support scheme	Input parameters		Modeling Method	Scenario	Displacement (mm)								
					Point C			Point D			Point H		
	Rock mass properties	In-situ stress			Mean	SD	COV	Mean	SD	COV	Mean	SD	COV
Numerical calculation without support	Deterministic	Deterministic	Deterministic	1	29	0	0	25.1	0	0	25.1	0	0
		Probabilistic	PEM	2	29	0.98	3%	25.2	0.1	0.4%	25.2	0.1	0.4%
			MCS	3	29	0.689	2%	25.2	0.11	0.4%	25.2	0.11	0.4%
	Probabilistic	Deterministic	PEM	4	38.7	19.6	51%	33.9	17.4	51%	33.9	17.4	51%
			MCS	5	40.5	25.1	62%	35.4	21.9	62%	35.4	22.0	62%
		Probabilistic	PEM	6	38.8	19	49%	34.1	16.9	50%	34.1	16.9	50%
			MCS	7	40.5	24.8	61%	35.6	21.9	62%	35.6	21.9	62%
	UDEC calculation results by Vardakos et al., (2007)			8	30~40	N/A							
Empirical results from the Barton approach (Eq. 4.14)				9	28.9	36.9	128%	N/A					
With support	Probabilistic	Probabilistic	PEM	10	19.1	9.08	48%	15.7	7.44	47%	15.7	7.44	47%
	Actually measured value			11	11.5	N/A		13	N/A		12	N/A	

Crown C has a mean of 19.1 mm and an SD value of 9.1 mm while the displacement at Crown D and H are similar, with a mean of 15.7 mm and an SD value of 7.4 mm. The actually measured displacement value at these crown points are also included.

Table 4.7 Standard support system used in the section STA 913+65

Sprayed concrete lining		Steel arch		Rock bolts		
UCS (MPa)	Thickness (cm)	Type	Spacing (m)	Tensile capacity (MN)	Length (m)	Circumferential spacing (m)
17.6	20	H200	1.5	0.176	6	1.2

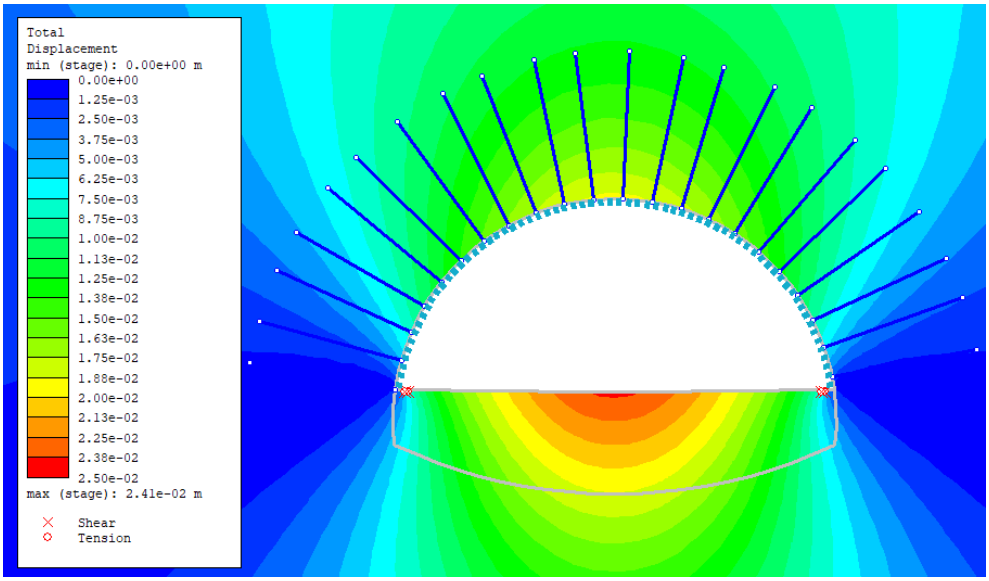

Figure 4.9 The support scheme and PEM-based displacement contour of the supported tunnel.

The predicted and actually measured displacement at tunnel crown points are compared in Table 4.6. The deterministic and PEM-based probabilistic predicted tunnel displacement before support are also included for comparison. The Crown C and D points are symmetrical, and the predicted and actually measured displacement values at these two points are almost the same, so only the Crown C case is demonstrated. The predicted tunnel displacement is lognormally distributed, consistent with the results obtained by (Hoek, 1998a). It is clearly that the tunnel displacement values, both mean and SD values, reduce significantly with the tunnel support installed. The actually measured displacements are single values at tunnel crown points, as marked in Figure 4.10. At the Crown C point, the deterministic measured value (11.5 mm) is close to the mode (14 mm) and within the range of one standard deviation of the mean (10~28.2 mm) in the PDF of the predicted tunnel displacement after support using RS2. The measured displacement

value (11.5 mm) at the Crown C point is also between the mode (7 mm) and median (18 mm) and has a high probability of occurrence in the PDF of tunnel displacement estimated using the Barton approach. Similar case is also observed at the Crown D. This indicates that the actual measurement values generally agree well with the mean or mode of the predicted displacement distribution. Thus, the predicted displacement distributions obtained using the PEM sampling in the RS2 model and the Barton approach are reasonably accurate and can provide possible range and dispersion in addition to the best estimate of tunnel displacement.

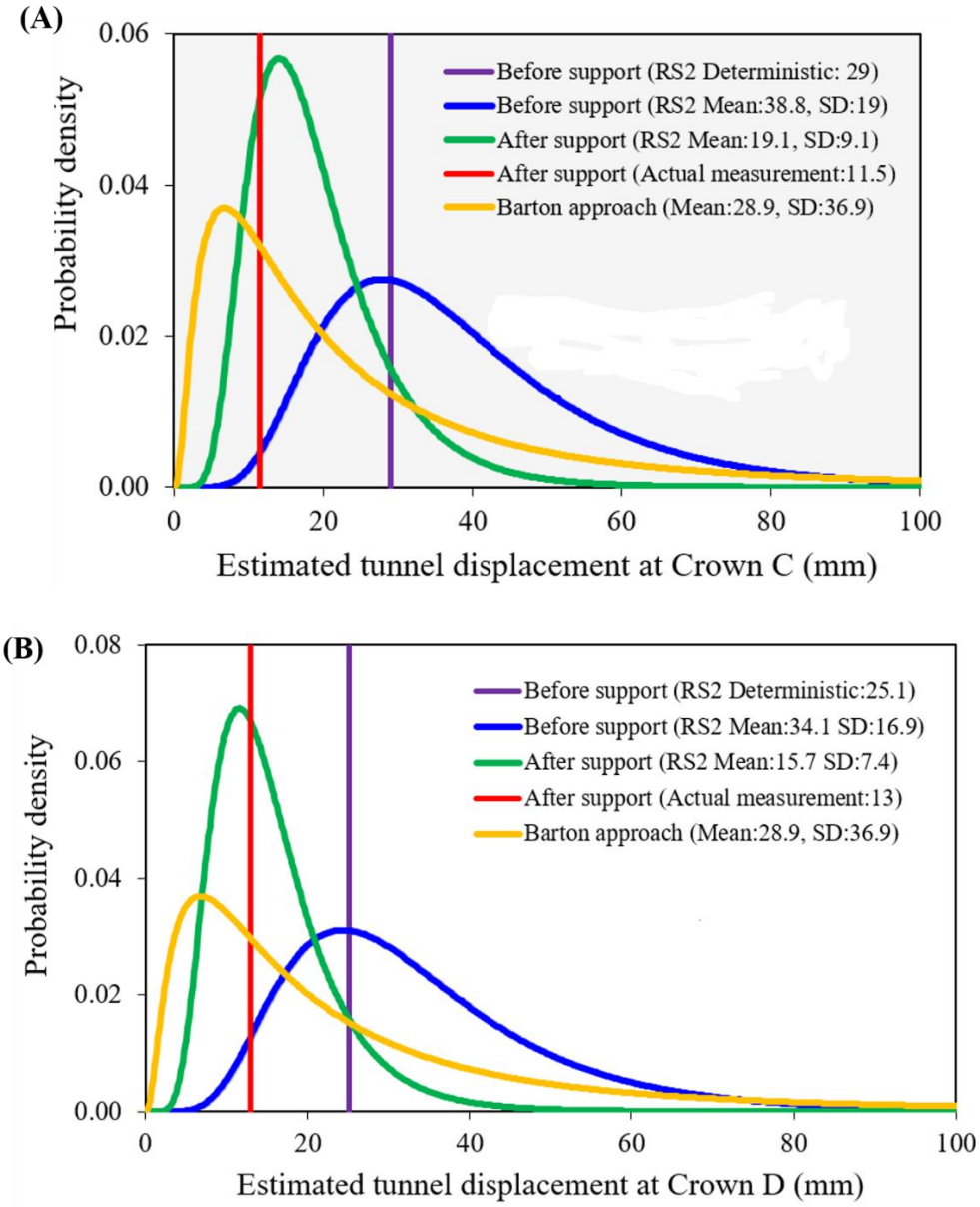

Figure 4.10 Distribution of displacements at the tunnel crown. (A) at Crown C point; (B) at Crown D point

4.4.3 Probabilistic sensitivity analysis

Sensitivity analysis has also been carried out during the MCS of the Q value in the @RISK program to examine the impact of the Q-parameters. Figure 4.11 depicts the tornado graphs for the different ranking techniques used in the Shimizu tunnel case study. In general, the results show that the SRF, J_a and RQD parameters have the most impact on the Q value, while the J_n, J_r, and J_w parameters are less important. The regression coefficient and the contribution to variance tornado graphs in Figure 4.11 (a) and (c) share the same rankings because both graphs are derived from the regression analysis. Figure 4.12 illustrates the spider graph generated in the @RISK program. The changes in the mean of the Q value relative to the changes in the values of the input parameters are shown. The mean Q value increases as RQD, J_r, and J_w increase but declines with increases in J_n, J_a and SRF. The spider graph provides similar sensitivity analysis results compared with the tornado graph by displaying the effect on the output mean. The input parameters J_a, SRF, and RQD have a greater impact on the Q value, and this is also obviously reflected in the spider graph because the rates of change for these parameters are larger compared to other Q-parameters.

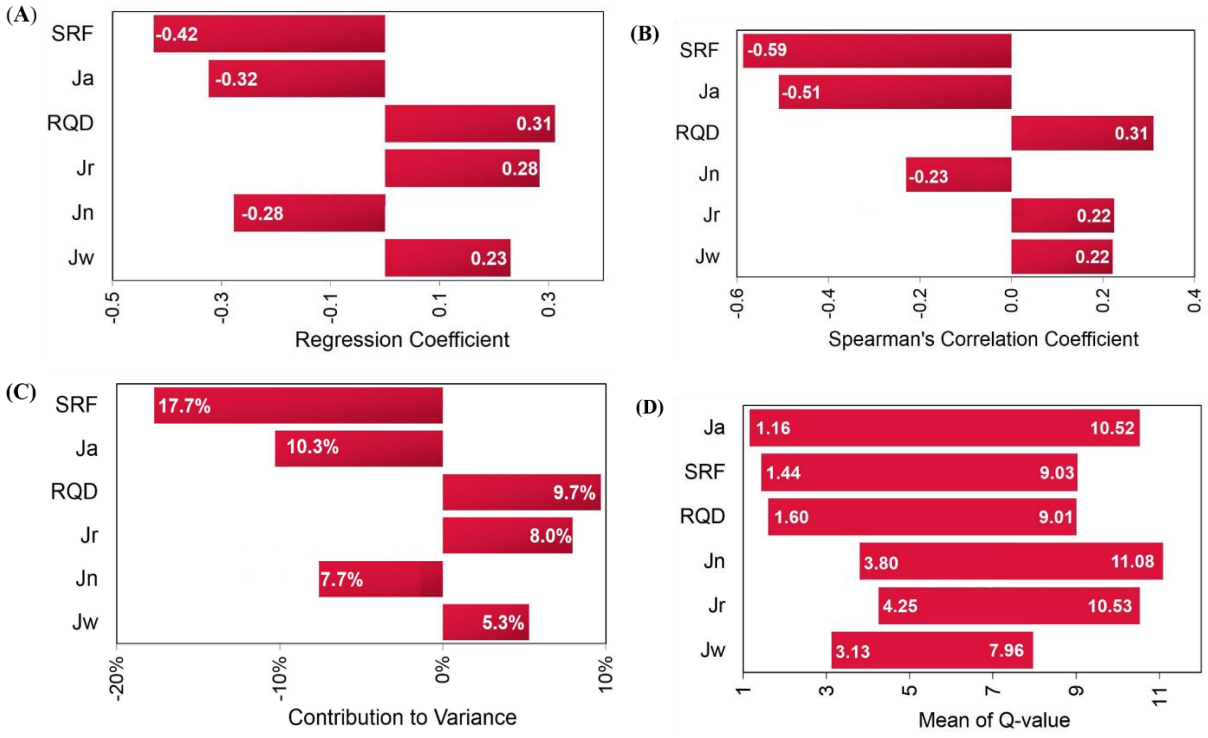

Figure 4.11 Rank of the relative importance of Q-parameters based on different ranking criteria: (A) ranked by regression coefficient; (B) ranked by Spearman's correlation coefficient; (C) ranked by contribution to variance; (D) ranked by effect on output mean

Traditionally, one-way sensitivity analysis is used to investigate the impact of the input parameters on the output by changing one input parameter while keeping the other parameters constant. The sensitivity index (SI) is a measure of the impact that the input parameters have on the output variable in the one-way sensitivity analysis, and is calculated as the percentage difference in the output when an input parameter varies across its entire range (Hamby, 1994). The SI can be obtained as follows:

$$SI = \frac{D_{max} - D_{min}}{D_{max}} * 100\% \qquad (4.20)$$

where D_{min} and D_{max} are the minimum and maximum output values, respectively, which result from varying the input over its entire range.

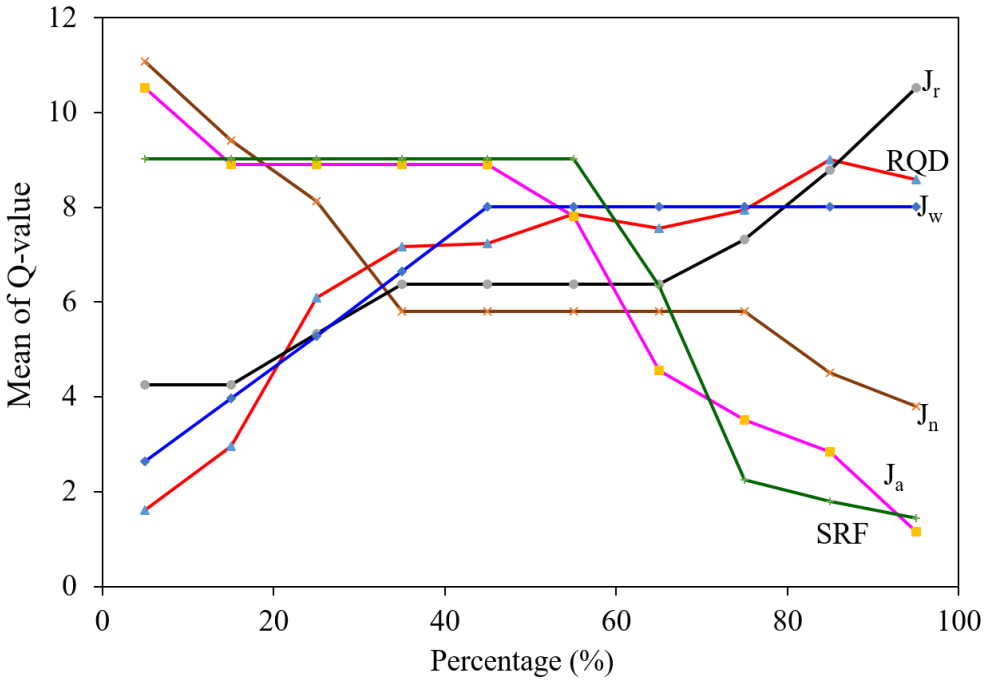

Figure 4.12 Spider graph of the mean of the Q value across the range of the input parameters.

In this case study, the D_{min} and D_{max} are taken as the minimum and maximum Q values calculated, according to Eq. (2.1), by inputting the minimum and maximum values of the specified input parameter while keeping the other five input parameters constant at their mean values. The SI was obtained by substituting the calculated D_{min} and D_{max} in Eq. (4.20) for each input parameter. The greater the SI is for an input parameter, the greater the influence of the input parameter on the output parameter is. Table 4.8 compares the sensitivity analysis results obtained by different ranking techniques. The COV of each Q-parameter is also included since a larger COV value

indicates more variability in the input parameter which may contribute more to the variation in the output Q value. Regarding the rank of relative importance, the smaller the rank number for an input parameter, the more important the parameter. Despite minor differences in the ranking results obtained by different ranking techniques, in general, the results show that the SRF, J_a and RQD are more important than the J_n, J_r, and J_w.

Table 4.8 Sensitivity analysis results using different ranking methods.

Q-parameter	Relative importance ranked by different methods				
	COV	Sensitivity index	Regression coefficient	Spearman correlation coefficient	Effect on output mean
RQD	34.8% (3)	90% (3)	0.31 (3)	0.31 (3)	7.41 (3)
J_n	30.7% (5)	73.3% (4)	-0.285 (4)	-0.23 (4)	7.28 (4)
J_r	31.3% (4)	66.7% (5)	-0.281 (5)	0.226 (5)	6.28 (5)
J_a	113% (1)	92.5% (2)	-0.32 (2)	-0.51 (2)	9.36 (1)
J_w	24.4% (6)	67% (6)	0.23 (6)	0.220 (6)	4.83 (6)
SRF	87.5% (2)	93.3% (1)	-0.42 (1)	-0.59 (1)	7.59 (2)
Note: The number in the parentheses is the ranking					

The aforementioned SI-based sensitivity analysis, which is a one-way sensitivity analysis, fails to account for the distribution form and the probability function of the input parameter and their effects on the sensitivity analysis. In contrast, the sensitivity analysis for the MCS in the @RISK program is capable of performing a multi factor sensitivity analysis, in which the effect of changes in several input parameters can be investigated by simultaneously varying different parameters. In this way, the compounded effect of a given variable can be evaluated. It is thus a probabilistic sensitivity analysis in which probabilistic distributions are utilized to consider the variations of input parameters rather than assigning certain values to input parameters. The calculation of the regression coefficients can reflect the simultaneous random sampling from the input distributions by displaying the sampled input values versus the output values calculated. Additionally, Fatemi et al. (2018) used spider graphs to analyze the sensitivity of the input parameters for measuring TBM performance on the output mean using @Risk software. A sensitivity analysis of the GSI, estimated from different quantitative methods, has also been conducted and used to rank the inputs relative to their contribution to the variance of the output

(Morelli, 2015). In a rock tunnel case study, the probabilistic input parameters in the Q-system were also ranked by their effect on the output mean, regression coefficient, Spearman correlation coefficient and contribution to variance using the @RISK program (Lu et al., 2018a).

A sensitivity analysis is a useful tool to characterize the relationship between the input parameters and the output parameters as well as identify the most influential input parameters. However, in ground characterization and rock mass classification, sensitivity analyses of geological parameters are not adequately conducted. Instead, it is often assumed that all the geological parameters are equally important, which obviously fails to realistically assess the different impact that input parameters have on output parameters. Thus, it is essential to perform sensitivity analyses on ground parameters in the site investigation stage, especially for complex and challenging ground conditions. It is also beneficial to know which input parameter is the most influential overall to the rock mass quality, so that precautionary measures (e.g., dewatering, grouting, freezing, pre-blasting) can be taken in advance to improve the rock mass quality before excavation. The different ranking techniques in the sensitivity analysis can be used for comparative and checking purposes.

4.4.4 Effects of the correlation between the RQD and J_n

The effect of the negative correlation between the RQD and J_n on the Q value, rock mass properties and the displacement estimated by the Barton approach is shown in Table 4.9. In general, the stronger the negative correlation is between the RQD and J_n, the greater the mean and the variation are, as described by the calculated COV of the output parameters. Wang and Akeju (2016) also reported that the output would be affected to a greater degree by the combination of correlated input parameters. The mean and range of the Q value, rock mass properties and displacement may be underestimated if the negative correlation is not taken into account. The SI was also calculated according to Eq. (4.20) to investigate the sensitivity of the mean and COV of the output parameters to the correlation coefficient, as displayed in the last row in Table 4.9. Regarding the sensitivity indices for all the output parameters, the SI for the displacement is the largest, followed by the SI for cohesion and the Q value, with the smallest SI being that for the deformation modulus and the UCS. This demonstrates that the negative correlation between the RQD and J_n has a greater impact on the displacement, cohesion and the Q value than on the deformation modulus and the UCS. This is related to the empirical correlations on which the output parameters are calculated, as shown in Table 4.1. For example, the displacement estimated by the Barton approach is associated

with the reciprocal of the Q value, while the deformation modulus and UCS are calculated based on the logarithm of the Q value as shown in Table 4.1. Results also show that SI for COV is generally greater than that for the mean, and this is because the SI values are greater (not shown here) for SD than for the mean values. This indicate the dispersion parameter (SD and COV) is more sensitive to the correlation compared to the mean values.

Table 4.9 Effect of the correlation between the RQD and J_n on the Q value, rock mass properties and displacement.

Correlation coefficient between RQD and Jn	Q-value		Rock mass properties						Displacement by Barton approach (mm)	
			UCS (MPa)		Deformation modulus (GPa)		Cohesion (MPa)			
	Mean	COV	Mean	COV	Mean	COV	Mean	COV	Mean	COV
-1	7.09	1.20	9.69	0.39	1.03	0.50	3.68	0.85	36.75	3.79
-0.9	7.08	1.20	9.69	0.39	1.02	0.50	3.67	0.86	36.39	3.39
-0.8	7.07	1.19	9.68	0.39	1.02	0.50	3.63	0.85	34.47	3.24
-0.7	7.01	1.18	9.67	0.39	1.02	0.49	3.61	0.85	34.24	3.29
-0.6	7.00	1.18	9.67	0.39	1.02	0.49	3.59	0.85	33.38	3.04
-0.5	6.97	1.18	9.67	0.39	1.02	0.49	3.57	0.84	33.59	3.30
-0.4	6.90	1.18	9.66	0.39	1.02	0.49	3.52	0.83	33.53	3.50
-0.3	6.86	1.17	9.65	0.38	1.02	0.49	3.50	0.82	31.97	2.73
-0.2	6.77	1.16	9.64	0.38	1.01	0.48	3.47	0.81	31.97	3.23
-0.1	6.66	1.15	9.62	0.38	1.01	0.48	3.44	0.81	29.77	2.84
0	6.63	1.14	9.62	0.37	1.01	0.47	3.40	0.80	30.17	2.93
Sensitivity Index	6.4%	5.2%	0.8%	4.9%	1.5%	5.0%	7.6%	7.1%	19.0%	27.9%

Lanaro and Bäckström (2007) plotted the RQD values against J_n based on field data collected from two boreholes and obtained the negative relation between the RQD and J_n at the Simpevarp site in Sweden. Interdependencies among input parameters were also observed and reported in other rock mass or ground classifications, such as the RQD and discontinuity spacing (Bieniawski, 1989; Priest and Hudson, 1976; Sen and Kazi, 1984); the UCS and discontinuity spacing observed by Hamidi et al. (2010); and the degree of jointing or faulting and the availability of groundwater (Chan, 1981) in a ground classification. Similarly, correlations were also encountered among geological parameters in the field of underground construction, including the cohesion and friction angle of rocks and soils (Baecher and Christian, 2003; Fenton and Griffiths, 2008; Li and Low, 2010; Lumb, 1970; Palmstrom and Stille, 2010), or the UCS and elastic modulus of rocks (Arslan et al., 2008; Deere, 1968; Palchik, 1999) Sari (2009) suggested that distributions in a probabilistic

model will often have to be correlated to ensure that only meaningful scenarios are generated during the model's iterations. For example, a weathered discontinuity may have a wider opening, while a strong rock is expected to have a narrower aperture (Sari, 2009). Leu and Adi (2011) also proposed that it is more realistic to correlate geological parameters in ground classification because one parameter may depend on the status of the other parameters.

Unfortunately, few studies have focused on the correlation among input parameters in rock mass or ground classification. The interdependencies among ground parameters are mostly overlooked, and it is assumed that all the input parameters are independent. However, dependencies among ground parameters can be critical to obtaining proper numerical results in engineering practice, particularly in probabilistic assessments and reliability analyses of geotechnical structures (Baecher and Christian, 2003; Wang and Akeju, 2016; Wang and Aladejare, 2016). The significant effect of correlations between ground parameters on a reliability analysis and probabilistic design in underground construction has been highlighted (Li and Low, 2010; Lü and Low, 2011; Lü et al., 2011). If the correlation between input parameters in a probabilistic analysis is neglected, the estimated probability of failure may be severely underestimated or overestimated and might differ by orders of magnitude (Lü et al., 2012; Wang and Aladejare, 2016). Therefore, it is advisable to account for and appropriately quantify the negative correlation between the RQD and J_n in estimating the probability distribution of the Q value.

4.4.5 Effects of distribution types of Q-parameters

To investigate the effect of the Q-parameters distribution types on the Q value and associated output parameters, different commonly used distribution types have been assigned, based on the relative frequency histogram in Scenario 1, to each Q-parameter. The uniform distribution in Scenario 2, also called the "noninformative priors" distribution, is commonly used when the available information is vague and only the bounds of the parameter are given. This distribution was also used to model all the input parameters in this case. The truncated triangular distribution, for which the typical range definition is adopted from Barton et al. (1974), is used in Scenario 15 and was also used to model each Q-parameter. The minimum and maximum values of the actual histogram data were used as the truncated values. Panthi (2006) used the truncated triangular distribution for the Q-parameters to simulate the rock mass quality Q in tunnels in regions of the Himalayas. In Scenario 16, the best fitting distributions relative to the histogram data for all the Q-parameters were obtained using the distribution fit function in the @RISK

program, the Kumaraswamy distribution for the RQD, triangular distribution for J_n, exponential distribution for J_r, inverse Gaussian distribution for J_a, triangular distribution for J_w and Pareto distribution for the SRF (Palisade Corporation, 2016). The simulation scenarios are shown in Table 4.10 with combinations of different distribution types for the Q-parameters. The statistics for all the assumed distributions, including the minimum, maximum, mean, mode, and standard deviation, are taken from those estimated in the relative frequency histogram for each Q-parameter, as summarized in Table 4.4. All the scenarios were performed simultaneously using the MCS functions in the @RISK program. Latin hypercube sampling was used with a total of 10,000 iterations.

Table 4.10 Effect of the distribution types of the Q-parameters on the Q value, rock mass properties and displacement.

Scenario	Distribution patterns of Q-parameters			Q-value		Rock mass properties						Displacement by Barton approach (mm)	
	RQD	Jr,Ja	Other input parameters			UCS (MPa)		Deformation modulus (GPa)		Cohesion (MPa)			
				Mean	COV	Mean	COV	Mean	COV	Mean	COV	Mean	COV
1	Histogram			6.64	1.13	9.62	0.38	1.01	0.47	3.42	0.81	29	2.57
2	Uniform			0.68	1.77	5.19	0.38	0.42	0.51	1.00	1.01	224	1.49
3	Normal	Lognormal	Triangular	4.38	1.60	8.53	0.38	0.85	0.49	1.74	0.77	43	1.72
4		Normal		1.65	1.16	6.93	0.32	0.73	0.73	1.56	0.74	55	1.24
5		Triangular		1.66	1.26	6.87	0.34	0.62	0.42	1.73	0.76	66	1.27
6	Lognormal	Lognormal		4.26	1.77	8.44	0.37	0.84	0.50	1.74	0.77	35	1.71
7		Normal		1.62	1.12	6.92	0.31	0.74	0.92	1.54	0.72	52	1.03
8		Triangular		1.66	1.27	6.89	0.33	0.62	0.42	1.75	0.77	57	1.09
9	Exponential	Lognormal		4.16	2.36	7.73	0.48	0.75	0.65	1.76	1.36	79	1.50
10		Normal		1.12	1.31	6.12	0.35	0.66	0.87	1.06	0.92	103	1.39
11		Triangular		1.70	1.96	6.31	0.45	0.56	0.59	1.76	1.34	124	1.39
12	Triangular	Lognormal		3.74	1.66	8.17	0.38	0.80	0.50	1.53	0.87	42	1.76
13		Normal		1.62	1.18	6.89	0.32	0.69	0.72	1.53	0.75	57	1.18
14		Triangular		1.46	1.22	6.65	0.33	0.59	0.42	1.53	0.74	68	1.17
15	Truncated Triangular			1.09	1.47	6.04	0.36	0.51	0.46	1.40	0.84	105	1.22
16	Best fit distribution			4.85	1.05	9.12	0.34	0.93	0.42	2.76	0.70	28	2.87

Note: The best distributions for input parameters are Kumaraswamy distribution (RQD), Triangular distribution (Jn), Exponential distribution (Jr), Inverse Gaussian distribution (Ja), Triangular distribution (Jw), and Pareto distribution (SRF).

Table 4.10 compares the generated mean and COV of the output parameters in all the scenarios with different distribution types. The simulation results from Scenarios 12, 6 and 3 are closest to the results from Scenario 1, which were generated by the actual relative frequency histograms. This is because the lognormal distributions, assumed for J_r and J_a in these three scenarios, are approximately closer to the actual histograms than to the other distribution types assumed in other

simulation scenarios. Although the best fit for J_r and J_a is an exponential distribution and an inverse Gaussian distribution, respectively, the lognormal distribution also captures the distribution characteristics of J_r and J_a, as shown in Figure 4.3 (c) and (d). Comparing the results generated in Scenarios 3, 6, 9 and 12, in which J_r and J_a are assumed to be lognormally distributed, the triangular distribution assumption for RQD in Scenario 12 performed best. This is because the distribution of the RQD is negatively skewed, as shown in Figure 4.3 (a), and the negatively skewed triangular distribution can better capture this type of data than the normal or lognormal distribution can. Barton and Grimstad (2014) stated that a lognormally distributed RQD with positive skewness is commonly found in "very poor" rock masses with a Q-range of 0.1−1, while a normally distributed RQD is found in "poor" rock masses with a Q-range of 1−4 and a negatively skewed RQD distribution is found in "fair" to "good" rock masses with a Q-range of 4−40. In the Shimizu case study, the average rock mass quality is "fair" with a mean value of 6.63, and the negatively skewed triangular RQD distribution in Scenario 12 matches better with the actual relative frequency histogram in Figure 4.3(a) than does the positively skewed lognormal distribution in Scenario 6 or the normal distribution in Scenario 3. It is also shown that in Scenario 2, in which all the input parameters are assumed to be uniformly distributed, a much smaller mean and a larger COV is generated than in Scenario 1. This demonstrates that Scenario 2, with a uniform distribution assumption, provides a greatly underestimated mean value with a larger variation. The triangular distribution without truncation in Scenario 14 achieves better results than the triangular distribution with truncations in Scenario 15. The best fit distribution used in Scenario 16 generates results closest to those generated from the actual relative frequency histograms of all the simulation scenarios used in Scenario 1. Thus, it is desirable to assign an appropriate distribution (e.g., best fit distribution) to each input parameter to generate more realistic results for the output parameters.

If a theoretical distribution is well fitted to the empirical frequency data (e.g., the relative frequency histogram), then random samples can be drawn from the fitted distribution in the MCS (Fenton and Griffiths, 2008). A continuous probability distribution function, which has a scientific rationale and is mathematically or computationally tractable, is a useful tool in probabilistic risk analysis for addressing uncertainties and making informed decisions. The advantages of a probability distribution function over a relative frequency histogram are summarized by Fenton and Griffiths (2008): first, the irregularities, commonly encountered in the histogram due to a finite amount of sampled data, are smoothed by fitting a continuous distribution; second, the fitted

distribution can produce values outside the range of the finite sampled data, meaning that the effects of extreme values can also be taken into account; third, the fitted distribution has descriptive statistical parameters while the detailed fluctuations in a histogram will change if the interval sizes are changed; most notably, the fitted distribution also enables making estimations of stochastic model parameters and drawing inferences, which allows one to make probabilistic inferential statements for an entire site where data are limited or not available.

If sufficient data are available, the distribution that best fits the histogram of the data should be selected. However, in rock engineering the subsurface information is often scarce, and only a limited number of samples in limited regions are used for estimating the rock mass quality in the site investigation stage (Fenton and Griffiths, 2008; Langford, 2013). Thus, it may be difficult or inappropriate to obtain the best fit distribution for such insufficient and incomplete frequency data. Fortunately, certain probability distribution models are found to be suitable for explicitly modeling the uncertainty or variability in some geological parameters, as reported by previous studies in the geotechnical literature (Adoko et al., 2013). For example, probabilistic models such as the normal, lognormal and beta distributions have been successfully utilized to describe the variability in rock and soil properties, including the UCS, elastic modulus, cohesion and friction angle based on an extensive literature review and case studies (Ang and Tang, 2007; Baecher and Christian, 2003; Fenton and Griffiths, 2008; Hoek, 1998a; Lacasse and Nadim, 1996; Lumb, 1970; Phoon and Kulhawy, 1999). Therefore, it is advisable to properly assume certain probability distribution types for the input parameters in the Q-system to realistically estimate the probability distribution of the Q value based on published literature and empirical experience. Additionally, the selected distributions should be as simple as possible while still reflecting the basic nature of the variability (Fenton and Griffiths, 2008). In the Shimizu study, the best fit for the RQD is the Kumaraswamy distribution, a Beta-like distribution, but it is not commonly used in geotechnical engineering. Instead, a negatively skewed triangular distribution, despite not being the best fit, matches the histogram data of the RQD well and can be used as an alternative. The triangular distribution of the RQD also generates similar results those of the best fit distribution.

4.5 Conclusions

An MCS-based uncertainty analysis framework for the Q-system has been developed to probabilistically assess the uncertainty in the Q-parameters and its effect on the Q value and

associated rock mass parameters. A case study of the Shimizu highway tunnel was adopted to implement the proposed framework. Based on the analysis and discussion of the obtained results, it is concluded that the MCS-based probabilistic analysis allows for the quantitative characterization of uncertainty and variability in the input parameters and its impact on the output parameters. The probabilistic distribution of the Q value was obtained with the MCS technique based on relative frequency histograms of the input parameters. The MCS-derived Q statistics are more reasonable than the conventional estimation results using the interval analysis. The former can more realistically take into account the correlations in input parameters in the estimation as well as providing the full probabilistic distribution of the Q value, while the estimation in the latter approach is based on assumptions of perfect correlations which are rarely met in practice. Based on the empirical correlations between rock mass parameters and the Q value, probabilistic estimates of the rock mass parameters can be obtained, which can also be used as inputs to numerical models for stress analysis and stability assessment. Caution should be exercised when selecting appropriate empirical correlations during the probabilistic calculation process. In this case study, the empirically estimated probabilistic tunnel displacement, obtained by the Barton approach, generally agreed well with that generated from the probabilistic analysis of the FEM RS2 numerical model with the PEM and MCS sampling techniques.

In addition, the results of the uncertainty analysis of the probabilistic Q-system suggest that the probabilistic sensitivity analysis provides a quantitative ranking of the impact of the input distributions of Q-parameters on the Q value. Different from traditional one-way sensitivity analysis, the probabilistic sensitivity analysis is a multi-factor analysis technique, in which the distributions of input parameters are taken into account and simultaneous variations of all the input parameters are allowed. Probabilistic sensitivity analysis results obtained in the MCS process generally agreed well with those derived from other sensitivity analysis techniques in this case study; the mean and variation of the Q value and the associated rock mass parameters have been underestimated if the negative correlation is not modeled in this case study. For the probabilistic assessment of the Q value and associated rock mass parameters, it is advisable to select appropriate distribution types for uncertain Q-parameters when insufficient input parameter data are available. The selection of proper distributions for input parameters is vital and should be conducted by combining site knowledge, local experience, and professional judgment.

The proposed framework of the MCS-based uncertainty analysis in the probabilistic Q-system provides an approach for systematically assessing the uncertainty in the rock mass quality and its propagation to rock mass characterization and ground response evaluation by applying the MCS technique with appropriate empirical correlations. The probabilistic sensitivity analysis in the MCS process can also be performed to identify the most influential input parameters in conjunction with traditional one-way sensitivity analysis techniques. The framework are helpful in providing insightful information for the probabilistic evaluation of ground responses and rock support performance of underground structures.

CHAPTER 5

RELIABILITY EVALUATION OF STABILITY FOR UNDERGROUND EXCAVATIONS USING AN EMPIRICAL APPROACH

5.1 Abstract

The critical strain concept has been widely used in analytical or numerical approaches to evaluate the stability of underground excavations with a strain-based failure criterion. However, analytical solutions are often based on simplistic assumptions and numerical procedures are generally computationally expensive, in which deterministic critical strain values are often used. To address this issue, reliability assessment using an empirical approach has been performed for the preliminary evaluation on the excavation stability with the First Order Reliability Method (FORM) algorithm. The probabilistic critical strain, which takes into account uncertainties in rock mass parameters, and the tunnel strain empirically estimated based on the rock mass classification Q index were incorporated in the limit state function for reliability evaluation. Monte Carlo simulation was also conducted for comparing the reliability analysis results with that derived from the FORM algorithm. A highway tunnel case study was utilized as an example to perform reliability evaluation on the excavation stability. The probabilistic sensitivity analysis has been carried out to identify the most influential parameter. The effects of the correlation, distribution types and coefficient of variation in input parameters on the reliability have also been investigated. The reliability analysis results show that the tunnel is not expected to experience instability after excavation. The excavation stability has also been evaluated using analytical and numerical approaches, and obtained results were consistent with that derived from the reliability assessment, which has also verified the effectiveness of the reliability-based evaluation on excavation stability using the empirical approach. Thus, reliability assessment using the FORM algorithm with the Q-based empirical approach can be used as a complement to analytical and numerical approaches for the preliminary evaluation of the stability of underground excavations.

5.2 Introduction

Uncertainty is inevitable in engineering geology, and inherent uncertainty in geologic conditions and geotechnical parameters plays a key role in the field of geotechnical engineering, including the construction of underground structures. Evaluation and consideration of uncertainty

have becoming an increasingly important part in the engineering design and construction (Einstein and Baecher, 1982). However, traditional deterministic design methods inadequately deal with the inherent uncertainty and variability, and this may result in over- or under-design of underground structures and associated risks. For example, in the traditional allowable stress design (ASD) approach, only the expected case is discussed and an overall margin of safety is applied. The ASD also does not consider the effects of actual variabilities in load and strength and insufficiently provides the level of site understanding on the probability of failure (Fenton and Griffiths, 2008). Fortunately, a more quantitative and systemic approach with the use of probability, statistics and reliability can provide rational analysis of uncertainty and complement the traditional deterministic approaches (Einstein and Baecher, 1982).

Reliability assessment represents a rational method to describe design risks by directly quantifying uncertainties in input parameters in the design process (Langford, 2013). It is capable of systematically quantifying safety risks and is regarded as a useful tool in solving challenging geotechnical engineering problems subjected to inherent uncertainty and variability (Zhang and Goh, 2018). Reliability approaches also provide a more consistent and complete measure of the risk level since they not only consider the expected case but also offer a measure of design performance based on the reliability index or probability of failure (Langford, 2013). Reliability-based design approaches, including the load resistance factor design within a probabilistic framework, have been widely used in evaluating the reliability and risk level in geotechnical engineering. Despite its benefits, the reliability analysis in the geotechnical engineering field has been focused on surface and gravity-driven geotechnical projects where loads and resistances can be dealt with separately. It has not yet achieved widespread use in the design of underground construction, and this is attributed to the complex ground-support interaction since the system performance is dependent on interdependency among rock loads, deformation and support resistance (Langford, 2013). The load and resistance are difficult to differentiate in underground construction since the rock mass itself both acts both as the load and support resistance. Thus, it is not appropriate to independently separate the loads and resistances in underground construction in a performance function, which is often used to define the acceptance criterion for the system performance. Instead, the limit state function that is defined with respect to a limiting value for rock mass response is generally taken as the performance function. Accordingly, the probability

of failure, which refers to the violation of the limit state, can be calculated as the likelihood of exceeding of a prescribed limit state.

The limit states with regard to the stability evaluation of underground structures can be mainly described by the stress-based failure criteria and strain-based failure criteria. As for the stress-based failure criteria, Li (1990) stated that the in-situ stresses are generally not directly measurable and are converted from the displacement or strain through behavior equations. It was also pointed out that the conversion is normally based on assumptions such as the plane stress condition and Hooke's law, which rarely represents actual in-situ conditions and rock mass properties. In addition, the strength parameters of rock masses in the stress-based failure criteria are often difficult to obtain since the in-situ tests are expensive and time-consuming (Hoek, 2007). Moreover, Sakurai (2017) presented that the stress-based yielding criteria, which are used in elasto-plastic analysis for stability assessment of geo-structures, lead to calculated stress levels that never go beyond the yield point. As a result, the stress keeps constant while the strain increase beyond the yielding point till failure, which implies the failure criteria to some extent should be defined in terms of strain. It is also stated that the apparent factor of safety, defined in terms of stress, will always be one as the stress state in a plastic zone cannot exceed the yield stress point. In these scenarios, however, tunnels may still be adequately stable as the plastic zone or failure region is always surrounded by stable elastic zone (Sakurai, 2017). In contrast, the advantages of strain-based failure criteria have been summarized over the stress-based failure criteria (Gaede et al., 2014): the consideration of both elastic and inelastic strain, the direct and observable effects instead of inferred effects, and the ability of modeling complete stress-strain curves. The displacement or percent strain is also more practical and easier to measure in underground construction. Based on these reasons, strain-based failure criteria are of particular interests and have been widely applied in the underground design and construction (Daraei and Zare, 2018; Fujii et al., 1998; Hoek, 1998b; Li and Villaescusa, 2005; Li et al., 2000; Li, 1990; Sakurai, 1981; Singh et al., 2007; Stacey, 1981).

In recent decades, numerous researchers have employed limit state functions with strain-based failure criteria using the First Order Reliability Method (FORM) or Monte Carlo simulation (MCS) techniques to evaluate the reliability of underground excavations, and productive results have been achieved (Li and Low, 2010; Liu and Low, 2017; Lü et al., 2012; Lü and Low, 2011; Lü et al., 2011; Song et al., 2016). Among these reliability evaluations, analytical expressions based on the

ground-support interaction in circular tunnels were used to construct the performance function (Li and Low, 2010; Su et al., 2011). However, the analytical solution was basically derived with assumptions of a circular tunnel in isotropic and homogeneous ground subjected to hydrostatic stress with uniform internal support pressure. These assumed conditions in the analytical solution are ideal and seldom met in the practice of underground excavation. Alternatively, numerical procedures with finite element or finite difference models using different algorithms were developed to implicitly approximate the strain-based performance function for the tunnel reliability assessment, including the response surface method (RSM) (Hamrouni et al., 2017; Lü and Low, 2011; Lü et al., 2011; Mollon et al., 2009b, 2010), Regression Method (Basarir, 2008; Goh and Zhang, 2012; Zhang and Goh, 2015; Zhang and Goh, 2012; Zhu et al., 2008), Artificial Neural Network (Adoko et al., 2013; Goh and Zhang, 2012; Lü et al., 2012; Mahdevari and Torabi, 2012; Rafiai and Moosavi, 2012), Support Vector Machine (Tan et al., 2011; Zhao, 2008; Zhao et al., 2014) and Augmented Radial Basis Function (Bai et al., 2012; Fang et al., 2005; Wang et al., 2016). Reliability approaches, including the First Order Second Moment method, Point Estimate Method, FORM and MCS techniques, have been used to perform reliability analysis based on these implicitly constructed performance functions with satisfactory results achieved. It should be noted, however, that the numerical procedures are generally computationally expensive, which requires a great number of numerical experimentations or iterations. Actually, in addition to the analytically or numerically derived performance functions, there are some empirical correlations related to the displacement or percent strain based on collected case histories of underground excavations (Barton, 2002; Barton et al., 1994; Chern et al., 1998a; Chern et al., 1998b; Hoek, 1999; Hoek, 2001; Sakurai, 1983) which are useful in the preliminary evaluation of excavation stability. Nevertheless, few attempts have been made to adopt the empirically derived performance function with the strain-based failure criterion to assess the reliability and risk levels of underground excavations. In addition, in regard to reliability evaluations using both the simplistic analytical solution and sophisticated numerical procedures, as mentioned above, the focus was primarily the illustration of proposed analysis approaches or numerical algorithms, and hypothetical examples with assumed statistical moments of rock mass parameters were mostly used. In other words, few case studies with real statistical data of rock mass properties have been utilized to verify the validity of proposed approaches or algorithms. Moreover, single deterministic

limiting strain values were subjectively determined and used in the strain-based performance functions, and the uncertainties involved were not accounted for.

To address these issues, in this chapter, reliability assessment using the FORM algorithm, which incorporates probabilistic critical strain and the Q-based empirically estimated tunnel strain, has been carried out. The reliability-based assessment allows for the consideration of inherent uncertainties in rock masses and has been applied in the preliminary evaluation of the excavation stability of the Shimizu highway tunnel case study.

5.3 Methodology

5.3.1 Reliability index

Reliability analysis deals with the relation between the loads a system must carry and its capacity to carry those loads (Baecher and Christian, 2003). Hasofer and Lind (1974) proposed an approach known as geometric reliability or the FORM to analyze the reliability of a system. The matrix formulation of the FORM for uncorrelated normal parameters can be found in the literature (Ditlevsen, 1981; Hasofer and Lind, 1974). Low and Tang (1997) proposed a practical approach with the optimization features using the spreadsheet to calculate the reliability index. In this approach, an alternative interpretation of the reliability index is performed based on an expanding ellipsoid in the original space of the basic random variables, and the reliability index can be expressed as (Low and Tang, 1997):

$$\beta = \min_{x \in F} \sqrt{\left(\frac{x_i - \mu_i}{\sigma_i}\right)^T R^{-1} \left(\frac{x_i - \mu_i}{\sigma_i}\right)} \tag{5.1}$$

where x_i is the original normal variable, R is the correlation matrix among input parameters, μ_i and σ_i are the mean and standard deviation of random variable x_i, respectively, and F is the failure domain. For correlated non-normal input parameters, the equivalent normal mean and standard deviation should be used, and the reliability index can be calculated as (Low and Tang, 2004):

$$\beta = \min_{x \in F} \sqrt{\left(\frac{x_i - \mu_i^N}{\sigma_i^N}\right)^T R^{-1} \left(\frac{x_i - \mu_i^N}{\sigma_i^N}\right)} \tag{5.2}$$

where μ_i^{N} and σ_i^{N} are the equivalent normal mean and standard deviation of non-normal random variable x_i, respectively. The equivalent normal mean and standard deviation values for

non-normal random variables can be computed using the Rackwitz and Flessler (1978) two-parameter equivalent normal transformation or other transformation techniques.

In the framework of the FORM algorithm using the spreadsheet, the design point is a point on the boundary (the limit state surface) that separates safe combinations of parametric values from the unsafe combinations. The design point is the most probable failure combination of parametric values (Low, 2008b). In reliability analysis using FORM, the uncertainties and correlation structure of the parameters are represented by a one-standard deviation dispersion ellipsoid centered at the mean-value point, as shown in Figure 5.1. The safety is expressed by a reliability index which is the shortest distance (measured in units of directional standard deviations, *R/r*) from the mean-value point to the most probable failure combination of parameters ("the design point") on the limit state surface (Low, 2018; Low, 2008b). For more information about the constrained optimization approach from the ellipsoidal perspective, the literature (Low, 2018; Low and Tang, 1997, 2007; Low, 2008b; Low and Tang, 2004) can be referred to. Based on the reliability index, the probability of failure can be evaluated by (Baecher and Christian, 2003):

$$p_f \approx 1-\Phi(\beta) \tag{5.3}$$

where p_f is the probability of failure, $\Phi(\cdot)$ is the cumulative distribution function of the standard normal variable.

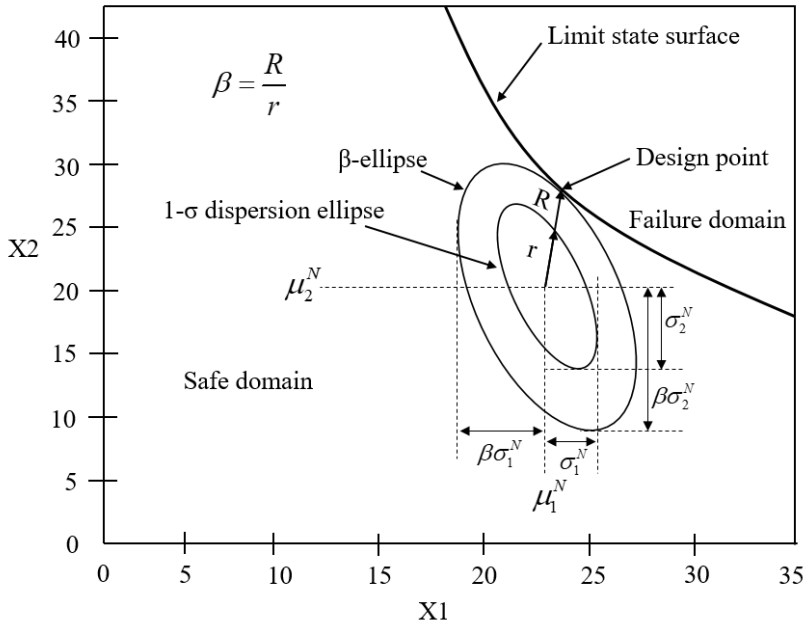

Figure 5.1 Design point and equivalent ellipsoids (modified from Low and Tang, 2004)

A new efficient spreadsheet algorithm for the FORM was proposed and expressed as follows (Low and Tang, 2007):

$$\beta = \min_{x \in F} \sqrt{[n]^T R^{-1} [n]} \tag{5.4}$$

$$n_i = \frac{x_i - \mu_i^N}{\sigma_i^N} = \Phi^{-1}[F(x_i)] \tag{5.5}$$

where n is a column vector of n_i; when the value of n_i is varied during the constrained optimization, the corresponding value of x_i is automatically calculated; F is the non-normal cumulative probability distribution at x_i; $\Phi(n_i)$ is the cumulative distribution function of the standard normal variable n_i.

The reliability index as expressed in Eq. (5.4) can be calculated using the FORM algorithm by the Excel's built-in optimization routine "Solver", subjected to the constraint that the performance function $G(X)=0$, where the x values are calculated from Eq. (5.4), and by automatically changing the values of n_i.

5.3.2 Reliability analysis with the critical strain-based limit state function

The implementation procedures of the critical strain-based reliability analysis of the tunnel using the FORM algorithm are shown as follows:

(1) Establish critical strain-based limit state function

The estimated strain is a function of the Q value using the Barton (2002) estimation approach. Thus, the limit state function can be expressed as follows:

$$G(X) = \varepsilon_C - \varepsilon(Q) \tag{5.6}$$

$$G(X) = \varepsilon_C - \Delta_v / R_0 \tag{5.7}$$

$$\Delta_v = \frac{SPAN}{100Q} \sqrt{\frac{\sigma_v}{\sigma_{ci}}} \tag{5.8}$$

$$G(X) = \varepsilon_C - \frac{SPAN}{100Q} \sqrt{\frac{\sigma_v}{\sigma_{ci}}} \Big/ R_0 \tag{5.9}$$

where $G(X)$ is the performance function of the system, ε_C is the critical strain; Δ_v is the vertical displacement (in units of mm); $SPAN$ is the tunnel span (in units of mm); σ_v is the vertical stress; σ_{ci} is the uniaxial compressive strength of intact rock; R_0 is the tunnel radius.

In terms of the critical strain, it can be treated as a deterministic value or a random variable. In the case of deterministic critical strain, the critical strain is set to certain single value (e.g. 0.5%, 1%). If the critical strain is viewed as a random variable, it can be calculated, according to the critical strain concept proposed by Sakurai (1981), as the ratio of the UCS over the elastic modulus of rock mass, which is as follows:

$$\varepsilon_C = \frac{\sigma_{cm}}{E_m} \tag{5.10}$$

$$G(X) = \frac{\sigma_{cm}}{E_m} - \frac{SPAN}{100Q}\sqrt{\frac{\sigma_v}{\sigma_c}}\Big/Ro = \frac{\sigma_c \exp(0.6\log Q - 2)}{E_i \exp(0.8625\log Q - 2.875)} - \frac{SPAN}{100Q}\sqrt{\frac{\sigma_v}{\sigma_c}}\Big/Ro \tag{5.11}$$

where σ_{cm} is the UCS of rock mass, E_m is the elastic modulus of rock mass. σ_c is the uniaxial compressive strength of intact rock; E_i is the elastic modulus of intact rock.

(2) Reliability analysis using the FORM spreadsheet

Once the critical strain-based limit state function is determined, the reliability analysis can be performed using the FORM spreadsheet, and the reliability index and the probability of failure can be obtained.

5.4 Reliability analysis with deterministic critical strain

5.4.1 The concept of critical strain

In underground excavations, there are mainly two failure mechanisms, i.e. stress-controlled failure mechanism due to the excavation-induced stresses and structurally-controlled failure mechanism caused by intersecting discontinuities (Li and Low, 2010). In this study, the stress-induced failure mechanism is investigated. The critical strain is normally required to evaluate the tunnel deformation before excavation. The concept of critical strain was introduced by Sakurai (1981) and is defined as the ratio of strength to the Young's modulus of rock. It can be used as the limiting strain and is interpreted as the strain value above which instability problems are likely to occur. The critical strain is always smaller than the failure strain or the peak strain on the stress-strain curve, thus it may be used as a warning strain level which can guarantee the structural safety (Sakurai, 1981). This also implies that if the predicted tunnel strain is below the critical strain, then the tunnel will be stable during the excavation process. The concept of critical strain has been extensively reviewed by Li (2004) based on laboratory tests on intact rock samples, and the critical strain is re-evaluated considering three typical stress-strain relationships of rocks, i.e. elastic

behavior, elastic-plastic behavior and plastic-elastic-plastic behavior. With regard to rocks with the plastic-elastic-plastic behavior, the modified tangential modulus is used using the axis translation technique instead of the initial tangential modulus considering the initial plastic deformation at the beginning of loading. This can greatly reduce the conservativeness caused by the use of the initial tangential modulus and more realistically reflect the deformational behavior of rocks (Daraei and Zare, 2018; Li, 2004).

Based on field observations and measurements, Sakurai (1983) suggested the critical strain value of 1% since the onset of tunnel instability with support problems took place when the tunnel strain was larger than approximately 1%. Field observations by Chern et al. (1998b) and Hoek (2001) confirmed the critical strain value of 1%. Hoek (1999) also defined the critical strain value of 2% as the boundary between stable tunnels requiring minimal support and unstable tunnels necessitating special support. However, it should be noted that some tunnels which have experienced strains as high as 5% did not show stability problems (Hoek, 2001). Hoek (2001) also presented that it is allowable for tunnels within squeezing conditions to suffer strains as much as 5% before the activation of the tunnel support. Thus, there is no universally accepted critical strain value and the critical strain is dependent on the ground characteristics and in-situ stress levels in different cases.

In this study, a critical strain-based performance function is empirically established, and the Shimizu highway tunnel case is illustrated as an example to perform the reliability analysis. Table 5.1 summarizes the statistical moments of relevant parameters for the Shimizu tunnel. Table 5.2 compares the estimates of the mean critical strain value using different calculations summarized from literatures. Eq. (5.10) is the definition of the critical strain. Other equations are the extension of the critical strain concept based on results obtained from laboratory tests, physical modeling tests, empirical correlations, and field observations or measurements. The mean values are also given for the tunnel strain at the tunnel crown derived from the numerical calculation with RS2 modeling and from the empirical Barton approach (Barton, 2002) in Table 5.2 for comparison purpose. The obtained critical strain values are different, varying from about 0.3% to 2%. This may be due to the fact that these equations, based on which the critical values are calculated, are derived from case histories or numerical studies with different ground characteristics. Thus, the determination of the single critical strain value of rock mass is not an easy task and caution should be exercised. The site knowledge, local experience, and engineering judgement should be

combined to determine the critical strain value based on some numerical calculations or field measurements.

Table 5.1 Summary of statistics of parameters in the Shimizu tunnel case study.

	Parameters						
Statistics	SPAN (m)	HEIGHT (m)	Q	Intact UCS σ_c (MPa)	Intact elastic modulus E_i (GPa)	Rock mass UCS σ_{cm} (MPa)	Rock mass elastic modulus E_m (GPa)
Distribution	N/A	N/A	Lognormal	Normal	Lognormal	Lognormal	Lognormal
Mean	18	12	6.63	49	10.2	9.62	1.01
SD	0	0	7.52	9.66	1.6	3.62	0.47

Table 5.2 Summarized critical strain estimated using different approaches.

Equation	Equation No.	Critical Strain	Remarks	Source
$\varepsilon_C = \sigma_{cm} / E_m$	5.10	0.95%	By definition	Sakurai 1983
$\varepsilon_C = 10^{(-0.3601\log\sigma_c + 0.0702)}$	5.12	0.29%	For intact rocks	Idris et al., 2016
$\varepsilon_C = 1.073\sigma_{cm}^{-0.318}$	5.13	0.52%	Curve fitting based on data from 3 case studies in Taiwan	Hoek, 1998
$\varepsilon_P = 50(\frac{E_m}{\sigma_m})^{-0.75}$	5.14		Peak strain correspoing to the peak stress	Ramamurthy, 2001; Singh et al., 2007
$\varepsilon_C \approx 0.67\varepsilon_P$	5.15	1.02%	Combine Eqs. 5.14 and 5.15	Singh et al., 2007
$\varepsilon_C = \frac{\sigma_{ci}}{E_m^{0.37} E_i^{0.63}}$	5.16	1.13%	Derived from physical modeling tests of jointed rock mass	
$\varepsilon_C = 31.1\frac{\sigma_c^{1.6}}{E_i\gamma^{0.6}Q^{0.2}}$	5.17	0.15%	Combine Eq. 5.16 and Singh et al. (1997) correlation	Singh et al., 2007; Singh et al., 1997
$\varepsilon_C = 5.84\frac{\sigma_c^{0.88}}{Q^{0.2}E_i^{0.63}}$	5.18	0.43%	Combine Eq. 6 and Barton (2002) correlation	Singh et al., 2007; Barton, 2002
$\varepsilon_C = f(Q, B/H)$	5.19	0.50%	FLAC3D code utilized to estimate strain in caverns	Zhang & Goh (2015)
$\varepsilon_C = f(GSI, p_0, \eta)$	5.20		Finite difference method used considering softening behaviors	Cui et al., 2017
1%				Sakurai, 1983; Hoek, 1998; Chern et al., 1998; Hoek, 2001; British Tunneling Society, 2004; Song et al., 2016
2%				Hoek, 1999; Lü et al., 2011;Lü et al., 2013, 2017
		0.44%	Mean strain value estimated by RS2 FEM analysis	
		0.32%	Mean strain estimated by Barton's approach	Barton, 2002

5.4.2 Critical strain for intact rock and rock mass

The relationships between critical strain and uniaxial compressive strength (UCS) as well as Young's modulus of rocks and soils are summarized by (Sakurai, 2017), as seen in Figure 5.2. Note that these relationships were established originally based on laboratory tests on rocks and soils, however, Sakurai (1983) pointed out that the critical strain of in-situ rock mass is almost the same order of magnitude as that of intact rocks based on in-situ tests (plate bearing tests and direct shear tests) and back-calculations in rock masses. The critical strain for rock masses also falls within the bounds shown in Figure 5.2 since the effects of joins are canceled out by taking the ratio of the strength to the elastic modulus of rock mass (Sakurai, 1997). The hazard waring levels were also proposed in the critical strain chart for preliminary evaluation of the stability of tunnels prior to the start of tunnel excavation, which have three stages depending on the degree of stability. As can be seen in Table 5.2 (A), the warning level III is the upper bound of the strain, above which many different types of excavation problems are likely to occur; the warning level I is the lower bound, below which tunnels are stable without excavation problems; and the warning level II in between is the centerline between warning level I (lower bound) and warning level III (upper bound). The upper bound and lower bound are also shown in Table 5.2 (B) in terms of the relationship between critical strain and elastic modulus.

Based on the relationships shown in Figure 5.2, the hazard warning levels were estimated using the strength and elastic moduli of intact rocks and rock mass in the Shimizu tunnel case, as marked in Figure 5.2. The obtained hazard warning levels of critical strain are summarized in Table 5.3. The critical strain values for intact rocks vary from about 0.1% to 0.8% based on the intact UCS and elastic modulus according to Figure 5.2. In contrast, the critical strain values for the rock mass are in the range of about 0.2% to about 1.5% based on the rock mass UCS and elastic modulus values. Thus, it reveals that the critical strain values estimated for the rock mass are about 2 times that for intact rocks in this case study.

Sakurai (1997) stated that the critical strain of the rock mass is always greater (1 to 3 times more) than that for intact rocks. Based on this, it is also suggested that the critical strain obtained from intact rocks can be used as the permissible strain for rock mass since a certain amount of safety allowance can be guaranteed. However, Daraei and Zare (2019) pointed out that the use of critical strain derived from intact rocks is too conservative due to the following reasons: first, there is a scale effect between rock mass and intact rocks and the critical strain for rock mass is about 1

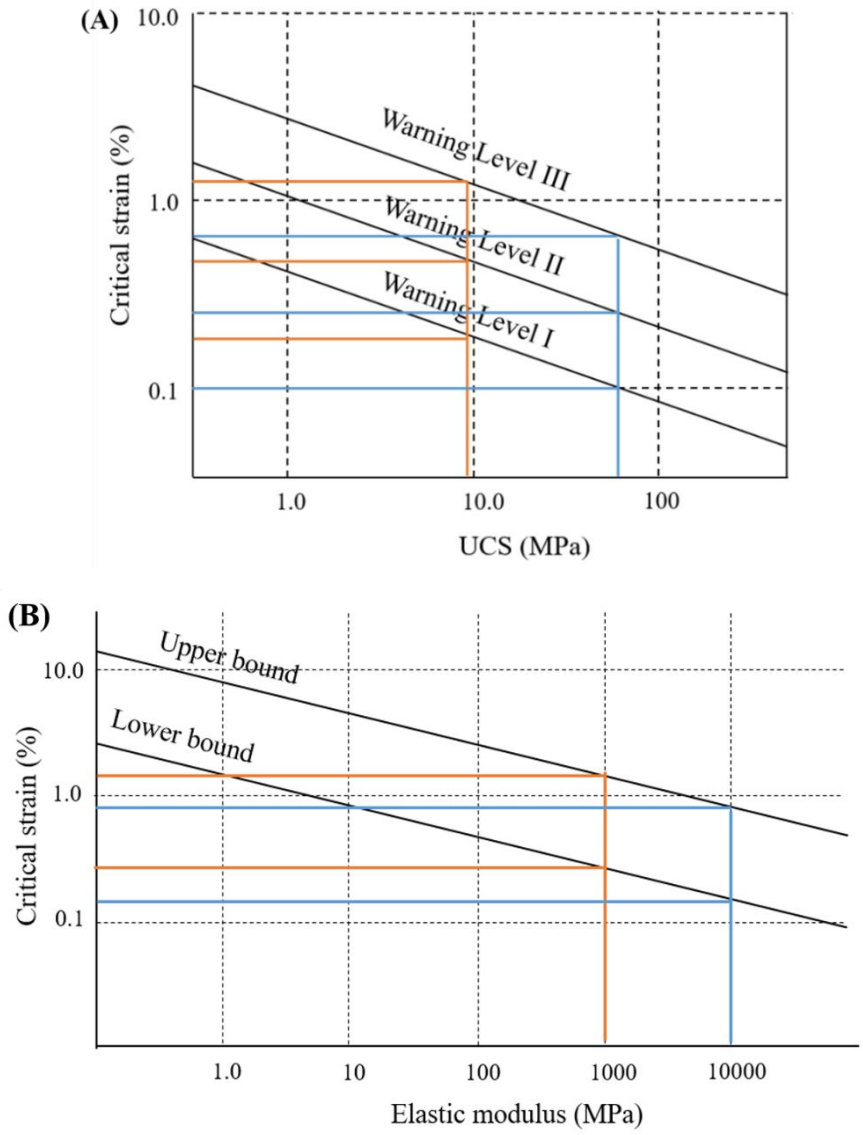

Figure 5.2 Relationship between critical strain and rock properties (Sakurai, 2017; Sakurai, 1997): (A) critical strain vs. UCS; (B) critical strain vs. elastic modulus

to 3 times that for the intact rock as noted by Sakurai (1997). Thus, a sufficient safety factor (1 to 3) has already been automatically taken into account due to this scale effect. Especially for rocks with the plastic-elastic-plastic behavior, critical strain values estimated from intact rocks can be considerably smaller than those for rock masses. If these critical strain values for intact rocks are used in evaluating the excavation stability in rock masses, over-conservativeness will be encountered. In addition, the difference between the critical strain and failure strain at the peak strength should also be considered in intact rocks. The failure strain of intact rocks will be 1 to 5 times the critical strain, indicating another safety factor is also included in the critical strain

criterion (Daraei and Zare, 2018). Thus, the critical strain determined from intact rocks should not be directly used for rock masses to avoid over-conservatism. Instead, to lessen the conservativeness and more realistically capture the characteristics of rock mass, the critical strain for rock mass should be estimated based on the mechanical properties of the rock mass itself. Since the in-situ tests for directly estimating the rock mass properties are expensive and time-consuming, empirical rock mass classifications can be used as an alternative to provide initial estimates of rock mass properties.

Table 5.3 Comparison of critical strain estimated using intact and rock mass properties.

Rock property index	Critical strain (%)		
	Upper bound	Mean	Lower bound
σ_c	0.65	0.25	0.093
σ_{cm}	1.27	0.48	0.20
E_i	0.81		0.14
E_m	1.46		0.25

5.4.3 Effects of deterministic critical strains on the reliability

To investigate the effects of critical strain values on the tunnel reliability, performance functions with different deterministic critical strain values were used within the FORM framework. Figure 5.3 illustrates the FORM example with a critical strain value of 1%. The input parameters, including the Q index, the UCS of intact rocks, and the vertical stress, were treated random variables with respective statistical moments. The UCS of intact rocks was assumed to follow a normal distribution and the standard deviation was estimated using 3 sigma rule (Duncan, 2000; Hoek, 1998a; Sari, 2009; Tiwari et al., 2017). The vertical stress was also assumed to be normally distributed, and the COV was assumed 25% based on published data in literature and practice (Cai, 2011; Hadjigeorgiou and Harrison, 2011; Lü et al., 2013; Şen and Sadagah, 2002). In the FORM spreadsheet shown in Figure 5.3, the reliability index value was calculated as 2.575 and the estimated probability of failure is 0.5%. For comparison, the MCS technique was also carried out to directly estimate the probability of failure, which is the likelihood that the performance function value is no greater than zero.

		Span (m)	Radius Ro (m)	△v (cm)	εv (%)				
		18	9	9.0	1.00				
Random Variable	Distribution	Para1	Para2	Para3	Para4	Design point x_i^*	Correlation matrix [R]		n_i
Q	Lognormal	6.63	7.52			0.44	1	0	0	-2.54
σc	Normal	49	9.66			46.18	0	1	0	-0.29
σv	Normal	2.03	0.51			2.19	0	0	1	0.32

limiting strain εc	Performance function G(X)	Reliability index β	Probability of failure Pf=Φ(-β)
1.0%	-8.0E-07	2.575	0.50%

$$G(X) = \varepsilon_C - \frac{SPAN}{100Q}\sqrt{\frac{\sigma_v}{\sigma_c}}\Big/R_0$$

β=SQRT(MMULT(TRANSPOSE [R],MMULT(MINVERSE [ni], [R])))

array formula:ctrl+shift, then enter

Figure 5.3 FORM spreadsheet with deterministic critical strain.

Figure 5.4 shows the effects of critical strain values on the reliability index and probability of failure. The reliability index increases while the probability of failure decreases with the increase of critical strain values. Note that the reliability index is negative and the probability of failure is greater than 50% when the critical strain value is less than 0.1%. The performance function values under these circumstances are negative at mean values of input parameters, indicating that the mean-value points are already inside the failure region (Low, 2008b). The resultant reliability index is negative and correspondingly the probability of failure is greater than 50%. Results in Figure 5.4 (B) also reveal that the probability of failure results calculated from the MCS technique are in good agreement with that estimated from the FORM approach, which also verifies the accuracy of the FORM approach. The good agreement achieved between the FORM and MCS approaches has also been previously reported in reliability analysis results in the field of geotechnical engineering (Jimenez-Rodriguez and Sitar, 2007; Li and Low, 2010; Low and Einstein, 2013; Lü et al., 2012; Lü and Low, 2011; Lü et al., 2011).

5.4.4 Sensitivity analysis with deterministic critical strain

In the FORM spreadsheet, the design point values are determined automatically for each input parameter and can reflect sensitivities of the performance function to all the input parameters (Low, 2008a). The n_i values, as calculated by Eq. (5.5), are standard normal variables, which provide a

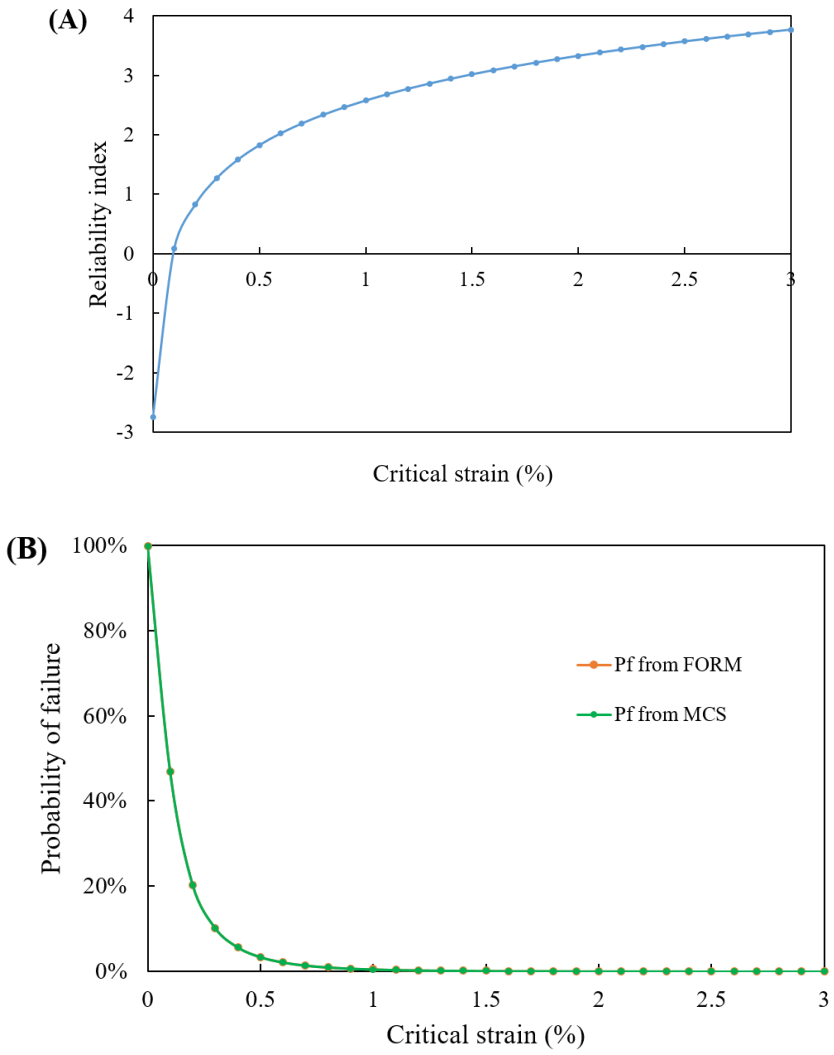

Figure 5.4 Effects of the critical strain on the reliability: (A) reliability index; (B) probability of failure

measure of relative parametric sensitivity. The greater the n_i value for an input parameter is, the farther the design point is from the mean value point, and thus the more significant the input parameter is. It is clearly seen in the n_i column in Figure 5.3 that the n_i value for the Q index is the largest, followed by the vertical stress and the UCS. Using the MCS technique, the sensitivities of input distributions can also be obtained with tornado graphs. Figure 5.5 illustrates the rank of relative importance of input parameters in tornado graphs derived from the regression analysis in the MCS process. The input parameter Q index is the most important, followed by the verticalstress and the UCS, which is consistent with the sensitivity results derived from n_i values in the FORM spreadsheet.

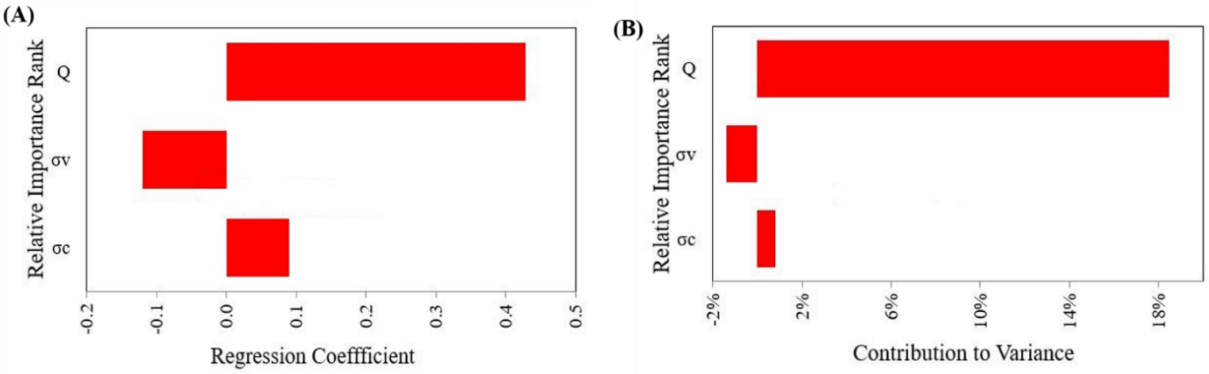

Figure 5.5 The rank of relative importance of input parameters: (A) ranked by regression coefficient; (B) ranked by the contribution to variance

5.4.5 Probability density function of the estimated strain

The effects of distribution types of Q-parameters on the probability density function (PDF) of the estimated strain were also studied using the MCS technique. The distribution effects of Q-parameters RQD, J_r and J_a are focused in this study with different distribution types assigned, while other Q-parameters J_n, J_w and SRF are assumed triangularly distributed. According to the summarized commonly used distribution types for RQD, J_r and J_a parameters, as mentioned in Section 3.4.7 in Chapter 3, three distribution types were assigned, i.e. normal, lognormal and triangular distributions for RQD, Jr and Ja parameters. The scenario with histograms of the relative frequency data for all the Q-parameters was also included for comparison.

Figure 5.6 compares the estimated PDFs of tunnel strain with different distribution assumptions. The scenario with histogram frequency data generated the smallest statistical moments (mean of 0.32%, standard deviation of 0.41%). This indicates that the obtained strain values are overestimated under other distribution assumptions, thus being conservative. Results also show that the scenario with the lognormal distribution assumption generates results closest to that derived from the histogram frequency data. This is because that J_a is the second most important input parameter (the SRF parameter is most significant with the assumed triangular distribution in all scenarios), as can be seen in Section 4.4.3, and that the lognormal distribution is a better fit for J_a compared to other distributions (normal distribution and triangular distribution). It was also reported by Lu et al. (2019) that scenarios with lognormally distributed J_r and J_a parameters produced better estimates of the Q value and associated rock mass parameters in the Shimizu tunnel case study. Thus, it is of great significance to identify the most influential input parameters

using sensitivity analysis and assign appropriate distribution types since variations in these important input parameters contribute the most to the overall uncertainty of the output parameter.

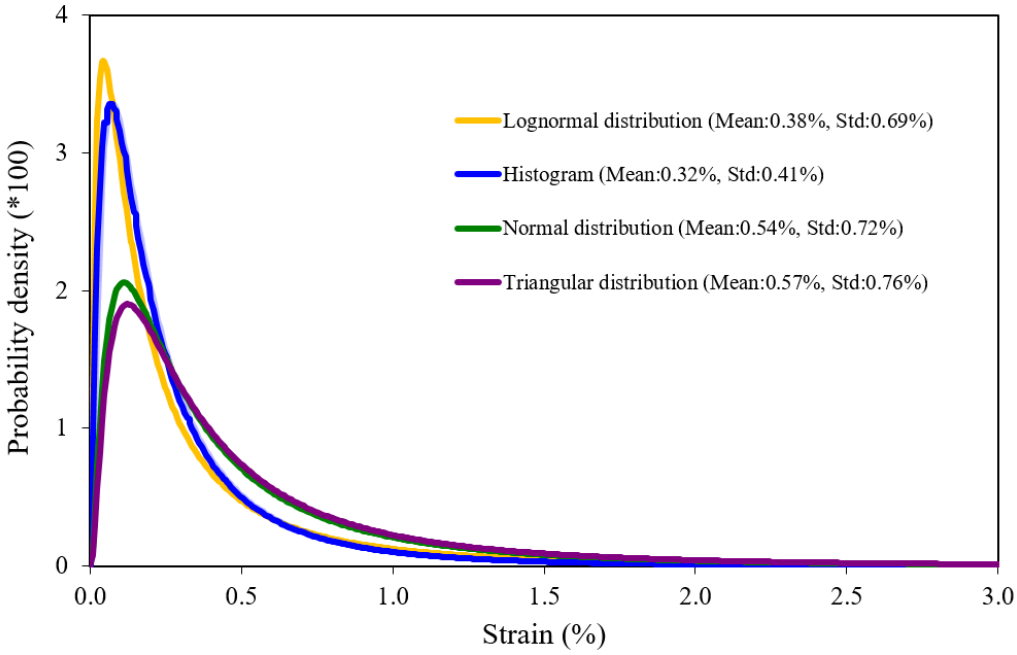

Figure 5.6 Comparison of PDFs of estimated strain.

It is also observed that the scenario with the normal distribution assignment generates PDF of estimated strain with greater mean and standard deviation than that of the lognormal distribution scenario. This phenomenon can be explained as follows: the lognormally distributed parameter J_a, one of the most influential parameters, with positive skewness, leads to a higher probability of smaller J_a values being sampled in the MCS process than that in the scenario of non-skewed normally distributed Ja. As a result, larger Q values are more likely to be calculated, meaning better rock mass quality, in the scenario with the lognormally distributed J_a parameter. This also results in a smaller mean value of the estimated tunnel strain in the lognormal distribution scenario than in the normal distribution scenario, indicating the conservativeness of the normal distribution assumption. The greater conservativeness achieved in the normal distribution assumption than in the non-normal distributions for rock mass input parameters has also been reported by numerous researchers in the analyses of underground structures, which includes scenarios of rock mass input parameters of cohesion, friction angle and deformation modulus of Mohr-Coulomb material (Hamrouni et al., 2017; Li and Low, 2010; Lü and Low, 2011; Lü et al., 2011), input parameters of GSI, the constant mi, the disturbance factor D and intact UCS of Hoek Brown material (Pan and Dias, 2018; Zeng et al., 2014), or input parameters of rock mass strength, deformation modulus,

Hoek-Brown criterion parameter m and dilation angle (Song et al., 2016). It is also found in Figure 5.6 that the scenario with triangular distribution assignment has the largest statistics of estimated strain, generating the greatest differences compared to the results obtained from the histogram scenario. This implies that the triangular distribution might not be suggested for use despite the relative ease and simplicity in defining the distribution (min, most likely and max).

5.4.6 Effects of correlation between RQD and J_n on the reliability

The effects of the negative correlation between RQD and J_n on the reliability were also studied. Figure 5.7 describes the variation of the reliability index and the probability of failure with the changes of correlation coefficient between RQD and J_n. Results show that the lower safety levels are achieved, represented by lower reliability index and higher probability of failure, with stronger correlation between RQD and J_n. This indicates that the level of safety and reliability is overestimated if the negative correlation is neglected. Recall that the greater mean of the Q value is achieved with the stronger correlation between RQD and J_n, as mentioned in Section 3.4.6 in Chapter 3 and Section 4.4.5 in Chapter 4, and this may lead to better rock mass quality as well as higher reliability level. It should be noted, however, that the standard deviation and the COV which are the measure of variation also become greater with stronger correlation between RQD and J_n. As mentioned in Section 4.4.5 in Chapter 4, the standard deviation and COV are more sensitive to the correlation between RQD and J_n compared to the mean values. Thus, it is indicated that the dispersion in the derived distribution of the Q value may have greater effects on the overall level of safety and reliability than the mean value.

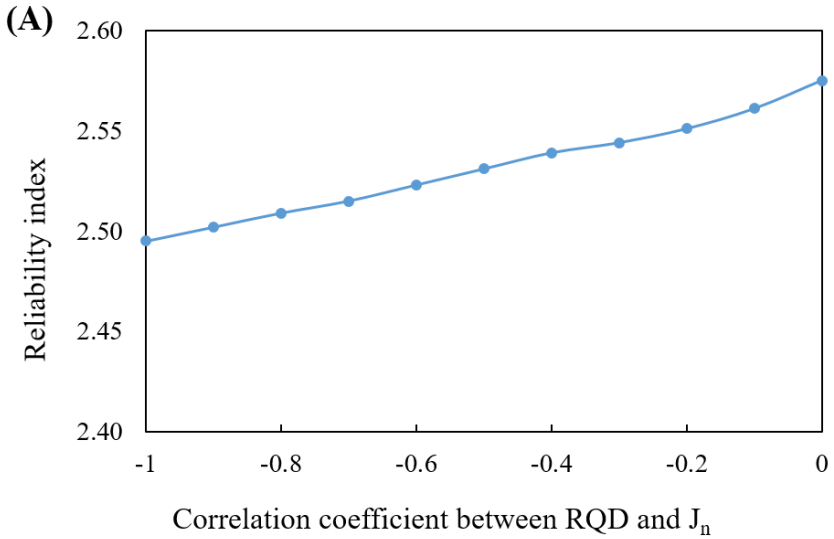

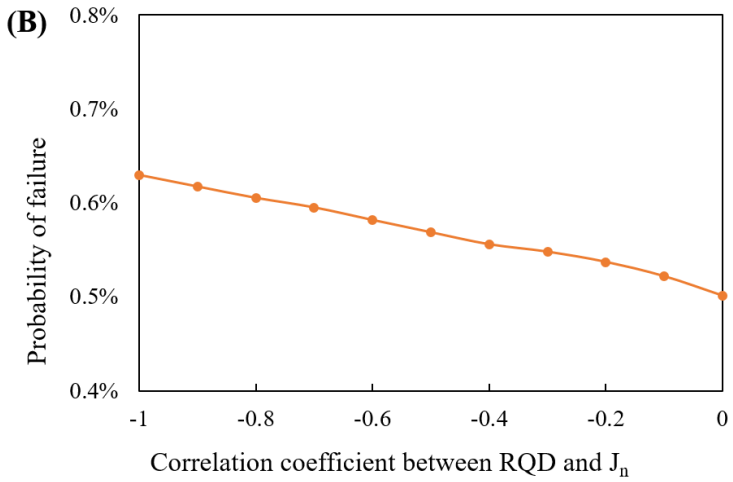

Figure 5.7 Effects of correlation between RQD and J_n on reliability: (A) reliability index; (B) probability of failure

The reliability index decreases from 2.575 to 2.495 and the corresponding probability of failure increases from 0.5% to 0.63% when the correlation coefficient varies from 0 to -1.The sensitivity indices, as introduced in Section 4.3.4 in Chapter 4, were also calculated to assess the sensitivity of both the reliability index and the probability of failure to the correlation coefficient. Results show the obtained sensitivity indices are 3.1% and 20.4% for the reliability index and the probability of failure, respectively. This indicates that the negative correlation between RQD and J_n has greater impact on the probability of failure than on the reliability index in this Shimizu tunnel case.

5.5 Reliability analysis with probabilistic critical strain

5.5.1 Performance function based on probabilistic critical strain

In Section 5.4, deterministic critical strain values were used in the performance function for conducting the reliability analysis. However, the uncertainties involved in the selection of the critical strain values are not considered. The probabilistic critical strain, which enables the consideration of inherent uncertainties in rock mass parameters, is capable of overcoming the difficulty when choosing the appropriate single critical strain value in the deterministic critical strain approach. The following study will introduce the probabilistic critical strain into the calculation. Uncertainties in the critical strain, according to the definition of the critical strain, are derived from the uncertainties in the rock mass strength and elastic modulus of rock mass. As

mentioned in Section 4.3.2 in Chapter 4, the normalized estimation approach with the consideration of intact rock properties works well in estimating the strength and elastic modulus of rock mass, and the rock mass properties estimated using this approach were adopted to calculate the critical strain. Figure 5.8 illustrates the FORM spreadsheet with probabilistic critical strain in the limit state function.

		Span (m)	Radius Ro(m)	△v (cm)	εv (%)					
		18	9	10.20	1.13					
Random Variable	Distribution	Para1	Para2	Para3	Para4	Design point x_i^*	Correlation matrix [R]			n_i
Q	Lognormal	6.63	7.52			0.41	1	0	0	0	-2.61
σc	Normal	49	9.66			41.30	0	1	0.67	0	-0.80
Ei	Lognormal	10.2	1.6			9.68	0	0.67	1	0	-0.26
σv	Normal	2.03	0.5075			2.22	0	0	0	1	0.37

limiting strain εc	Performance function G(X)	Reliability index β	Probability of failure pf=Φ(-β)
σ_{cm}/E_m	9.0E-07	2.778	0.27%

$$G(X)=\frac{\sigma_{cm}}{E_m}-\frac{SPAN}{100Q}\sqrt{\frac{\sigma_v}{\sigma_c}}\Big/Ro=\frac{\sigma_c\exp(0.61\log Q-2)}{E_i\exp(0.8625\log Q-2.875)}-\frac{SPAN}{100Q}\sqrt{\frac{\sigma_v}{\sigma_c}}\Big/Ro$$

β=SQRT(MMULT(TRANSPOSE [R],MMULT(MINVERSE [ni], [R])))

array formula:ctrl+shift, then enter

Figure 5.8 FORM spreadsheet with probabilistic critical strain.

In the FORM spreadsheet in Figure 5.8, the input parameters are the Q index, the intact UCS, the intact elastic modulus, and the vertical stress. As mentioned in Section 5.4.3, the intact UCS was assumed to be normally distributed and the standard deviation was estimated using 3 sigma rule. Similarly, the intact elastic modulus was assumed to follow lognormal distribution and the standard deviation was also estimated using 3 sigma rule (Tiwari et al., 2017). Based on laboratory tests on intact rock samples in the Shimizu tunnel case study, the intact UCS and elastic modulus data was collected, and the correlation coefficient between the UCS and elastic modulus was determined to be 0.67, as depicted in Figure 5.9. The correlation coefficient between the intact UCS and elastic modulus was considered in the correlation matrix in the reliability analysis shown in Figure 5.8. The obtained reliability index is 2.778 and the corresponding probability of failure is 0.27%. Figure 5.10 illustrates the PDF of the estimated critical strain, in which the statistical

moments and the 90% confidence interval are also listed. The critical strain is a random variable with the mean value of 1.04% and the standard deviation of 0.31%.

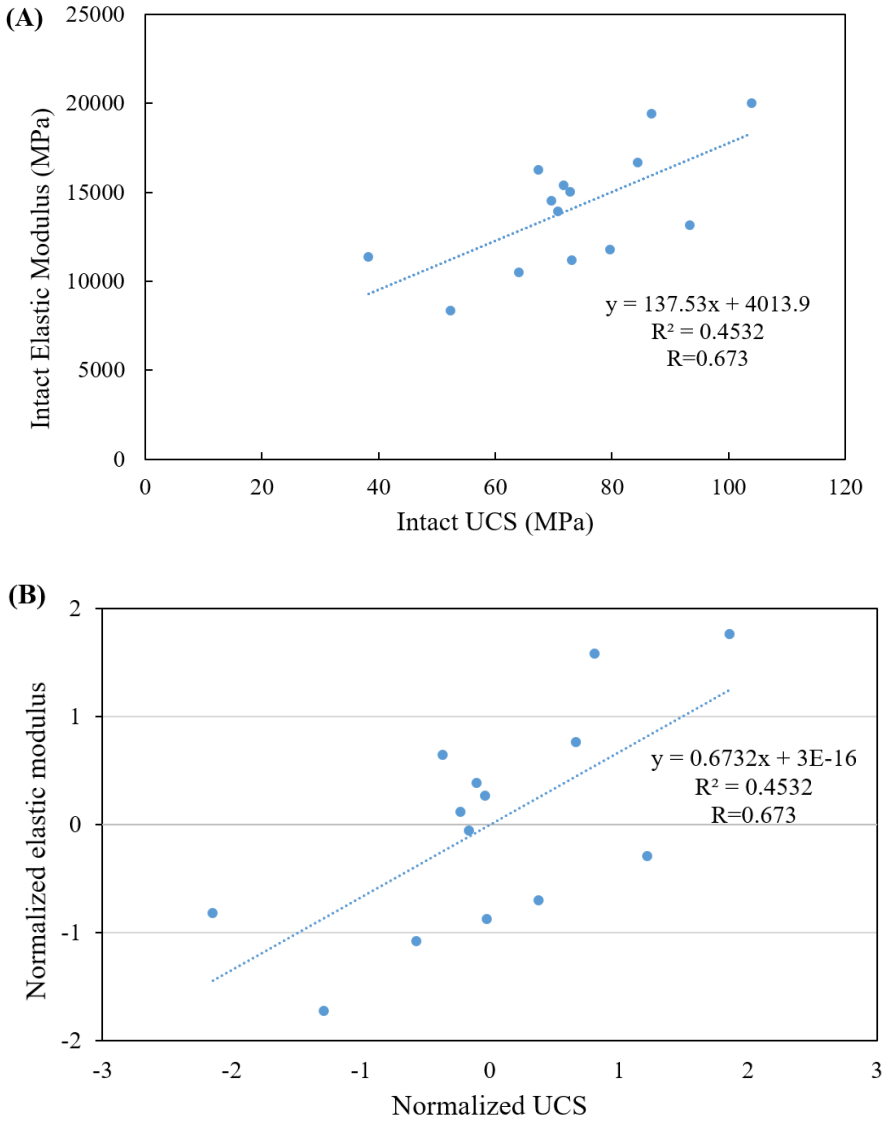

Figure 5.9 The positive correlation between UCS and elastic modulus of intact rock: (A) original data set; (B) normalized data set

Reliability analysis with the probabilistic critical strain has also been conducted using the MCS technique with 50,000 iterations. The obtained probability of failure is 0.28%, which also agrees well with the value of 0.27% derived from the FORM results. This also confirms the agreement of reliability results derived from the FORM algorithm and the MCS simulations.

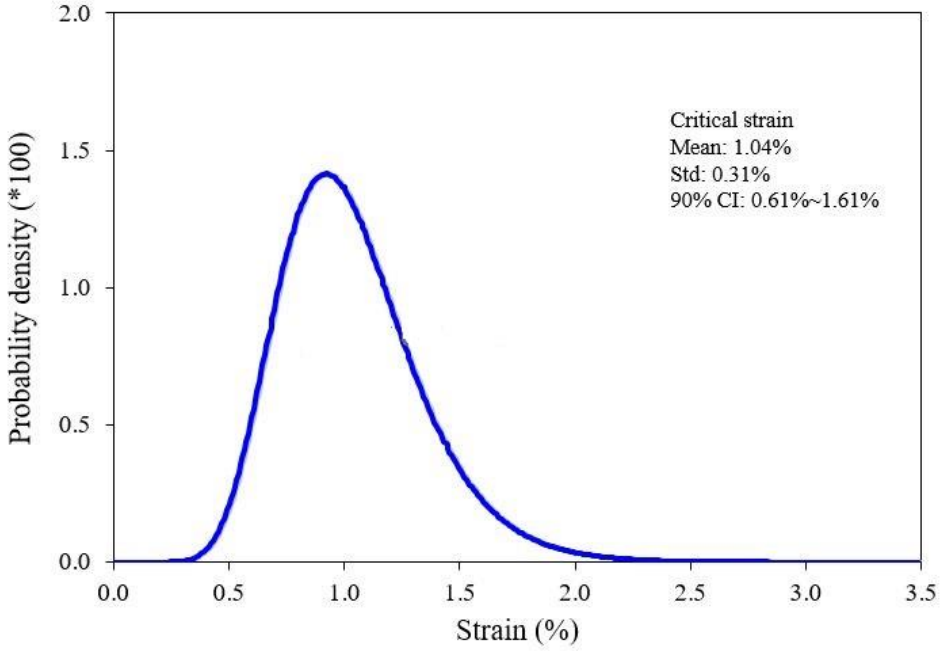

Figure 5.10 The distribution of critical strain.

5.5.2 Sensitivity analysis with probabilistic critical strain

Sensitivity analysis has also been carried out during the MCS process and Figure 5.11 shows the sensitivity analysis results with tornado graph displaying relative importance of input parameters. Results show that the intact UCS is the most influential input parameter based on the regression analysis. The ranking criteria of the regression coefficient and the contribution to variance demonstrate the same ranking order, and the intact UCS and elastic modulus are more significant than the Q index and the vertical stress. This is because the results ranked by the regression coefficient and the contribution to variance of output were both obtained in the regression analysis. In contrast, according to the n_i column in the FORM spreadsheet in Figure 5.8, the Q index has the largest effects on the reliability, followed by the intact UCS, the vertical stress and intact elastic modulus. The ranking order is different to that generated from the MCS process. This may be caused by the complicated performance function, in which the input parameters Q index and the intact UCS are involved in both the first and second terms in the limit state function. Due to the non-linear performance function in this study, the limit state surface at the design point may be non-linear. Under this circumstance, the FORM algorithm might not provide very accurate sensitivity analysis results. This is due to the fact that the FORM is essentially a linear approximation of the actual limit state surface at the design point and does not adequately deal

with highly non-linear problems. Instead, the second order reliability method (SORM) can be used owing to its advantage in capturing the non-linearity of limit state surface at the design point. In view of the complex computational procedures of the SORM, the SORM is not focused on herein and could be included in the future work for the verification of reliability results derived from the FORM algorithm. However, the MCS technique is a versatile simulation tool and is capable of handling highly non-linear performance functions with a large amount of random sampling (Fenton and Griffiths, 2008). The MCS technique can serve as a complementary tool to the FORM algorithm and provide reliable sensitivity analysis results especially in highly non-linear problems.

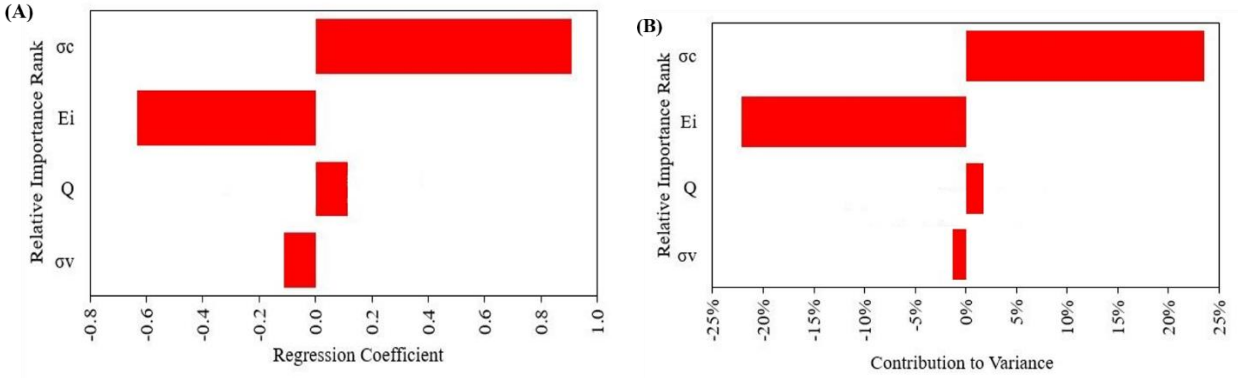

Figure 5.11 The rank of relative importance of input parameters: (A) ranked by regression coefficient; (B) ranked by the contribution to variance

5.5.3 Effects of correlation between intact UCS and elastic modulus

Effects on reliability index and probability of failure

It is well-recognized that the UCS and elastic modulus or rocks are correlated and a positive correlation between the intact UCS and elastic modulus has been reported in the published literature and geotechnical practice (Arslan et al., 2008; Hoek and Diederichs, 2006; Palchik, 1999; Palmstrom and Stille, 2010; Wang and Aladejare, 2016). The significant impact of the correlation structure between ground parameters on the reliability analysis and probabilistic design of geotechnical structures has also been highlighted in previously published literature (Lü and Low, 2011; Lü et al., 2011; Wang and Akeju, 2016; Wang and Aladejare, 2016).

The effects of the correlation between intact UCS and elastic modulus on the reliability have been studied using the FORM spreadsheet, and the obtained results are shown in Figure 5.12. The probability of failure results calculated from the MCS simulation process are also included for comparison. The MCS-derived results of probability of failure agree well with those generated in the reliability analysis with the FORM spreadsheet. Results also reveal that the stronger the

correlation between the intact UCS and elastic modulus, the higher the safety level achieved with greater reliability index and smaller probability of failure. This indicates that the level of reliability and safety is underestimated if the correlation is neglected. It is often perceived as conservative to neglect the correlation between ground parameters, and various research (Li and Low, 2010; Mollon et al., 2009b; Pan and Dias, 2018; Zeng et al., 2014) in the field of underground construction has confirmed this point. With regard to this conservativeness, Langford (2013) pointed out that it introduces errors to an uncertainty-based assessment and can result in the development of incorrect geomechanical models as well as unreasonable extreme output values. Thus, it is necessary and essential to more realistically account for the correlation between input parameters if the correlation exists and to reduce the conservativeness.

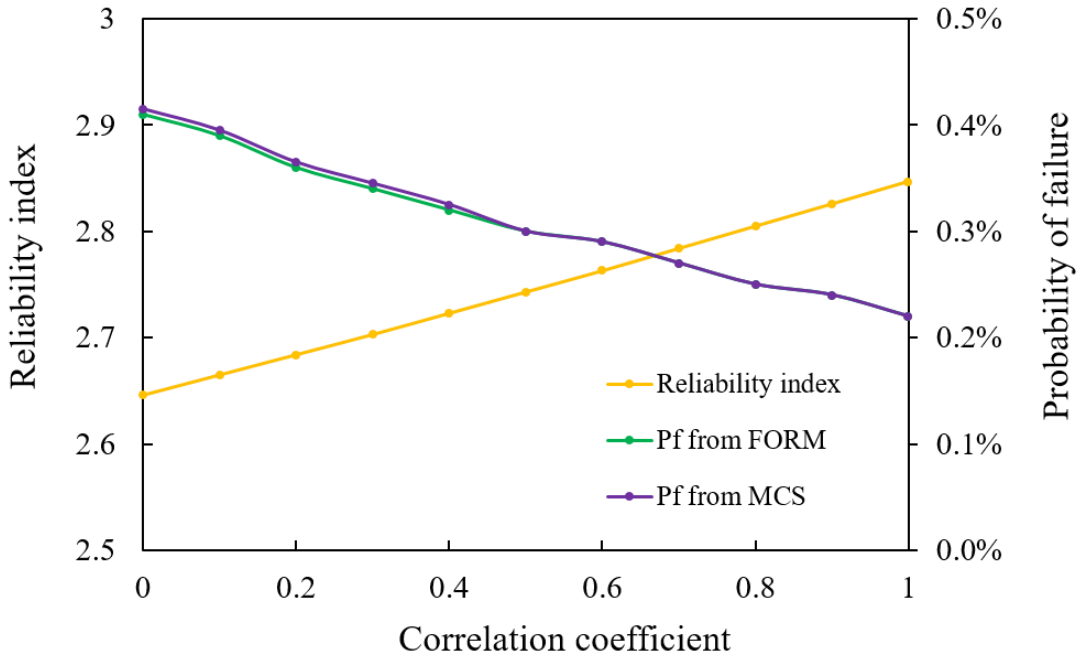

Figure 5.12 Effects of the correlation coefficient between UCS and elastic modulus on reliability

Song et al. (2016) reported that the reliability results were overestimated if the correlation between the UCS and elastic modulus of intact rock was neglected based on limit state functions of plastic zone and radial tunnel displacement. Lü et al. (2012) suggested that the reliability results are conservative in the plastic zone criterion while not conservative in the tunnel convergence criterion if the correlation between the deformation modulus of rock mass and the intact strength is not modeled. It was further concluded that the complicated influences of correlation structure on the reliability results depend on the orientation of the limit state surface and the direction of the correlation structure. This can be intuitively appreciated using the perspective of the expanding

dispersion ellipsoid (Lü et al., 2012; Lü et al., 2011). To be more specific, in the case of a positively inclined limit state surface, the positively correlated dispersion ellipsoid has to expand more (i.e. greater reliability index) than the non-correlated dispersion ellipsoid to touch the limit state surface; in contrast, in the case of a negatively inclined limit state surface, the positively correlated dispersion ellipsoid has to expand less than the un-correlated dispersion ellipsoid, thus leading to smaller reliability index. In this study, the limit state surface in the space of the intact UCS and elastic modulus is positively inclined, and thus the positive correlation between the intact UCS and elastic modulus results in a larger reliability index.

Effects on sensitivity analysis

The effects of the correlation between the intact UCS and elastic modulus on the relative importance of input parameters were also investigated in the MCS process, and the results are shown in Figure 5.13. Results show that the correlation has insignificant effects on the sensitivities in the regression analysis. Similar to the results in Section 5.5.2, the sensitivity results obtained based on the criteria of regression coefficient and contribution to variance are consistent, in which the intact UCS and elastic modulus are most influential while the Q index and the vertical stress have minimal impact. It is also found that the sensitivity results based on the criterion of the contribution to variance are more sensitive than those based on the criterion of regression coefficient to the correlation structure between the intact UCS and elastic modulus.

5.5.4 Effects of distribution types for intact UCS and elastic modulus

Uncertainty and variability exist in rock properties and probability distribution models can be used to explicitly characterize them. Table 5.4 summarizes the commonly used distribution types for the intact UCS and elastic modulus from published studies. Both the intact UCS and elastic modulus can be described by normal, lognormal and beta distributions. The lognormal distribution and the beta distribution are often used as alternatives to the normal distribution to rule out negative values, which are not physically meaningful, when the COV of the ground parameters is over 25% (Li and Low, 2010). The bounded beta distribution with a lower and an upper bound is versatile and can be used in lieu of the normal distribution (Low, 2008b). The beta distribution is characterized by four parameters (alpha1, alpha2, min, max) in which the first two parameters are shape parameters while the latter two parameters define the bounds of the distribution. The mean and standard deviation of a beta distribution can be calculated as follows (Benjamin and Cornell, 2014):

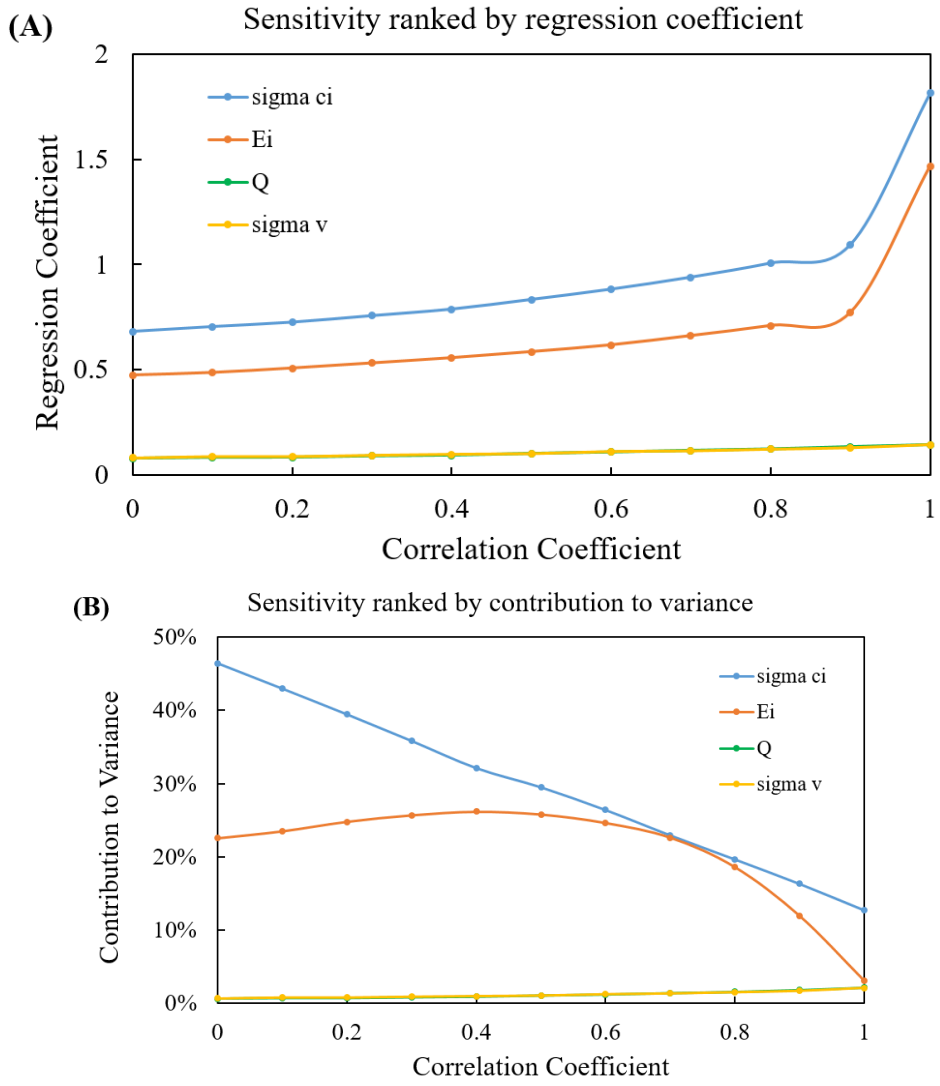

Figure 5.13 Effects of correlation on sensitivity: (A) ranked by regression coefficient; (B) ranked by the contrition to variance

$$\mu = \min + (\max - \min)\frac{\alpha_1}{\alpha_1 + \alpha_2} \tag{5.21}$$

$$\sigma = \frac{\max - \min}{\alpha_1 + \alpha_2}\sqrt{\frac{\alpha_1 \alpha_2}{\alpha_1 + \alpha_2 + 1}} \tag{5.22}$$

The comparison among the normal distribution, lognormal distribution and beta distribution for the intact UCS and elastic modulus with respective statistics is demonstrated in Figure 5.14. The effects of distribution types for the intact UCS and elastic modulus on the reliability were investigated and are shown in Figure 5.15. Three scenarios, including the normal, lognormal and beta distributions for both the intact UCS and elastic modulus, were compared to

the scenario with the combination of normal (UCS) and lognormal distributions (the elastic modulus), which was used in the reliability analysis shown in Figure 5.8. It can be seen in Figure 5.15 that all these three assumed distribution types generated lower reliability index and higher probability of failure than the scenario with combined distributions. The normal distribution scenario produces the lowest level of reliability, indicating the most conservativeness for the normal distribution assumption.

Table 5.4 Summary of distribution types for the UCS and elastic modulus of rocks.

Rock property	Distribution type	Literature
UCS	Normal distribution	Yamaguchi, 1970; Hoek 1998; Grasso et al., 1992; Hsu and Nelson, 2002; Pathak and Nelson, 2004; Gill et al., 2005; Sari and Karpuz, 2006
	Lognormal distribution	Lv et al., 2013; Song et al., 2016; Zeng et al., 2014; Lv et al., 2017; Pan et al., 2018
	Beta distribution	Baecher and Christian, 2003; Ang and Tang, 2007; Fenton and Griffiths, 2008; Song et al., 2016
Elastic modulus	Normal distribution	Hoek, 1998; Li and Low, 2010; Cai, 2011; Lv et al., 2011; Su et al., 2011; Song et al., 2016; Bjureland et al., 2017
	Lognormal distribution	Li and Low, 2010; Low and Einstein, 2013; Lv et al., 2011; Lv et al., 2013; Song et al., 2016; Tiwari et al., 2017; Lv et al., 2017
	Beta distribution	Li and Low, 2010; Lv et al., 2011; Song et al., 2016; Ang and Tang, 2007

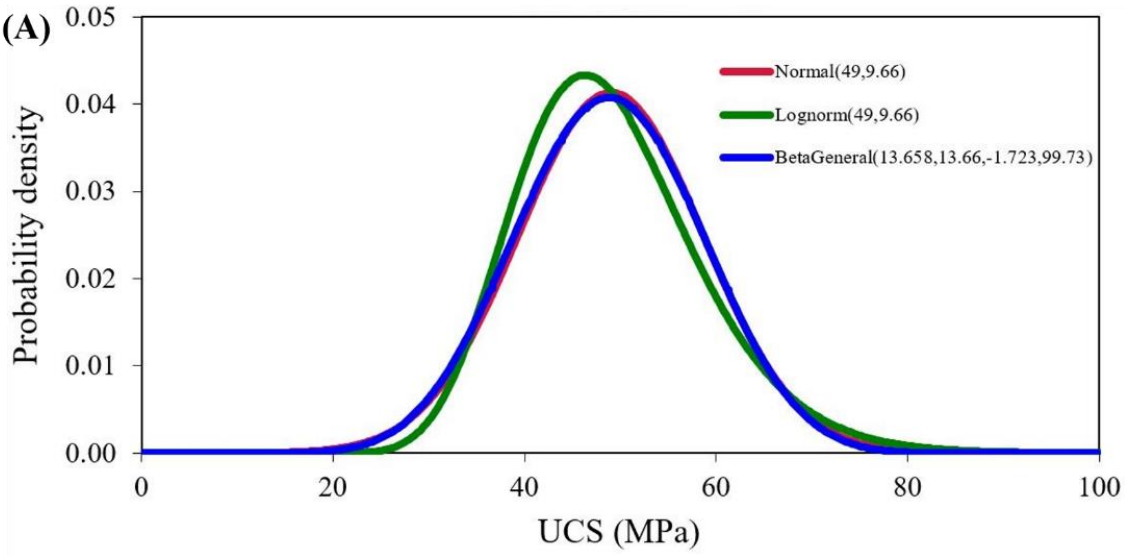

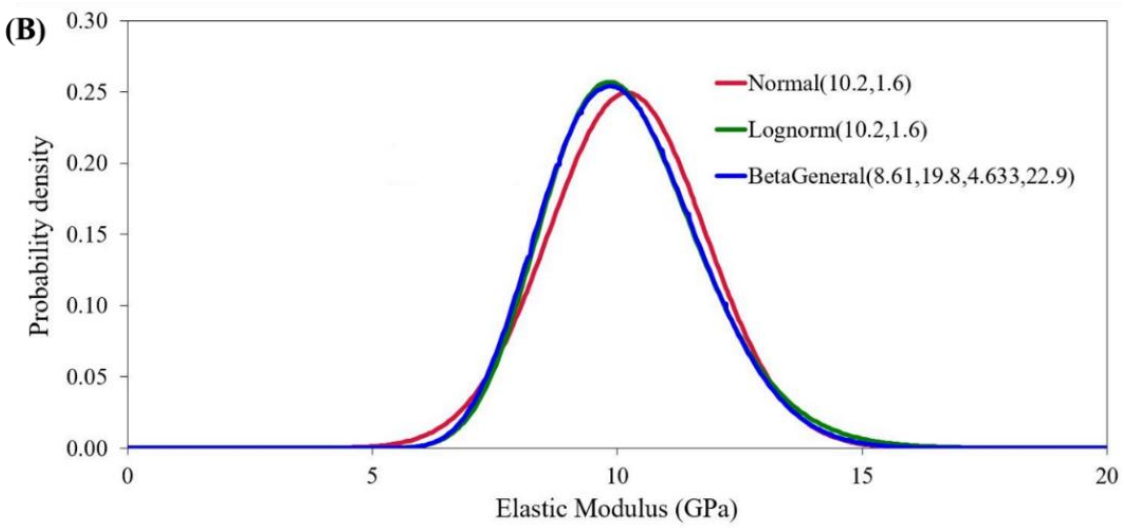

Figure 5.14 Comparison of PDFs of elastic modulus with different distribution assignments: (A) UCS; (B) elastic modulus

It is generally considered conservative to assume a normal distribution for geotechnical parameters according to published studies (Li and Low, 2010; Lü et al., 2013; Lü et al., 2011; Mollon et al., 2009b, 2010; Pan and Dias, 2018; Zeng et al., 2014), and the results in this study also confirm this statement. It is also found that the results generated from the beta distribution are closest to those produced from the scenario of the combined distributions. The characteristic of the bounded beta distribution being an appropriate approximation distribution for geotechnical parameters in reliability analysis has also been reported in literature (Li and Low, 2010; Lü et al., 2011; Mollon et al., 2009a, b, 2010; Pan and Dias, 2018; Song et al., 2016; Zeng et al., 2014). Note that the effects of different distribution types for the intact UCS and elastic modulus on the reliability are limited in this study. This may be due to the relatively high reliability in this case and the low variations of the intact UCS and elastic modulus with COV of 19.7% and 15.7%, respectively. The impact of different distribution assignments may be more significant given greater uncertainty and variability in the geotechnical input parameters. The advantage of excluding irrational negative values from lognormal and bounded beta distributions may also be more appreciated in scenarios of geotechnical parameters with more variability.

5.5.5 Effects of COV of intact UCS and elastic modulus

COV is a statistical measure of the overall dispersion in a geotechnical parameter and it has been widely used to describe the inherent variability of rocks and soils (Baecher and Christian, 2003; Fenton and Griffiths, 2008; Lacasse and Nadim, 1996; Phoon and Kulhawy, 1999).

Gunsallus and Kulhawy (1984) compiled a database of rock property measures, including the UCS and elastic modulus of intact rocks, from eight sedimentary rock units from the northeastern United States. The obtained results showed that the COV of UCS varied from 7% to 59% while the COV of elastic modulus were in the range between 7% and 48%. In this study, the COV of the intact UCS and elastic modulus was assumed to vary from 10% to 50%, and the effects of COV on the reliability were examined.

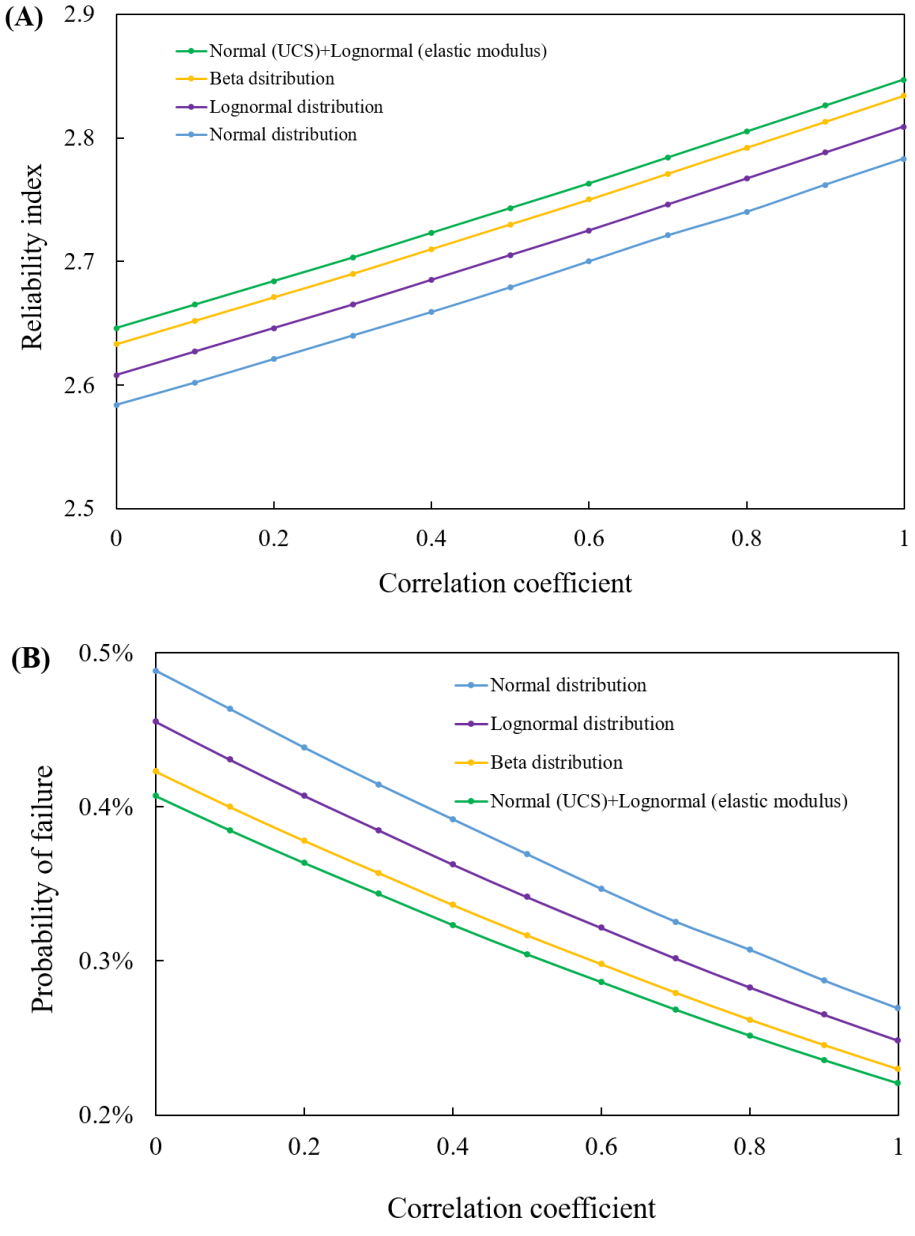

Figure 5.15 Effects of distribution types on the probability of failure: (A) reliability index; (B) probability of failure.

For the effects of the UCS on the reliability, the elastic modulus was set to follow lognormal distribution with COV of 15.7%, and the COV of UCS was varied from 10% to 50% to study its effect on the reliability index and the probability of failure. Similarly, for the effects of the elastic modulus on the reliability, the UCS was set to follow a normal distribution with COV of 19.7%, and the COV of the elastic modulus was changed from 10% to 50% to investigate its influence on the reliability. For the combined effects of UCS and elastic modulus, the COVs of these two parameters were changed to the same values simultaneously from 10% to 50%.

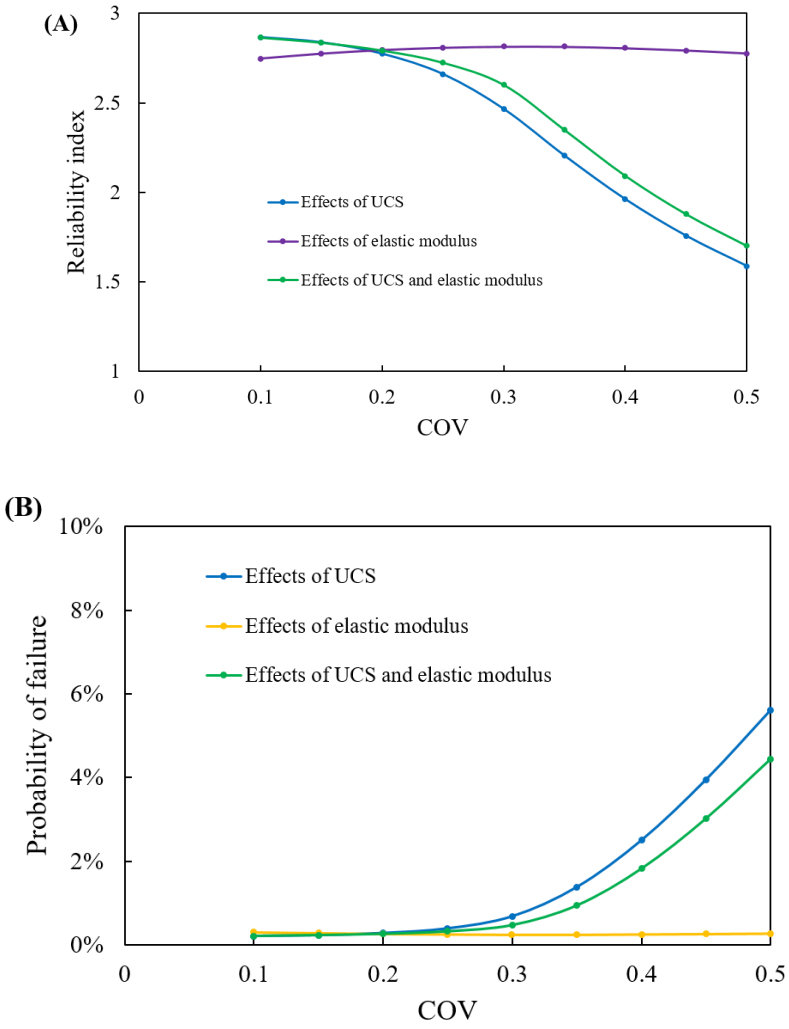

Figure 5.16 Effects of COV on the probability of failure: (A) reliability index; (B) probability of failure.

Figure 5.16 shows the effects of the COV on the reliability index and probability of failure. It is clear that the effects of the COV for the intact UCS on the reliability are significant. The

reliability index decreases from 2.87 to 1.59 and the probability of failure increases from 0.21% to 5.61% when the COV of UCS increases from 10% to 50%. By contrast, the reliability index and the probability of failure are insensitive to the variation of the COV of the elastic modulus. The reliability index changes from 2.75 to 2.78 and the probability of failure varies from 0.3% to 0.27% when the COV of the elastic modulus varies from 10% to 50%. This also verifies the greater significance of the UCS than the elastic modulus, which is consistent with the obtained sensitivity analysis results as described in Section 5.5.2. Interestingly, the simultaneous variation of the UCS and the elastic modulus has less influence on the reliability than that caused by the variation of the UCS alone even when the COV of the elastic modulus for the former (over 20%) is larger than the latter (19.7%). This may be due to the fact that the increase of the COV of the elastic modulus alone results in a slight increase of the reliability, as can be seen in Figure 5.16.

To investigate the effects of the variability on the reliability for scenarios with different distribution assumptions, the influences of the COV of the UCS and elastic modulus were compared under different distribution assignments, as shown in Figure 5.17. With regard to the effects of UCS on the reliability, similar to the scenarios in Figure 5.16, the elastic modulus was set to follow lognormal distribution with COV of 19.7% and the influences of the COV of the UCS under different distribution assignments on the reliability were compared. The effects of the elastic modulus and the combined effects of these two rock properties were also examined analogously. Results in Figure 5.17 show that the reliability results are most sensitive to the normal distribution, followed by the lognormal distribution and the beta distribution. This may be related to the non-skewness (or symmetry) of the normal distribution. The normal distribution also generates the most conservative results with lower reliability index and higher probability of failure than other distribution types, similar to the results in Section 5.5.4. It is also obvious to see that the reliability results are much more sensitive to the variability of the UCS than that of the elastic modulus. The reliability results generated in the normal distribution scenario are closer to those produced in the scenario with combined distributions than non-normal distribution scenarios. This may be due to the fact that the UCS is much more influential than the elastic modulus and that the normal distribution scenario has the same UCS distribution as the combined distribution scenario. Similar to what has been discussed in Section 5.4.5, this also indicates the importance to identify the most influential input parameter and assign appropriate distribution type to it due to its greatest contribution to the output parameter.

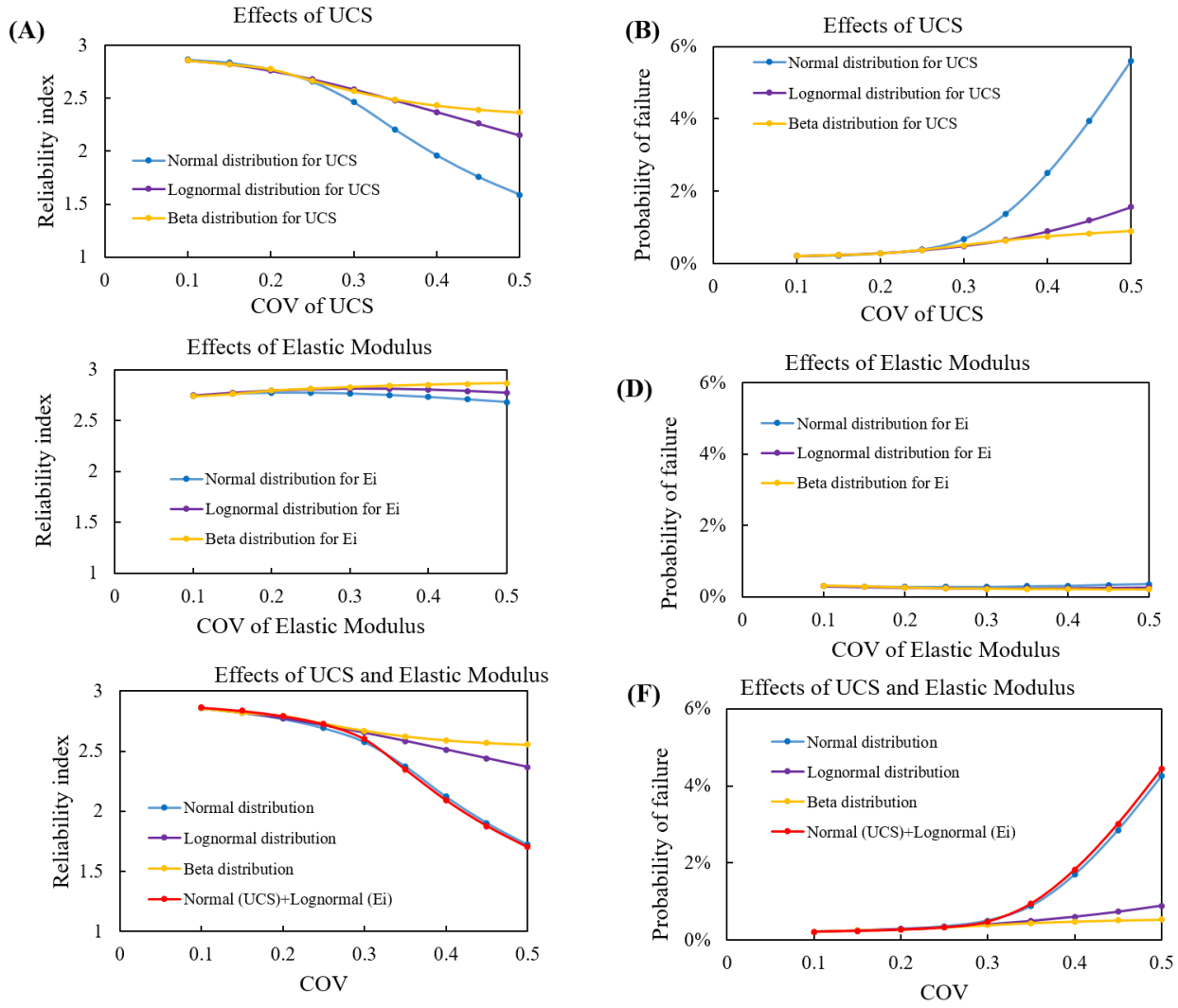

Figure 5.17 The effects of distribution types on the influences of COV on the probability of failure.

5.5.6 Reliability evaluation on the excavation stability

Excavation stability evaluation using different approaches

Recall that the obtained reliability index is 2.778 and the probability of failure is 0.27% with the probabilistic critical strain in the performance function, as shown in Figure 5.8. The target reliability indices and corresponding probability of failure are summarized by USACE (1997) for general structures in the geotechnical engineering field, as shown in Table 5.5. The probability of failure value for the excavated Shimizu tunnel is 0.27%. The expected performance level is worse than “above average” and better than “below average”.

Table 5.5 Target reliability indices (USACE, 1997)

Expected Performance Level	Reliability index	Probability of Unsatisfactory Performance
High	5	0.00003%
Good	4	0.003%
Above average	3	0.1%
Below average	2.5	0.6%
Poor	2.0	2.3%
Unsatisfactory	1.5	7%
Hazardous	1.0	16%

To verify the reliability evaluation results for the excavation stability, the stability of the excavated Shimizu tunnel was also assessed using analytical and numerical approaches for the comparative and check purposes for the same tunnel station STA 913+65 as in Chapter 4, The estimated PDFs of the tunnel strain were compared using analytical, numerical and empirical approaches. With regard to the analytical approach, the convergence-confinement method (CCM) (Carranza-Torres and Fairhurst, 2000; Panet and Guenot, 1983) was used. In the CCM method, the equivalent radius of 7 m was used. The calculated critical support pressure result is negative, indicating no plastic behavior took place. The radial elastic displacement was calculated and used in the study; in terms of the numerical approach, Rocsupport and RS2 FEM software were employed; as for the empirical approach, the tunnel displacement estimation approach developed by Barton (2002) was utilized in this study for reliability analysis.

These obtained PDFs of tunnel strain are summarized with respective statistical moments in Figure 5.18 in comparison to the PDF of estimated critical strain. In the critical strain-based limit state function, the estimated strains using different approaches can be regarded as the load component in the realm of LRFD, while the critical strain may be viewed as the resistance component. All the estimated PDFs of tunnel strain are on the left of the PDF of critical strain, and the potential for failure can be represented by the overlapping area between PDF curves of the estimated strain (load component) and critical strain (resistance component). As mentioned above, the probability of failure derived from the empirical Barton approach (Barton, 2002) is 0.27% using the FORM algorithm. Results in Figure 5.18 show that the overlapping areas in the scenarios with other approaches are larger than that in the scenario with the Barton approach (Barton, 2002), indicating probability of failure values greater than 0.27%.

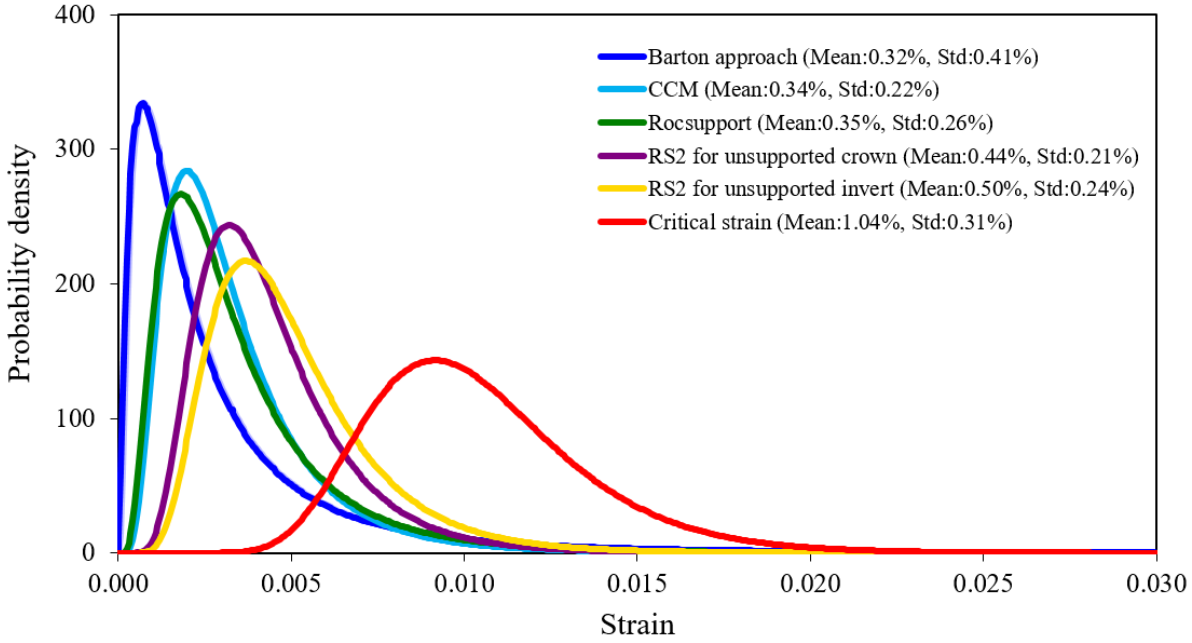

Figure 5.18 Comparison of PDFs of estimated strain and critical strain.

The CCM and Rocsupport results show the elastic behavior in the excavated tunnel, meaning no plastic zone generated around the excavated tunnel. Note that the equivalent radius of 7 m is used in the CCM and Rocsupport, and the mean displacement is 2.38 and 2.45 cm, respectively. These relatively small elastic displacements indicate the unsupported tunnel is stable.

The unsupported tunnel strains estimated using the RS2 FEM software, which have higher mean values, result in larger overlapping areas, as seen in Figure 5.18. Figure 5.19 illustrates the calculated displacement contours around the tunnel excavation. There is no significant plastic behavior, and the sheared or tensioned yielding mainly takes place around the tunnel periphery. The maximum displacement occurs at the invert with mean of 4.5 cm and SD of 2.2 cm, corresponding to a mean strain of 0.75% and a strain SD value of 0.36%. The crown displacement has the mean of about 4 cm and SD value of about 2 cm, corresponding to a mean strain of 0.66% and a strain SD value of 0.33%.

To evaluate the crown displacement for the unsupported tunnel, the ground reaction curves have been generated using the RS2 software. The tunnel is assumed to be full-face excavated, and the mean and lower bound (one standard deviation below the mean) rock mass properties have been considered. Figure 5.20 shows the ground reaction curves for mean and lower bound cases.

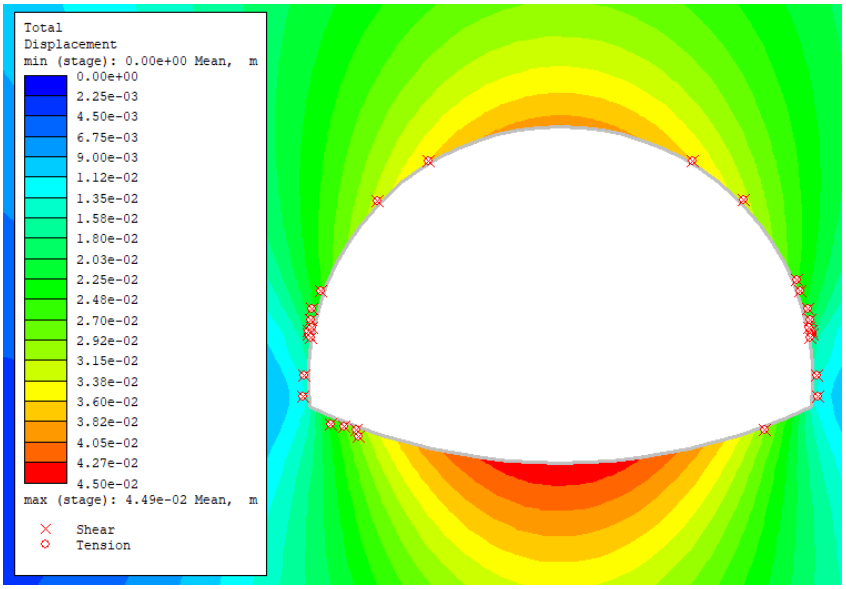

Figure 5.19 Displacement contour of the unsupported tunnel.

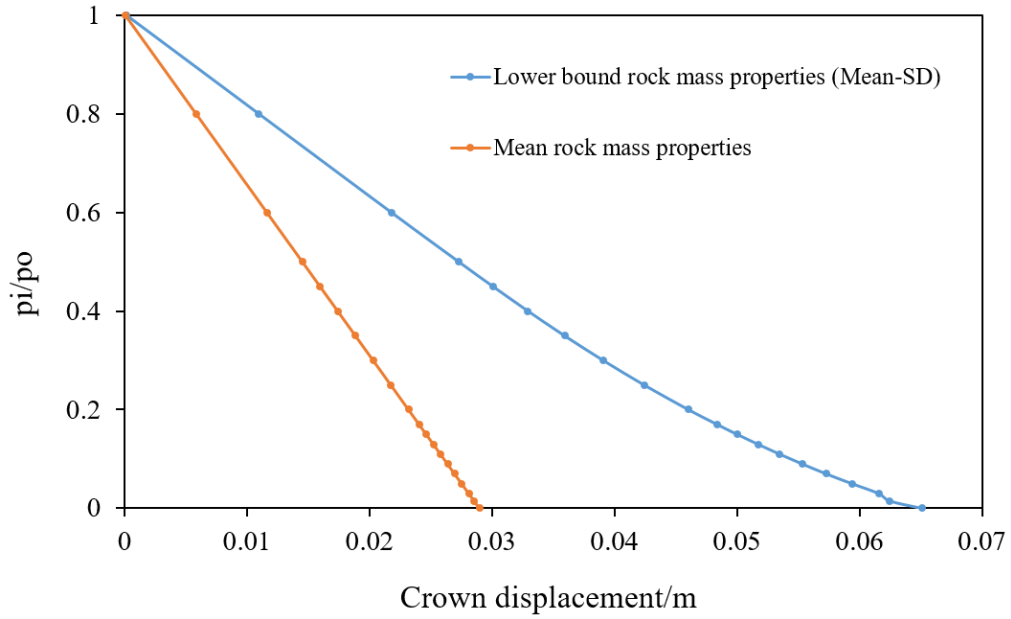

Figure 5.20 Ground reaction curves using mean and low bound rock mass properties

The ground reaction curves are linear, indicating the elastic behavior in the tunnel. Total elastic crown displacements for the fully relaxed tunnel are 2.9 and 6.5 cm for the mean and lower bound cases, respectively. Considering the large span and height of the tunnel, the elastic displacement on the order of 4 cm is not expected to cause failure or instability during the construction. In addition, the strength factor, a measure of safety level in terms of strength-to-stress ratio, has been obtained and its contour is shown in Figure 5.21.The strength factor at the crown

has a mean value of 2.9 with COV of 37%. The minimum strength factor is observed at the corner with a mean value of 1.51 and COV of 25%. Thus, it is highly likely that the unsupported Shimizu tunnel is not expected to encounter instability after excavation.

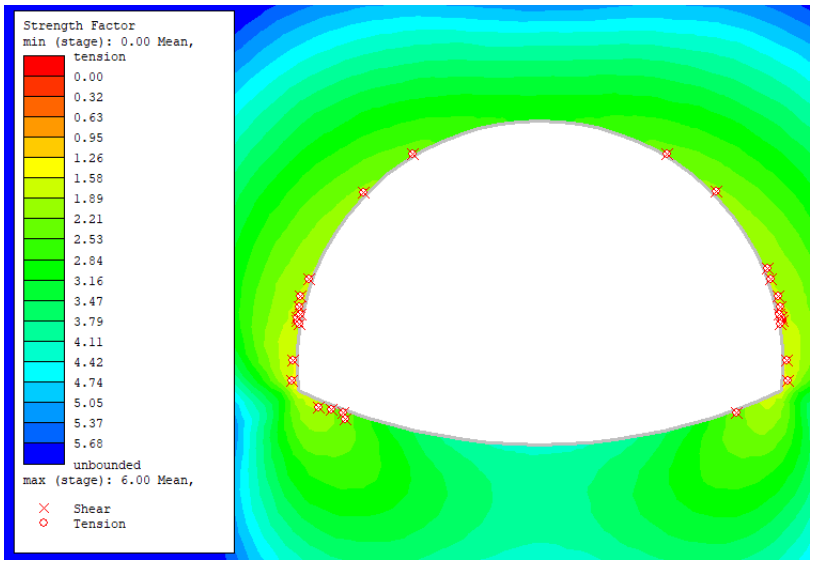

Figure 5.21 The strength factor contour of the unsupported tunnel.

Comparison between unsupported and supported case

As mentioned in Section 4.4.3 in Chapter 4, the primary support was designed based on Japanese highway rock mass classification systems in the Shimizu tunnel, and it was a combination of rockbolts, shotcrete and steel arch. The tunnel construction using the heading and bench method was modeled using the RS2 software with the prescribed support installed.

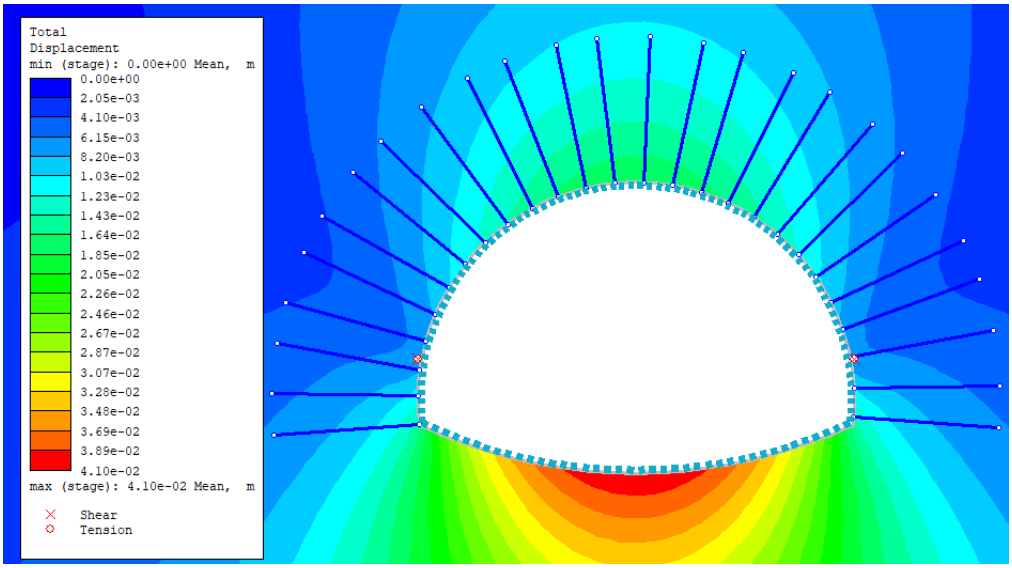

Figure 5.22 The displacement contour of the supported tunnel

Figure 5.22 shows the displacement contour of the fully excavated tunnel after support. The tunnel displacements with and without support are compared in Table 5.6. The supported tunnel crown has the mean value of 1.85 cm and SD value of 0.87 cm, corresponding to a mean strain of 0.31% and a strain SD value of 0.15%. Compared to the unsupported tunnel case, the crown displacement reduced significantly with the tunnel support installed. The distributions of crown displacement between unsupported and supported tunnel are compared in Figure 5.23. The distributions of empirically estimated strain using Barton approach and the critical strain are also included for comparison. It is seen that the mean and SD decrease by about 50% from the unsupported case to supported case. It also reveals that the overlapping area between the tunnel crown strain in the supported case and the critical strain is much smaller than that derived from the Barton approach, indicating a smaller probability of failure in the supported tunnel case (<0.27%). Thus, the reliability of the tunnel has increased significantly with the support installed.

Table 5.6 Comparison of tunnel displacement before and after the support installation

Scenario	Displacement (cm)						Strain			
	Crown C			Invert			Crown C		Invert	
	Mean	SD	COV	Mean	SD	COV	Mean	SD	Mean	SD
Without support	3.95	1.97	50%	4.49	2.19	49%	0.44%	0.22%	0.06%	0.50%
With support	1.85	0.87	47%	4.1	1.98	48%	0.21%	0.10%	0.05%	0.46%

The Q-based support chart is shown in Figure 5.24. The 1.5ESR and 5Q can be used for the temporary support for underground openings (Barton and Grimstad, 2014). Figure 5.24 shows the suggested temporary support based on the Q-support chart (NGI, 2015). Support category 3 is recommended, including systematic bolting and fiber reinforced sprayed concrete of 5-6 cm thickness. Clearly, the heavy and rigid support adopted in the Shimizu tunnel, selected based on Japanese highway rock mass classification system, is much more conservative than the Q-based support recommendation.

Based on the stability evaluation results mentioned above, it is shown that the unsupported tunnel is not expected to encounter instability after excavation. However, note that the analyses and discussion aim to provide a preliminary evaluation on the excavation stability and only stress-induced instability is considered. In reality, there may be some structurally-controlled instability issues for the excavated tunnel especially considering three dominant joint sets in the Shimizu

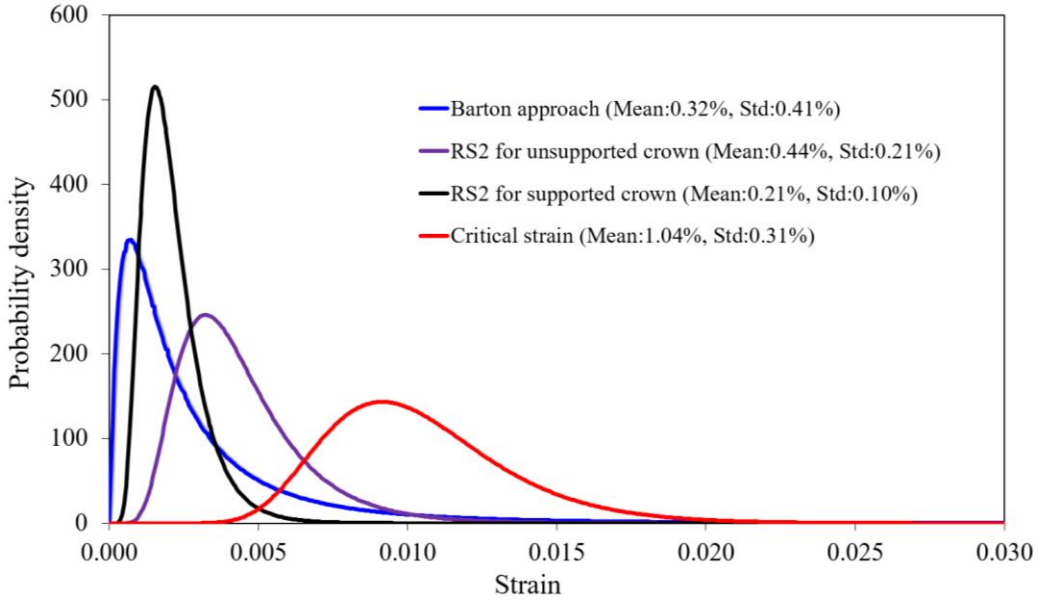

Figure 5.23 Distribution comparison of estimated strain between unsupported and supported tunnel cases

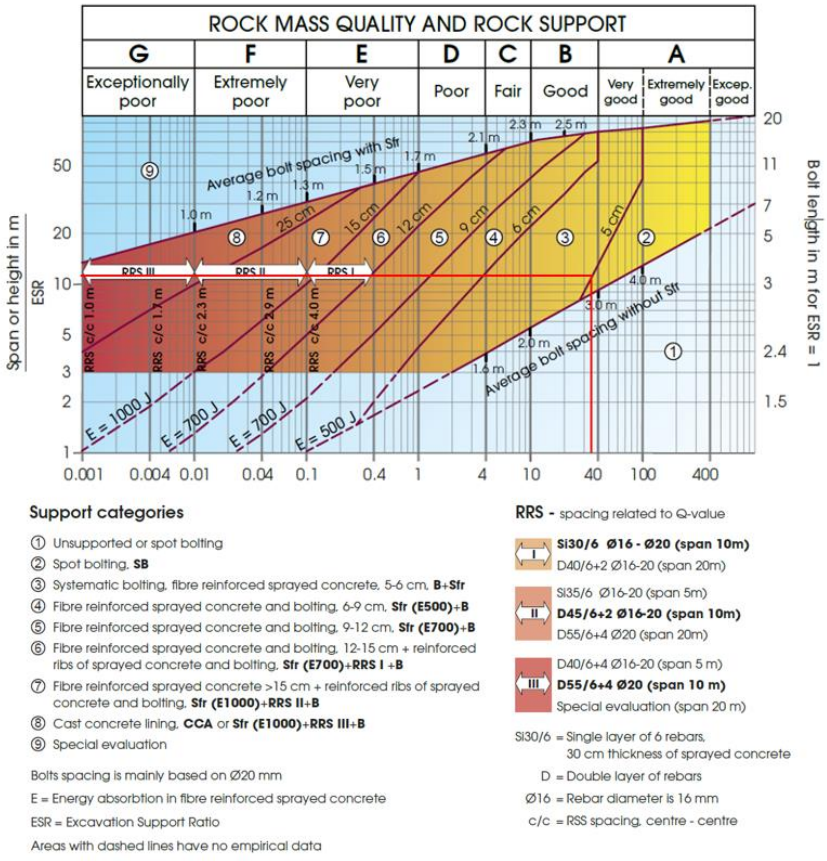

Figure 5.24 Temporary support based on the Q-support chart (NGI, 2015)

tunnel area. As a result, rockbolts and shotcrete may be required to support the loose blocks formed by the intersection of joint sets. Actual construction practice is more complicated than the modeled scenario since there are more factors involved, such as the heterogeneity and spatial variability of rock mass, the varying overburden, the seismic consideration, the safety of the workforce during construction etc. The overly-conservative support system used in the Shimizu tunnel may be designed to have considered the weak and very weak rock mass near the fault zones at the eastern sector and portal areas. In this study, the stability of the tunnel excavation has been evaluated from a perspective of reliability, and the reliability evaluation results have confirmed the stability of the excavated tunnel, which is also consistent with the stability assessment results using analytical and numerical approaches.

5.6 Conclusions

The reliability assessment with a strain-based failure criterion for the stability evaluation of underground excavation has been performed using the FORM algorithm with the Q-based empirical approach. The Shimizu highway tunnel case study was utilized as an example to perform the reliability evaluation. Reliability analyses were conducted using the FORM algorithm with both the deterministic and probabilistic critical strain which accounts for uncertainties in rock mass parameters. The reliability analysis using the MCS simulation was also performed for comparison. The reliability analysis results obtained from the FORM algorithm agreed well with those derived from the MCS technique. The FORM algorithm can be used as a complement to the MCS simulation in reliability analysis when dealing with complicated problems that require considerable computation efforts for MCS iterations.

Reliability analysis results show that the reliability level increased, represented by the increase of the reliability index and the decrease of the probability of failure, with the increase of deterministic critical strain value. However, the deterministic critical strain does not consider inherent uncertainties in rock masses. The selection of an appropriate deterministic critical strain value is also not an easy task, which may require the site knowledge, local construction experience as well as engineering judgement based on some numerical calculations or field measurements. However, the probabilistic critical strain, which enables the consideration of uncertainties in rock mass parameters, is capable of overcoming these difficulties when choosing appropriate single critical strain value in the deterministic critical strain approach.

The effects of correlation in input parameters on the reliability were investigated. Results show that the negative correlation between RQD and J_n had limited influence on the reliability. The positive correlation between the intact UCS and elastic modulus was also examined, and it was found that the reliability results would be conservative if the positive correlation between the intact UCS and elastic modulus is overlooked. In addition, the effects of distribution types for the intact UCS and elastic modulus were also studied. The normal distribution assignment generated the most conservative reliability results. Thus, the assumption of uncorrelated and normally distributed input parameters (intact UCS and elastic modulus) has generated more conservative reliability results in this case study.

The influence of COV in input parameters on the reliability has also been examined. Results show that its effect on the reliability was dependent on the relative importance of the input parameter. Probabilistic sensitivity analysis indicates the intact UCS was the most influential input parameter while the elastic modulus had limited influence. The variations in COV for the intact UCS had a great effect on the reliability while the reliability results were insensitive to variations in COV for the intact elastic modulus.

The reliability analysis results show that the Shimizu tunnel had a relatively high reliability (reliability index of 2.78 and probability of failure of 0.27%) and was not expected to experience instability after excavation. The excavation stability has also been evaluated using analytical and numerical approaches, and the obtained results were consistent with reliability assessment results, which has also verified the effectiveness of the reliability-based excavation stability evaluation. The reliability of the supported tunnel with the actually installed support system has also been examined, and results show that the reliability has greatly improved compared to the unsupported tunnel case. The reliability assessment using the FORM algorithm with the Q-based empirical approach can be used as a complement to analytical and numerical approaches in the preliminary evaluation of the stability of underground excavations.

CHAPTER 6

CONCLUSIONS AND RECOMMENDATIONS

The research presented in this report attempts to improve the understanding of the inherent uncertainties in rock mass classifications and investigate the uncertainty propagation into the analysis and design process of underground construction. A systematic assessment of uncertainties in rock mass classification systems, using the Q-system as an example in this study, was performed. The Markov Chain technique has been incorporated in the Q-based prediction model to provide the probabilistic distribution of the Q value in unexcavated tunnel sections. The results can be used to complement geology exploration in planning and preliminary stages of tunnel projects. In addition, an MCS-based uncertainty analysis framework of the probabilistic Q-system has also been developed to characterize the uncertainty in input parameters of the Q-system and investigate its effects on the rock mass property characterization and ground response evaluation in tunneling. The developed framework can be helpful in providing insightful information for the probabilistic evaluation of excavation-induced ground behavior and the probabilistic tunnel design. Moreover, the research performed reliability analysis using the Q-based empirical approach, which incorporates probabilistic critical strain and Q-based empirically estimated strain, to preliminarily evaluate the stability of underground opening. The reliability analysis using the Q-based empirical approach can supplement analytical and numerical approaches in the preliminary evaluation of tunnel excavation stability. The chapter summarizes major findings and conclusions from each chapter of the report, and some recommendations for future research are also presented.

6.1 Specific conclusions from each chapter

6.1.1 Probabilistic prediction of rock mass quality

In Chapter 3, a Markovian Q-based prediction model has been proposed using the MCS technique to provide the probability distribution of rock mass quality along the tunnel alignment before construction. In addition to the MCS-based predicted results, an analytical approximation approach to deriving the statistics (mean, standard deviation, COV) of the Q value has also been developed given the statistics of input parameters in the Q-system. The proposed probabilistic prediction model and the developed analytical approach have been applied to a water tunnel section for the purpose of validation. The MCS-derived and analytically calculated Q values were

comparable to the actually recorded Q results, which has also proved the validity of the proposed prediction model and developed analytical approach.

Probabilistic sensitivity analysis was also carried out in the MCS process and the most influential input parameters in the Q-system are J_n and RQD in the tornado graphs in this case study, consistent with the greater variations in the predicted probabilistic profile of Q-parameters J_n and RQD. In addition, the negative correlation between RQD and J_n was presented, and the mean and dispersion of the Q value were found to be underestimated if the correlation was neglected. The effects of distribution type for RQD on the Q value have also been examined. The normal distribution was a good fit for the actually recorded RQD data in this case study, and the simulated statistics of the Q value under this normal distribution assumption agreed well with the actually recorded Q results.

The proposed Q-based prediction model is helpful in reducing uncertainties and risks involved in rock mass classifications and can serve as a complement to geology exploration in the planning and preliminary design stage of underground construction. It can also provide insights into the decision support for the design of excavation sequence and support schemes for the underground structures.

6.1.2 Uncertainty analysis in probabilistic Q-system

In Chapter 4, an MCS-based uncertainty analysis framework in the Q-system has been developed to probabilistically characterize the uncertainty in input parameter of Q-system and its effects on rock mass characterization and ground response by applying the MCS technique with appropriate empirical correlations. A case study of the Shimizu highway tunnel was adopted to implement the developed framework. The probabilistic distribution of the Q value was obtained using the MCS technique based on relative frequency histograms of the Q-parameters. The MCS-derived Q statistics are more reasonable than the conventional estimation results using the interval analysis. The MCS technique can more realistically take into account the correlations in input parameters in the estimation as well as providing the full probabilistic distribution of the Q value, while the estimation using the conventional approach is based on assumptions of perfect correlations which are rarely met in practice. Similarly, based on appropriate Q-based empirical correlations, probabilistic estimates of rock mass properties were obtained, which were subsequently used as inputs in numerical models for excavation response evaluation. The empirically estimated probabilistic tunnel displacement, obtained by the Barton approach,

generally agreed with that derived from the probability analysis in the FEM RS2 numerical models with the PEM and MCS sampling techniques.

The advantage of probabilistic sensitivity analysis in the MCS process has been pointed out over the traditional one-way sensitivity analysis. The probabilistic sensitivity analysis takes the input distributions into account and enables simultaneous variations of all the input parameters based on their respective distributions. The probabilistic sensitivity analysis results agreed well with those obtained from other sensitivity analysis techniques in the probabilistic Q-system in this case study. The use of different sensitivity analysis methods is suggested for comparative and checking purposes.

The effects of the negative correlation between RQD and J_n have also been examined. The mean and dispersion of the Q value and associated rock mass parameters would be underestimated if the negative correlation was not modeled in this case study. The effects of the distribution types of Q-parameters on the Q value and associated rock mass parameters were significant. Caution should be exercised when selecting appropriate distribution types for Q-parameters when only limited site investigation data are available, and a combination of site knowledge, local experience and professional engineering judgement should be used.

The proposed framework of the MCS-based uncertainty analysis in the probabilistic Q-system provides an approach for systematically characterizing the uncertainty in the rock mass classification and its propagation to associated rock mass parameters. The framework can also serve as a useful tool to obtain insightful information for the probabilistic evaluation of ground responses and support performance of underground structures.

6.1.3 Reliability evaluation on tunnel excavation stability

In Chapter 5, reliability assessment with the strain-based failure criterion has been performed using the FORM algorithm. The probabilistic critical strain and Q-based empirically estimated tunnel strain were incorporated in the limit state function. The Shimizu highway tunnel case study was also utilized as an example to perform the reliability evaluation on the excavation stability. Reliability analysis using the MCS technique was also performed for comparison. The reliability analysis results obtained from the FORM algorithm agreed well with those derived from the MCS technique.

The effects of correlation in the input parameters on the reliability have also been investigated. The negative correlation between RQD and J_n had limited influence on the reliability in this

Shimizu tunnel case study. The positive correlation between the UCS and elastic modulus of intact rocks was also presented based on available data. The impact of the positive correlation on the reliability was significant, and the reliability would be conservative if the positive correlation is overlooked. In addition, the effects of distribution types for the UCS and elastic modulus of intact rocks were also studied. The normal distribution assignment generated the most conservative reliability results than other distributions. Thus, the assumption of uncorrelated and normally distributed input parameters (intact UCS and elastic modulus) generated more conservative reliability results in this case study.

The influence of COV in input parameters on the reliability has also been examined. Results show that its effect on the reliability was dependent on the relative importance of the input parameters. Probabilistic sensitivity analysis indicated the intact UCS was the most influential input parameter while the elastic modulus has limited influence in this case study. The variations in COV for the intact UCS had great effects on the reliability while the reliability results were insensitive to variations in COV for the intact elastic modulus.

The reliability analysis results show that the Shimizu tunnel had a relatively high reliability (reliability index of 2.78 and probability of failure of 0.27%) and was not expected to experience instability after excavation. The excavation stability has also been evaluated using analytical and numerical approaches, and the obtained results were consistent with reliability assessment results, which has verified the effectiveness of the reliability-based evaluation on tunnel excavation stability. Thus, the reliability assessment using the Q-based empirical approach can be used as a complement to analytical and numerical approaches in the preliminary evaluation of the stability of underground excavations.

6.2 Recommendations for future research

The aim of this research is to advance understanding of uncertainty analysis in rock mass classification systems in the current research, using the rock mass classification Q-system in this study, and apply it to the reliability-based evaluation on the stability of underground excavations. Due to the limited availability of rock mass classification data, only two tunnel cases with available Q data have been used. Thus, the research presented in this report should be applied to more case studies with Q data to test the performance of the prediction model and to verify the validity of the developed uncertainty analysis framework. In addition, the extension of the research should also

be made to other rock mass classification systems such as RMR and GSI. With regard to the proposed probabilistic prediction model, the predicted Q values for the unexcavated tunnel sections have been validated by the actually recorded Q results during construction. However, the probabilistic prediction model has not been incorporated and updated based on newly available data during tunnel construction. Moreover, in terms of the reliability-based analysis, the focus in this research was the preliminary evaluation on the tunnel excavation stability. The performance of the actually installed support was verified, but the reliability-based design for the underground excavations, e.g. the design for the required support systems, has not been conducted.

In view of the needs of this research mentioned above, the following future research can be performed to have an improved understanding of the uncertainty in rock mass classifications and its effect on the tunnel design aspect:

- Implementation of the research to more tunnel case studies with Q data should be performed. Tunnel case examples with Q data should be used to test the performance of the proposed probabilistic prediction model and to verify the validity of the developed uncertainty analysis framework in this study.
- Extension of the research to other rock mass classifications (RMR, GSI) should be conducted. Different rock mass classification (RMR, GSI) data available from various tunnel projects should be collected and utilized to verify the proposed prediction model and developed uncertainty analysis framework.
- Incorporation of the proposed probabilistic prediction model using the Bayesian updating technique or equivalent should be conducted based on the newly available data during construction. Newly available rock mass classification data or tunnel response data (displacement, strain, load, pressure etc.), observed or measured during tunnel construction, can be used to update the previous predictions.
- Reliability-based design should be performed to optimize tunnel support. For example, the required tunnel support can be estimated according to prescribed target reliability index or maximum allowable probability of failure within the framework of reliability-based design. Support design parameters, such as the shotcrete thickness or the distance of the support installation behind the tunnel face, can be evaluated and optimized to achieve the desired reliability level for the tunnel support design.

ACKNOWLEDGEMENTS

Support from the University Transportation Center for Underground Transportation Infrastructure (UTC-UTI) at the Colorado School of Mines for funding this research under Grant No. 69A3551747118 from the U.S. Department of Transportation (DOT) is gratefully acknowledged.

REFERENCES

Adoko, A.-C., Jiao, Y.-Y., Wu, L., Wang, H., Wang, Z.-H., 2013. Predicting tunnel convergence using multivariate adaptive regression spline and artificial neural network. Tunnelling and Underground Space Technology 38, 368-376.

Andrade, P.S., Saraiva, A.A., 2008. Estimating the joint roughness coefficient of discontinuities found in metamorphic rocks. Bulletin of Engineering Geology and the Environment 67, 425-434.

Ang, A.H.-S., Tang, W.H., 2007. Probability concepts in engineering: emphasis on applications in civil & environmental engineering. Wiley New York.

Arslan, A., Koca, M., Aydogmus, T., Klapperich, H., Yılmaz, H., 2008. Correlation of unconfined compressive strength with young's modulus and poisson's ratio in gypsum from Sivas (Turkey). Rock mechanics and rock engineering 41, 941-950.

Baecher, G.B., Christian, J.T., 2003. Reliability and statistics in geotechnical engineering. John Wiley & Sons, New York.

Bai, Y., Han, X., Jiang, C., Liu, J., 2012. Comparative study of metamodeling techniques for reliability analysis using evidence theory. Advances in Engineering Software 53, 61-71.

Barton, 1993. Application of Q-System and Index Tests to Estimate Shear Strength and Deformability of Rock Masses. Workshop on Norwegian Method of Tunneling.

Barton, 2002. Some new Q-value correlations to assist in site characterisation and tunnel design. International journal of rock mechanics and mining sciences 39, 185-216.

Barton, Grimstad, E., 2014. Forty years with the Q-system in Norway and abroad. Fjellsprengningsteknikk, NFF: Olso, Norway.

Barton, Gutierrez, M., Løset, F., 1995. Shimizu Tunnel No. 3–Tomei II Highway Project. Application of Q system, UDEC-BB and NMT principles to Shimizu No. 3 tunnel design–Phase I, 951024-951021.

Barton, N., 1996. Estimating rock mass deformation modulus for excavation disturbed zone studies, Proc. of excavation disturbed zone workshop, eds. JB Montino & CD Martin, pp. 133-144.

Barton, N., By, T., Chryssanthakis, P., Tunbridge, L., Kristiansen, J., Løset, F., Bhasin, R., Westerdahl, H., Vik, G., 1994. Predicted and measured performance of the 62 m span Norwegian Olympic Ice Hockey Cavern at Gjøvik, International Journal of Rock Mechanics and Mining Sciences & Geomechanics Abstracts. Elsevier, pp. 617-641.

Barton, N., Chrysanthakis, P., 1996. Shimizu Tunnel No. 3–Tomei II Highways Project. Preliminary NMT modeling using UDEC-BB, UDEC-S (fr) and 3DEC, with M= 1 GPa and M= 2 GPa deformation moduli. Norwegian Geotechnical Institute Report, 1.

Barton, N., Lien, R., Lunde, J., 1974. Engineering classification of rock masses for the design of tunnel support. Rock mechanics 6, 189-236.

Basarir, H., 2008. Analysis of rock–support interaction using numerical and multiple regression modeling. Canadian Geotechnical Journal 45, 1-13.

Bedi, A., 2013. A proposed framework for characterising uncertainty and variability in rock mechanics and rock engineering. Imperial College London, London, United Kingdom.

Bedi, A., 2014. A proposed framework for characterising uncertainty and variability in rock mechanics and rock engineering. Imperial College London.

Beer, A., Stead, D., Coggan, J., 2002. Technical note estimation of the joint roughness coefficient (JRC) by visual comparison. Rock mechanics and rock engineering 35, 65-74.

Benhalima, M., 2016. Evaluation of the differences in characterization and classification of the rock mass quality: A comparison between pre-investigation, engineering geological forecast and tunnel mapping in the Northern Link project and the Cityline project.

Benjamin, J.R., Cornell, C.A., 2014. Probability, statistics, and decision for civil engineers. Courier Corporation.

Bi, L., Ren, B., Zhong, D., Hu, L., 2015. Real-Time Construction Schedule Analysis of Long-Distance Diversion Tunnels Based on Lithological Predictions Using a Markov Process. J Constr Eng Manag 141, 04014076.

Bieniawski, Z., 1976. Rock mass classification in rock engineering applications, Proceedings of a Symposium on Exploration for Rock Engineering, 1976, pp. 97-106.

Bieniawski, Z., 1989. Engineering rock mass classifications: a complete manual for engineers and geologists in mining, civil, and petroleum engineering. John Wiley & Sons, New York.

Bieniawski, Z., 1993. Classification of rock masses for engineering: the RMR system and future trends, Rock Testing and Site Characterization. Elsevier, pp. 553-573.

Bjureland, W., Spross, J., Johansson, F., Prästings, A., Larsson, S., 2017. Reliability aspects of rock tunnel design with the observational method. International Journal of Rock Mechanics and Mining Sciences 98, 102-110.

Brox, D., 2017. Practical Guide to Rock Tunneling. CRC Press.

Cai, M., 2011. Rock mass characterization and rock property variability considerations for tunnel and cavern design. Rock mechanics and rock engineering 44, 379-399.

Cai, M., Kaiser, P., Uno, H., Tasaka, Y., Minami, M., 2004. Estimation of rock mass deformation modulus and strength of jointed hard rock masses using the GSI system. International Journal of Rock Mechanics and Mining Sciences 41, 3-19.

Carle, S., 2000. Use of a transition probability/Markov approach to improve geostatistical simulation of facies architecture, Hedberg symposium: applied reservoir characterization using geostatistics. American association of petroleum geologists (AAPG), The Woodlands, TX, pp. 3-6.

Carranza-Torres, C., Fairhurst, C., 2000. Application of the convergence-confinement method of tunnel design to rock masses that satisfy the Hoek-Brown failure criterion. Tunnelling and Underground Space Technology 15, 187-213.

Carter, T., 1992. Prediction and uncertainties in geological engineering and rock mass characterization assessments, Proc. 4th. int. rock mechanics and rock engineering conf.

Chan, M.H.C., 1981. A geological prediction and updating model in tunneling. Massachusetts Institute of Technology.

Chen, J., Li, X., Zhu, H., Rubin, Y., 2017. Geostatistical method for inferring RMR ahead of tunnel face excavation using dynamically exposed geological information. Eng Geol 228, 214-223.

Chern, J., Shiao, F., Yu, C., 1998a. An empirical safety criterion for tunnel construction, Proceedings of the regional symposium on sedimentary rock engineering, Taipei, Taiwan, pp. 222-227.

Chern, J., Yu, C., Shiao, F., 1998b. Tunnelling in squeezing ground and support estimation, Proc. Regional Symposium on Sedimentary Rock Engineering, Taipei, pp. 192-202.

Daraei, A., Zare, S., 2018. A new strain-based criterion for evaluating tunnel stability. Geomechanics and Engineering 16, 205-215.

Daraei, A., Zare, S., 2019. Modifying Tunnel's Hazard Warning Levels based on the Laboratory Studies on Different Rock Types. KSCE Journal of Civil Engineering 23, 2384-2390.

Deere, D., 1968. Geological considerations. Rock Mechanics in Engineering Practice, Stagg and Zienkiewicz. John Wiley, London.

Ditlevsen, O., 1981. Uncertainty modeling with applications to multidimensional civil engineering systems. McGraw-Hill New York.

Duncan Fama, 1993. Numerical modeling of yield zones in weak rock, Analysis and design methods. Elsevier, pp. 49-75.

Duncan, J.M., 2000. Factors of safety and reliability in geotechnical engineering. Journal of geotechnical and geoenvironmental engineering 126, 307-316.

Einstein, H., Baecher, G., 1982. Probabilistic and statistical methods in engineering geology I. Problem statement and introduction to solution, Ingenieurgeologie und Geomechanik als Grundlagen des Felsbaues/Engineering Geology and Geomechanics as Fundamentals of Rock Engineering. Springer, pp. 47-61.

Einstein, H.H., Baecher, G.B., 1983. Probabilistic and statistical methods in engineering geology. Rock mechanics and rock engineering 16, 39-72.

Elandt-Johnson, R.C., Johnson, N.L., 1980. Survival Models and Data Analysis. John Wiley & Sons, New York.

Elfeki, A., Dekking, M., 2001. A Markov chain model for subsurface characterization: theory and applications. Math Geol 33, 569-589.

Elfeki, A.M.M., Dekking, F.M., 2005. Modelling Subsurface Heterogeneity by Coupled Markov Chains: Directional Dependency, Walther's Law and Entropy. Geotech Geol Eng 23, 721-756.

Esfahani, N.M., Asghari, O., 2013. Fault detection in 3D by sequential Gaussian simulation of Rock Quality Designation (RQD). Arabian Journal of Geosciences 6, 3737-3747.

Ewan, V., West, G., Temporal, J., 1983. Variation in measuring rock joints for tunnelling. Tunnels & Tunnelling International 15.

Fang, H., Rais-Rohani, M., Liu, Z., Horstemeyer, M., 2005. A comparative study of metamodeling methods for multiobjective crashworthiness optimization. Computers & Structures 83, 2121-2136.

Fatemi, S.A., Ahmadi, M., Rostami, J., 2018. Evaluation of TBM performance prediction models and sensitivity analysis of input parameters. Bulletin of Engineering Geology and the Environment 77, 501-513.

Felletti, F., Beretta, G.P., 2009. Expectation of boulder frequency when tunneling in glacial till: A statistical approach based on transition probability. Eng Geol 108, 43-53.

Fenton, G., Griffiths, V., 2008. Risk assessment in geotechnical engineering. John Wiley & Sons, New York.

Ferrari, F., Apuani, T., Giani, G.P., 2014. Rock Mass Rating spatial estimation by geostatistical analysis. Int J Rock Mech Min Sci 70, 162-176.

Fujii, Y., Kiyama, T., Ishijima, Y., Kodama, J., 1998. Examination of a rock failure criterion based on circumferential tensile strain. pure and applied geophysics 152, 551-577.

Gaede, O., Schrank, C., Canbulat, I., Karrech, A., 2014. A strain-based failure criterion for pillar stability analysis, Proceedings AusRock 2014: Third Australasian Ground Control in Mining Conference. The Australasian Institute of Mining and Metallurgy, pp. 393-398.

Gentle, J.E., 2013. Random number generation and Monte Carlo methods. Springer Science & Business Media.

Goel, R.K., Singh, B., Zhao, J., 2012. Underground infrastructures: planning, design, and construction. butterworth-heinemann.

Goh, A.T.C., Zhang, W., 2012. Reliability assessment of stability of underground rock caverns. International Journal of Rock Mechanics and Mining Sciences 55, 157-163.

Goovaerts, P., 2001. Geostatistical modelling of uncertainty in soil science. Geoderma 103, 3-26.

Grenon, M., Hadjigeorgiou, J., 2003. Evaluating discontinuity network characterization tools through mining case studies. Soil Rock America 1, 13.

Griffiths, D.V., Fenton, G.A., 2007. Probabilistic methods in geotechnical engineering. Springer Science & Business Media.

Grimstad, E., 1993. Updating the Q-system for NMT, Proceedings of the International Symposium on Sprayed Concrete-Modern use of wet mix sprayed concrete for underground support, Fagemes, Oslo, Norwegian Concrete Association, 1993.

Guan et al., 2014. Probabilistic estimation of ground condition and construction cost for mountain tunnels. Tunnelling and Underground Space Technology 42, 175-183.

Guan, Z., Deng, T., Du, S., Li, B., Jiang, Y., 2012. Markovian geology prediction approach and its application in mountain tunnels. Tunn Undergr Sp Technol 31, 61-67.

Gunsallus, K.t., Kulhawy, F., 1984. A comparative evaluation of rock strength measures, International Journal of Rock Mechanics and Mining Sciences & Geomechanics Abstracts. Elsevier, pp. 233-248.

Haas, C., Einstein, H.H., 2002. Updating the decision aids for tunneling. J Constr Eng Manag 128, 40-48.

Hadjigeorgiou, J., Harrison, J., 2011. Uncertainty and sources of error in rock engineering, 12th ISRM Congress. International Society for Rock Mechanics and Rock Engineering.

Hamby, D., 1994. A review of techniques for parameter sensitivity analysis of environmental models. Environmental monitoring and assessment 32, 135-154.

Hamidi, J.K., Shahriar, K., Rezai, B., Rostami, J., 2010. Performance prediction of hard rock TBM using Rock Mass Rating (RMR) system. Tunnelling and Underground Space Technology 25, 333-345.

Hamrouni, A., Dias, D., Sbartai, B., 2017. Reliability analysis of shallow tunnels using the response surface methodology. Underground Space 2, 246-258.

Hasofer, A.M., Lind, N.C., 1974. Exact and invariant second-moment code format. Journal of the Engineering Mechanics division 100, 111-121.

Hoek, Brown, 2018. The Hoek-Brown failure criterion and GSI–2018 edition. Journal of Rock Mechanics and Geotechnical Engineering.

Hoek, Marinos, 2000a. Predicting tunnel squeezing problems in weak heterogeneous rock masses. Tunnels and tunnelling international 32, 45-51.

Hoek, E., 1998a. Reliability of Hoek-Brown estimates of rock mass properties and their impact on design. International Journal of Rock Mechanics and Mining Sciences 35, 63-68.

Hoek, E., 1998b. Tunnel support in weak rock, Keynote address, Symposium of Sedimentary Rock Engineering, Taipei, Taiwan.

Hoek, E., 1999. Support for very weak rock associated with faults and shear zones. Rock Support and Reinforcement Practice in Mining. Villaescusa, Windsor and Thompson (eds), Rotterdam: Balkema.

Hoek, E., 2001. Big tunnels in bad rock. Journal of Geotechnical and Geoenvironmental Engineering 127, 726-740.

Hoek, E., 2007. Practical rock engineering. 2007, Online. ed. Rocscience.

Hoek, E., Brown, E.T., 1997. Practical estimates of rock mass strength. International journal of rock mechanics and mining sciences 34, 1165-1186.

Hoek, E., Carranza-Torres, C., Corkum, B., 2002. Hoek-Brown failure criterion-2002 edition. Proceedings of NARMS-Tac 1, 267-273.

Hoek, E., Carter, T., Diederichs, M., 2013. Quantification of the geological strength index chart, 47th US rock mechanics/geomechanics symposium. American Rock Mechanics Association.

Hoek, E., Diederichs, M., 2006. Empirical estimation of rock mass modulus. International journal of rock mechanics and mining sciences 43, 203-215.

Hoek, E., Marinos, P., 2000b. Predicting tunnel squeezing problems in weak heterogeneous rock masses. Tunnels and tunnelling international 32, 45-51.

Hoek, E., Marinos, P., Benissi, M., 1998. Applicability of the Geological Strength Index (GSI) classification for very weak and sheared rock masses. The case of the Athens Schist Formation. Bulletin of Engineering Geology and the Environment 57, 151-160.

Idris, M.A., Saiang, D., Nordlund, E., 2015. Stochastic assessment of pillar stability at Laisvall mine using Artificial Neural Network. Tunnelling and Underground Space Technology 49, 307-319.

Ioannou, P.G., 1987. Geologic prediction model for tunneling. J Constr Eng Manag 113, 569-590.

Jimenez-Rodriguez, R., Sitar, N., 2007. Rock wedge stability analysis using system reliability methods. Rock Mechanics and Rock Engineering 40, 419-427.

Jimenez, R., Sitar, N., 2009. The importance of distribution types on finite element analyses of foundation settlement. Computers and Geotechnics 36, 474-483.

Lacasse, S., Nadim, F., 1996. Uncertainties in characterising soil properties, Uncertainty in the geologic environment: From theory to practice. ASCE, pp. 49-75.

Lanaro, F., Bäckström, A., 2007. Empirical characterisation of the rock mass along borehole KBH02 and comparison with the results of the EXPECT project.

Langford, J.C., 2013. Application of reliability methods to the design of underground structures. Queen's University

Langford, J.C., Diederichs, M., 2013. Reliability based approach to tunnel lining design using a modified point estimate method. International Journal of Rock Mechanics and Mining Sciences 60, 263-276.

Law, A.M., Kelton, W.D., Kelton, W.D., 1991. Simulation modeling and analysis. McGraw-Hill New York.

Leu, S.-S., Adi, T.J.W., 2011. Probabilistic prediction of tunnel geology using a Hybrid Neural-HMM. Eng Appl Artif Intell 24, 658-665.

Li, H.-Z., Low, B.K., 2010. Reliability analysis of circular tunnel under hydrostatic stress field. Computers and Geotechnics 37, 50-58.

Li, J., 2004. Critical strain of intact rock and rock masses. Curtin University of Technology.

Li, J., Villaescusa, E., 2005. Determination of rock mass compressive strength using critical strain theory, Proc. 40th US Symposium on Rock Mechanics, p. 663.

Li, X., Wu, Z., Takahashi, M., Yasuhara, K., 2000. An experimental study on strain-based failure criteria of brittle materials. Journal of applied mechanics 3, 387-394.

Li, Z., 1990. A new approach to rock failure: Criterion of failure in plastical strain space. Engineering Fracture Mechanics 35, 739-742.

Lilly, P., Li, J., 2000. Estimating excavation reliability from displacement modelling. International Journal of Rock Mechanics and Mining Sciences 37, 1261-1265.

Liu, H., Low, B.K., 2017. System reliability analysis of tunnels reinforced by rockbolts. Tunnelling and Underground Space Technology 65, 155-166.

Low, B.-K., 2018. Reliability-based design: practical procedures, geotechnical examples, and insights, Risk and Reliability in Geotechnical Engineering. CRC Press, pp. 385-424.

Low, B., 2008a. Efficient probabilistic algorithm illustrated for a rock slope. Rock Mechanics and Rock Engineering 41, 715-734.

Low, B., Tang, W.H., 1997. Efficient reliability evaluation using spreadsheet. Journal of Engineering Mechanics 123, 749-752.

Low, B., Tang, W.H., 2007. Efficient spreadsheet algorithm for first-order reliability method. Journal of engineering mechanics 133, 1378-1387.

Low, B.K., 2008b. Practical reliability approach using spreadsheet. Reliability-based design in geotechnical engineering: Computations and applications, 134-168.

Low, B.K., Einstein, H., 2013. Reliability analysis of roof wedges and rockbolt forces in tunnels. Tunnelling and Underground Space Technology 38, 1-10.

Low, B.K., Tang, W.H., 2004. Reliability analysis using object-oriented constrained optimization. Structural Safety 26, 69-89.

Lu, H., Kim, E., Gutierrez, M., 2018a. A Markovian Rock Mass Quality Q-based Prediction Model for Tunneling, 52nd US Rock Mechanics/Geomechanics Symposium. American Rock Mechanics Association.

Lu, H., Kim, E., Gutierrez, M., 2018b. A study of a probabilistic Q-system using a Markov chain model to predict rock mass quality in tunneling Rock Mechanics and rock engineering (Submitted).

Lu, H., Kim, E., Gutierrez, M., 2019. Monte Carlo simulation (MCS)-based uncertainty analysis of rock mass quality Q in underground construction. Tunnelling and Underground Space Technology 94, 103089.

Lü, Q., Chan, C.L., Low, B.K., 2012. Probabilistic evaluation of ground-support interaction for deep rock excavation using artificial neural network and uniform design. Tunnelling and Underground Space Technology 32, 1-18.

Lü, Q., Chan, C.L., Low, B.K., 2013. System reliability assessment for a rock tunnel with multiple failure modes. Rock mechanics and rock engineering 46, 821-833.

Lü, Q., Low, B.K., 2011. Probabilistic analysis of underground rock excavations using response surface method and SORM. Computers and Geotechnics 38, 1008-1021.

Lü, Q., Sun, H.-Y., Low, B.K., 2011. Reliability analysis of ground–support interaction in circular tunnels using the response surface method. International Journal of Rock Mechanics and Mining Sciences 48, 1329-1343.

Lumb, P., 1970. Safety factors and the probability distribution of soil strength. Canadian Geotechnical Journal 7, 225-242.

Mahdevari, S., Torabi, S.R., 2012. Prediction of tunnel convergence using artificial neural networks. Tunnelling and Underground Space Technology 28, 218-228.

Marinos, P., Hoek, E., 2000. GSI: a geologically friendly tool for rock mass strength estimation, ISRM international symposium. International Society for Rock Mechanics and Rock Engineering.

Marinos, V., Marinos, P., Hoek, E., 2005. The geological strength index: applications and limitations. Bulletin of Engineering Geology and the Environment 64, 55-65.

Min, S., Kim, T., Lee, J., Einstein, H., 2008. Design and construction of a road tunnel in Korea including application of the decision aids for tunneling–a case study. Tunn Undergr Sp Technol 23, 91-102.

Mollon, G., Dias, D., Soubra, A.-H., 2009a. Probabilistic analysis and design of circular tunnels against face stability. International Journal of Geomechanics 9, 237-249.

Mollon, G., Dias, D., Soubra, A.-H., 2009b. Probabilistic analysis of circular tunnels in homogeneous soil using response surface methodology. Journal of Geotechnical and Geoenvironmental Engineering 135, 1314-1325.

Mollon, G., Dias, D., Soubra, A.-H., 2010. Probabilistic analysis of pressurized tunnels against face stability using collocation-based stochastic response surface method. Journal of Geotechnical and Geoenvironmental Engineering 137, 385-397.

Morelli, G.L., 2015. Variability of the GSI index estimated from different quantitative methods. Geotechnical and Geological Engineering 33, 983-995.

NGI, 2015. Using the Q system: Rock mass classification and support design (handbook). Norwegian Geotechnical Institute.

Onsel, I.E., Ozturk, C.A., Ozkan, M., Nasuf, S.E., 2011. Software for RQD and rock mass evaluation.

Palchik, V., 1999. Influence of porosity and elastic modulus on uniaxial compressive strength in soft brittle porous sandstones. Rock Mechanics and Rock Engineering 32, 303-309.

Palisade Corporation, 2016. @RISK program and user manual. Palisade Corporation, New York.

Palmstrom, A., 2005. Measurements of and correlations between block size and rock quality designation (RQD). Tunnelling and Underground Space Technology 20, 362-377.

Palmstrom, A., Broch, E., 2006. Use and misuse of rock mass classification systems with particular reference to the Q-system. Tunnelling and underground space technology 21, 575-593.

Palmstrom, A., Stille, H., 2007. Ground behaviour and rock engineering tools for underground excavations. Tunn Undergr Sp Technol 22, 363-376.

Palmstrom, A., Stille, H., 2010. Rock engineering. Thomas Telford, London.

Pan, Q., Dias, D., 2018. Probabilistic Analysis of a Rock Tunnel Face Using Polynomial Chaos Expansion Method. International Journal of Geomechanics 18, 04018013.

Panet, M., Guenot, A., 1983. Analysis of convergence behind the face of a tunnel: Tunnelling 82, proceedings of the 3rd international symposium, Brighton, 7–11 June 1982, P197–204. Publ London: IMM, 1982, International Journal of Rock Mechanics and Mining Sciences & Geomechanics Abstracts. Pergamon, p. A16.

Panthi, K.K., 2006. Analysis of engineering geological uncertainties related to tunnelling in Himalayan rock mass conditions. Norwegian University of Science and Technology.

Panthi, K.K., Nilsen, B., 2007. Predicted versus actual rock mass conditions: A review of four tunnel projects in Nepal Himalaya. Tunn Undergr Sp Technol 22, 173-184.

Panthi, K.K., Nilsen, B., 2010. Uncertainty analysis for assessing leakage through water tunnels: A case from Nepal Himalaya. Rock mechanics and rock engineering 43, 629-639.

Park, E., Elfeki, A., Dekking, M., 2005. Characterization Of Subsurface Heterogeneity: Integration of Soft and Hard Information using Multidimensional Coupled Markov Chain Approach, Developments in water science, pp. 193-202.

Phoon, K.-K., Kulhawy, F.H., 1999. Characterization of geotechnical variability. Canadian geotechnical journal 36, 612-624.

Phoon, K., Becker, D., Kulhawy, F., Honjo, Y., Ovesen, N., Lo, S., 2003. Why consider reliability analysis for geotechnical limit state design?, Limit State Design In Geotechnical Engineering Practice: (With CD-ROM). World Scientific.

Priest, S.D., Hudson, J.A., 1976. Discontinuity spacings in Rock.

Qi, X.-H., Li, D.-Q., Phoon, K.-K., Cao, Z.-J., Tang, X.-S., 2016. Simulation of geologic uncertainty using coupled Markov chain. Eng Geol 207, 129-140.

Rackwitz, R., Flessler, B., 1978. Structural reliability under combined random load sequences. Computers & Structures 9, 489-494.

Rafiai, H., Moosavi, M., 2012. An approximate ANN-based solution for convergence of lined circular tunnels in elasto-plastic rock masses with anisotropic stresses. Tunnelling and Underground Space Technology 27, 52-59.

Ramamurthy, T., 2004. A geo-engineering classification for rocks and rock masses. International Journal of Rock Mechanics and Mining Sciences 41, 89-101.

Ravnjak, K., Grget, G., Kovacevic, M., 2014. Comparison of predicted and actual conditions of the rock mass in the Tunnel Stražina, ISRM Regional Symposium-EUROCK 2014. International Society for Rock Mechanics.

Rosenblueth, E., 1975. Point estimates for probability moments. Proceedings of the National Academy of Sciences 72, 3812-3814.

Rosenblueth, E., 1981. Two-point estimates in probabilities. Appl. Math. Modeling 5, 329-335.

Ruwanpura, J.Y., AbouRizk, S.M., Allouche, M., 2004. Analytical methods to reduce uncertainty in tunnel construction projects. Can J Civ Eng 31, 345-360.

Sakurai, 2017. Back analysis in rock engineering. CRC Press.

Sakurai, S., 1981. Direct strain evaluation technique in construction of underground opening, The 22nd US Symposium on Rock Mechanics (USRMS). American Rock Mechanics Association.

Sakurai, S., 1983. Displacement measurements associated with the design of underground openings. Proc. Int. Sympo. Field Measurements in Geomechanics 2, 1163-1178.

Sakurai, S., 1997. Lessons learned from field measurements in tunnelling. Tunnelling and underground space technology 12, 453-460.

Sari, M., 2009. The stochastic assessment of strength and deformability characteristics for a pyroclastic rock mass. International Journal of Rock Mechanics and Mining Sciences 46, 613-626.

Sari, M., Karpuz, C., Ayday, C., 2010. Estimating rock mass properties using Monte Carlo simulation: Ankara andesites. Computers & Geosciences 36, 959-969.

Sen, Z., 2016. Spatial modeling principles in earth sciences. Springer.

Sen, Z., Kazi, A., 1984. Discontinuity spacing and RQD estimates from finite length scanlines, International Journal of Rock Mechanics and Mining Sciences & Geomechanics Abstracts. Elsevier, pp. 203-212.

Şen, Z., Sadagah, B.H., 2002. Probabilistic horizontal stress ratios in rock. Mathematical geology 34, 845-855.

Singh, B., Goel, R.K., 1999. Rock mass classification: a practical approach in civil engineering. Elsevier.

Singh, B., Villadkar, M., Samadhiya, N., Mehrotra, V., 1997. Rock mass strength parameters mobilised in tunnels. Tunnelling and Underground Space Technology 12, 47-54.

Singh, M., Singh, B., Choudhari, J., 2007. Critical strain and squeezing of rock mass in tunnels. Tunnelling and underground space technology 22, 343-350.

Song, L., Li, H.-Z., Chan, C.L., Low, B.K., 2016. Reliability analysis of underground excavation in elastic-strain-softening rock mass. Tunnelling and Underground Space Technology 60, 66-79.

Sousa, R.L., Einstein, H.H., 2012. Risk analysis during tunnel construction using Bayesian Networks: Porto Metro case study. Tunn Undergr Sp Technol 27, 86-100.

Spackova, O., 2012. Risk management of tunnel construction projects. Czech technical University, p. 180.

Stacey, T., 1981. A simple extension strain criterion for fracture of brittle rock, International Journal of Rock Mechanics and Mining Sciences & Geomechanics Abstracts. Elsevier, pp. 469-474.

Stille, H., Palmström, A., 2003. Classification as a tool in rock engineering. Tunnelling and underground space technology 18, 331-345.

Su, Y.-H., Li, X., Xie, Z.-Y., 2011. Probabilistic evaluation for the implicit limit-state function of stability of a highway tunnel in China. Tunnelling and Underground Space Technology 26, 422-434.

Tan, X.-h., Bi, W.-h., Hou, X.-l., Wang, W., 2011. Reliability analysis using radial basis function networks and support vector machines. Computers and Geotechnics 38, 178-186.

Tapia, A., Contreras, L., Jefferies, M., Steffen, O., 2007. Risk evaluation of slope failure at the Chuquicamata Mine, Proceedings of the 2007 international symposium on rock slope stability in open pit mining and civil engineering. Australian Centre for Geomechanics, pp. 477-495.

Tavakoli, H., Ranjbar, H., 2004. Statistical analysis of discontinuities, with a special reference to Rock Quality Designation, Mining Science and Technology: Proceedings of the 5th International Symposium on Mining Science and Technology, Xuzhou, China 20-22 October 2004. CRC Press, p. 415.

Tiwari, G., Pandit, B., Latha, G.M., Babu, G.S., 2017. Probabilistic analysis of tunnels considering uncertainty in peak and post-peak strength parameters. Tunnelling and Underground Space Technology 70, 375-387.

USACE, 1997. Engineering and Design: Introduction to Probability and Reliability Methods for Use in Geotechnical Engineering. CORPS OF ENGINEERS WASHINGTON DC.

Valley, B., Kaiser, P., Duff, D., 2010. Consideration of uncertainty in modelling the behaviour of underground excavations, Proceedings Fifth International Seminar on Deep and High Stress Mining (Deep Mining 2010), M. Van Sint Jan and Y. Potvin (eds), pp. 6-8.

Vardakos, 2003. Distinct Element Modeling of the Shimizu Tunnel No. 3 in Japan. Virginia Tech.

Vardakos, Gutierrez, M.S., Barton, N.R., 2007. Back-analysis of Shimizu Tunnel No. 3 by distinct element modeling. Tunnelling and Underground Space Technology 22, 401-413.

Vásárhelyi, B., Kovács, D., 2017. Empirical methods of calculating the mechanical parameters of the rock mass. Periodica Polytechnica Civil Engineering 61, 39-50.

Vose, D., 2008. Risk analysis: a quantitative guide. John Wiley & Sons.

Wang, Q., Fang, H., Shen, L., 2016. Reliability analysis of tunnels using a metamodeling technique based on augmented radial basis functions. Tunnelling and Underground Space Technology 56, 45-53.

Wang, Y., Akeju, O.V., 2016. Quantifying the cross-correlation between effective cohesion and friction angle of soil from limited site-specific data. Soils and Foundations 56, 1055-1070.

Wang, Y., Aladejare, A.E., 2016. Bayesian characterization of correlation between uniaxial compressive strength and Young's modulus of rock. International Journal of Rock Mechanics and Mining Sciences 85, 10-19.

Wines, D.R., Lilly, P.A., 2001. A comparative analysis of rock mass classification schemes in part of the Fimiston Open Pit Operation in Kalgoorlie, Western Australia. Australian Geomechanics 36, 59-72.

Ye, M., Khaleel, R., 2008. A Markov chain model for characterizing medium heterogeneity and sediment layering structure. Water Resour Res 44.

You, K., Lee, J.S., 2006. Estimation of rock mass classes using the 3-dimensional multiple indicator kriging technique. Tunn Undergr Sp Technol 21, 3-4.

Zeng, P., Senent, S., Jimenez, R., 2014. Reliability analysis of circular tunnel face stability obeying Hoek–Brown failure criterion considering different distribution types and correlation structures. Journal of Computing in Civil Engineering 30, 04014126.

Zhang, L., 2017. Evaluation of rock mass deformability using empirical methods–A review. Underground Space 2, 1-15.

Zhang, W., Goh, A., 2015. Regression models for estimating ultimate and serviceability limit states of underground rock caverns. Engineering geology 188, 68-76.

Zhang, W., Goh, A.T., 2012. Reliability assessment on ultimate and serviceability limit states and determination of critical factor of safety for underground rock caverns. Tunnelling and Underground Space Technology 32, 221-230.

Zhang, W., Goh, A.T.C., 2018. Reliability analysis of geotechnical infrastructures: Introduction.

Zhao, H.-b., 2008. Slope reliability analysis using a support vector machine. Computers and Geotechnics 35, 459-467.

Zhao, H., Ru, Z., Chang, X., Yin, S., Li, S., 2014. Reliability analysis of tunnel using least square support vector machine. Tunnelling and Underground Space Technology 41, 14-23.

Zhu, W., Sui, B., Li, X., Li, S., Wang, W., 2008. A methodology for studying the high wall displacement of large scale underground cavern complexes and it's applications. Tunnelling and Underground Space Technology 23, 651-664.

APPENDIX A - DEFINITIONS AND RATINGS FOR STATES OF Q-PARAMETERS (MODIFIED FROM BARTON 2002)

Table A. 1 States, descriptions and ratings for RQD.

States	Descriptions	Rating
1	Very poor	0-25
2	Poor	26-50
3	Fair	51-75
4	Good	76-100

Table A. 2 States, descriptions and ratings for J_n.

States	Descriptions	Rating
1	None	0.5
2	One	2
3	One plus	3
4	Two	4
5	Two plus	6
6	Three	9
7	Three plus	12
8	Four or more	15
9	Earth	20

Table A. 3 States, descriptions and ratings for J_r.

States	Descriptions		Rating
1	Discontinuous		4
2	Undulating	Rough undulating	3
3		Smooth undulating	2
4	Slickensided undulating or Rough planar		1.5
5	Planar	Smooth planar	1
6		Slickensided planar	0.5
7	No contact when sheared		1

Table A. 4 States, descriptions and ratings for J_a.

States	Descriptions		Rating
1	No fills	Healed	0.75
2		Unaltered joint wall	1
3		Slightly altered wall	2
4		Coated non-softening	3
5		Coated softening or disintegrated sandy particles	4
6	Thin fills	Thin non-softening clay fillings	6
7		Thin softening clay fillings	8
8		Thin swelling clays	12
9	Thick fills	Thick, continuous; clay band; medium to low over-consolidated	13
10		Thick, continuous; clay band; swelling clay	20

Table A. 5 States, descriptions and ratings for J_w.

States	Descriptions	Approx. water press. (kg/cm^2)	Rating
1	Dry	<1	1
2	Wet	1~2.5	0.66
3	High pressure in unfilled joints	2.5~10	0.5
4	High pressure with fillings outwash	2.5~10	0.33
5	Exc. inflows with decay	>10	0.1
6	Exc. inflows without decay	>10	0.05

Table A. 6 States, descriptions and ratings for SRF.

States	Descriptions	Sigma c/Sigma 1	Rating
1	Multiple clay zones		10
2	Multiple non-clay zones		7.5
3	Single weak zone (Depth<50m) or heavily jointed		5
4	Single weak zone (Depth>50m) or low stress(>200)		2.5
5	Medium stress	200-10	1
6	High stress with tight structure	10~5	2
7	Moderate slabbing	5~3	50
8	Slabbing and rock burst	3~2	200
9	Heavy rock burst	<2	400

APPENDIX B - TRANSITION PROBABILITY AND TRANSITION INTENSITY COEFFICIENT OF Q-PARAMETERS

Table B. 1 Transition probability and intensity coefficient of RQD states.

State i	P_{ij} for RQD				c_i
	State j				
	1	2	3	4	
1	0	0.2	0.4	0.4	10
2	0	0	0.4	0.6	0.098
3	0	0.3	0	0.7	0.083
4	0	0.2	0.8	0	0.071

Table B. 2 Transition probability and intensity coefficient of J_n states.

State i	P_{ij} for J_n									c_i
	State j									
	1	2	3	4	5	6	7	8	9	
1	0	0	0.25	0.375	0.375	0	0	0	0	10
2	0	0	0.176	0.353	0.471	0	0	0	0	10
3	0	0	0	0.5	0.5	0	0	0	0	0.116
4	0	0	0	0	1	0	0	0	0	0.162
5	0	0	0.333	0.667	0	0	0	0	0	0.014
6	0	0	0.176	0.353	0.471	0	0	0	0	10
7	0	0	0.176	0.353	0.471	0	0	0	0	10
8	0	0	0.176	0.353	0.471	0	0	0	0	10
9	0	0	0.176	0.353	0.471	0	0	0	0	10

Table B. 3 Transition probability and intensity coefficient of J_r states.

State i	P_{ij} for J_r							c_i
	State j							
	1	2	3	4	5	6	7	
1	0	0	0	1	0	0	0	0.25
2	0	0	0	0.455	0.545	0	0	10
3	0	0	0	0.455	0.545	0	0	10
4	0.25	0	0	0	0.75	0	0	0.015
5	0	0	0	1	0	0	0	0.389
6	0	0	0	0.455	0.545	0	0	10
7	0	0	0	0.455	0.545	0	0	10

Table B. 4 Transition probability and intensity coefficient of J_a states.

State i	P_{ij} for J_a										c_i
	State j										
	1	2	3	4	5	6	7	8	9	10	
1	0	0.1	0.5	0.4	0	0	0	0	0	0	10
2	0	0	1	0	0	0	0	0	0	0	0.5
3	0	0.2	0	0.8	0	0	0	0	0	0	0.025
4	0	0	1	0	0	0	0	0	0	0	0.041
5	0	0.1	0.5	0.4	0	0	0	0	0	0	10
6	0	0.1	0.5	0.4	0	0	0	0	0	0	10
7	0	0.1	0.5	0.4	0	0	0	0	0	0	10
8	0	0.1	0.5	0.4	0	0	0	0	0	0	10
9	0	0.1	0.5	0.4	0	0	0	0	0	0	10
10	0	0.1	0.5	0.4	0	0	0	0	0	0	10

Table B. 5 Transition probability and intensity coefficient of J_w states.

State i	P_{ij} for J_w						c_i
	State j						
	1	2	3	4	5	6	
1	0	1	0	0	0	0	0.014
2	1	0	0	0	0	0	0.160
3	0.444	0.556	0	0	0	0	10
4	0.444	0.556	0	0	0	0	10
5	0.444	0.556	0	0	0	0	10
6	0.444	0.556	0	0	0	0	10

Table B. 6 Transition probability and intensity coefficient of SRF states.

State i	P_{ij} for SRF									c_i
	State j									
	1	2	3	4	5	6	7	8	9	
1	0	0	0	0	1	0	0	0	0	10
2	0	0	0	0	1	0	0	0	0	10
3	0	0	0	0	1	0	0	0	0	10
4	0	0	0	0	1	0	0	0	0	10
5	0	0	0	0.5	0	0.5	0	0	0	0.0025
6	0	0	0	0	1	0	0	0	0	10
7	0	0	0	0	1	0	0	0	0	10
8	0	0	0	0	1	0	0	0	0	10
9	0	0	0	0	1	0	0	0	0	10

APPENDIX C - LIKELIHOOD MATRIX FOR EACH STATE OF Q-PARAMETERS

Table C. 1 Likelihood matrix of RQD states.

State i	L_{ij}=P[Y(k)=j|X(k)=i] for RQD			
	State j			
	1	2	3	4
1	0.95	0.05	0	0
2	0.05	0.9	0.05	0
3	0	0.05	0.9	0.05
4	0	0	0.05	0.95

Table C. 2 Likelihood matrix of J_n states.

State i	L_{ij}=P[Y(k)=j|X(k)=i] for J_n								
	State j								
	1	2	3	4	5	6	7	8	9
1	0.95	0.05	0	0	0	0	0	0	0
2	0.05	0.9	0.05	0	0	0	0	0	0
3	0	0.05	0.9	0.05	0	0	0	0	0
4	0	0	0.05	0.9	0.05	0	0	0	0
5	0	0	0	0.05	0.9	0.05	0	0	0
6	0	0	0	0	0.05	0.9	0.05	0	0
7	0	0	0	0	0	0.05	0.9	0.05	0
8	0	0	0	0	0	0	0.05	0.9	0.05
9	0	0	0	0	0	0	0	0.05	0.95

Table C. 3 Likelihood matrix of J_r states.

State i	$L_{ij}=P[Y(k)=j\|X(k)=i]$ for J_r						
	State j						
	1	2	3	4	5	6	7
1	0.95	0.05	0	0	0	0	0
2	0	0.9	0.05	0.05	0	0	0
3	0	0.05	0.85	0.05	0.05	0	0
4	0	0.05	0.05	0.85	0.05	0	0
5	0	0	0.05	0.05	0.85	0.05	0
6	0	0	0	0.05	0.05	0.9	0
7	0	0	0	0	0	0.05	0.95

Table C. 4 Likelihood matrix of J_a states.

State i	$L_{ij}=P[Y(k)=j\|X(k)=i]$ for J_a									
	State j									
	1	2	3	4	5	6	7	8	9	10
1	0.9	0.05	0.05	0	0	0	0	0	0	0
2	0.05	0.85	0.05	0.05	0	0	0	0	0	0
3	0	0.05	0.85	0.05	0.05	0	0	0	0	0
4	0	0.05	0.05	0.85	0.05	0	0	0	0	0
5	0	0	0.05	0.05	0.85	0.05	0	0	0	0
6	0	0	0	0.05	0.05	0.85	0.05	0	0	0
7	0	0	0	0	0.05	0.05	0.85	0.05	0	0
8	0	0	0	0	0	0.05	0.05	0.85	0.05	0
9	0	0	0	0	0	0	0.05	0.05	0.85	0.05
10	0	0	0	0	0	0	0	0	0.1	0.9

Table C. 5 Likelihood matrix of J_w states.

State i	$L_{ij}=P[Y(k)=j\|X(k)=i]$ for J_w					
	State j					
	1	2	3	4	5	6
1	0.95	0.05	0	0	0	0
2	0.05	0.9	0.05	0	0	0
3	0	0.05	0.9	0.05	0	0
4	0	0	0.05	0.9	0.05	0
5	0	0	0	0.05	0.9	0.05
6	0	0	0	0	0.1	0.9

Table C. 6 Likelihood matrix of SRF states.

State i	$L_{ij}=P[Y(k)=j\|X(k)=i]$ for SRF								
	State j								
	1	2	3	4	5	6	7	8	9
1	0.9	0.1	0	0	0	0	0	0	0
2	0.1	0.9	0	0	0	0	0	0	0
3	0	0.05	0.9	0.05	0	0	0	0	0
4	0	0.05	0.05	0.9	0	0	0	0	0
5	0	0	0	0	0.9	0.1	0	0	0
6	0	0	0	0	0.1	0.9	0	0	0
7	0	0	0	0	0	0.05	0.9	0.05	0
8	0	0	0	0	0	0	0.05	0.9	0.05
9	0	0	0	0	0	0	0	0.1	0.9

APPENDIX - D ACCURACY PLOTS OF PROBABILISTIC PREDICTION MODEL USING INPUT DATA FROM SUBSECTION 1 WITH 200M AND 300M

The prediction accuracy has been evaluated using the accuracy plots for the probabilistic prediction models using the input Q data from Subsection 1 with 200 m and 300 m. The accuracy plots have been made for the predicted Q-parameters, including RQD and J_n, Q value, Q-based rock class, GC1 with "good" rock and GC2 with "fair" rock. The comparison results have also been summarized at the end of this section.

(1) RQD

The accuracy plots of predicted RQD for the 200 m and 300 m cases are shown in Figure D.1. It is found that the calculated R^2 value is higher for the 300m case (0.70) than the 200 m case (0.58) and that the RMSE value is lower for the former (0.11) than the latter (0.13). This has indicated that the prediction accuracy is higher with more Q data as the input for the prediction model.

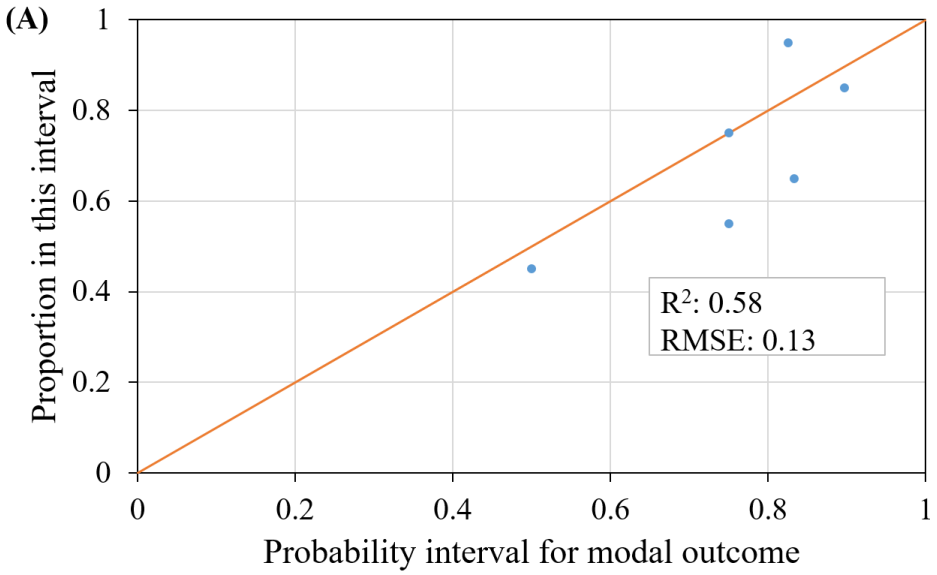

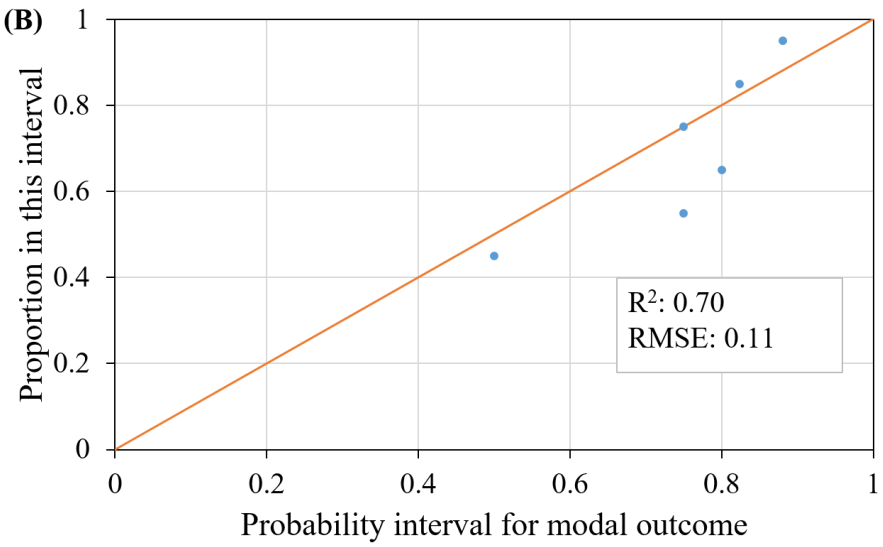

Figure D. 1 Accuracy plots for predicted RQD: (A): the 200 m case; (B): the 300 m case

(2) J_n

The accuracy plots for the predicted J_n are demonstrated in Figure D.2. Similar to the predicted results for RQD, the prediction accuracy is higher for the 300 m case than the 200 m case. However, it is seen that the R2 values for the predicted J_n are lower than those for the RQD and the RMSE values are higher for the former compared to the latter. This reveals the predicted RQD has higher prediction accuracy than the predicted J_n results, which is consistent with the results derived from the 400 m case.

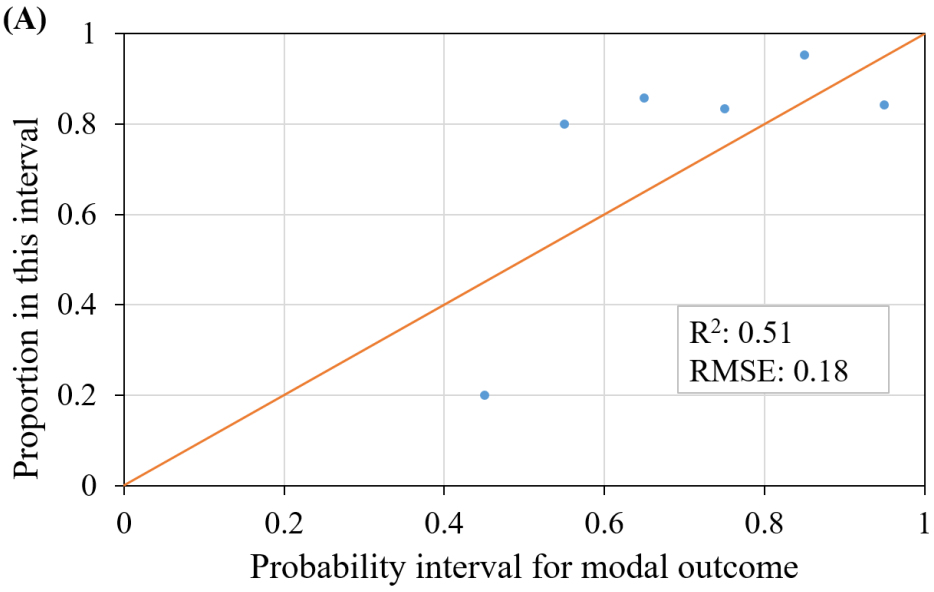

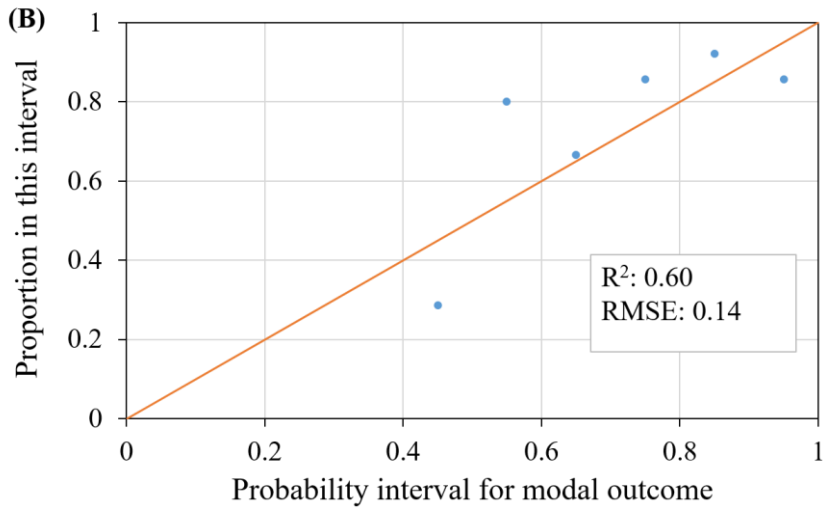

Figure D. 2 Accuracy plots for predicted J_n: (A) the 200 m case; (B) the 300 m case

(3) Q value

The accuracy plots for the predicted Q value are depicted in Figure D.3. It is seen that both the accuracy plots for both the 200 m and 300 m cases are close to the 1:1 line, indicating the very good prediction accuracy based on the comparison criterion of the Q value. The derived R^2 values are as high as 0.99 and the RMSE values are as low as around 0.05. It reveals that the difference of prediction accuracy for these two cases is insignificant. This may be related to the approach used for generating accuracy plots. In this study, the probability intervals, i.e. $(1-p)/2 \sim (1+p)/2$, are relatively wide using the symmetric probability interval centered on the cumulative distribution function proposed by Goovaerts (2001) for generating accuracy plots of Q value. Accuracy plots can be generated using other approaches for comparison.

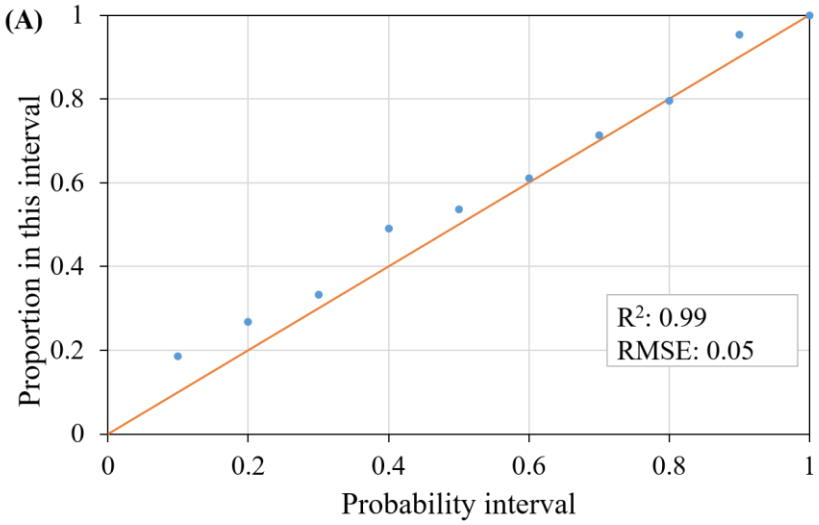

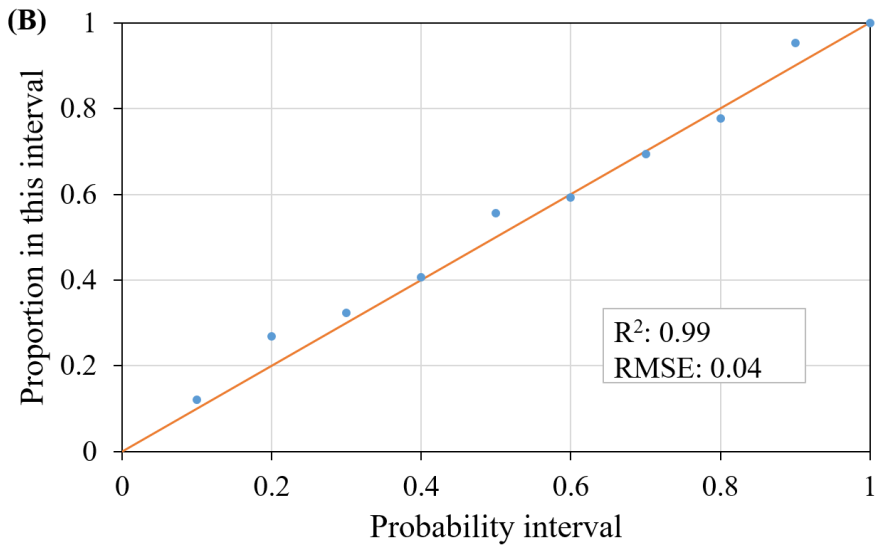

Figure D. 3 Accuracy plots for predicted Q value: (A) the 200 m case; (B) the 300 m case

(4) Q-based rock class

The accuracy plots for Q-based rock class have also been generated, as shown in Figure D.4. Similar to the predicted results for Q-parameters, it is clearly seen that the prediction accuracy has increased significantly, especially based on the measure of R^2 value, with more input Q data from a subsection with additional 100 m. In addition, the accuracy plots for predicted dominant GC1 with "good" rock and GC2 with "fair" rock have also been made, as demonstrated in Figure D. 5 and Figure D. 6.

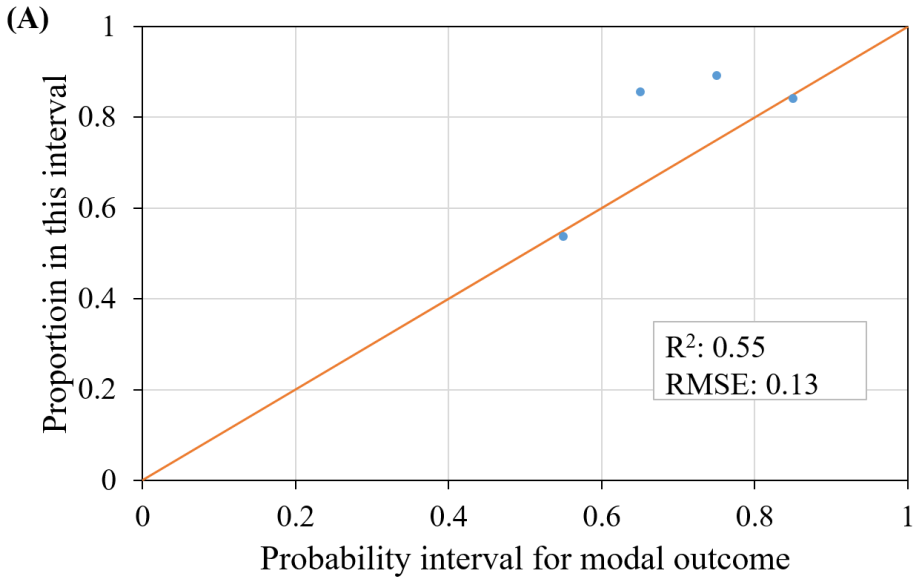

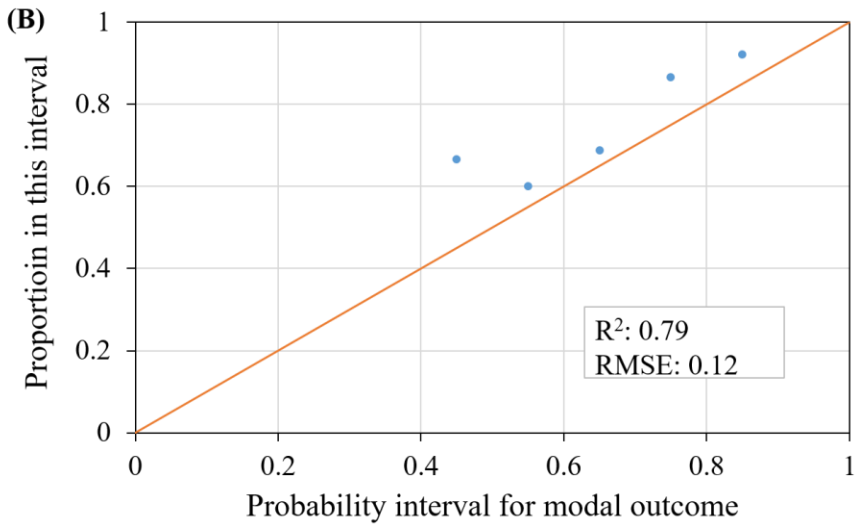

Figure D. 4 Accuracy plots for predicted Q class: (A) the 200 m case; (B) the 300 m case

As can be seen in Figure D.5, for the accuracy plot of GC1, the significant increase of the prediction accuracy can be clearly seen from the 200 m case to the 300 m case. However, for the accuracy plot of GC2, there is a slight increase of the R^2 value from the 200 m case (0.84) to the 300 m case (0.87). It means that the predicted GC1 results are more sensitive to the increase of input data than the predicted GC2 results. Overall, both predicted GC1 and GC2 results show that the prediction accuracy increases with the additional Q data as the input.

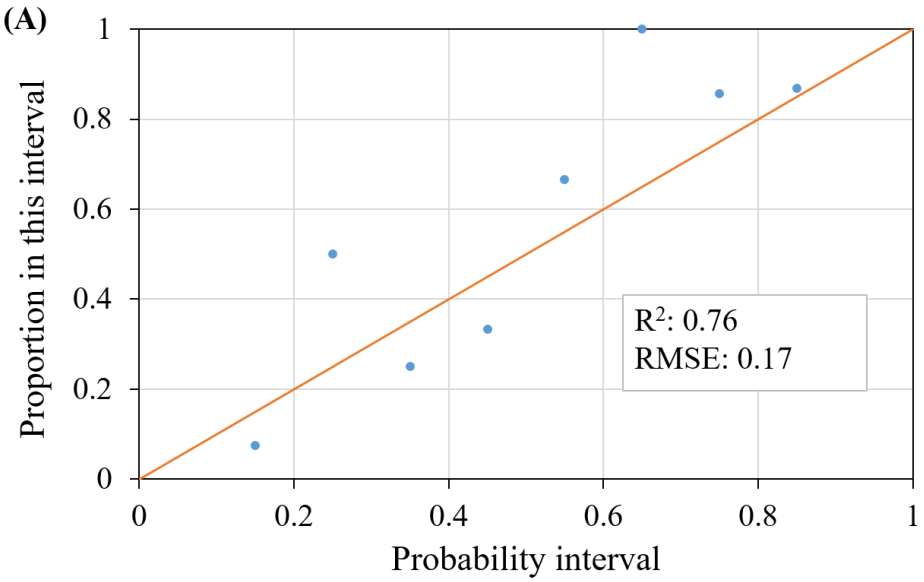

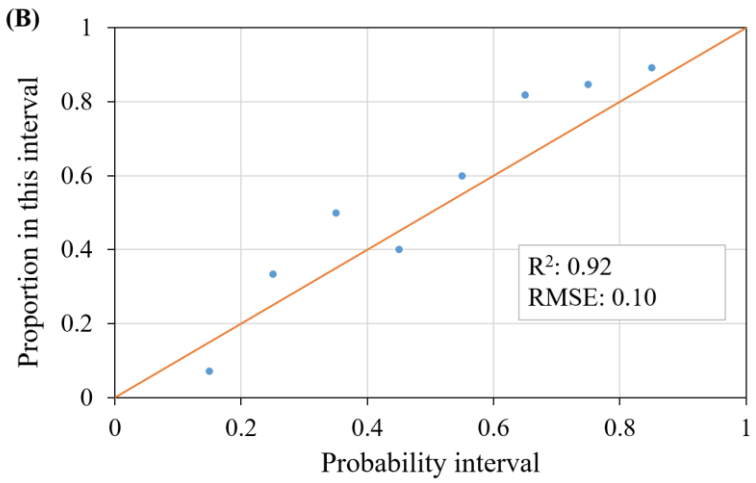

Figure D. 5 Accuracy plots for predicted GC1: (A) the 200 m case; (B) the 300 m case

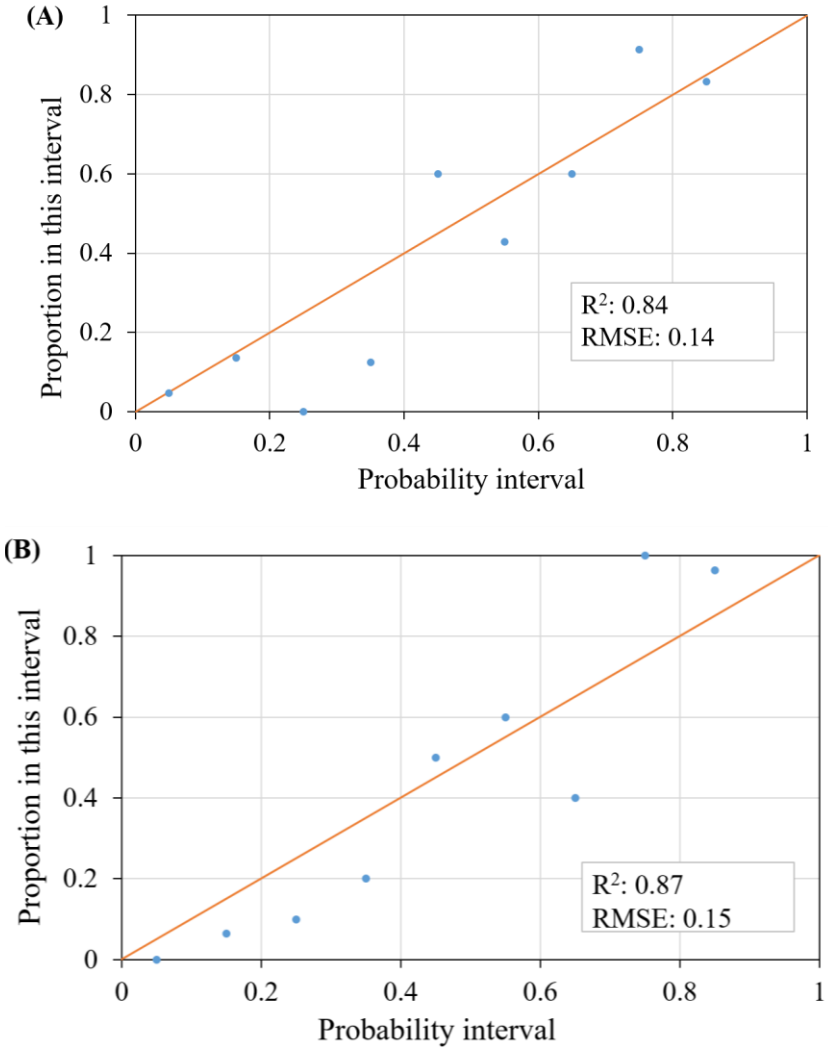

Figure D. 6 Accuracy plots for predicted GC2: (A) the 200 m case; (B) the 300 m case

The comparison of prediction accuracy from the accuracy plots is summarized in Table D. 1 for three cases, including the 200 m, 300 m and 400 cases. It can be seen that the prediction accuracy increases with the input data from Subsection 1 with longer length based on comparison criteria of Q-parameters, Q-based rock class and individual dominant GC1 and GC2. The prediction accuracy based on the Q value criterion is insensitive to the more input data. Note that the accuracy plot for the predicted Q value was generated using the approach proposed by Goovaerts (2001), and prediction accuracy can also be evaluated for the accuracy plot using other approaches for comparison. It is suggested to validate the predicted results using more comparison criteria between the predicted and actual results. In this study, the prediction accuracy is improved with input Q data from longer Subsection 1 based on all the comparison criteria, and the best prediction accuracy is achieved in the 400 m case.

Table D. 1 Summary of measures of prediction accuracy from accuracy plots

Criterion for validation	Length of Subsection 1 as model input (m)	RMSE (Root Mean Square Error)	R^2
RQD	200	0.13	0.58
	300	0.11	0.7
	400	0.08	0.88
J_n	200	0.18	0.51
	300	0.14	0.6
	400	0.11	0.81
Q value	200	0.05	0.99
	300	0.04	0.99
	400	0.04	0.99
Q class	200	0.13	0.55
	300	0.12	0.79
	400	0.07	0.92
GC1	200	0.17	0.76
	300	0.10	0.92
	400	0.10	0.96
GC2	200	0.14	0.84
	300	0.15	0.87
	400	0.10	0.98

APPENDIX E - APPROXIMATE CALCULATION APPROACH FOR STATISTICS OF Q VALUE

1. Statistics of the product of three random variables

(1) Statistics of the product of three random variables

$$X = A \times B \times C \tag{E.1}$$

It is seen in Eq. (E.1) that the dependent variable is the product of random variables A, B and C. It is assumed herein that random variables A, B and C are mutually independent. Statistics (expected value $E(X)$, variance $Var(X)$, coefficient of variation (COV) $\Omega(X)$) of variable X can be obtained given statistics of A, B and C as follows (Benjamin and Cornell 2014):

$$E(X) = E(ABC) = E(AB)E(C) = E(A)E(B)E(C) \tag{D.2}$$

$$\begin{aligned} Var(X) = Var(ABC) &= E\left[(ABC)^2\right] - \left[E(ABC)\right]^2 \\ &= E(A^2B^2C^2) - \left[E(A)E(B)E(C)\right]^2 \\ &= E(A^2)E(B^2)E(C^2) - [E(A)]^2[E(B)]^2[E(C)]^2 \\ &= (Var(A) + [E(A)]^2) * (Var(B) + [E(B)]^2) * (Var(C) + [E(C)]^2) - [E(A)]^2[E(B)]^2[E(C)]^2 \end{aligned} \tag{E.3}$$

$$\begin{aligned} \Omega(X) = \Omega(ABC) &= \frac{\sqrt{VAR(ABC)}}{E(ABC)} \\ &= \frac{\sqrt{(Var(A) + [E(A)]^2) * (Var(B) + [E(B)]^2) * (Var(C) + [E(C)]^2) - [E(A)]^2[E(B)]^2[E(C)]^2}}{E(A)E(B)E(C)} \\ &= \sqrt{\frac{(Var(A) + [E(A)]^2) * (Var(B) + [E(B)]^2) * (Var(C) + [E(C)]^2) - [E(A)]^2[E(B)]^2[E(C)]^2}{[E(A)]^2[E(B)]^2[E(C)]^2}} \\ &= \sqrt{([\Omega(A)]^2 + 1)([\Omega(B)]^2 + 1)([\Omega(C)]^2 + 1) - 1} \end{aligned} \tag{E.4}$$

(2) Statistics of the ratio of two random variables

It is defined the dependent variable G is the ratio of random variable R to S, and it can be expressed as $G = g(R,S) = \frac{R}{S}$ $(R, S > 0)$. The approximations for $E(G)$ and $Var(G)$ can be derived using Taylor expansions of function as follows $g()$ (Elandt-Johnson and Johnson 1980; Stuart and Ord 1998):

$$E(G) = E(\frac{R}{S}) \approx \frac{E(R)}{E(S)} - \frac{Cov(R,S)}{[E(S)]^2} + \frac{Var(S)E(R)}{[E(S)]^3} \tag{E.5}$$

$$Var(G) = Var(\frac{R}{S}) \approx \frac{Var(R)}{[E(S)]^2} - 2\frac{E(R)}{[E(S)]^3}Cov(R,S) + \frac{[E(R)]^2}{[E(S)]^4}Var(S)$$

$$= \frac{[E(R)]^2}{[E(S)]^2}\left(\frac{Var(R)}{[E(R)]^2} - 2\frac{Cov(R,S)}{[E(R)E(S)]} + \frac{Var(S)}{[E(S)]^2}\right) \tag{E.6}$$

In particular, if random variables R and S are independent, $Cov(R,S) = 0$. Eqs. (E.5) and (E.6) can be written as Eqs. (E.7) and (E.8), respectively.

$$E\left(\frac{R}{S}\right) \approx \frac{E(R)}{E(S)} + \frac{Var(S)E(R)}{[E(S)]^3} \tag{E.7}$$

$$Var\left(\frac{R}{S}\right) \approx \frac{[E(R)]^2}{[E(S)]^2}\left(\frac{Var(R)}{[E(R)]^2} + \frac{Var(S)}{[E(S)]^2}\right) \tag{E.8}$$

The approximate calculation for the COV of dependent variable G can be derived as follows:

$$\Omega(G) = \Omega\left(\frac{R}{S}\right) = \frac{\sqrt{VAR\left(\frac{R}{S}\right)}}{E\left(\frac{R}{S}\right)} \approx \frac{\sqrt{\frac{[E(R)]^2}{[E(S)]^2}\left(\frac{Var(R)}{[E(R)]^2} + \frac{Var(S)}{[E(S)]^2}\right)}}{\frac{E(R)}{E(S)} + \frac{Var(S)E(R)}{[E(S)]^3}} \approx \frac{\sqrt{\frac{[E(R)]^2}{[E(S)]^2}\left([(\Omega(R)]^2 + [(\Omega(S)]^2\right)}}{\frac{E(R)}{E(S)}(1 + [\Omega(S)]^2)} \approx \frac{\sqrt{[(\Omega(R)]^2 + [(\Omega(S)]^2}}{1 + [\Omega(S)]^2} \tag{E.9}$$

2. Statistics of the Q value

Recall

$$Q = \frac{RQD}{Jn} \times \frac{Jr}{Ja} \times \frac{Jw}{SRF} \tag{E.10}$$

and

$$X = A \times B \times C \tag{E.11}$$

where

$$A = \frac{RQD}{Jn},\ B = \frac{Jr}{Ja}, C = \frac{Jw}{SRF} \tag{E.12}$$

Integrating Eqs. (E.7), (E.11) and (E.12), the expected value of Q value can be derived as:

$$\begin{aligned} E(Q) &= E\left(\frac{RQD}{Jn} \times \frac{Jr}{Ja} \times \frac{Jw}{SRF}\right) = E\left(\frac{RQD}{Jn}\right)E\left(\frac{Jr}{Ja}\right)E\left(\frac{Jw}{SRF}\right) \\ &\approx \left(\frac{E(RQD)}{E(Jn)} + \frac{Var(Jn)E(RQD)}{[E(Jn)]^3}\right)\left(\frac{E(Jr)}{E(Ja)} + \frac{Var(Ja)E(Jr)}{[E(Ja)]^3}\right)\left(\frac{E(Jw)}{E(SRF)} + \frac{Var(SRF)E(Jw)}{[E(SRF)]^3}\right) \end{aligned} \tag{E.13}$$

Integrating Eqs. (E.8), (E.11) and (E.12), the standard deviation of Q value can be derived as:

$$\begin{aligned} Var(Q) &= Var\left(\frac{RQD}{Jn} \times \frac{Jr}{Ja} \times \frac{Jw}{SRF}\right) \\ &\approx \left(Var\left(\frac{RQD}{Jn}\right) + [E(\frac{RQD}{Jn})]^2\right) * \left(Var\left(\frac{Jr}{Ja}\right) + [E(\frac{Jr}{Ja})]^2\right) * \left(Var\left(\frac{Jw}{SRF}\right) + [E(\frac{Jw}{SRF})]^2\right) - [E(\frac{RQD}{Jn})]^2[E(\frac{Jr}{Ja})]^2[E(\frac{Jw}{SRF})]^2 \\ &\approx \left(\frac{[E(RQD)]^2}{[E(Jn)]^2}\left(\frac{Var(RQD)}{[E(RQD)]^2} + \frac{Var(Jn)}{[E(Jn)]^2}\right) + \frac{E(RQD)}{E(Jn)} + \frac{Var(Jn)E(RQD)}{[E(Jn)]^3}\right) * \left(\frac{[E(Jr)]^2}{[E(Ja)]^2}\left(\frac{Var(Jr)}{[E(Ja)]^2} + \frac{Var(Ja)}{[E(Ja)]^2}\right) + \frac{E(Jr)}{E(Ja)} + \frac{Var(Ja)E(Jr)}{[E(Ja)]^3}\right) \\ &* \left(\frac{[E(Jw)]^2}{[E(SRF)]^2}\left(\frac{Var(Jw)}{[E(SRF)]^2} + \frac{Var(SRF)}{[E(SRF)]^2}\right) + \frac{E(Jw)}{E(SRF)} + \frac{Var(SRF)E(Jw)}{[E(SRF)]^3}\right) - \left(\frac{E(RQD)}{E(Jn)} + \frac{Var(Jn)E(RQD)}{[E(Jn)]^3}\right)^2 \\ &* \left(\frac{E(JR)}{E(Ja)} + \frac{Var(Ja)E(Jr)}{[E(Ja)]^3}\right)^2 * \left(\frac{E(Jw)}{E(SRF)} + \frac{Var(SRF)E(Jw)}{[E(SRF)]^3}\right)^2 \end{aligned} \tag{E.14}$$

Integrating Eqs. (E.9), (E.11) and (E.12), the COV of Q value can be derived as:

$$\begin{aligned}
&\Omega(Q)=\frac{\sqrt{VAR(Q)}}{E(Q)}\\
&=\frac{\sqrt{VAR(\frac{RQD}{Jn}\times\frac{Jr}{Ja}\times\frac{Jw}{SRF})}}{E(\frac{RQD}{Jn}\times\frac{Jr}{Ja}\times\frac{Jw}{SRF})}\approx\sqrt{([\Omega(\frac{RQD}{Jn})]^2+1)([\Omega(\frac{Jr}{Ja})]^2+1)([\Omega(\frac{Jw}{SRF})]^2+1)-1}\\
&\approx\sqrt{(\frac{([(\Omega(RQD)]^2+[(\Omega(Jn)]^2)}{(1+[\Omega(Jn)]^2)^2}+1)(\frac{([(\Omega(Jr)]^2+[(\Omega(Ja)]^2)}{(1+[\Omega(Ja)]^2)^2}+1)(\frac{([(\Omega(Jw)]^2+[(\Omega(SRF)]^2)}{(1+[\Omega(SRF)]^2)^2}+1)-1}
\end{aligned}\tag{E.15}$$

The COV of Q value can also be calculated based on its definition, which is the ratio of standard deviation to its expected value. In this way, it is calculated by dividing the square root of result in Eq. (E.14) by the result in Eq. (E.13)

APPENDIX F – DATA AND RESULTS

INPUT AND OUTPUT OF PROBABILISTIC PREDICTION MODEL

Table F.1 Input of the probabilistic prediction model in Subsection 1

Chainage (m)		Actual Q-parameter value and state											
From	To	RQD	RQD state	J_n	J_n state	J_r	J_r state	J_a	J_a state	J_w	J_w state	SRF	SRF state
1610	1615	80	4	6	5	1.5	4	2	3	1	1	1	5
1615	1620	80	4	6	5	1.5	4	2	3	1	1	1	5
1620	1625	80	4	6	5	1.5	4	2	3	1	1	1	5
1625	1630	80	4	6	5	1.5	4	2	3	1	1	1	5
1630	1635	60	3	6	5	1.5	4	2	3	1	1	1	5
1635	1640	60	3	6	5	1.5	4	2	3	1	1	1	5
1640	1645	60	3	6	5	1.5	4	2	3	1	1	1	5
1645	1650	85	4	6	5	1.5	4	2	3	1	1	1	5
1650	1655	85	4	6	5	1.5	4	2	3	1	1	1	5
1655	1660	85	4	6	5	1.5	4	2	3	1	1	1	5
1660	1665	55	3	6	5	1.5	4	3	4	1	1	1	5
1665	1670	55	3	6	5	1.5	4	3	4	1	1	1	5
1670	1675	55	3	6	5	1.5	4	3	4	1	1	1	5
1675	1680	40	2	6	5	1.5	4	3	4	1	1	1	5
1680	1685	40	2	6	5	1.5	4	3	4	1	1	1	5
1685	1690	70	3	6	5	1.5	4	2	3	1	1	1	5
1690	1695	45	2	6	5	1.5	4	3	4	1	1	1	5
1695	1700	45	2	6	5	1.5	4	3	4	1	1	1	5
1700	1705	45	2	6	5	1.5	4	3	4	1	1	1	5
1705	1710	45	2	6	5	1.5	4	3	4	1	1	1	5
1710	1715	45	2	6	5	1.5	4	3	4	1	1	1	5
1715	1720	80	4	6	5	1.5	4	3	4	1	1	1	5
1720	1725	80	4	6	5	1.5	4	3	4	1	1	1	5
1725	1730	80	4	6	5	1.5	4	3	4	1	1	1	5
1730	1735	80	4	6	5	1.5	4	3	4	1	1	1	5
1735	1740	80	4	6	5	1.5	4	3	4	1	1	1	5
1740	1745	40	2	6	5	1.5	4	3	4	1	1	1	5
1745	1750	40	2	6	5	1.5	4	3	4	1	1	1	5
1750	1755	95	4	4	4	1.5	4	2	3	1	1	1	5
1755	1760	95	4	4	4	1.5	4	2	3	1	1	1	5
1760	1765	95	4	4	4	1.5	4	2	3	1	1	1	5
1765	1770	100	4	3	3	4	1	1	2	1	1	1	5
1770	1775	85	4	3	3	1.5	4	2	3	1	1	1	5

Chainage (m)		Actual Q-parameter value and state											
From	**To**	**RQD**	**RQD state**	**J_n**	**J_n state**	**J_r**	**J_r state**	**J_a**	**J_a state**	**J_w**	**J_w state**	**SRF**	**SRF state**
1775	1780	85	4	3	3	1.5	4	2	3	1	1	1	5
1780	1785	85	4	3	3	1.5	4	2	3	0.66	2	1	5
1785	1790	85	4	6	5	1.5	4	2	3	1	1	1	5
1790	1795	70	3	6	5	1.5	4	2	3	1	1	1	5
1795	1800	70	3	6	5	1.5	4	2	3	1	1	1	5
1800	1805	50	2	6	5	1	1	2	3	0.66	2	1	5
1805	1810	70	3	6	5	1.5	4	2	3	1	1	1	5
1810	1815	80	4	6	5	1.5	4	2	3	0.66	2	1	5
1815	1820	80	4	6	5	1.5	4	2	3	0.66	2	1	5
1820	1825	60	3	6	5	1.5	4	2	3	1	1	1	5
1825	1830	60	3	6	5	1.5	4	2	3	1	1	1	5
1830	1835	60	3	6	5	1.5	4	2	3	1	1	1	5
1835	1840	60	3	6	5	1.5	4	2	3	1	1	1	5
1840	1845	40	3	6	5	1.5	4	2	3	1	1	1	5
1845	1850	40	3	6	5	1.5	4	2	3	1	1	1	5
1850	1855	40	3	6	5	1.5	4	2	3	0.66	2	1	5
1855	1860	40	3	6	5	1.5	4	2	3	0.66	2	1	5
1860	1865	80	4	6	5	1.5	4	2	3	1	1	1	5
1865	1870	80	4	6	5	1.5	4	2	3	1	1	1	5
1870	1875	60	3	6	5	1.5	4	3	4	1	1	1	5
1875	1880	60	3	6	5	1.5	4	3	4	1	1	1	5
1880	1885	80	4	6	5	1.5	4	2	3	1	1	1	5
1885	1890	70	3	6	5	1.5	4	2	3	1	1	1	5
1890	1895	70	3	6	5	1.5	4	2	3	1	1	1	5
1895	1900	70	3	6	5	1.5	4	2	3	1	1	1	5
1900	1905	80	4	6	5	1.5	4	2	3	1	1	1	5
1905	1910	80	4	6	5	1.5	4	2	3	1	1	1	5
1910	1915	70	3	3	3	1.5	4	2	3	1	1	1	5
1915	1920	80	4	4	4	1.5	4	3	4	1	1	1	5
1920	1925	80	4	4	4	1.5	4	3	4	1	1	1	5
1925	1930	80	4	4	4	1.5	4	3	4	1	1	1	5
1930	1935	80	4	4	4	1.5	4	3	4	1	1	1	5
1935	1940	60	3	4	4	1.5	4	3	4	1	1	1	5
1940	1945	80	4	6	5	1.5	4	2	3	1	1	1	5
1945	1950	80	4	6	5	1.5	4	2	3	1	1	1	5
1950	1955	80	4	6	5	1.5	4	2	3	1	1	1	5
1955	1960	80	4	6	5	1.5	4	2	3	1	1	1	5
1960	1965	80	4	6	5	1.5	4	2	3	1	1	1	5
1965	1970	80	4	6	5	1.5	4	2	3	1	1	1	5

Chainage (m)		Actual Q-parameter value and state											
From	To	RQD	RQD state	J_n	J_n state	J_r	J_r state	J_a	J_a state	J_w	J_w state	SRF	SRF state
1970	1975	60	3	4	4	1.5	4	2	3	1	1	1	5
1975	1980	70	3	4	4	1.5	4	2	3	1	1	1	5
1980	1985	70	3	4	4	1.5	4	2	3	1	1	1	5
1985	1990	60	3	4	4	1	5	2	3	1	1	1	5
1990	1995	70	3	6	5	1.5	4	2	3	1	1	1	5
1995	2000	70	3	6	5	1.5	4	2	3	1	1	1	5
2000	2005	70	3	6	5	1.5	4	2	3	1	1	1	5
2005	2010	70	3	6	5	1.5	4	2	3	1	1	1	5
2010	2015	80	4	6	5	1.5	4	2	3	1	1	1	5

Table F.2 Comparison between predicted and actual RQD in Subsection 2

Chainage (m)		Predicted state probability				Actual value and state	
From	To	State 1	State 2	State 3	State 4	Actual value	Actual state
2010	2015	0.0%	0.0%	5.0%	95.0%	80	4
2015	2020	0.0%	1.3%	13.8%	84.9%	80	4
2020	2025	0.0%	2.4%	22.1%	75.5%	80	4
2025	2030	0.0%	3.4%	30.1%	66.5%	80	4
2030	2035	0.0%	4.2%	37.9%	57.9%	80	4
2035	2040	0.0%	4.7%	45.7%	49.5%	80	3
2040	2045	0.0%	5.1%	53.7%	41.1%	60	3
2045	2050	0.0%	5.4%	62.0%	32.7%	80	4
2050	2055	0.0%	5.4%	70.6%	23.9%	50	3
2055	2060	0.0%	5.3%	79.9%	14.8%	70	3
2060	2065	0.0%	5.0%	90.0%	5.0%	30	3
2065	2070	0.0%	5.6%	86.6%	7.7%	70	3
2070	2075	0.0%	6.1%	84.1%	9.8%	65	3
2075	2080	0.0%	6.4%	82.3%	11.3%	65	3
2080	2085	0.0%	6.6%	81.2%	12.2%	70	3
2085	2090	0.0%	6.6%	80.9%	12.6%	70	3
2090	2095	0.0%	6.5%	81.2%	12.3%	70	3
2095	2100	0.0%	6.3%	82.3%	11.5%	70	3
2100	2105	0.0%	5.9%	84.1%	10.0%	70	3
2105	2110	0.0%	5.5%	86.6%	7.8%	70	3
2110	2115	0.0%	5.0%	90.0%	5.0%	75	3
2115	2120	0.0%	5.6%	86.6%	7.7%	75	3
2120	2125	0.0%	6.1%	84.1%	9.8%	60	3
2125	2130	0.0%	6.4%	82.3%	11.3%	65	3
2130	2135	0.0%	6.6%	81.2%	12.2%	65	3
2135	2140	0.0%	6.6%	80.9%	12.6%	80	4

Chainage (m)		Predicted state probability				Actual value and state	
From	To	State 1	State 2	State 3	State 4	Actual value	Actual state
2140	2145	0.0%	6.5%	81.2%	12.3%	70	3
2145	2150	0.0%	6.3%	82.3%	11.5%	70	3
2150	2155	0.0%	5.9%	84.1%	10.0%	70	3
2155	2160	0.0%	5.5%	86.6%	7.8%	70	3
2160	2165	0.0%	5.0%	90.0%	5.0%	60	3
2165	2170	0.0%	5.6%	86.6%	7.7%	80	4
2170	2175	0.0%	6.1%	84.1%	9.8%	80	4
2175	2180	0.0%	6.4%	82.3%	11.3%	65	3
2180	2185	0.0%	6.6%	81.2%	12.2%	70	3
2185	2190	0.0%	6.6%	80.9%	12.6%	70	3
2190	2195	0.0%	6.5%	81.2%	12.3%	60	3
2195	2200	0.0%	6.3%	82.3%	11.5%	60	3
2200	2205	0.0%	5.9%	84.1%	10.0%	65	3
2205	2210	0.0%	5.5%	86.6%	7.8%	65	3
2210	2215	0.0%	5.0%	90.0%	5.0%	70	3
2215	2220	0.0%	6.3%	79.4%	14.3%	70	3
2220	2225	0.0%	7.1%	69.7%	23.2%	70	3
2225	2230	0.0%	7.6%	60.7%	31.7%	70	3
2230	2235	0.0%	7.6%	52.2%	40.1%	80	3
2235	2240	0.0%	7.3%	44.2%	48.5%	80	3
2240	2245	0.0%	6.6%	36.4%	57.0%	85	4
2245	2250	0.0%	5.6%	28.7%	65.7%	85	4
2250	2255	0.0%	4.1%	21.0%	74.9%	85	4
2255	2260	0.0%	2.3%	13.2%	84.6%	85	4
2260	2265	0.0%	0.0%	5.0%	95.0%	80	4
2265	2270	0.0%	0.8%	7.3%	91.9%	70	3
2270	2275	0.0%	1.4%	9.1%	89.5%	60	3
2275	2280	0.0%	1.9%	10.3%	87.8%	60	3
2280	2285	0.0%	2.2%	10.9%	86.8%	70	3
2285	2290	0.0%	2.4%	11.1%	86.5%	80	3
2290	2295	0.0%	2.3%	10.9%	86.8%	80	4
2295	2300	0.0%	2.1%	10.1%	87.8%	80	4
2300	2305	0.0%	1.6%	8.9%	89.5%	90	4
2305	2310	0.0%	0.9%	7.2%	91.9%	90	4
2310	2315	0.0%	0.0%	5.0%	95.0%	90	4
2315	2320	0.0%	0.8%	7.3%	91.9%	90	4
2320	2325	0.0%	1.4%	9.1%	89.5%	90	4
2325	2330	0.0%	1.9%	10.3%	87.8%	90	4
2330	2335	0.0%	2.2%	10.9%	86.8%	85	4

Chainage (m)		Predicted state probability				Actual value and state	
From	To	State 1	State 2	State 3	State 4	Actual value	Actual state
2335	2340	0.0%	2.4%	11.1%	86.5%	85	4
2340	2345	0.0%	2.3%	10.9%	86.8%	80	4
2345	2350	0.0%	2.1%	10.1%	87.8%	80	4
2350	2355	0.0%	1.6%	8.9%	89.5%	70	3
2355	2360	0.0%	0.9%	7.2%	91.9%	85	4
2360	2365	0.0%	0.0%	5.0%	95.0%	80	4
2365	2370	0.0%	0.8%	7.3%	91.9%	80	4
2370	2375	0.0%	1.4%	9.1%	89.5%	90	4
2375	2380	0.0%	1.9%	10.3%	87.8%	90	4
2380	2385	0.0%	2.2%	10.9%	86.8%	80	4
2385	2390	0.0%	2.4%	11.1%	86.5%	80	4
2390	2395	0.0%	2.3%	10.9%	86.8%	50	2
2395	2400	0.0%	2.1%	10.1%	87.8%	80	4
2400	2405	0.0%	1.6%	8.9%	89.5%	80	4
2405	2410	0.0%	0.9%	7.2%	91.9%	90	4
2410	2415	0.0%	0.0%	5.0%	95.0%	90	4
2415	2420	0.0%	0.8%	7.3%	91.9%	95	4
2420	2425	0.0%	1.4%	9.1%	89.5%	95	4
2425	2430	0.0%	1.9%	10.3%	87.8%	95	4
2430	2435	0.0%	2.2%	10.9%	86.8%	95	4
2435	2440	0.0%	2.4%	11.1%	86.5%	95	4
2440	2445	0.0%	2.3%	10.9%	86.8%	90	4
2445	2450	0.0%	2.1%	10.1%	87.8%	90	4
2450	2455	0.0%	1.6%	8.9%	89.5%	95	4
2455	2460	0.0%	0.9%	7.2%	91.9%	95	4
2460	2465	0.0%	0.0%	5.0%	95.0%	90	4
2465	2470	0.0%	0.8%	7.3%	91.9%	90	4
2470	2475	0.0%	1.4%	9.1%	89.5%	85	4
2475	2480	0.0%	1.9%	10.3%	87.8%	85	4
2480	2485	0.0%	2.2%	10.9%	86.8%	85	4
2485	2490	0.0%	2.4%	11.1%	86.5%	70	3
2490	2495	0.0%	2.3%	10.9%	86.8%	50	2
2495	2500	0.0%	2.1%	10.1%	87.8%	50	2
2500	2505	0.0%	1.6%	8.9%	89.5%	60	3
2505	2510	0.0%	0.9%	7.2%	91.9%	80	4
2510	2515	0.0%	0.0%	5.0%	95.0%	90	4
2515	2520	0.0%	0.8%	7.3%	91.9%	90	4
2520	2525	0.0%	1.4%	9.1%	89.5%	85	4
2525	2530	0.0%	1.9%	10.3%	87.8%	85	4

Chainage (m)		Predicted state probability				Actual value and state	
From	To	State 1	State 2	State 3	State 4	Actual value	Actual state
2530	2535	0.0%	2.2%	10.9%	86.8%	80	4
2535	2540	0.0%	2.4%	11.1%	86.5%	80	4
2540	2545	0.0%	2.3%	10.9%	86.8%	80	4
2545	2550	0.0%	2.1%	10.1%	87.8%	70	3
2550	2555	0.0%	1.6%	8.9%	89.5%	70	3
2555	2560	0.0%	0.9%	7.2%	91.9%	85	4
2560	2565	0.0%	0.0%	5.0%	95.0%	90	4
2565	2570	0.0%	0.8%	7.3%	91.9%	90	4
2570	2575	0.0%	1.4%	9.1%	89.5%	100	4
2575	2580	0.0%	1.9%	10.3%	87.8%	100	4
2580	2585	0.0%	2.2%	10.9%	86.8%	100	4
2585	2590	0.0%	2.4%	11.1%	86.5%	100	4
2590	2595	0.0%	2.3%	10.9%	86.8%	100	4
2595	2600	0.0%	2.1%	10.1%	87.8%	100	4
2600	2605	0.0%	1.6%	8.9%	89.5%	100	4
2605	2610	0.0%	0.9%	7.2%	91.9%	100	4
2610	2615	0.0%	0.0%	5.0%	95.0%	100	4

Table F.3 Comparison between predicted and actual J_n in Subsection 2

Chainage (m)		Predicted state probability									Actual value	Actual state
From	To	State 1	State 2	State 3	State 4	State 5	State 6	State 7	State 8	State 9		
2010	2015	0.0%	0.0%	0.0%	5.0%	90.0%	5.0%	0.0%	0.0%	0.0%	6	5
2015	2020	0.0%	0.0%	1.2%	6.4%	92.4%	0.0%	0.0%	0.0%	0.0%	6	5
2020	2025	0.0%	0.0%	1.7%	6.1%	92.2%	0.0%	0.0%	0.0%	0.0%	6	5
2025	2030	0.0%	0.0%	2.1%	5.9%	92.0%	0.0%	0.0%	0.0%	0.0%	6	5
2030	2035	0.0%	0.0%	2.5%	5.7%	91.8%	0.0%	0.0%	0.0%	0.0%	6	5
2035	2040	0.0%	0.0%	2.9%	5.5%	91.5%	0.0%	0.0%	0.0%	0.0%	6	4
2040	2045	0.0%	0.0%	3.3%	5.4%	91.3%	0.0%	0.0%	0.0%	0.0%	4	5
2045	2050	0.0%	0.0%	3.7%	5.3%	91.0%	0.0%	0.0%	0.0%	0.0%	6	5
2050	2055	0.0%	0.0%	4.2%	5.2%	90.6%	0.0%	0.0%	0.0%	0.0%	6	5
2055	2060	0.0%	0.0%	4.6%	5.1%	90.3%	0.0%	0.0%	0.0%	0.0%	6	5
2060	2065	0.0%	0.0%	0.0%	5.0%	90.0%	5.0%	0.0%	0.0%	0.0%	4	5
2065	2070	0.0%	0.0%	1.2%	6.4%	92.4%	0.0%	0.0%	0.0%	0.0%	6	5
2070	2075	0.0%	0.0%	1.7%	6.1%	92.2%	0.0%	0.0%	0.0%	0.0%	6	5
2075	2080	0.0%	0.0%	2.1%	5.9%	92.0%	0.0%	0.0%	0.0%	0.0%	6	5
2080	2085	0.0%	0.0%	2.5%	5.7%	91.8%	0.0%	0.0%	0.0%	0.0%	6	5
2085	2090	0.0%	0.0%	2.9%	5.5%	91.5%	0.0%	0.0%	0.0%	0.0%	6	5
2090	2095	0.0%	0.0%	3.3%	5.4%	91.3%	0.0%	0.0%	0.0%	0.0%	6	5
2095	2100	0.0%	0.0%	3.7%	5.3%	91.0%	0.0%	0.0%	0.0%	0.0%	6	5

Chainage (m)		Predicted state probability									Actual value	Actual state
From	To	State 1	State 2	State 3	State 4	State 5	State 6	State 7	State 8	State 9		
2100	2105	0.0%	0.0%	4.2%	5.2%	90.6%	0.0%	0.0%	0.0%	0.0%	6	5
2105	2110	0.0%	0.0%	4.6%	5.1%	90.3%	0.0%	0.0%	0.0%	0.0%	6	5
2110	2115	0.0%	0.0%	0.0%	5.0%	90.0%	5.0%	0.0%	0.0%	0.0%	6	5
2115	2120	0.0%	0.0%	1.2%	6.4%	92.4%	0.0%	0.0%	0.0%	0.0%	6	5
2120	2125	0.0%	0.0%	1.7%	6.1%	92.2%	0.0%	0.0%	0.0%	0.0%	6	5
2125	2130	0.0%	0.0%	2.1%	5.9%	92.0%	0.0%	0.0%	0.0%	0.0%	6	5
2130	2135	0.0%	0.0%	2.5%	5.7%	91.8%	0.0%	0.0%	0.0%	0.0%	6	5
2135	2140	0.0%	0.0%	2.9%	5.5%	91.5%	0.0%	0.0%	0.0%	0.0%	6	5
2140	2145	0.0%	0.0%	3.3%	5.4%	91.3%	0.0%	0.0%	0.0%	0.0%	6	5
2145	2150	0.0%	0.0%	3.7%	5.3%	91.0%	0.0%	0.0%	0.0%	0.0%	6	5
2150	2155	0.0%	0.0%	4.2%	5.2%	90.6%	0.0%	0.0%	0.0%	0.0%	6	5
2155	2160	0.0%	0.0%	4.6%	5.1%	90.3%	0.0%	0.0%	0.0%	0.0%	6	5
2160	2165	0.0%	0.0%	0.0%	5.0%	90.0%	5.0%	0.0%	0.0%	0.0%	6	5
2165	2170	0.0%	0.0%	1.2%	6.4%	92.4%	0.0%	0.0%	0.0%	0.0%	4	4
2170	2175	0.0%	0.0%	1.7%	6.1%	92.2%	0.0%	0.0%	0.0%	0.0%	4	4
2175	2180	0.0%	0.0%	2.1%	5.9%	92.0%	0.0%	0.0%	0.0%	0.0%	4	4
2180	2185	0.0%	0.0%	2.5%	5.7%	91.8%	0.0%	0.0%	0.0%	0.0%	6	5
2185	2190	0.0%	0.0%	2.9%	5.5%	91.5%	0.0%	0.0%	0.0%	0.0%	6	5
2190	2195	0.0%	0.0%	3.3%	5.4%	91.3%	0.0%	0.0%	0.0%	0.0%	6	5
2195	2200	0.0%	0.0%	3.7%	5.3%	91.0%	0.0%	0.0%	0.0%	0.0%	6	5
2200	2205	0.0%	0.0%	4.2%	5.2%	90.6%	0.0%	0.0%	0.0%	0.0%	6	5
2205	2210	0.0%	0.0%	4.6%	5.1%	90.3%	0.0%	0.0%	0.0%	0.0%	6	5
2210	2215	0.0%	0.0%	0.0%	5.0%	90.0%	5.0%	0.0%	0.0%	0.0%	4	5
2215	2220	0.0%	0.0%	8.9%	4.9%	86.2%	0.0%	0.0%	0.0%	0.0%	4	5
2220	2225	0.0%	0.0%	14.8%	4.3%	80.9%	0.0%	0.0%	0.0%	0.0%	6	5
2225	2230	0.0%	0.0%	21.3%	3.9%	74.7%	0.0%	0.0%	0.0%	0.0%	6	5
2230	2235	0.0%	0.0%	28.6%	3.6%	67.7%	0.0%	0.0%	0.0%	0.0%	3	3
2235	2240	0.0%	0.0%	36.8%	3.4%	59.7%	0.0%	0.0%	0.0%	0.0%	3	3
2240	2245	0.0%	0.0%	45.9%	3.4%	50.6%	0.0%	0.0%	0.0%	0.0%	3	3
2245	2250	0.0%	0.0%	56.2%	3.5%	40.3%	0.0%	0.0%	0.0%	0.0%	3	3
2250	2255	0.0%	0.0%	67.7%	3.7%	28.5%	0.0%	0.0%	0.0%	0.0%	6	3
2255	2260	0.0%	0.0%	80.6%	4.2%	15.1%	0.0%	0.0%	0.1%	0.0%	6	3
2260	2265	0.0%	5.0%	90.0%	5.0%	0.0%	0.0%	0.0%	0.0%	0.0%	3	3
2265	2270	0.0%	0.0%	75.8%	11.8%	12.4%	0.0%	0.0%	0.0%	0.0%	3	3
2270	2275	0.0%	0.0%	62.7%	15.1%	22.2%	0.0%	0.0%	0.0%	0.0%	6	5
2275	2280	0.0%	0.0%	51.2%	16.9%	31.8%	0.0%	0.0%	0.0%	0.0%	6	5
2280	2285	0.0%	0.0%	41.3%	17.5%	41.2%	0.0%	0.0%	0.0%	0.0%	6	5
2285	2290	0.0%	0.0%	32.6%	17.2%	50.2%	0.0%	0.0%	0.0%	0.0%	6	5
2290	2295	0.0%	0.0%	25.2%	16.0%	58.8%	0.0%	0.0%	0.0%	0.0%	6	5

Chainage (m)		Predicted state probability									Actual value	Actual state
From	To	State 1	State 2	State 3	State 4	State 5	State 6	State 7	State 8	State 9		
2295	2300	0.0%	0.0%	18.8%	14.1%	67.1%	0.0%	0.0%	0.0%	0.0%	6	5
2300	2305	0.0%	0.0%	13.3%	11.6%	75.0%	0.0%	0.0%	0.0%	0.0%	3	3
2305	2310	0.0%	0.0%	8.8%	8.6%	82.6%	0.0%	0.0%	0.0%	0.0%	3	3
2310	2315	0.0%	0.0%	0.0%	5.0%	90.0%	5.0%	0.0%	0.0%	0.0%	6	5
2315	2320	0.0%	0.0%	8.9%	4.9%	86.2%	0.0%	0.0%	0.0%	0.0%	6	5
2320	2325	0.0%	0.0%	14.8%	4.3%	80.9%	0.0%	0.0%	0.0%	0.0%	6	5
2325	2330	0.0%	0.0%	21.3%	3.9%	74.7%	0.0%	0.0%	0.0%	0.0%	6	5
2330	2335	0.0%	0.0%	28.6%	3.6%	67.7%	0.0%	0.0%	0.0%	0.0%	3	5
2335	2340	0.0%	0.0%	36.8%	3.4%	59.7%	0.0%	0.0%	0.0%	0.0%	3	3
2340	2345	0.0%	0.0%	45.9%	3.4%	50.6%	0.0%	0.0%	0.0%	0.0%	3	3
2345	2350	0.0%	0.0%	56.2%	3.5%	40.3%	0.0%	0.0%	0.0%	0.0%	3	3
2350	2355	0.0%	0.0%	67.7%	3.7%	28.5%	0.0%	0.0%	0.0%	0.0%	3	3
2355	2360	0.0%	0.0%	80.6%	4.2%	15.1%	0.0%	0.0%	0.1%	0.0%	3	3
2360	2365	0.0%	5.0%	90.0%	5.0%	0.0%	0.0%	0.0%	0.0%	0.0%	3	3
2365	2370	0.0%	0.0%	75.8%	11.8%	12.4%	0.0%	0.0%	0.0%	0.0%	3	3
2370	2375	0.0%	0.0%	62.7%	15.1%	22.2%	0.0%	0.0%	0.0%	0.0%	3	3
2375	2380	0.0%	0.0%	51.2%	16.9%	31.8%	0.0%	0.0%	0.0%	0.0%	3	3
2380	2385	0.0%	0.0%	41.3%	17.5%	41.2%	0.0%	0.0%	0.0%	0.0%	3	3
2385	2390	0.0%	0.0%	32.6%	17.2%	50.2%	0.0%	0.0%	0.0%	0.0%	6	5
2390	2395	0.0%	0.0%	25.2%	16.0%	58.8%	0.0%	0.0%	0.0%	0.0%	4	4
2395	2400	0.0%	0.0%	18.8%	14.1%	67.1%	0.0%	0.0%	0.0%	0.0%	6	5
2400	2405	0.0%	0.0%	13.3%	11.6%	75.0%	0.0%	0.0%	0.0%	0.0%	6	5
2405	2410	0.0%	0.0%	8.8%	8.6%	82.6%	0.0%	0.0%	0.0%	0.0%	6	5
2410	2415	0.0%	0.0%	0.0%	5.0%	90.0%	5.0%	0.0%	0.0%	0.0%	6	5
2415	2420	0.0%	0.0%	2.7%	11.3%	86.0%	0.0%	0.0%	0.0%	0.0%	6	5
2420	2425	0.0%	0.0%	4.1%	15.3%	80.5%	0.0%	0.0%	0.0%	0.0%	6	5
2425	2430	0.0%	0.0%	5.4%	20.1%	74.5%	0.0%	0.0%	0.0%	0.0%	6	5
2430	2435	0.0%	0.0%	6.4%	25.7%	67.9%	0.0%	0.0%	0.0%	0.0%	6	5
2435	2440	0.0%	0.0%	7.3%	32.3%	60.4%	0.0%	0.0%	0.0%	0.0%	6	5
2440	2445	0.0%	0.0%	7.8%	40.2%	52.0%	0.0%	0.0%	0.0%	0.0%	4	4
2445	2450	0.0%	0.0%	7.9%	49.6%	42.4%	0.0%	0.0%	0.0%	0.0%	4	4
2450	2455	0.0%	0.0%	7.6%	60.8%	31.6%	0.0%	0.0%	0.0%	0.0%	4	4
2455	2460	0.0%	0.0%	6.7%	74.1%	19.2%	0.0%	0.0%	0.1%	0.0%	4	4
2460	2465	0.0%	0.0%	5.0%	90.0%	5.0%	0.0%	0.0%	0.0%	0.0%	4	4
2465	2470	0.0%	0.0%	6.2%	68.8%	25.0%	0.0%	0.0%	0.0%	0.0%	4	4
2470	2475	0.0%	0.0%	8.7%	51.9%	39.3%	0.0%	0.0%	0.0%	0.0%	4	4
2475	2480	0.0%	0.0%	12.8%	38.5%	48.6%	0.0%	0.0%	0.0%	0.0%	4	4
2480	2485	0.0%	0.0%	18.5%	28.0%	53.4%	0.0%	0.0%	0.0%	0.0%	3	3
2485	2490	0.0%	0.0%	25.9%	20.0%	54.0%	0.0%	0.0%	0.0%	0.0%	3	3

Chainage (m)		Predicted state probability									Actual value	Actual state
From	To	State 1	State 2	State 3	State 4	State 5	State 6	State 7	State 8	State 9		
2490	2495	0.0%	0.0%	35.2%	14.1%	50.7%	0.0%	0.0%	0.0%	0.0%	3	3
2495	2500	0.0%	0.0%	46.6%	9.8%	43.6%	0.0%	0.0%	0.0%	0.0%	3	3
2500	2505	0.0%	0.0%	60.2%	7.0%	32.8%	0.0%	0.0%	0.1%	0.0%	3	3
2505	2510	0.0%	0.0%	76.3%	5.4%	18.2%	0.0%	0.0%	0.1%	0.0%	3	3
2510	2515	0.0%	5.0%	90.0%	5.0%	0.0%	0.0%	0.0%	0.0%	0.0%	3	3
2515	2520	0.0%	0.0%	92.6%	4.8%	2.6%	0.0%	0.0%	0.0%	0.0%	3	3
2520	2525	0.0%	0.0%	91.8%	4.3%	3.9%	0.0%	0.0%	0.0%	0.0%	3	3
2525	2530	0.0%	0.0%	91.3%	3.9%	4.7%	0.0%	0.0%	0.0%	0.0%	3	3
2530	2535	0.0%	0.0%	91.1%	3.7%	5.3%	0.0%	0.0%	0.0%	0.0%	3	3
2535	2540	0.0%	0.0%	91.1%	3.5%	5.4%	0.0%	0.0%	0.0%	0.0%	3	3
2540	2545	0.0%	0.0%	91.3%	3.6%	5.1%	0.0%	0.0%	0.0%	0.0%	3	3
2545	2550	0.0%	0.0%	91.8%	3.7%	4.5%	0.0%	0.0%	0.0%	0.0%	3	3
2550	2555	0.0%	0.0%	92.6%	4.0%	3.4%	0.0%	0.0%	0.0%	0.0%	3	3
2555	2560	0.0%	0.0%	93.6%	4.4%	1.9%	0.0%	0.0%	0.0%	0.0%	3	3
2560	2565	0.0%	5.0%	90.0%	5.0%	0.0%	0.0%	0.0%	0.0%	0.0%	3	3
2565	2570	0.0%	0.0%	92.6%	4.8%	2.6%	0.0%	0.0%	0.0%	0.0%	3	3
2570	2575	0.0%	0.0%	91.8%	4.3%	3.9%	0.0%	0.0%	0.0%	0.0%	3	3
2575	2580	0.0%	0.0%	91.3%	3.9%	4.7%	0.0%	0.0%	0.0%	0.0%	3	3
2580	2585	0.0%	0.0%	91.1%	3.7%	5.3%	0.0%	0.0%	0.0%	0.0%	3	3
2585	2590	0.0%	0.0%	91.1%	3.5%	5.4%	0.0%	0.0%	0.0%	0.0%	3	3
2590	2595	0.0%	0.0%	91.3%	3.6%	5.1%	0.0%	0.0%	0.0%	0.0%	3	3
2595	2600	0.0%	0.0%	91.8%	3.7%	4.5%	0.0%	0.0%	0.0%	0.0%	3	3
2600	2605	0.0%	0.0%	92.6%	4.0%	3.4%	0.0%	0.0%	0.0%	0.0%	3	3
2605	2610	0.0%	0.0%	93.6%	4.4%	1.9%	0.0%	0.0%	0.0%	0.0%	3	3
2610	2615	0.0%	5.0%	90.0%	5.0%	0.0%	0.0%	0.0%	0.0%	0.0%	3	3

Table F.4 Comparison between predicted and actual J_r in Subsection 2

Chainage (m)		Predicted state probability							Actual value	Actual state
From	To	State 1	State 2	State 3	State 4	State 5	State 6	State 7		
2010	2015	0.0%	5.0%	5.0%	85.0%	5.0%	0.0%	0.0%	1.5	4
2015	2020	0.4%	0.0%	0.0%	91.3%	8.3%	0.0%	0.0%	1.5	4
2020	2025	0.8%	0.0%	0.0%	92.5%	6.7%	0.0%	0.0%	1.5	4
2025	2030	1.1%	0.0%	0.0%	93.1%	5.8%	0.0%	0.0%	1.5	4
2030	2035	1.4%	0.0%	0.0%	93.3%	5.2%	0.0%	0.0%	1.5	4
2035	2040	1.8%	0.0%	0.0%	93.2%	5.0%	0.0%	0.0%	1.5	4
2040	2045	2.3%	0.0%	0.0%	92.6%	5.1%	0.0%	0.0%	1.5	4
2045	2050	2.8%	0.0%	0.0%	91.6%	5.6%	0.0%	0.0%	1.5	4
2050	2055	3.4%	0.0%	0.0%	90.1%	6.5%	0.0%	0.0%	1.5	4
2055	2060	4.2%	0.0%	0.0%	87.9%	7.9%	0.0%	0.0%	1.5	4

Chainage (m)		Predicted state probability							Actual value	Actual state
From	To	State 1	State 2	State 3	State 4	State 5	State 6	State 7		
2060	2065	0.0%	5.0%	5.0%	85.0%	5.0%	0.0%	0.0%	1	5
2065	2070	0.4%	0.0%	0.0%	91.3%	8.3%	0.0%	0.0%	1.5	4
2070	2075	0.8%	0.0%	0.0%	92.5%	6.7%	0.0%	0.0%	1.5	4
2075	2080	1.1%	0.0%	0.0%	93.1%	5.8%	0.0%	0.0%	1.5	4
2080	2085	1.4%	0.0%	0.0%	93.3%	5.2%	0.0%	0.0%	1.5	4
2085	2090	1.8%	0.0%	0.0%	93.2%	5.0%	0.0%	0.0%	1.5	4
2090	2095	2.3%	0.0%	0.0%	92.6%	5.1%	0.0%	0.0%	1.5	4
2095	2100	2.8%	0.0%	0.0%	91.6%	5.6%	0.0%	0.0%	1.5	4
2100	2105	3.4%	0.0%	0.0%	90.1%	6.5%	0.0%	0.0%	1.5	4
2105	2110	4.2%	0.0%	0.0%	87.9%	7.9%	0.0%	0.0%	1.5	4
2110	2115	0.0%	5.0%	5.0%	85.0%	5.0%	0.0%	0.0%	1.5	4
2115	2120	0.4%	0.0%	0.0%	91.3%	8.3%	0.0%	0.0%	1.5	4
2120	2125	0.8%	0.0%	0.0%	92.5%	6.7%	0.0%	0.0%	1.5	4
2125	2130	1.1%	0.0%	0.0%	93.1%	5.8%	0.0%	0.0%	1.5	4
2130	2135	1.4%	0.0%	0.0%	93.3%	5.2%	0.0%	0.0%	1.5	4
2135	2140	1.8%	0.0%	0.0%	93.2%	5.0%	0.0%	0.0%	1.5	4
2140	2145	2.3%	0.0%	0.0%	92.6%	5.1%	0.0%	0.0%	1.5	4
2145	2150	2.8%	0.0%	0.0%	91.6%	5.6%	0.0%	0.0%	1.5	4
2150	2155	3.4%	0.0%	0.0%	90.1%	6.5%	0.0%	0.0%	1.5	4
2155	2160	4.2%	0.0%	0.0%	87.9%	7.9%	0.0%	0.0%	1.5	4
2160	2165	0.0%	5.0%	5.0%	85.0%	5.0%	0.0%	0.0%	1.5	4
2165	2170	0.4%	0.0%	0.0%	91.3%	8.3%	0.0%	0.0%	1.5	4
2170	2175	0.8%	0.0%	0.0%	92.5%	6.7%	0.0%	0.0%	1.5	4
2175	2180	1.1%	0.0%	0.0%	93.1%	5.8%	0.0%	0.0%	1	5
2180	2185	1.4%	0.0%	0.0%	93.3%	5.2%	0.0%	0.0%	1.5	4
2185	2190	1.8%	0.0%	0.0%	93.2%	5.0%	0.0%	0.0%	1.5	4
2190	2195	2.3%	0.0%	0.0%	92.6%	5.1%	0.0%	0.0%	1.5	4
2195	2200	2.8%	0.0%	0.0%	91.6%	5.6%	0.0%	0.0%	1.5	4
2200	2205	3.4%	0.0%	0.0%	90.1%	6.5%	0.0%	0.0%	1.5	4
2205	2210	4.2%	0.0%	0.0%	87.9%	7.9%	0.0%	0.0%	1.5	4
2210	2215	0.0%	5.0%	5.0%	85.0%	5.0%	0.0%	0.0%	1.5	4
2215	2220	0.4%	0.0%	0.0%	91.3%	8.3%	0.0%	0.0%	1.5	4
2220	2225	0.8%	0.0%	0.0%	92.5%	6.7%	0.0%	0.0%	1.5	4
2225	2230	1.1%	0.0%	0.0%	93.1%	5.8%	0.0%	0.0%	1	5
2230	2235	1.4%	0.0%	0.0%	93.3%	5.2%	0.0%	0.0%	1.5	4
2235	2240	1.8%	0.0%	0.0%	93.2%	5.0%	0.0%	0.0%	1.5	4
2240	2245	2.3%	0.0%	0.0%	92.6%	5.1%	0.0%	0.0%	1.5	4
2245	2250	2.8%	0.0%	0.0%	91.6%	5.6%	0.0%	0.0%	1.5	4
2250	2255	3.4%	0.0%	0.0%	90.1%	6.5%	0.0%	0.0%	1.5	4

Chainage (m)		Predicted state probability							Actual value	Actual state
From	To	State 1	State 2	State 3	State 4	State 5	State 6	State 7		
2255	2260	4.2%	0.0%	0.0%	87.9%	7.9%	0.0%	0.0%	1.5	4
2260	2265	0.0%	5.0%	5.0%	85.0%	5.0%	0.0%	0.0%	1.5	4
2265	2270	0.4%	0.0%	0.0%	91.3%	8.3%	0.0%	0.0%	1.5	4
2270	2275	0.8%	0.0%	0.0%	92.5%	6.7%	0.0%	0.0%	1.5	4
2275	2280	1.1%	0.0%	0.0%	93.1%	5.8%	0.0%	0.0%	1.5	4
2280	2285	1.4%	0.0%	0.0%	93.3%	5.2%	0.0%	0.0%	1.5	4
2285	2290	1.8%	0.0%	0.0%	93.2%	5.0%	0.0%	0.0%	1.5	4
2290	2295	2.3%	0.0%	0.0%	92.6%	5.1%	0.0%	0.0%	1.5	4
2295	2300	2.8%	0.0%	0.0%	91.6%	5.6%	0.0%	0.0%	1.5	4
2300	2305	3.4%	0.0%	0.0%	90.1%	6.5%	0.0%	0.0%	1.5	4
2305	2310	4.2%	0.0%	0.0%	87.9%	7.9%	0.0%	0.0%	1.5	4
2310	2315	0.0%	5.0%	5.0%	85.0%	5.0%	0.0%	0.0%	1.5	4
2315	2320	0.4%	0.0%	0.0%	91.3%	8.3%	0.0%	0.0%	1.5	4
2320	2325	0.8%	0.0%	0.0%	92.5%	6.7%	0.0%	0.0%	1.5	4
2325	2330	1.1%	0.0%	0.0%	93.1%	5.8%	0.0%	0.0%	1.5	4
2330	2335	1.4%	0.0%	0.0%	93.3%	5.2%	0.0%	0.0%	1.5	4
2335	2340	1.8%	0.0%	0.0%	93.2%	5.0%	0.0%	0.0%	1.5	4
2340	2345	2.3%	0.0%	0.0%	92.6%	5.1%	0.0%	0.0%	1.5	4
2345	2350	2.8%	0.0%	0.0%	91.6%	5.6%	0.0%	0.0%	1.5	4
2350	2355	3.4%	0.0%	0.0%	90.1%	6.5%	0.0%	0.0%	1.5	4
2355	2360	4.2%	0.0%	0.0%	87.9%	7.9%	0.0%	0.0%	1.5	4
2360	2365	0.0%	5.0%	5.0%	85.0%	5.0%	0.0%	0.0%	1.5	4
2365	2370	0.2%	0.0%	0.0%	88.7%	11.0%	0.0%	0.0%	1.5	4
2370	2375	0.4%	0.0%	0.0%	88.4%	11.2%	0.0%	0.0%	1.5	4
2375	2380	0.5%	0.0%	0.0%	87.2%	12.3%	0.0%	0.0%	1.5	4
2380	2385	0.5%	0.0%	0.0%	84.9%	14.6%	0.0%	0.0%	1.5	4
2385	2390	0.5%	0.0%	0.0%	81.2%	18.3%	0.0%	0.0%	1.5	4
2390	2395	0.4%	0.0%	0.0%	75.5%	24.1%	0.0%	0.0%	1.5	4
2395	2400	0.3%	0.0%	0.0%	66.8%	32.9%	0.0%	0.0%	1	5
2400	2405	0.2%	0.0%	0.0%	53.7%	46.1%	0.0%	0.0%	1	5
2405	2410	0.1%	0.0%	0.0%	34.0%	65.9%	0.0%	0.0%	1	5
2410	2415	0.0%	0.0%	5.0%	5.0%	85.0%	5.0%	0.0%	1	5
2415	2420	0.1%	0.0%	0.0%	37.6%	62.3%	0.0%	0.0%	1	5
2420	2425	0.3%	0.0%	0.0%	56.4%	43.3%	0.0%	0.0%	1	5
2425	2430	0.6%	0.0%	0.0%	68.7%	30.6%	0.0%	0.0%	1	5
2430	2435	1.0%	0.0%	0.0%	76.8%	22.2%	0.0%	0.0%	1	5
2435	2440	1.4%	0.0%	0.0%	81.9%	16.7%	0.0%	0.0%	1.5	4
2440	2445	1.8%	0.0%	0.0%	85.0%	13.2%	0.0%	0.0%	1.5	4
2445	2450	2.4%	0.0%	0.0%	86.6%	11.0%	0.0%	0.0%	1.5	4

Chainage (m)		Predicted state probability							Actual value	Actual state
From	To	State 1	State 2	State 3	State 4	State 5	State 6	State 7		
2450	2455	3.1%	0.0%	0.0%	87.0%	9.9%	0.0%	0.0%	1.5	4
2455	2460	4.0%	0.0%	0.0%	86.4%	9.6%	0.0%	0.0%	1.5	4
2460	2465	0.0%	5.0%	5.0%	85.0%	5.0%	0.0%	0.0%	1.5	4
2465	2470	0.4%	0.0%	0.0%	91.3%	8.3%	0.0%	0.0%	1.5	4
2470	2475	0.8%	0.0%	0.0%	92.5%	6.7%	0.0%	0.0%	1.5	4
2475	2480	1.1%	0.0%	0.0%	93.1%	5.8%	0.0%	0.0%	1.5	4
2480	2485	1.4%	0.0%	0.0%	93.3%	5.2%	0.0%	0.0%	1.5	4
2485	2490	1.8%	0.0%	0.0%	93.2%	5.0%	0.0%	0.0%	1.5	4
2490	2495	2.3%	0.0%	0.0%	92.6%	5.1%	0.0%	0.0%	1	5
2495	2500	2.8%	0.0%	0.0%	91.6%	5.6%	0.0%	0.0%	1	5
2500	2505	3.4%	0.0%	0.0%	90.1%	6.5%	0.0%	0.0%	1.5	4
2505	2510	4.2%	0.0%	0.0%	87.9%	7.9%	0.0%	0.0%	1.5	4
2510	2515	0.0%	5.0%	5.0%	85.0%	5.0%	0.0%	0.0%	1.5	4
2515	2520	0.4%	0.0%	0.0%	91.3%	8.3%	0.0%	0.0%	1.5	4
2520	2525	0.8%	0.0%	0.0%	92.5%	6.7%	0.0%	0.0%	1.5	4
2525	2530	1.1%	0.0%	0.0%	93.1%	5.8%	0.0%	0.0%	1.5	4
2530	2535	1.4%	0.0%	0.0%	93.3%	5.2%	0.0%	0.0%	1.5	4
2535	2540	1.8%	0.0%	0.0%	93.2%	5.0%	0.0%	0.0%	1.5	4
2540	2545	2.3%	0.0%	0.0%	92.6%	5.1%	0.0%	0.0%	1.5	4
2545	2550	2.8%	0.0%	0.0%	91.6%	5.6%	0.0%	0.0%	1.5	4
2550	2555	3.4%	0.0%	0.0%	90.1%	6.5%	0.0%	0.0%	1.5	4
2555	2560	4.2%	0.0%	0.0%	87.9%	7.9%	0.0%	0.0%	1.5	4
2560	2565	0.0%	5.0%	5.0%	85.0%	5.0%	0.0%	0.0%	1.5	4
2565	2570	0.4%	0.0%	0.0%	91.3%	8.3%	0.0%	0.0%	1.5	4
2570	2575	0.8%	0.0%	0.0%	92.5%	6.7%	0.0%	0.0%	1.5	4
2575	2580	1.1%	0.0%	0.0%	93.1%	5.8%	0.0%	0.0%	1.5	4
2580	2585	1.4%	0.0%	0.0%	93.3%	5.2%	0.0%	0.0%	1.5	4
2585	2590	1.8%	0.0%	0.0%	93.2%	5.0%	0.0%	0.0%	1.5	4
2590	2595	2.3%	0.0%	0.0%	92.6%	5.1%	0.0%	0.0%	1.5	4
2595	2600	2.8%	0.0%	0.0%	91.6%	5.6%	0.0%	0.0%	1.5	4
2600	2605	3.4%	0.0%	0.0%	90.1%	6.5%	0.0%	0.0%	1.5	4
2605	2610	4.2%	0.0%	0.0%	87.9%	7.9%	0.0%	0.0%	1.5	4
2610	2615	0.0%	5.0%	5.0%	85.0%	5.0%	0.0%	0.0%	1.5	4

Table F.5 Comparison between predicted and actual J_a in Subsection 2

Chainage (m)		Predicted state probability										Actual value	Actual state
From	To	State 1	State 2	State 3	State 4	State 5	State 6	State 7	State 8	State 9	State 10		
2010	2015	0%	5.0%	85.0%	5.0%	5%	0%	0%	0%	0%	0%	2	3

Chainage (m)		Predicted state probability											
From	To	State 1	State 2	State 3	State 4	State 5	State 6	State 7	State 8	State 9	State 10	Actual value	Actual state
2015	2020	0%	3.9%	89.1%	7.0%	0%	0%	0%	0%	0%	0%	2	3
2020	2025	0%	2.8%	89.5%	7.7%	0%	0%	0%	0%	0%	0%	2	3
2025	2030	0%	2.2%	89.5%	8.3%	0%	0%	0%	0%	0%	0%	2	3
2030	2035	0%	1.8%	89.3%	8.8%	0%	0%	0%	0%	0%	0%	2	3
2035	2040	0%	1.7%	89.0%	9.2%	0%	0%	0%	0%	0%	0%	2	3
2040	2045	0%	1.8%	88.6%	9.6%	0%	0%	0%	0%	0%	0%	2	3
2045	2050	0%	2.0%	88.1%	9.8%	0%	0%	0%	0%	0%	0%	2	3
2050	2055	0%	2.6%	87.5%	10.0%	0%	0%	0%	0%	0%	0%	2	3
2055	2060	0%	3.5%	86.5%	10.1%	0%	0%	0%	0%	0%	0%	2	3
2060	2065	0%	5.0%	85.0%	5.0%	5%	0%	0%	0%	0%	0%	2	3
2065	2070	0%	3.9%	89.1%	7.0%	0%	0%	0%	0%	0%	0%	2	3
2070	2075	0%	2.8%	89.5%	7.7%	0%	0%	0%	0%	0%	0%	2	3
2075	2080	0%	2.2%	89.5%	8.3%	0%	0%	0%	0%	0%	0%	2	3
2080	2085	0%	1.8%	89.3%	8.8%	0%	0%	0%	0%	0%	0%	2	3
2085	2090	0%	1.7%	89.0%	9.2%	0%	0%	0%	0%	0%	0%	2	3
2090	2095	0%	1.8%	88.6%	9.6%	0%	0%	0%	0%	0%	0%	2	3
2095	2100	0%	2.0%	88.1%	9.8%	0%	0%	0%	0%	0%	0%	2	3
2100	2105	0%	2.6%	87.5%	10.0%	0%	0%	0%	0%	0%	0%	2	3
2105	2110	0%	3.5%	86.5%	10.1%	0%	0%	0%	0%	0%	0%	2	3
2110	2115	0%	5.0%	85.0%	5.0%	5%	0%	0%	0%	0%	0%	2	3
2115	2120	0%	3.9%	89.1%	7.0%	0%	0%	0%	0%	0%	0%	2	3
2120	2125	0%	2.8%	89.5%	7.7%	0%	0%	0%	0%	0%	0%	2	3
2125	2130	0%	2.2%	89.5%	8.3%	0%	0%	0%	0%	0%	0%	2	3
2130	2135	0%	1.8%	89.3%	8.8%	0%	0%	0%	0%	0%	0%	2	3
2135	2140	0%	1.7%	89.0%	9.2%	0%	0%	0%	0%	0%	0%	2	3
2140	2145	0%	1.8%	88.6%	9.6%	0%	0%	0%	0%	0%	0%	2	3
2145	2150	0%	2.0%	88.1%	9.8%	0%	0%	0%	0%	0%	0%	2	3
2150	2155	0%	2.6%	87.5%	10.0%	0%	0%	0%	0%	0%	0%	2	3
2155	2160	0%	3.5%	86.5%	10.1%	0%	0%	0%	0%	0%	0%	2	3
2160	2165	0%	5.0%	85.0%	5.0%	5%	0%	0%	0%	0%	0%	3	4
2165	2170	0%	3.9%	89.1%	7.0%	0%	0%	0%	0%	0%	0%	2	3
2170	2175	0%	2.8%	89.5%	7.7%	0%	0%	0%	0%	0%	0%	2	3
2175	2180	0%	2.2%	89.5%	8.3%	0%	0%	0%	0%	0%	0%	2	3
2180	2185	0%	1.8%	89.3%	8.8%	0%	0%	0%	0%	0%	0%	2	3
2185	2190	0%	1.7%	89.0%	9.2%	0%	0%	0%	0%	0%	0%	2	3
2190	2195	0%	1.8%	88.6%	9.6%	0%	0%	0%	0%	0%	0%	2	3
2195	2200	0%	2.0%	88.1%	9.8%	0%	0%	0%	0%	0%	0%	2	3
2200	2205	0%	2.6%	87.5%	10.0%	0%	0%	0%	0%	0%	0%	2	3

Chainage (m)		Predicted state probability											
From	To	State 1	State 2	State 3	State 4	State 5	State 6	State 7	State 8	State 9	State 10	Actual value	Actual state
2205	2210	0%	3.5%	86.5%	10.1%	0%	0%	0%	0%	0%	0%	2	3
2210	2215	0%	5.0%	85.0%	5.0%	5%	0%	0%	0%	0%	0%	2	3
2215	2220	0%	3.9%	89.1%	7.0%	0%	0%	0%	0%	0%	0%	2	3
2220	2225	0%	2.8%	89.5%	7.7%	0%	0%	0%	0%	0%	0%	2	3
2225	2230	0%	2.2%	89.5%	8.3%	0%	0%	0%	0%	0%	0%	2	3
2230	2235	0%	1.8%	89.3%	8.8%	0%	0%	0%	0%	0%	0%	2	3
2235	2240	0%	1.7%	89.0%	9.2%	0%	0%	0%	0%	0%	0%	2	3
2240	2245	0%	1.8%	88.6%	9.6%	0%	0%	0%	0%	0%	0%	2	3
2245	2250	0%	2.0%	88.1%	9.8%	0%	0%	0%	0%	0%	0%	2	3
2250	2255	0%	2.6%	87.5%	10.0%	0%	0%	0%	0%	0%	0%	2	3
2255	2260	0%	3.5%	86.5%	10.1%	0%	0%	0%	0%	0%	0%	2	3
2260	2265	0%	5.0%	85.0%	5.0%	5%	0%	0%	0%	0%	0%	2	3
2265	2270	0%	3.9%	89.1%	7.0%	0%	0%	0%	0%	0%	0%	2	3
2270	2275	0%	2.8%	89.5%	7.7%	0%	0%	0%	0%	0%	0%	3	4
2275	2280	0%	2.2%	89.5%	8.3%	0%	0%	0%	0%	0%	0%	3	4
2280	2285	0%	1.8%	89.3%	8.8%	0%	0%	0%	0%	0%	0%	3	4
2285	2290	0%	1.7%	89.0%	9.2%	0%	0%	0%	0%	0%	0%	2	3
2290	2295	0%	1.8%	88.6%	9.6%	0%	0%	0%	0%	0%	0%	2	3
2295	2300	0%	2.0%	88.1%	9.8%	0%	0%	0%	0%	0%	0%	2	3
2300	2305	0%	2.6%	87.5%	10.0%	0%	0%	0%	0%	0%	0%	2	3
2305	2310	0%	3.5%	86.5%	10.1%	0%	0%	0%	0%	0%	0%	2	3
2310	2315	0%	5.0%	85.0%	5.0%	5%	0%	0%	0%	0%	0%	2	3
2315	2320	0%	3.9%	89.1%	7.0%	0%	0%	0%	0%	0%	0%	2	3
2320	2325	0%	2.8%	89.5%	7.7%	0%	0%	0%	0%	0%	0%	2	3
2325	2330	0%	2.2%	89.5%	8.3%	0%	0%	0%	0%	0%	0%	2	3
2330	2335	0%	1.8%	89.3%	8.8%	0%	0%	0%	0%	0%	0%	2	3
2335	2340	0%	1.7%	89.0%	9.2%	0%	0%	0%	0%	0%	0%	2	3
2340	2345	0%	1.8%	88.6%	9.6%	0%	0%	0%	0%	0%	0%	2	3
2345	2350	0%	2.0%	88.1%	9.8%	0%	0%	0%	0%	0%	0%	2	3
2350	2355	0%	2.6%	87.5%	10.0%	0%	0%	0%	0%	0%	0%	2	3
2355	2360	0%	3.5%	86.5%	10.1%	0%	0%	0%	0%	0%	0%	2	3
2360	2365	0%	5.0%	85.0%	5.0%	5%	0%	0%	0%	0%	0%	2	3
2365	2370	0%	3.9%	89.1%	7.0%	0%	0%	0%	0%	0%	0%	2	3
2370	2375	0%	2.8%	89.5%	7.7%	0%	0%	0%	0%	0%	0%	2	3
2375	2380	0%	2.2%	89.5%	8.3%	0%	0%	0%	0%	0%	0%	2	3
2380	2385	0%	1.8%	89.3%	8.8%	0%	0%	0%	0%	0%	0%	2	3
2385	2390	0%	1.7%	89.0%	9.2%	0%	0%	0%	0%	0%	0%	2	3
2390	2395	0%	1.8%	88.6%	9.6%	0%	0%	0%	0%	0%	0%	1	2

Chainage (m)		Predicted state probability											
From	To	State 1	State 2	State 3	State 4	State 5	State 6	State 7	State 8	State 9	State 10	Actual value	Actual state
2395	2400	0%	2.0%	88.1%	9.8%	0%	0%	0%	0%	0%	0%	2	3
2400	2405	0%	2.6%	87.5%	10.0%	0%	0%	0%	0%	0%	0%	2	3
2405	2410	0%	3.5%	86.5%	10.1%	0%	0%	0%	0%	0%	0%	1	2
2410	2415	0%	5.0%	85.0%	5.0%	5%	0%	0%	0%	0%	0%	2	3
2415	2420	0%	5.4%	88.4%	6.2%	0%	0%	0%	0%	0%	0%	2	3
2420	2425	0%	5.3%	88.3%	6.4%	0%	0%	0%	0%	0%	0%	2	3
2425	2430	0%	6.0%	87.6%	6.4%	0%	0%	0%	0%	0%	0%	2	3
2430	2435	0%	7.5%	86.1%	6.4%	0%	0%	0%	0%	0%	0%	2	3
2435	2440	0%	10.2%	83.6%	6.2%	0%	0%	0%	0%	0%	0%	2	3
2440	2445	0%	14.8%	79.2%	6.0%	0%	0%	0%	0%	0%	0%	2	3
2445	2450	0%	22.4%	71.8%	5.7%	0%	0%	0%	0%	0%	0%	1	2
2450	2455	0%	35.1%	59.5%	5.4%	0%	0%	0%	0%	0%	0%	1	2
2455	2460	0%	55.9%	38.9%	5.1%	0%	0%	0%	0%	0%	0%	1	2
2460	2465	5%	85.0%	5.0%	5.0%	0%	0%	0%	0%	0%	0%	1	2
2465	2470	0%	52.7%	41.2%	6.1%	0%	0%	0%	0%	0%	0%	1	2
2470	2475	0%	32.8%	60.9%	6.4%	0%	0%	0%	0%	0%	0%	1	2
2475	2480	0%	20.7%	72.4%	6.8%	0%	0%	0%	0%	0%	0%	1	2
2480	2485	0%	13.5%	79.1%	7.4%	0%	0%	0%	0%	0%	0%	2	3
2485	2490	0%	9.1%	82.9%	7.9%	0%	0%	0%	0%	0%	0%	2	3
2490	2495	0%	6.6%	84.9%	8.5%	0%	0%	0%	0%	0%	0%	2	3
2495	2500	0%	5.2%	85.9%	9.0%	0%	0%	0%	0%	0%	0%	2	3
2500	2505	0%	4.5%	86.1%	9.4%	0%	0%	0%	0%	0%	0%	2	3
2505	2510	0%	4.5%	85.8%	9.8%	0%	0%	0%	0%	0%	0%	2	3
2510	2515	0%	5.0%	85.0%	5.0%	5%	0%	0%	0%	0%	0%	2	3
2515	2520	0%	3.9%	89.1%	7.0%	0%	0%	0%	0%	0%	0%	2	3
2520	2525	0%	2.8%	89.5%	7.7%	0%	0%	0%	0%	0%	0%	2	3
2525	2530	0%	2.2%	89.5%	8.3%	0%	0%	0%	0%	0%	0%	2	3
2530	2535	0%	1.8%	89.3%	8.8%	0%	0%	0%	0%	0%	0%	2	3
2535	2540	0%	1.7%	89.0%	9.2%	0%	0%	0%	0%	0%	0%	2	3
2540	2545	0%	1.8%	88.6%	9.6%	0%	0%	0%	0%	0%	0%	2	3
2545	2550	0%	2.0%	88.1%	9.8%	0%	0%	0%	0%	0%	0%	2	3
2550	2555	0%	2.6%	87.5%	10.0%	0%	0%	0%	0%	0%	0%	2	3
2555	2560	0%	3.5%	86.5%	10.1%	0%	0%	0%	0%	0%	0%	2	3
2560	2565	0%	5.0%	85.0%	5.0%	5%	0%	0%	0%	0%	0%	2	3
2565	2570	0%	3.9%	89.1%	7.0%	0%	0%	0%	0%	0%	0%	2	3
2570	2575	0%	2.8%	89.5%	7.7%	0%	0%	0%	0%	0%	0%	2	3
2575	2580	0%	2.2%	89.5%	8.3%	0%	0%	0%	0%	0%	0%	2	3
2580	2585	0%	1.8%	89.3%	8.8%	0%	0%	0%	0%	0%	0%	2	3

Chainage (m)		Predicted state probability										Actual value	Actual state
From	To	State 1	State 2	State 3	State 4	State 5	State 6	State 7	State 8	State 9	State 10		
2585	2590	0%	1.7%	89.0%	9.2%	0%	0%	0%	0%	0%	0%	2	3
2590	2595	0%	1.8%	88.6%	9.6%	0%	0%	0%	0%	0%	0%	2	3
2595	2600	0%	2.0%	88.1%	9.8%	0%	0%	0%	0%	0%	0%	2	3
2600	2605	0%	2.6%	87.5%	10.0%	0%	0%	0%	0%	0%	0%	2	3
2605	2610	0%	3.5%	86.5%	10.1%	0%	0%	0%	0%	0%	0%	2	3
2610	2615	0%	5.0%	85.0%	5.0%	5%	0%	0%	0%	0%	0%	2	3

Table F.6 Comparison between predicted and actual J_w in Subsection 2

Chainage (m)		Predicted state probability						Actual value	Actual state
From	To	State 1	State 2	State 3	State 4	State 5	State 6		
2010	2015	95%	5%	0%	0%	0%	0%	1	1
2015	2020	95%	5%	0%	0%	0%	0%	1	1
2020	2025	95%	5%	0%	0%	0%	0%	1	1
2025	2030	94%	6%	0%	0%	0%	0%	1	1
2030	2035	94%	6%	0%	0%	0%	0%	1	1
2035	2040	94%	6%	0%	0%	0%	0%	1	1
2040	2045	94%	6%	0%	0%	0%	0%	1	1
2045	2050	94%	6%	0%	0%	0%	0%	1	1
2050	2055	95%	5%	0%	0%	0%	0%	1	1
2055	2060	95%	5%	0%	0%	0%	0%	1	1
2060	2065	95%	5%	0%	0%	0%	0%	1	1
2065	2070	95%	5%	0%	0%	0%	0%	1	1
2070	2075	95%	5%	0%	0%	0%	0%	1	1
2075	2080	94%	6%	0%	0%	0%	0%	1	1
2080	2085	94%	6%	0%	0%	0%	0%	1	1
2085	2090	94%	6%	0%	0%	0%	0%	1	1
2090	2095	94%	6%	0%	0%	0%	0%	1	1
2095	2100	94%	6%	0%	0%	0%	0%	1	1
2100	2105	95%	5%	0%	0%	0%	0%	1	1
2105	2110	95%	5%	0%	0%	0%	0%	1	1
2110	2115	95%	5%	0%	0%	0%	0%	1	1
2115	2120	95%	5%	0%	0%	0%	0%	1	1
2120	2125	95%	5%	0%	0%	0%	0%	1	1
2125	2130	94%	6%	0%	0%	0%	0%	1	1
2130	2135	94%	6%	0%	0%	0%	0%	1	1
2135	2140	94%	6%	0%	0%	0%	0%	1	1
2140	2145	94%	6%	0%	0%	0%	0%	1	1
2145	2150	94%	6%	0%	0%	0%	0%	1	1
2150	2155	95%	5%	0%	0%	0%	0%	1	1
2155	2160	95%	5%	0%	0%	0%	0%	1	1
2160	2165	95%	5%	0%	0%	0%	0%	1	1
2165	2170	95%	5%	0%	0%	0%	0%	1	1
2170	2175	95%	5%	0%	0%	0%	0%	0.66	2
2175	2180	94%	6%	0%	0%	0%	0%	0.5	3
2180	2185	94%	6%	0%	0%	0%	0%	0.66	2

Chainage (m)		Predicted state probability						Actual value	Actual state
From	To	State 1	State 2	State 3	State 4	State 5	State 6		
2185	2190	94%	6%	0%	0%	0%	0%	0.66	2
2190	2195	94%	6%	0%	0%	0%	0%	1	1
2195	2200	94%	6%	0%	0%	0%	0%	1	1
2200	2205	95%	5%	0%	0%	0%	0%	1	1
2205	2210	95%	5%	0%	0%	0%	0%	1	1
2210	2215	95%	5%	0%	0%	0%	0%	1	1
2215	2220	95%	5%	0%	0%	0%	0%	1	1
2220	2225	95%	5%	0%	0%	0%	0%	1	1
2225	2230	94%	6%	0%	0%	0%	0%	1	1
2230	2235	94%	6%	0%	0%	0%	0%	1	1
2235	2240	94%	6%	0%	0%	0%	0%	1	1
2240	2245	94%	6%	0%	0%	0%	0%	0.66	2
2245	2250	94%	6%	0%	0%	0%	0%	0.66	2
2250	2255	95%	5%	0%	0%	0%	0%	1	1
2255	2260	95%	5%	0%	0%	0%	0%	1	1
2260	2265	95%	5%	0%	0%	0%	0%	1	1
2265	2270	95%	5%	0%	0%	0%	0%	1	1
2270	2275	95%	5%	0%	0%	0%	0%	0.66	2
2275	2280	94%	6%	0%	0%	0%	0%	0.66	2
2280	2285	94%	6%	0%	0%	0%	0%	0.66	2
2285	2290	94%	6%	0%	0%	0%	0%	1	1
2290	2295	94%	6%	0%	0%	0%	0%	1	1
2295	2300	94%	6%	0%	0%	0%	0%	1	1
2300	2305	95%	5%	0%	0%	0%	0%	1	1
2305	2310	95%	5%	0%	0%	0%	0%	1	1
2310	2315	95%	5%	0%	0%	0%	0%	1	1
2315	2320	95%	5%	0%	0%	0%	0%	1	1
2320	2325	95%	5%	0%	0%	0%	0%	1	1
2325	2330	94%	6%	0%	0%	0%	0%	1	1
2330	2335	94%	6%	0%	0%	0%	0%	1	1
2335	2340	94%	6%	0%	0%	0%	0%	1	1
2340	2345	94%	6%	0%	0%	0%	0%	1	1
2345	2350	94%	6%	0%	0%	0%	0%	1	1
2350	2355	95%	5%	0%	0%	0%	0%	1	1
2355	2360	95%	5%	0%	0%	0%	0%	1	1
2360	2365	95%	5%	0%	0%	0%	0%	1	1
2365	2370	95%	5%	0%	0%	0%	0%	1	1
2370	2375	95%	5%	0%	0%	0%	0%	1	1
2375	2380	94%	6%	0%	0%	0%	0%	1	1
2380	2385	94%	6%	0%	0%	0%	0%	1	1
2385	2390	94%	6%	0%	0%	0%	0%	1	1
2390	2395	94%	6%	0%	0%	0%	0%	1	1
2395	2400	94%	6%	0%	0%	0%	0%	1	1
2400	2405	95%	5%	0%	0%	0%	0%	1	1
2405	2410	95%	5%	0%	0%	0%	0%	1	1
2410	2415	95%	5%	0%	0%	0%	0%	1	1
2415	2420	95%	5%	0%	0%	0%	0%	1	1
2420	2425	95%	5%	0%	0%	0%	0%	1	1
2425	2430	94%	6%	0%	0%	0%	0%	1	1

Chainage (m)		Predicted state probability						Actual value	Actual state
From	To	State 1	State 2	State 3	State 4	State 5	State 6		
2430	2435	94%	6%	0%	0%	0%	0%	1	1
2435	2440	94%	6%	0%	0%	0%	0%	1	1
2440	2445	94%	6%	0%	0%	0%	0%	1	1
2445	2450	94%	6%	0%	0%	0%	0%	1	1
2450	2455	95%	5%	0%	0%	0%	0%	1	1
2455	2460	95%	5%	0%	0%	0%	0%	1	1
2460	2465	95%	5%	0%	0%	0%	0%	1	1
2465	2470	95%	5%	0%	0%	0%	0%	1	1
2470	2475	95%	5%	0%	0%	0%	0%	1	1
2475	2480	94%	6%	0%	0%	0%	0%	1	1
2480	2485	94%	6%	0%	0%	0%	0%	1	1
2485	2490	94%	6%	0%	0%	0%	0%	1	1
2490	2495	94%	6%	0%	0%	0%	0%	1	1
2495	2500	94%	6%	0%	0%	0%	0%	1	1
2500	2505	95%	5%	0%	0%	0%	0%	1	1
2505	2510	95%	5%	0%	0%	0%	0%	1	1
2510	2515	95%	5%	0%	0%	0%	0%	1	1
2515	2520	95%	5%	0%	0%	0%	0%	1	1
2520	2525	95%	5%	0%	0%	0%	0%	1	1
2525	2530	94%	6%	0%	0%	0%	0%	1	1
2530	2535	94%	6%	0%	0%	0%	0%	1	1
2535	2540	94%	6%	0%	0%	0%	0%	1	1
2540	2545	94%	6%	0%	0%	0%	0%	1	1
2545	2550	94%	6%	0%	0%	0%	0%	1	1
2550	2555	95%	5%	0%	0%	0%	0%	1	1
2555	2560	95%	5%	0%	0%	0%	0%	1	1
2560	2565	95%	5%	0%	0%	0%	0%	1	1
2565	2570	95%	5%	0%	0%	0%	0%	1	1
2570	2575	95%	5%	0%	0%	0%	0%	1	1
2575	2580	94%	6%	0%	0%	0%	0%	1	1
2580	2585	94%	6%	0%	0%	0%	0%	1	1
2585	2590	94%	6%	0%	0%	0%	0%	1	1
2590	2595	94%	6%	0%	0%	0%	0%	1	1
2595	2600	94%	6%	0%	0%	0%	0%	1	1
2600	2605	95%	5%	0%	0%	0%	0%	1	1
2605	2610	95%	5%	0%	0%	0%	0%	1	1
2610	2615	95%	5%	0%	0%	0%	0%	1	1

Table F.7 Comparison between predicted and actual SRF in Subsection 2

Chainage (m)		Predicted state probability									Actual value	Actual state
From	To	State 1	State 2	State 3	State 4	State 5	State 6	State 7	State 8	State 9		
2010	2015	0.00	0.00	0.00	0.05	0.90	0.05	0.00	0.00	0.00	1	5
2015	2020	0.00	0.00	0.00	0.00	1.00	0.00	0.00	0.00	0.00	1	5
2020	2025	0.00	0.00	0.00	0.00	1.00	0.00	0.00	0.00	0.00	1	5
2025	2030	0.00	0.00	0.00	0.00	1.00	0.00	0.00	0.00	0.00	1	5
2030	2035	0.00	0.00	0.00	0.00	1.00	0.00	0.00	0.00	0.00	1	5
2035	2040	0.00	0.00	0.00	0.00	1.00	0.00	0.00	0.00	0.00	1	5
2040	2045	0.00	0.00	0.00	0.00	1.00	0.00	0.00	0.00	0.00	1	5

Chainage (m)		Predicted state probability									Actual value	Actual state
From	To	State 1	State 2	State 3	State 4	State 5	State 6	State 7	State 8	State 9		
2045	2050	0.00	0.00	0.00	0.00	1.00	0.00	0.00	0.00	0.00	1	5
2050	2055	0.00	0.00	0.00	0.00	1.00	0.00	0.00	0.00	0.00	1	5
2055	2060	0.00	0.00	0.00	0.00	1.00	0.00	0.00	0.00	0.00	1	5
2060	2065	0.00	0.00	0.00	0.05	0.90	0.05	0.00	0.00	0.00	2.5	4
2065	2070	0.00	0.00	0.00	0.00	1.00	0.00	0.00	0.00	0.00	1	5
2070	2075	0.00	0.00	0.00	0.00	1.00	0.00	0.00	0.00	0.00	1	5
2075	2080	0.00	0.00	0.00	0.00	1.00	0.00	0.00	0.00	0.00	1	5
2080	2085	0.00	0.00	0.00	0.00	1.00	0.00	0.00	0.00	0.00	1	5
2085	2090	0.00	0.00	0.00	0.00	1.00	0.00	0.00	0.00	0.00	1	5
2090	2095	0.00	0.00	0.00	0.00	1.00	0.00	0.00	0.00	0.00	1	5
2095	2100	0.00	0.00	0.00	0.00	1.00	0.00	0.00	0.00	0.00	1	5
2100	2105	0.00	0.00	0.00	0.00	1.00	0.00	0.00	0.00	0.00	1	5
2105	2110	0.00	0.00	0.00	0.00	1.00	0.00	0.00	0.00	0.00	1	5
2110	2115	0.00	0.00	0.00	0.05	0.90	0.05	0.00	0.00	0.00	1	5
2115	2120	0.00	0.00	0.00	0.00	1.00	0.00	0.00	0.00	0.00	1	5
2120	2125	0.00	0.00	0.00	0.00	1.00	0.00	0.00	0.00	0.00	1	5
2125	2130	0.00	0.00	0.00	0.00	1.00	0.00	0.00	0.00	0.00	1	5
2130	2135	0.00	0.00	0.00	0.00	1.00	0.00	0.00	0.00	0.00	1	5
2135	2140	0.00	0.00	0.00	0.00	1.00	0.00	0.00	0.00	0.00	1	5
2140	2145	0.00	0.00	0.00	0.00	1.00	0.00	0.00	0.00	0.00	1	5
2145	2150	0.00	0.00	0.00	0.00	1.00	0.00	0.00	0.00	0.00	1	5
2150	2155	0.00	0.00	0.00	0.00	1.00	0.00	0.00	0.00	0.00	1	5
2155	2160	0.00	0.00	0.00	0.00	1.00	0.00	0.00	0.00	0.00	1	5
2160	2165	0.00	0.00	0.00	0.05	0.90	0.05	0.00	0.00	0.00	1	5
2165	2170	0.00	0.00	0.00	0.00	1.00	0.00	0.00	0.00	0.00	1	5
2170	2175	0.00	0.00	0.00	0.00	1.00	0.00	0.00	0.00	0.00	1	5
2175	2180	0.00	0.00	0.00	0.00	1.00	0.00	0.00	0.00	0.00	1	5
2180	2185	0.00	0.00	0.00	0.00	1.00	0.00	0.00	0.00	0.00	1	5
2185	2190	0.00	0.00	0.00	0.00	1.00	0.00	0.00	0.00	0.00	1	5
2190	2195	0.00	0.00	0.00	0.00	1.00	0.00	0.00	0.00	0.00	1	5
2195	2200	0.00	0.00	0.00	0.00	1.00	0.00	0.00	0.00	0.00	1	5
2200	2205	0.00	0.00	0.00	0.00	1.00	0.00	0.00	0.00	0.00	1	5
2205	2210	0.00	0.00	0.00	0.00	1.00	0.00	0.00	0.00	0.00	1	5
2210	2215	0.00	0.00	0.00	0.05	0.90	0.05	0.00	0.00	0.00	1	5
2215	2220	0.00	0.00	0.00	0.00	1.00	0.00	0.00	0.00	0.00	1	5
2220	2225	0.00	0.00	0.00	0.00	1.00	0.00	0.00	0.00	0.00	1	5
2225	2230	0.00	0.00	0.00	0.00	1.00	0.00	0.00	0.00	0.00	1	5
2230	2235	0.00	0.00	0.00	0.00	1.00	0.00	0.00	0.00	0.00	1	5
2235	2240	0.00	0.00	0.00	0.00	1.00	0.00	0.00	0.00	0.00	1	5
2240	2245	0.00	0.00	0.00	0.00	1.00	0.00	0.00	0.00	0.00	1	5
2245	2250	0.00	0.00	0.00	0.00	1.00	0.00	0.00	0.00	0.00	1	5
2250	2255	0.00	0.00	0.00	0.00	1.00	0.00	0.00	0.00	0.00	1	5
2255	2260	0.00	0.00	0.00	0.00	1.00	0.00	0.00	0.00	0.00	1	5
2260	2265	0.00	0.00	0.00	0.05	0.90	0.05	0.00	0.00	0.00	1	5
2265	2270	0.00	0.00	0.00	0.00	1.00	0.00	0.00	0.00	0.00	1	5
2270	2275	0.00	0.00	0.00	0.00	1.00	0.00	0.00	0.00	0.00	1	5
2275	2280	0.00	0.00	0.00	0.00	1.00	0.00	0.00	0.00	0.00	1	5
2280	2285	0.00	0.00	0.00	0.00	1.00	0.00	0.00	0.00	0.00	1	5
2285	2290	0.00	0.00	0.00	0.00	1.00	0.00	0.00	0.00	0.00	1	5

Chainage (m)		Predicted state probability									Actual value	Actual state
From	To	State 1	State 2	State 3	State 4	State 5	State 6	State 7	State 8	State 9		
2290	2295	0.00	0.00	0.00	0.00	1.00	0.00	0.00	0.00	0.00	1	5
2295	2300	0.00	0.00	0.00	0.00	1.00	0.00	0.00	0.00	0.00	1	5
2300	2305	0.00	0.00	0.00	0.00	1.00	0.00	0.00	0.00	0.00	1	5
2305	2310	0.00	0.00	0.00	0.00	1.00	0.00	0.00	0.00	0.00	1	5
2310	2315	0.00	0.00	0.00	0.05	0.90	0.05	0.00	0.00	0.00	1	5
2315	2320	0.00	0.00	0.00	0.00	1.00	0.00	0.00	0.00	0.00	1	5
2320	2325	0.00	0.00	0.00	0.00	1.00	0.00	0.00	0.00	0.00	1	5
2325	2330	0.00	0.00	0.00	0.00	1.00	0.00	0.00	0.00	0.00	1	5
2330	2335	0.00	0.00	0.00	0.00	1.00	0.00	0.00	0.00	0.00	1	5
2335	2340	0.00	0.00	0.00	0.00	1.00	0.00	0.00	0.00	0.00	1	5
2340	2345	0.00	0.00	0.00	0.00	1.00	0.00	0.00	0.00	0.00	1	5
2345	2350	0.00	0.00	0.00	0.00	1.00	0.00	0.00	0.00	0.00	1	5
2350	2355	0.00	0.00	0.00	0.00	1.00	0.00	0.00	0.00	0.00	1	4
2355	2360	0.00	0.00	0.00	0.00	1.00	0.00	0.00	0.00	0.00	1	4
2360	2365	0.00	0.00	0.00	0.05	0.90	0.05	0.00	0.00	0.00	1	5
2365	2370	0.00	0.00	0.00	0.00	1.00	0.00	0.00	0.00	0.00	1	5
2370	2375	0.00	0.00	0.00	0.00	1.00	0.00	0.00	0.00	0.00	1	5
2375	2380	0.00	0.00	0.00	0.00	1.00	0.00	0.00	0.00	0.00	1	5
2380	2385	0.00	0.00	0.00	0.00	1.00	0.00	0.00	0.00	0.00	1	5
2385	2390	0.00	0.00	0.00	0.00	1.00	0.00	0.00	0.00	0.00	1	5
2390	2395	0.00	0.00	0.00	0.00	1.00	0.00	0.00	0.00	0.00	1	5
2395	2400	0.00	0.00	0.00	0.00	1.00	0.00	0.00	0.00	0.00	1	5
2400	2405	0.00	0.00	0.00	0.00	1.00	0.00	0.00	0.00	0.00	1	5
2405	2410	0.00	0.00	0.00	0.00	1.00	0.00	0.00	0.00	0.00	1	5
2410	2415	0.00	0.00	0.00	0.05	0.90	0.05	0.00	0.00	0.00	1	5
2415	2420	0.00	0.00	0.00	0.00	1.00	0.00	0.00	0.00	0.00	1	5
2420	2425	0.00	0.00	0.00	0.00	1.00	0.00	0.00	0.00	0.00	1	5
2425	2430	0.00	0.00	0.00	0.00	1.00	0.00	0.00	0.00	0.00	1	5
2430	2435	0.00	0.00	0.00	0.00	1.00	0.00	0.00	0.00	0.00	1	5
2435	2440	0.00	0.00	0.00	0.00	1.00	0.00	0.00	0.00	0.00	1	5
2440	2445	0.00	0.00	0.00	0.00	1.00	0.00	0.00	0.00	0.00	1	5
2445	2450	0.00	0.00	0.00	0.00	1.00	0.00	0.00	0.00	0.00	2.5	4
2450	2455	0.00	0.00	0.00	0.00	1.00	0.00	0.00	0.00	0.00	2.5	4
2455	2460	0.00	0.00	0.00	0.00	1.00	0.00	0.00	0.00	0.00	1	5
2460	2465	0.00	0.00	0.00	0.05	0.90	0.05	0.00	0.00	0.00	1	5
2465	2470	0.00	0.00	0.00	0.00	1.00	0.00	0.00	0.00	0.00	1	5
2470	2475	0.00	0.00	0.00	0.00	1.00	0.00	0.00	0.00	0.00	1	5
2475	2480	0.00	0.00	0.00	0.00	1.00	0.00	0.00	0.00	0.00	1	5
2480	2485	0.00	0.00	0.00	0.00	1.00	0.00	0.00	0.00	0.00	2.5	4
2485	2490	0.00	0.00	0.00	0.00	1.00	0.00	0.00	0.00	0.00	2.5	4
2490	2495	0.00	0.00	0.00	0.00	1.00	0.00	0.00	0.00	0.00	1	5
2495	2500	0.00	0.00	0.00	0.00	1.00	0.00	0.00	0.00	0.00	1	5
2500	2505	0.00	0.00	0.00	0.00	1.00	0.00	0.00	0.00	0.00	1	5
2505	2510	0.00	0.00	0.00	0.00	1.00	0.00	0.00	0.00	0.00	1	5
2510	2515	0.00	0.00	0.00	0.05	0.90	0.05	0.00	0.00	0.00	1	5
2515	2520	0.00	0.00	0.00	0.00	1.00	0.00	0.00	0.00	0.00	1	5
2520	2525	0.00	0.00	0.00	0.00	1.00	0.00	0.00	0.00	0.00	1	5
2525	2530	0.00	0.00	0.00	0.00	1.00	0.00	0.00	0.00	0.00	1	5
2530	2535	0.00	0.00	0.00	0.00	1.00	0.00	0.00	0.00	0.00	1	5

Chainage (m)		Predicted state probability									Actual value	Actual state
From	To	State 1	State 2	State 3	State 4	State 5	State 6	State 7	State 8	State 9		
2535	2540	0.00	0.00	0.00	0.00	1.00	0.00	0.00	0.00	0.00	1	5
2540	2545	0.00	0.00	0.00	0.00	1.00	0.00	0.00	0.00	0.00	1	5
2545	2550	0.00	0.00	0.00	0.00	1.00	0.00	0.00	0.00	0.00	1	5
2550	2555	0.00	0.00	0.00	0.00	1.00	0.00	0.00	0.00	0.00	1	5
2555	2560	0.00	0.00	0.00	0.00	1.00	0.00	0.00	0.00	0.00	1	5
2560	2565	0.00	0.00	0.00	0.05	0.90	0.05	0.00	0.00	0.00	1	5
2565	2570	0.00	0.00	0.00	0.00	1.00	0.00	0.00	0.00	0.00	1	5
2570	2575	0.00	0.00	0.00	0.00	1.00	0.00	0.00	0.00	0.00	1	5
2575	2580	0.00	0.00	0.00	0.00	1.00	0.00	0.00	0.00	0.00	1	5
2580	2585	0.00	0.00	0.00	0.00	1.00	0.00	0.00	0.00	0.00	1	5
2585	2590	0.00	0.00	0.00	0.00	1.00	0.00	0.00	0.00	0.00	1	5
2590	2595	0.00	0.00	0.00	0.00	1.00	0.00	0.00	0.00	0.00	1	5
2595	2600	0.00	0.00	0.00	0.00	1.00	0.00	0.00	0.00	0.00	1	5
2600	2605	0.00	0.00	0.00	0.00	1.00	0.00	0.00	0.00	0.00	1	5
2605	2610	0.00	0.00	0.00	0.00	1.00	0.00	0.00	0.00	0.00	1	5
2610	2615	0.00	0.00	0.00	0.05	0.90	0.05	0.00	0.00	0.00	1	5

Table F.8 Comparison between predicted and actual Q value in Subsection 2

Chainage (m)		Predicted Q value		Actual Q value
From	To	Mean	SD	
2010	2015	11.1	5.4	10.0
2015	2020	11.3	5.0	10.0
2020	2025	11.4	6.0	10.0
2025	2030	11.3	6.2	10.0
2030	2035	11.3	6.6	10.0
2035	2040	11.0	6.4	11.3
2040	2045	10.8	6.4	11.3
2045	2050	10.4	6.1	5.0
2050	2055	9.9	5.8	6.3
2055	2060	9.4	5.2	8.8
2060	2065	7.8	3.9	3.8
2065	2070	8.5	4.0	8.8
2070	2075	8.9	4.6	8.1
2075	2080	9.3	5.1	8.1
2080	2085	9.4	5.1	8.8
2085	2090	9.5	5.1	8.8
2090	2095	9.6	5.5	8.8
2095	2100	9.6	5.3	8.8
2100	2105	9.4	5.3	8.8
2105	2110	9.1	4.8	8.8
2110	2115	7.7	3.6	9.4
2115	2120	8.5	3.9	9.4

Chainage (m)		Predicted Q value		Actual Q value
From	To	Mean	SD	
2120	2125	9.0	4.8	7.5
2125	2130	9.2	5.0	8.1
2130	2135	9.5	5.4	8.1
2135	2140	9.6	5.3	10.0
2140	2145	9.5	5.2	8.8
2145	2150	9.5	5.2	8.8
2150	2155	9.4	5.2	8.8
2155	2160	9.1	5.0	8.8
2160	2165	7.8	3.9	5.0
2165	2170	8.5	4.1	15.0
2170	2175	8.9	4.7	9.9
2175	2180	9.2	5.0	4.1
2180	2185	9.4	5.1	5.8
2185	2190	9.6	5.4	5.8
2190	2195	9.6	5.4	7.5
2195	2200	9.6	5.3	7.5
2200	2205	9.4	5.3	8.1
2205	2210	9.2	5.1	8.1
2210	2215	7.7	3.9	13.1
2215	2220	9.3	5.0	13.1
2220	2225	10.5	6.0	8.8
2225	2230	11.8	7.0	5.8
2230	2235	12.9	8.3	17.5
2235	2240	14.3	9.1	20.0
2240	2245	15.8	10.2	14.0
2245	2250	17.2	11.0	14.0
2250	2255	18.9	11.8	10.6
2255	2260	20.7	12.0	10.6
2260	2265	22.1	10.1	18.8
2265	2270	20.1	9.9	17.5
2270	2275	19.3	11.0	3.3
2275	2280	18.5	11.0	3.3
2280	2285	17.6	10.9	3.9
2285	2290	16.7	10.2	10.0
2290	2295	15.9	9.8	10.0
2295	2300	14.9	8.8	10.0
2300	2305	13.9	8.1	22.5
2305	2310	13.0	7.4	22.5
2310	2315	12.1	6.0	11.3

Chainage (m)		Predicted Q value		Actual Q value
From	To	Mean	SD	
2315	2320	11.6	4.2	11.3
2320	2325	12.0	4.8	11.3
2325	2330	12.6	5.4	11.3
2330	2335	13.3	6.1	21.3
2335	2340	14.2	6.8	21.3
2340	2345	15.2	7.1	20.0
2345	2350	16.5	8.3	20.0
2350	2355	18.0	8.8	17.5
2355	2360	19.9	9.9	21.3
2360	2365	22.1	10.3	20.0
2365	2370	18.7	7.0	20.0
2370	2375	17.1	6.7	22.5
2375	2380	15.8	6.5	22.5
2380	2385	14.6	6.0	20.0
2385	2390	13.6	5.5	10.0
2390	2395	12.6	5.1	18.8
2395	2400	11.6	4.6	6.7
2400	2405	10.5	4.2	6.7
2405	2410	9.4	3.7	15.0
2410	2415	7.1	3.4	7.5
2415	2420	9.4	3.3	7.9
2420	2425	10.4	3.9	7.9
2425	2430	11.3	4.6	7.9
2430	2435	12.2	5.2	7.9
2435	2440	13.3	6.0	11.9
2440	2445	14.7	6.9	16.9
2445	2450	16.6	8.5	13.5
2450	2455	19.5	10.4	14.3
2455	2460	24.1	12.9	35.6
2460	2465	30.9	15.4	33.8
2465	2470	21.7	10.0	33.8
2470	2475	18.1	8.1	31.9
2475	2480	16.1	7.2	31.9
2480	2485	15.2	6.8	8.5
2485	2490	15.0	6.9	7.0
2490	2495	15.4	7.1	8.3
2495	2500	16.3	7.5	8.3
2500	2505	17.8	9.2	15.0
2505	2510	19.8	9.8	20.0

Chainage (m)		Predicted Q value		Actual Q value
From	To	Mean	SD	
2510	2515	22.2	10.5	22.5
2515	2520	20.3	6.4	22.5
2520	2525	20.0	6.4	21.3
2525	2530	19.8	6.7	21.3
2530	2535	19.7	7.0	20.0
2535	2540	19.8	7.3	20.0
2540	2545	19.9	7.7	20.0
2545	2550	20.2	8.2	17.5
2550	2555	20.7	8.8	17.5
2555	2560	21.4	9.3	21.3
2560	2565	22.2	10.3	22.5
2565	2570	20.3	6.7	22.5
2570	2575	19.9	6.7	25.0
2575	2580	19.8	7.1	25.0
2580	2585	19.7	7.2	25.0
2585	2590	19.7	7.6	25.0
2590	2595	19.9	7.9	25.0
2595	2600	20.2	8.2	25.0
2600	2605	20.7	8.8	25.0
2605	2610	21.4	9.5	25.0
2610	2615	22.0	10.1	25.0

APPENDIX G

Technology Transfer Activities

by
Hui Lu[1]
Dr. Marte Gutierrez[1]
[1] Colorado School of Mines

Sponsorship
(UTC-UTI and cost matching external sponsors)

For

University Transportation Center for
Underground Transportation Infrastructure
(UTC-UTI)

October 30, 2020

G.1 Accomplishments

G.1.1 What was done? What was learned?

- A Markovian Q-based prediction model has been proposed using the MCS technique to provide the probability distribution of rock mass quality along the tunnel alignment before construction.
- An MCS-based uncertainty analysis framework in the Q-system has been developed to probabilistically characterize the uncertainty in input parameter of Q-system and its effects on rock mass characterization and ground response by applying the MCS technique with appropriate empirical correlations.
- A reliability assessment with the strain-based failure criterion has been performed using the FORM (First-Order Reliability Model) algorithm.
- The reliability evaluation procedures were applied on the excavation stability The Shimizu Highway Tunnel in Japan and the engineering feasibility study of the future extension of the Eisenhower-Johnson Tunnel in Colorado.

G.2 How have the results been disseminated?

- The results were presented at the *2019 Society of Mining Engineers Annual Meeting*, Denver, Colorado, Feb. 26, 2019.
- One journal paper has been accepted and published in a journal.
- A second journal paper was submitted and reviewed in a journal and is under revision.
- A third journal paper is completed and is under review in a journal.
- The results were presented at UTC-UTI workshops.

G.3 Participants and Collaborating Organizations

Colorado Department of Transportation.

G.4 Outputs

Journal publications

Lu, H., Kim, E, and Gutierrez, M. (2020). "Monte Carlo Simulation (MCS)-Based Uncertainty Analysis of Rock Mass Quality Q in Underground Construction," Tunnelling and Underground Space Technology, 10.1016/j.tust.2019.103089.

Conference presentations and proceedings

Lu, H., Kim, E. and Gutierrez. M. (2019). "Probability-based uncertainty analysis of rock mass quality in underground excavations." SME 2019 Annual Meeting, Denver, Colorado, Feb. 26, 2019.

G.4 Outcomes

- The proposed Q-based prediction model was shown to be valuable in reducing uncertainties and risks involved in rock mass classifications and can serve as a complement to geology exploration in the planning and preliminary design stage of underground construction. It can also provide insights into the decision support for the design of excavation sequence and support schemes for the underground structures.
- The proposed framework of the MCS-based uncertainty analysis in the probabilistic Q-system can provide an approach for systematically characterizing the uncertainty in the rock mass classification and its propagation to associated rock mass parameters. The framework can also serve as a useful tool to obtain insightful information for the probabilistic evaluation of ground responses and support performance of underground structures.
- The reliability assessment using the Q-based empirical approach can be used as a complement to analytical and numerical approaches in the preliminary evaluation of the stability of underground excavations.

G.6 Impacts

- Using the improved tool developed in this research project, tunnel lining design can be more efficient resulting in more cost-effective, safer and more reliable tunnel structures.